Universitat Ramon Llull

DOCTORAL THESIS

Title	Development of novel vesicle-like nanocarriers for targeted drug delivery
Presented by	Maria Sánchez Purrà
Centre	IQS School of Engineering
Department	Bioengineering
Directed by	Dr. Salvador Borrós Gómez Dr. Víctor Ramos Pérez

C. Claravall, 1-3
08022 Barcelona
Tel. 936 022 200
Fax 936 022 249
E-mail: urlsc@sec.url.es
www.url.es

Als meus pares,

Science does not know its debt to imagination

Ralph Waldo Emerson

Acknowledgements

En primer lloc, voldria donar les gràcies al meu director de tesi, en Salvador Bórros, per brindar-me l'oportunitat de treballar al grup GEMAT. Gràcies, Chicho, per demostrar-me al llarg d'aquests anys la teva confiança en mi i fer possible estades a l'estranger com la de Boston, la participació en el projecte de Nanobiopharmaceutics i l'assistència a nombrosos cursos i congressos. Gràcies també, pel suport que m'has brindat en moments d'incertesa, no només en l'àmbit professional sinó també en el personal, i per suportar la meva pressió i exigència. Espero que em trobis a faltar ni que sigui una miqueta ;)

En segon lloc, voldria donar les gràcies també al meu co-director, en Víctor, per la seva infinita paciència, la total disposició i entrega, les grans idees que et salven el cul, per veure sempre la part positiva de tot allò que jo veig negre, negre, molt negre, pels mil·ligrams de cholaco gran reserva donats a fons perdut, i en definitiva, per les hores de coaching gratis i per aguantar-me. T'has guanyat el cel.

I would like to thank Prof. Vladimir Torchilin for letting me work in his lab and become a part of that nice family. Thank you for supporting me as a scientist and as a person, and for making me think with your clever advice and questions. I would also like to thank Dimitri, Tatyana, Bill and Boris for helping me carry out my work in the lab, and obviously all my colleagues to make of my stay such a pleasant and wonderful one. Thank you Shravan, Can and Sean for making of the lab such a funny place. Thank you Giusy and Sam for your support, company and happiness. Thanks to all those helpful smiley girls for being so sweet to me: Swati, Bhawani, Aditi, Pranali, Pooja and Madhura, and to all the others who helped me as well, Shuang, Tao, Karl, Sebastian, Rupa, Sara, Arjun and Lin. Last but not least, estaré eternamente agradecida a mis "victors" overseas. Gracias Gemma y Federico por ser mi norte y mi guía en mi aventura americana, además de unos cachondos, sin vuestra infinita y desinteresada ayuda, soporte y humor me hubieran dado los siete males.

I would like to thank as well all the members of the Nanobiopharmaceutics consortium that helped me and contributed to this work: Eleonore Fröhlich, Claudia Samberger, Peter Bingruber, Sofia Svedhem, Karin Pickl, Christian Grandfils and Christian Fresee.

La meva experiència a boston no hagués estat el mateix ni de bon tros sense "la família". Gracias de todo corazón a mis flores de Berkshire st, Helena y Majo, por hacer de nuestra casa un hogar, a la petita de la casa (Núria), per ser tan positiva i dolça, a la abuela, Nat, a l'Arnau per fer-me riure tant en les seves visites imprevistes, y en especial a Sagi, por ser mi sista del alma y compartirlo absolutamente todo. Gràcies a la resta de familia catalana per fer que em sentís com a casa amb les nostres trobades de germanor, Marcel, Jose, Jaume i Dèlia. Florian, Alba, Angie, Andreu, Eli, Joan, Ferran, Noel y el MIT Spain team. Gràcies en especial al Biel, per ser el millor company de viatge, pel teu compromís i per donar-me tant de suport en aquesta última etapa.

Als que de ben segur trobaré molt a faltar a partir d'ara és la gran familia de GEMAT, per fer d'aquest departament el més cool i divertit del món. Gràcies als membres de Can trunyo vell, Elena i Pere, per aguantar-nos quan només fem que demanar, i en especial a la Núria i a la Marina, pels seus cursets accelerats de formació d'auxiliars, per salvar-nos el cul quan es tracta de reanimar algun tros de ferralla del segle passat o per quan necessitem un vale aprovat per ahir. Gràcies als més xaladíssims del biosotano, Joan i Robert, per fer del soterrani una festa a diari, tot i que a vegades sigui

too much! I la fetsa no seria el mateix sense la resta d'assistents, Irene, MA (mil gracias por tu paciencia y por compartir tus conocimientos), Anna Mas, les meves graduades preferides, Mariana i Ingrid, la petarda de la Leti, Sara, Peri, Sejin, Pri, Òscar, Greg, Arbu i les noies de teixits. A tots vosaltres us diria que...con el triunvirato estábamos mejor!!!

Gràcies a aquells que han contribuït a l'elaboració d'aquest treball: Benjamí, Maria Burrial, Miquel Canudas, Gabi i Grace, the best undergrad assistant ever and a good friend wherever we are. Gràcies al BBB team, al Pau, per compartir amb mi els secrets de la BBB, i a la Caski, per respondre sempre als meus dubtes existencials sobre biologia molecular. Gracias a majo por ser la siesa más maja de todas, por escuchar las penas ajenas y por tu risa contagiosa. Y a Nathaly, por ser un festival, no hubiera sido tan divertido sin ti. Gracias también por ser mi compañera de penas, eres cobarde pero buena persona.

Agrair els bons moments a tots aquells amb els que vaig començar aquesta etapa i que ja no hi són, però que van marcar una època: Toni, Jorge, AnadP, Manolo, Jordan, Brotiano, Berta Albaigés, i sobretot al Jose, que a banda i banda de l'oceà és el pater famillias amb el que sempre pots comptar; gràcies pel temps que em vas dedicar a l'AFM (les teves fotos ho peten!) i per cuidar-me a boston. Tot i que em van deixar sola ante el peligro, sempre duré amb mi el meu triumvirat estimat. Gràcies a la Laura, per ser la mater familias, per comprometre't, donar-me suport i cuidar-me durant tots aquests anys. I gràcies a la meva zipi, l'Anna, amb la què ens hem fet sempre costat en les alegries i les penes, tot i que ja fa un temps que els nostres camins es van separar, sé que a mil milions de quilometres enllà hi ets pel que sigui.

No em vull oblidar de la gent de fora que també han contribuït i ajudat a fer més amè el camí. Com la bolet i la mertx, amb les birres d'entre setmana per Enric Granados per posar-nos al dia i vomitar les típiques penes del doctorand. Gràcies també a les nenes pels ànims i el suport, i per no tenir en compte les diverses negatives per motius de feina a l'hora de fer activitats, a la bea i la helen, i sobretot a la pollo i la marina, gràcies per ser-hi i comprendre-ho. Tot i que no les veig tant per desgràcia, la mindru, la laia, la Peguero i la Cris també aporten el seu granet de sorra en les diverses peripècies d'aquests anys, gràcies a totes noies.

I em guardo pel final el més profund dels agraïments pels que, dia rere dia des que sóc aquí, vetllen pel meu benestar i els meus èxits. Gràcies pares, perquè evidentment això no hagués estat possible sense el vostre suport i fe incondicional i pels vostres mimos.

Summary

The existing difficulties in the delivery of certain drugs, having a direct influence on their therapeutic efficiency, has lead to the exploration of a new field in pharmaceuticals, the use of polymers as drug carriers. Polymers are presented as carrier vehicles, which provide drug protection preventing its degradation and targeted delivery to the site of action diminishing side effects. An appropriate combination of the drug and the polymer allows the release of the drug in the tissue where it has to develop its therapeutic effect. However, in order to ensure the success of these drug delivery systems, they must fulfil a list of requirements according to size, surface charge, composition, drug loading capacity and release, targetability and biocompatibility.

In this work, the fabrication of diverse drug delivery systems has been explored in order to provide know-how regarding polymers' tunability to achieve delivery platforms that fulfil the aforementioned requirements.

On one hand, a versatile thermo-responsive delivery system has been obtained trough a core-shell approach, allowing the tailoring of its size and thermosensitivity, while providing a simple and fast method to decorate its surface by means of classic chemistry.

On the other hand, the preparation of polymersomic systems was explored by RAFT polymerization, a more sophisticated chemistry, which allowed the synthesis of self-assembling amphiphilic multiblock copolymers, ranging from diblock to pentablock, in a controlled manner, obtaining predetermined molecular weight polymers with narrow molecular weight distributions. Similarly to the previous system, the tunability of blocks ratio and number allowed the control over nanostructures size and loading capacity.

Finally, polymersomes have been compared with a very well established delivery system, such as liposomes, in terms of targeting and drug loading and release, as potential drug delivery systems to breast cancer metastasis in the brain through a dual-targeting approach, in order to evaluate the suitability of the system developed in this work.

Resum

Les dificultats existents en l'administració de certs fàrmacs, que es tradueix en una considerable reducció de la seva eficàcia terapèutica, ha portat a l'exploració d'un nou camp en la recerca de fàrmacs, l'ús de polímers per a transportar fàrmacs. Aquests polímers es presenten com a vehicles transportadors que aporten protecció al fàrmac, evitant la seva degradació, i permeten la seva distribució dirigida fins la diana terapèutica, disminuint així els efectes secundaris. Una combinació adequada del polímer transportador amb el fàrmac, permet l'alliberament d'aquest en el teixit on ha de desenvolupar el seu efecte terapèutic. Tot i així, per tal de garantir l'èxit d'aquests sistemes de distribució de fàrmacs, aquests han de complir una sèrie de requisits pel que fa a la mida, càrrega superficial, composició, capacitat d'encapsular i d'alliberar un fàrmac, funcionalització i biocompatibilitat.

En aquest treball, s'ha explorat la fabricació de diversos sistemes de distribució de fàrmacs per tal d'aportar coneixement sobre la modificació d'aquests polímers, que permetin obtenir plataformes de distribució de fàrmacs que reuneixi els requisits prèviament esmentats.

Per una banda, s'ha obtingut un sistema termosensible i versàtil a través d'una estratègia de core-shell, que permet ajustar la seva mida i el seu comportament termosensible, com també la seva modificació superficial mitjançant un mètode fàcil i ràpid basat en una química clàssica.

Per altra banda, la preparació de sistemes polimersòmics s'ha explorat per polimerització de tipus RAFT, és a dir, s'empra una química més sofisticada, que permet la síntesi de copolímers de multibloc amfifílics i auto-ensamblables, des de dos fins a cinc blocs, de manera controlada, obtenint polímers de pes molecular determinada amb distribucions de pes molecular molt estretes. De manera similar a l'anterior sistema, la modulació de la proporció entre blocs i del nombre de blocs permet el control de la mida de les nanoestructures formades i de la seva capacitat d'encapsular fàrmacs.

Finalment, els sistemes polimersòmics desenvolupats s'han comparat amb un sistema de distribució de fàrmacs molt ben establert, com ara els liposomes, pel que fa a funcionalització, encapsulació i alliberament de fàrmacs, com a potencials sistemes de distribució de fàrmacs per al tractament de metàstasis de càncer de mama al cervell a través d'una estratègia de doble funcionalització, per tal d'avaluar la idoneïtat del sistema desenvolupat en aquest treball.

Table of contents

Index of figures

Index of tables

Index of equations

Acronym list

3B: Polymersomes from amphiphilic triblock copolymer
ABC: Amphiphilic block copolymer

AFM: Atomic Forces Microscopy
AIBN: Azobisisobutyronitrile
BBB: Blood-Brain Barrier
BBMVECs: Bovine brain microvascular endothelial cells
BFA: Bafilomycin A1

C166: endothelial cells from mouse yolk sac
CNS: Central Nervous System
CTA: Chain Transfer Agent

DCMA: 2-(dodecylthiocarbonothioylthio)-2-methylpropionic acid
DDS: Drug Delivery System

DLS: Dynamic Light Scattering
DMAAm: N,N'-dimethylacrylamide
DMEM: Dulbecco's Modified Eagle's Medium
DMPG: MCF-7-specific phage fusion pVIII coat protein bearing DMPGTVLP peptide
DSPA: 4-cyano-4-[(dodecylsulfanylthiocarbonyl)sulfanyl]pentanoic acid
Dox: Doxorubicin
GPC: Gel Permeation Chromatography
HCMEC: Human Cardiac Microvascular Endothelial Cells
HDMEC: Human Dermal Microvascular Endothelial Cells
HEMA: 2-hydroxyethyl methacrylate
HUVEC: Human Umbilical Vein Endothelial Cells
Lipo: Liposomes

LRP-1: Low density lipoprotein receptor-related protein 1
LCST: Lower Critical Solution Temperature

Ma-acap-CHOL: methacryloylated cholesteroyl monomer
MBAAm: Methylenebisacrylamide

MCF-7: epithelial adenocarcinoma cell line

MEM: Minimum Essential Medium

$MPEG_{2k}$-DSPE: N-(Carbonyl-methoxypolyethyleneglycol 2000)-1,2-distearoyl-*sn*-glycero-3-phosphoethanolamine

MTS: 3-(4,5-dimethylthiazol-2-yl)-5-(3-carboxymethoxyphenyl)-2-(4-sulfophenyl)-2H-tetrazolium
MW: Molecular Weight
NIPAAm: N-isopropylacrylamide
NPs: Nanoparticles

NTA: Nanoparticle track analysis
pAAc: Poly(acrylic acid)
PBS: Phosphate Buffered Saline

pCHOL: poly (Ma-acap-CHOL)
PDI: Polydispersity index
PFM: Pentafluorophenyl methacrylate

pHEMA: poly (2-hydroxyethyl methacrylate)
PHPA: 4-cyano-4-(phenylcarbonylthioylthio)pentanoic acid
pNIPAAm: poly (N-isopropylacrylamide)
RAFT: Reversible Addition-Fragmentation chain Transfer polymerization
REG or RP3: Regulon peptide
SEM: Scanning electronic microscopy
TBDMS: t-butyldimethylsilyl chloride
TEM: Transmission electronic microscopy
TNPs: Targeted nanoparticles
U87MG: Glioblastoma cel lline
UCST: Upper Critical Solution Temperature

Chapter 1

Introduction

1.1 Background

Nowadays, cancer, the uncontrolled growth and spread of abnormal cells, remains to be one of the leading causes of death worldwide with approximately 14 million new cases and 8.2 million cancer related deaths in 2012. Among these statistics, lung cancer has shown the highest incidence and mortality, followed by breast cancer, which is the most commonly detected in woman (Figure 1.1). According to the World Health Organization (WHO), if the population continues to be exposed to certain risk factors, such as genetic or external factors (tobacco use, UV radiation, etc.), the number of cases is expected to rise by about 70% over the next two decades[1].

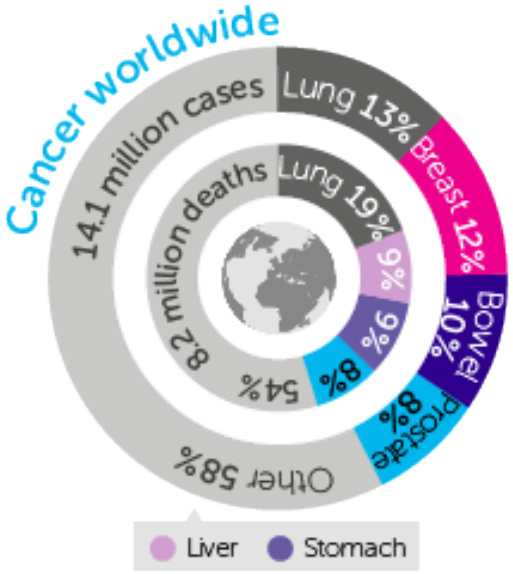

Figure 1.1: Incidence and mortality of cancer worldwide (2012) according to the International Agency of Research on Cancer (IARC)

Over the past several decades, significant advances have been made in our fundamental understanding of cancer biology, which has in turn lead to better diagnostic and treatment methods[2]. Current therapeutic strategies for most cancers involve a combination of surgical resection, radiation therapy and chemotherapy[3], being the latter, the most widely used. Since they began to be used in the 1940s[4] till today[5], the vast majority of clinically used chemotherapeutic agents are low-molecular-weight drugs of an extraordinary efficacy to kill rapid proliferating cells, such as tumour cells[6]. Among the most powerful agents, it can be found paclitaxel, a taxane that acts stabilizing microtubules and preventing mitosis[7], and doxorubicin, an anthracycline that has been shown to target the topoisomerase-II-DNA complex, disrupting the DNA and preventing cellular replication[8]. The major concern with the usage of the aforementioned chemotherapeutic agents is their inability to discern between healthy and tumour tissue[9]. Thus, these drugs attack all cells indistinctly, being particularly harmful to any rapid proliferating cells in the body, such as hair, intestinal epithelial cells and bone marrow[10]. Therefore, treatments involving these chemotherapeutic agents are associated to severe side effects like hair loss, bone marrow suppression, gastrointestinal tract lesions and nauseas among others[3]. In addition to the high overall cytotoxicity, most of these drugs exhibit low bioavailability,

generally due to low solubility, short half-life in the blood stream and a high overall clearance rate[11]. As a consequence, relatively small amounts of drug are able to reach the target site, thus decreasing therapy efficacy[5] and generating, in many cases, drug resistance by cancer cells due to drug tolerization[10,12]. Indeed, the use of drug "cocktails" to avoid drug resistance and to increase therapy efficacy by hitting two different targets is routinely used in cancer therapy. However, the difficulty to truly deliver several chemotherapeutic agents to the same cell simultaneously can compromise the efficacy of these combination therapies[12,13].

The need for more efficient therapies and the advances in nanotechnology has lead to the development of drug delivery systems (DDS) focused on optimizing marketed compounds, improving their effectiveness and tolerability, and simplifying their administration[14]. Generally, the new generation of drug delivery system consists in a carrier vehicle of nanometric size and varied composition, structure and surface characteristics, that allows its combination with the drug to be delivered in order to protect it from the body, increase its solubility, control its dosage and target it to the site of action. The proper design of these systems determines the amount and type of drug that can be encapsulated and the way this drug is released in the body, which may be constant over a long period, cyclic or upon activation or exposure to a stimulus or trigger[15]. In addition, the surface of this carrier vehicle can be chemically modified to attach targeting molecules that allow the steering of the system to the site of the disease[9]. The combination of these factors provides control over the delivery of drugs for the purpose of achieving more efficient therapies while eliminating the potential for both under- and overdosing. On the other hand, these systems can provide the maintenance of drug levels within a desired range, the need for fewer administrations, optimal use of the drug and a remarkable reduction of side effects due to their targeting towards specific cells or tissues[15].

A wide diversity of drug delivery systems have been investigated as well as several delivery routes such as oral, nasal, intravenous and transdermal delivery. Basically, all these systems can be classified in two groups depending on the way the drug is combined with the carrier, which are drug conjugates and carrier-based systems[16]. On one hand, drug conjugates consist of a matrix that is covalently bound to the drug through a linker, which must be stable during conjugate's transport and cleaved at the site of action[17]. On the other hand, carrier-based systems consist of non-covalent aggregates of carrier molecules entrapping the drug in the inner core[16]. The most typical systems include vesicles, which can be made out of lipids (liposomes) or out of polymers (polymersomes), polymeric micelles, polymeric nanoparticles, dendrimers, carbon-based nanocarriers and metal nanoparticles, being liposomes and polymer-based systems the most extended group (Figure 1.2).

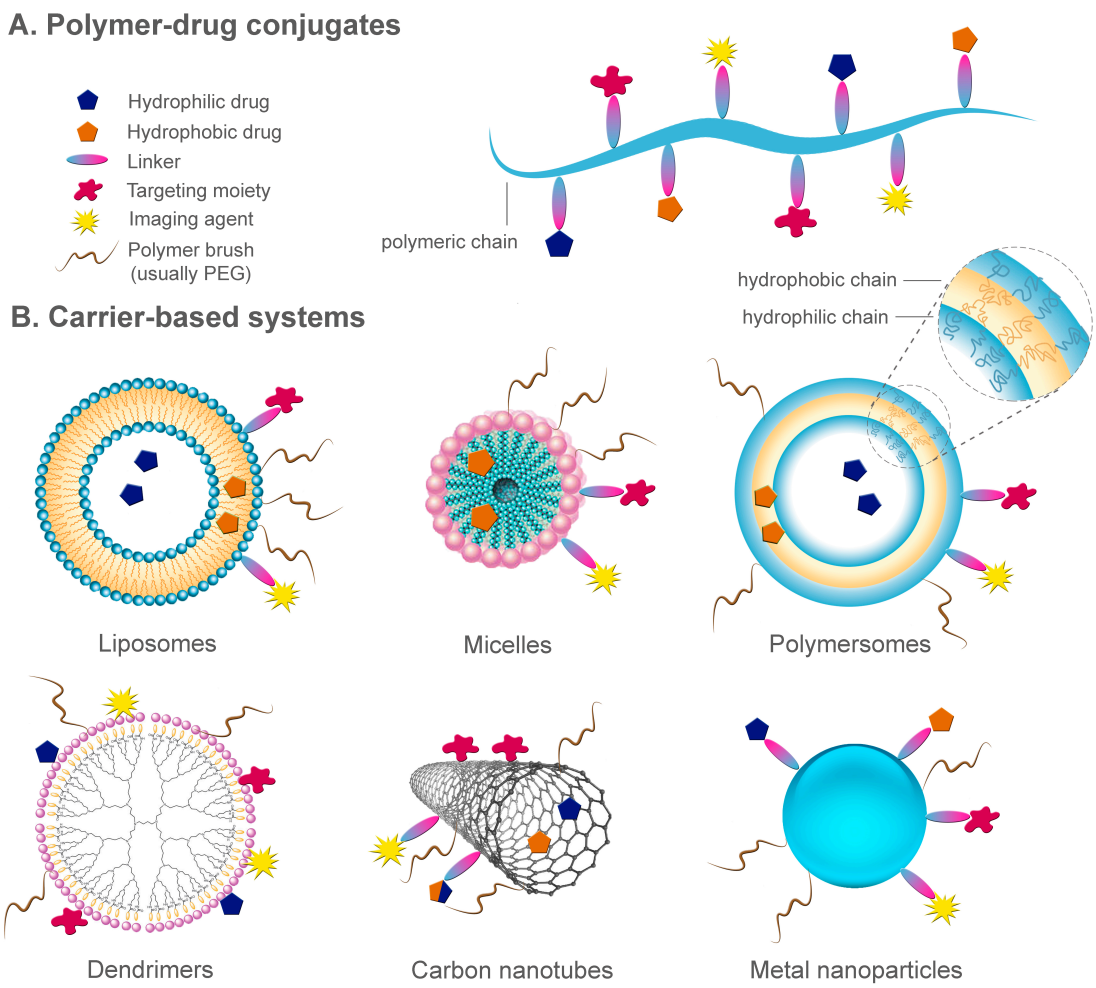

Figure 1.2: Schematic description of drug delivery systems, divided into drug conjugates (A) and carrier-based systems (B)[12].

As mentioned before, both systems can be modified to attach molecules that allow their targeting to the tissue to be treated. Concretely, the coupling of drugs to macromolecular carriers received an important impulse from 1975 onwards with the development of monoclonal antibodies by Milstein and Köhler[18] and with Ringsdorff's proposal[19] of a general drug-delivery system based on synthetic polymers, which consisted in a simplified version of Figure 1.2A. From then on, many of these polymers have been involved in clinical trials and some have already received market approval[5]. Regarding polymer-drug conjugates, the delivery of insoluble and unstable drugs has been successfully achieved. These systems provide a great increase in solubility and stability of the bound drug, reduce immunogenicity and extend its circulation time. An example of this success is Poliglumex™ (Xyotax) (CtiBiopharma), formerly known as Opaxio, based on poly(glutamic acid) with an enzymatically cleavable link to paclitaxel, which is currently undergoing phase III trials in combination with standard chemotherapy against ovarian cancer. As stated before, as well as paclitaxel, doxorubicin is also a widely used anti-caner drug. Its conjugation to a N-(2-hydroxypropyl)methacrylamide (HPMA) copolymer, also through an enzymatically cleavable link, was the first drug-polymer conjugate, PK1, to enter clinical trials, reaching phase II. Similarly to polymers, some proteins have also been used to deliver

chemotherapeutic drugs, such as paclitaxel. This is the case of Abraxane® (Celgene), albumin-bound paclitaxel nanoparticles for injectable suspension, approved for the treatment of metastatic breast cancer, non-small cell lung cancer (US, Japan) and advanced pancreatic cancer.

However, not only chemotherapeutics agents but also proteins can be employed as drugs. In the case of polymer-protein conjugates, the most frequently used polymer for conjugation is poly(ethylene glycol) (PEG), approved by Regulatory Authorities for routine clinical use in the early 1990s. PEGylation efficacy is shown in all the commercially available drugs using this technology, such as PEGINTRON®, PEGylated interferons for the treatment of Hepatitis C, or ONCASPAR®, a PEG-modified version of the enzyme L-asparaginsae used as a chemotherapeutic agent for acute lymphoblastic leukemia (ALL)[5,20].

Regarding carrier-based systems (Figure 1.2B), liposomes and their polymeric equivalent, polymersomes, are of special interest thanks to their compartmentalized structure that mimics the cell membrane, which provides them the capability to encapsulate both hydrophilic and hydrophobic compounds[21]. Liposomes have been widely used during the past 40 years[22] as pharmaceutical carriers for disease therapy or imaging. A proof of the suitability of these systems in drug delivery is the amount of approved liposomal drugs and in clinical trials, as a result of the breakthrough developments achieved in the past 25 years. Among the approved liposomal formulations it can be found liposomal doxorubicin for the treatment of ovarian cancer and recurrent breast cancer, such as Doxil® (Johnson & Johnson) and Caelyx®, or liposomal paclitaxel, such as Lipusu® (Luye Pharma) for the treatment of ovarian cancer as well. On the other hand, their polymeric equivalents, polymersomes, have gained increasing interest in the past decade thanks to their thicker and tougher membrane[23], which confers them higher mechanical stability compared to liposomes[24]. In addition, these synthetic membranes can be tuned at a molecular level varying polymers' structure, allowing the control over drug loading capacity and release rate[25]. Owing to the versatility presented by this system, polymersomes have reached advanced clinical trials. This is the case of PEO-PPO-PEO (Pluronic) triblock copolymer, developed to deliver doxorubicin, which is currently under phase III in Canada[26,27].

In order to successfully provide the aforementioned improvements, these drug delivery systems must fulfil several requirements to ensure they reach the target site and release their payload in a proper way. Among them, size and shape of these systems have been found to have an enormous impact on their interaction with the environment[28], which will determine their uptake, internalization and clearance. On one hand, they must be at least 10 nm in diameter to avoid clearance by first pass filtration by the kidney[29]; however, the upper bound on size is not well defined. Taking into account that endocytotic vesicles range in size from 40 to 100 nm in diameter, whereas caveolae range from 80 to 200 nm, it was postulated by many that significantly larger nanoparticulate systems will not fit into these receptacles, and therefore, they will be taken up by macrophages through phagocytosis, thus routing them into clearance by the reticulo-endothelial system (RES)[9]. Nevertheless, systems ranging from 20 nm up to 5 μm have been found to be successfully taken up by several mechanisms of entry, like experiments performed with folate-decorated PEG-p-

polycaprolactone nanoparticles, which showed that smaller nanoparticles (50 nm) preferred clathrin-mediated endocytosis (CME), whereas larger particles (250 nm) followed caveolae-meditaed preferentially[30]. Upper-size-limits were questioned by non-spherical particles up to 3 μm, which showed internalization through clathrin-mediated, caveolae-mediated and macropinocytosis routes in Hela cells[31]. Summarizing, it is difficult to define a general rule regarding nanocarriers' size, since the most appropriate features may ultimately depend on each application. Nevertheless, the drug delivery systems that are currently successfully being employed can be found in a range between 20 and 250 nm[32].

However, nanocarrier's size cannot be analysed individually to determine the preferred uptake pathway by cells. Nanoparticles' charge, shape and composition play also an important role in internalization[33]. Initially, it was thought that cationic nanocarriers achieved better cell penetration and action increase over anionic or neutral systems owing to the attraction between cationic nanoparticles and negatively charged plasma membranes of cells[34-37]. However, results have shown that this classification is in fact not as strict. Most of the reports suggest that positively charged nanomaterials of very different composition are predominantly internalized by CME with some fraction utilizing macropinocytosis, although there are some exceptions that utilize multiple pathways including caveolae-mediated[38]. On the other hand, negatively charged nanoparticles, such as Doxil®[39] or QDs[40], are more likely to use clathrin-mediated endocytosis. Nevertheless, both cationic and anionic nanoparticles rapidly bind a mixture of proteins present in serum resulting in an anionic serum protein-NP complex, which is what interacts with the cell surface[41,42]. Similarly, hydrophilic and hydrophobic surfaces of these nanoparticles are known to influence cell adhesion in the uptake process[43]. Concretely, some groups have reported that polymeric nanoparticles showed higher attachment on cells and a subsequent enhancement in internalization[44], which correlates with the increasing protein adsorption at the surface with increasing hydrophobicity. Regarding shape, some studies have shown that spherical gold nanoparticles were taken up 500% more than rod-shaped particles with similar sizes[45], which is explained by greater membrane wrapping for elongated particles[28]. Despite the popularity of spherical nanocarriers, disc-like, cylindrical and hemispherical particles substantially outperform spherical ones when it comes to evading uptake by phagocytic cells, flowing through capillaries and firmly adhering to the walls of blood vessels[46]. This difference is critical specially when targeting vasculature, where the adhesive interactions has to counteract the hemodynamic forces exerted over the particle by the blood flow, tending to dislodge the particle away from the target surface[47]. Again, as well as size, nanocarriers' shape requirements may be ultimately tailored for each concrete application.

Apart from these structural features that help ensure a longer circulation time and proper uptake by cells, the targeting of these systems is a crucial factor to guarantee their delivery to the disease site, as the failure to reach the target site means the failure of the therapy. For this reason, targeting has been one of the most important topics in drug delivery research throughout the years. Multiple physical barriers lie between the point of administration (intravenous) of these systems and the target that hinder their free access across them. As these platforms move from the bloodstream to their target located within a cell, they must pass the endothelial cells either by

transcytosis or by the paracellular path, then the subendothelial basement membranes and finally, the cell's plasma membrane[9]. In addition, assuming that the system will enter the cell through receptor-mediated endocytosis, it will be confined in the endosomal-lysosomal intracellular compartment, and therefore an additional barrier will separate them from the cytoplasm[48]. To overcome these obstacles, active targeting consists in modifying nanocarriers' surface with affinity ligands for specific retention and uptake by the disease cells targeted. For that purpose, ligands are selected to target surface molecules or receptors overexpressed in diseased organs, tissues, cells or subcellular domains, which will specifically recognize those ligands[49]. Representative ligands include antibodies, peptides, proteins, nucleic acids, sugars and small molecules, whereas target molecules can be proteins, sugars or lipids present in the diseased organs or on the cell surface[50]. Targeting upregulated receptors is a common strategy employed by therapies addressing cancer and inflammatory diseases. Since Köhler and Milstein[18] developed in 1976 a technique to obtain large quantities of monoclonal antibodies (mAbs) with a single specificity, their conjugation with nanocarriers gained an enormous interest because of the high specificity and affinity of antibody-antigen interaction[51]. However, the drawbacks that these immunoconjugates present, such as immunogenicity, high synthesis cost and large ligand size, led to the utilisation of alternative smaller molecules thanks to their simple conjugation chemistry, non-immunogenicity and low cost. For instance, folic acid has shown to facilitate tumour-specific delivery of nanocarriers due to its high affinity for folate receptor, which is frequently overexpressed in a number of human tumours such as ovarian, colorectal and breast cancer, while less expressed in normal tissues[49]. In addition, it has been found that folate receptor is overexpressed in activated macrophages as well, which are implicated in such pathologies as osteoarthritis, Crohn's disease, atherosclerosis or diabetes among others, thus folate targeting could also be proposed in most inflammatory diseases[52]. Other therapies employing small molecule targeting moieties are used for the treatment of Alzheimer's disease (AD), by using the conjugation with curcumin derivatives, known for their potential role in the prevention and treatment of AD[53].

However, targeting strategies can also provide an improvement of the therapy without targeting a specific receptor. This is the case of thiolated nanocarriers, which can prolong residence time at the local site allowing a sustained release thanks to the interaction between their thiol groups and cysteine-rich subdomains from the mucus layer covering GI-epithelia[54]. Similarly, coating nanocarriers with polyethylene glycol (PEG) can increase their blood circulation half-time[55], whereas their coating with albumin have shown a reduction of the association of serum proteins[56]. Concretely, these two last strategies have been successfully commercialized, as mentioned before.

The first generation of drug delivery systems mainly aimed to address single challenges, such as the need to increase drug stability in vivo and the circulation time in the blood, or the need to target a drug to a specific tissue or pathology. Now, research has led to the development of systems that can perform two or more functions (either simultaneously or sequentially) to overcome multiple physiological barriers to optimize delivery and deliver their loads (which can be single or multiple) to the required target sites[57]. For instance, dual-targeting strategies using several ligands to cross biological barriers and target certain tissues at a time are often used in brain

diseases due to the presence of the blood-brain barrier. This barrier is the most restrictive in the body as it protects the CNS structures from the diffusion of pathogens and large molecules, becoming the bottleneck in the treatment of brain disorders, such as Parkinson's disease, Alzheimer's disease or brain tumours, as the majority of conventional drugs are not able to cross it. An example of this kind of strategies is a drug delivery system bearing two ligands, which present affinity for two different receptors that demonstrate an increase in drug concentration in the brain[58]. On one hand, 4-aminophenyl-α-D-manno-pyranoside (MAN), a mannose analogue, that shows high affinity for GLUT1, a receptor present in the BBB involved in the transport of glucose into the brain, thus allowing the system to firstly cross the barrier. On the other hand, the use of transferrin as the second ligand, would help the binding to glioma cells inside the brain thanks to the presence of transferrin receptor, whose expression is much higher in tumour cells than in healthy tissue[59]. In addition, many of the drug delivery systems described, such as vesicles or polymer-drug conjugates, are able to encapsulate several drugs in one single nanocarrier, thus permitting the simultaneous delivery of several drugs to a single target cell that can act on different molecular targets of the same disease. Combination therapy of multiple active agents is of special interest in diseases showing multidrug resistance, such as HIV/AIDS, malaria or cancer[13]. For instance, biodegradable polymersomes loaded with doxorubicin and tetrandrine, a potent hydrophobic multidrug resistance (MDR) inhibitor, demonstrated an enhanced efficacy compared to loaded doxorubicin alone to treat glioma rats[60].

Once the drug delivery system reaches the target site, there are several ways to release their payload depending on the type of carrier or the type of drug. In general, drug diffusion and matrix swelling or degradation are suggested to be the main driving forces for drug release from the matrix to the external medium. This seemingly simple process is affected by multiple complex factors, such as the physicochemical properties of the drug, the structural characteristic of the matrix, the release environment and the possible interaction between these factors[61]. Among the most sophisticated systems in terms of release, it can be found polymer-drug conjugates with cleavable linkers and stimuli-responsive polymers. Regarding polymer-drug conjugates, the drug is covalently bound to the polymer by a linker that should be stable in blood and enzymatically or chemically cleaved at the site of action[13]. Meticulous research has led to the design of polymer-drug conjugates with specific peptidic linkers for selective cleavage in the lysosomal compartment. In addition, studies revealed that the selection of proper peptidic linkers can lead to different release rates, which can impact on the conjugate activity[62]. This strategy was popularized by the successful design of HPMA copolymer conjugated to doxorubicin trough a tetrapeptide linker, which was stable in circulation[63] but cleaved by the lysosomal thiol-dependent protease cathepsin B following endocytic uptake[64]. In parallel, pH sensitive cis-aconityl, hydrazone and acetal linkers have also been fashionable as an alternative for drug conjugation, thanks to the acidic intravesicular environment (pH 4-6.5) of lysosomes[17].

In the area of carrier-based systems, synthetic polymers that can undergo conformational or phase changes in response to variations of temperature, pH or light are of special interest in order to enhance drug release at the target site. In all these cases the key parameter defining the responsive behaviour of the polymer is a non-

linear response to the external signal, being the most widely studied the pH and thermosensitive ones[65]. Thermosensitive polymers, such as poly(N-isopropylacrylamide) (pNIPAAm), exhibit a coil-to-globule transition at a certain temperature, changing from a state of well solvated coils, at lower temperature, to a state of tightly packed globular particles, at higher temperature[66]. This transition results in a change of conformation of the polymer, which leads to the freeing of the entrapped water molecules from the polymer network along with the entrapped drug[67]. The temperature at which this transition takes place is known as Lower Critical Solution Temperature (LCST) and can be tuned as desired by modifying polymers' structure[68,69]. Therefore, these systems are especially useful to release their payload in areas of the body where temperature is typically higher (hyperthermic tissues), such as tumours[70], inflammations[71,72] or during digestion[73,74]. Similarly, nanocarriers based on polymers, such as poly(acrylic acid) and poly(methacrylic acid), exhibit a reversible swelling as well due to pH variations. The presence of ionisable groups in the polymer results in its swelling mainly because electrostatic repulsions among charges present on the polymer chain. Like thermosensitive polymers, pH-responsiveness can be also adjusted by introducing neutral comonomers into the polymeric chain[75].

Owing to the limitations that current therapies still possess, drug delivery arises as a promising tool to improve their efficacy. Summarizing, drug delivery systems allow the possibility to control the delivery of currently available active agents by protecting the drug from degradation, focus the therapy at the site of action and release the drug in a controlled manner. The combination of these properties lead to more efficient therapies, thanks to an increased drug's bioavailability with less side-effects, due to the localization of the treatment. However, these systems must accomplish several requirements regarding size, charge, shape and composition, among others, in order to guarantee a successful therapy. In addition, their fabrication, the drug encapsulation and surface decoration must be achieved in a simple and fast way. Therefore, drug delivery systems with high versatility in terms of tunability of their properties, ability to encapsulate a wide range of drugs and simplicity in attaching diverse targeting moieties are required to fulfil different applications, being this is the framework within this thesis has been developed.

1.2 Aims of this thesis

The main aim of this thesis is to provide knowhow on the fabrication of different drug delivery systems that fulfil the requirements of size, charge, targeting, loading, release and biocompatibility to be able to deliver an active agent to the target site and release their payload. Therefore, to accomplish this main aim, the goals of this thesis can be summarized as follows:

- Exploration of core-shell polymerization approach for the obtaining of versatile smart delivery systems easily decorated (Chapter 2)
- Design of a vesicle-like drug delivery system through the tunability of the polymer's characteristics by RAFT polymerization (Chapter 3)
- Comparative study of two vesicular drug delivery platforms, liposomes and polymersomes, for a dual-targeting approach to treat metastatic breast cancer in the brain, as a proof of concept (Chapter 4)

1.3 References

1. Stewart, B. & Wild, C. P. *World cancer report 2014*. (IARC Publications).

2. Steichen, S. D., Caldorera-Moore, M. & Peppas, N. A. A review of current nanoparticle and targeting moieties for the delivery of cancer therapeutics. *European journal of pharmaceutical sciences : official journal of the European Federation for Pharmaceutical Sciences* **48**, 416–427 (2013).

3. Nussbaumer, S., Bonnabry, P., Veuthey, J.-L. & Fleury-Souverain, S. Analysis of anticancer drugs: A review. *Talanta* **85**, 2265–2289 (2011).

4. Shewach, D. S. & Kuchta, R. D. Introduction to Cancer Chemotherapeutics. *Chemical reviews* **109**, 2859–2861 (2009).

5. Haag, R. & Kratz, F. Polymer therapeutics: concepts and applications. *Angewandte Chemie (International ed. in English)* **45**, 1198–1215 (2006).

6. Alexander, C. Drugs take control. *Nature materials* **7**, 767–768 (2008).

7. Rowinsky, E. K. The development and clinical utility of the taxane class of antimicrotubule chemotherapy agents. *Annual Review of Medicine* **48**, 353–374 (1997).

8. Hurley, L. H. DNA and its associated processes as targets for cancer therapy. *Nature Reviews Cancer* **2**, 188–200 (2002).

9. Debbage, P. Targeted drugs and nanomedicine: present and future. *Current pharmaceutical design* **15**, 153–172 (2009).

10. Feng, S.-S. & Chien, S. Chemotherapeutic engineering: Application and further development of chemical engineering principles for chemotherapy of cancer and other diseases. *Chemical Engineering Science* **58**, 4087–4114 (2003).

11. Morishita, M. & Peppas, N. A. Is the oral route possible for peptide and protein drug delivery? *Drug discovery today* **11**, 905–910 (2006).

12. Markman, J. L., Rekechenetskiy, A., Holler, E. & Ljubimova, J. Y. Nanomedicine therapeutic approaches to overcome cancer drug resistance. *Advanced Drug Delivery Reviews* **65**, 1866–1879 (2013).

13. Greco, F. & Vicent, M. J. Combination therapy: Opportunities and challenges for polymer–drug conjugates as anticancer nanomedicines. *Advanced Drug Delivery Reviews* **61**, 1203–1213 (2009).

14. Rosen, H. & Abribat, T. The rise and rise of drug delivery. *Nature reviews. Drug discovery* **4**, 381–385 (2005).

15. Brannon-peppas, L. Polymers in Controlled Drug Delivery. *Medical Plastics and Biomaterials* (1997).

16. Cassidy, J. & Schätzlein, A. G. Targeted delivery systems: carrier-based systems and drug conjugates. *Expert reviews in molecular medicine* **6**, 19 (2004).

17. Duncan, R. The dawning era of polymer therapeutics. *Nature reviews. Drug discovery* **2**, 347–360 (2003).

18. Köhler, G. & Milstein, C. Continuous cultures of fused cells secreting antibody of predefined specificity

. *Nature* **256**, 495–497 (1975).

19. Ringsdorf, H., Schlarb, B. & Venzmer, J. Molecular architecture and function of polymeric oriented systems: Models for the study of organization, surface recognition and dynamics of niomembranes. *Angewandte Chemie (International ed. in English)* **27**, 113–158 (2003).

20. Twaites, B., de las Heras Alarcón, C. & Alexander, C. Synthetic polymers as drugs and therapeutics. *Journal of Materials Chemistry* **15**, 441 (2005).

21. Chandrawati, R. & Caruso, F. Biomimetic Liposome- and Polymersome-Based Multicompartmentalized Assemblies. *Langmuir : the ACS journal of surfaces and colloids* **28**, 13798–13807 (2012).

22. Torchilin, V. P. Recent advances with liposomes as pharmaceutical carriers. *Nature reviews. Drug discovery* **4**, 145–160 (2005).

23. Meng, F., Zhong, Z. & Feijen, J. Stimuli-Responsive Polymersomes for Programmed Drug Delivery. *Biomacromolecules* **10**, 197–209 (2009).

24. Le Meins, J. F., Sandre, O. & Lecommandoux, S. Recent trends in the tuning of polymersomes' membrane properties. *Eur. Phys. J. E* **34**, 14 (2011).

25. Onaca, O., Enea, R., Hughes, D. W. & Meier, W. Stimuli-Responsive Polymersomes as Nanocarriers for Drug and Gene Delivery. *Macromolecular bioscience* **9**, 129–139 (2009).

26. Valle, J. W. *et al.* A phase 2 study of SP1049C, doxorubicin in P-glycoprotein-targeting pluronics, in patients with advanced adenocarcinoma of the esophagus and gastroesophageal junction. *Invest New Drugs* **29**, 1029–1037 (2010).

27. Kabanov, A. V., Batrakova, E. V. & Alakhov, V. Pluronic block copolymers for overcoming drug resistance in cancer. *Advanced Drug Delivery Reviews* **54**, 759–779 (2002).

28. Verma, A. & Stellacci, F. Effect of surface properties on nanoparticle-cell interactions. *Small (Weinheim an der Bergstrasse, Germany)* **6**, 12–21 (2010).

29. Davis, M. E., Chen, Z. G. & Shin, D. M. Nanoparticle therapeutics: an emerging treatment modality for cancer. *Nature Publishing Group* **7**, 771–782 (2008).

30. Suen, W.-L. L. & Chau, Y. Size-dependent internalisation of folate-decorated nanoparticles via the pathways of clathrin and caveolae-mediated endocytosis in ARPE-19 cells. *J Pharm Pharmacol* **66**, 564–573 (2013).

31. Graton, S. E. A. *et al.* The effect of particle design on cellular internalization pathways. *Proceedings of the National Academy of Sciences of the United States of America* **15**, 11613–11618 (2008).

32. Liu, Y., Tan, J., Thomas, A., Ou-Yang, D. & Muzykantov, V. R. The shape of things to come: importance of design in nanotechnology for drug delivery. *Therapeutic Delivery* **3**, 181–194 (2012).

33. Sahay, G., Alakhova, D. Y. & Kabanov, A. V. Endocytosis of nanomedicines. *Journal of controlled release : official journal of the Controlled Release Society* **145**, 182–195 (2010).

34. Harush-Frenkel, O., Rozentur, E., Benita, S. & Altschuler, Y. Surface Charge of Nanoparticles Determines Their Endocytic and Transcytotic Pathway in Polarized MDCK Cells. *Biomacromolecules* **9**, 435–443 (2008).

35. Panyam, J. & Labhasetwar, V. Dynamics of Endocytosis and Exocytosis of Poly(D,L-Lactide-co-Glycolide) Nanoparticles in Vascular Smooth Muscle Cells. *Pharmaceutical research* **20**, 212–220 (2003).

36. behrens, I., Vila Pena, A. I., Alonso, M. J. & Kissel, T. Comparative Uptake Studies of Bioadhesive and Non-Bioadhesive Nanoparticles in Human Intestinal Cell Lines and Rats: The Effect of Mucus on Particle Adsorptionand Transport. *Pharmaceutical research* **19**, 1185–1193 (2002).

37. Villanueva, A. *et al.* The influence of surface functionalization on the enhanced internalization of magnetic nanoparticles in cancer cells. *Nanotechnology* **20**, 115103 (2009).

38. Rejman, J., Bragonzi, A. & Conese, M. Role of clathrin- and caveolae-mediated endocytosis in gene transfer mediated by lipo- and polyplexes. *Molecular Therapy* **12**, 468–474 (2005).

39. Sahay, G., Kim, J. O., Kabanov, A. V. & Bronich, T. K. The exploitation of differential endocytic pathways in normal and tumor cells in the selective targeting of nanoparticulate chemotherapeutic agents. *Biomaterials* **31**, 923–933 (2010).

40. Zhang, L. & Monteiro-Riviere, N. A. Mechanism of Quantum Dot Nanoparticle Cellular Uptake. *Toxicological Sciences* **110**, 138–155 (2009).

41. Doorley, G. W. & Payne, C. K. Cellular binding of nanoparticles in the presence of serum proteins. *Chemical communications (Cambridge, England)* **47**, 466 (2010).

42. Fleischer, C. C., Kumar, U. & Payne, C. K. Cellular binding of anionic nanoparticles is inhibited by serum proteins independent of nanoparticle composition. *Biomater. Sci.* **1**, 975 (2013).

43. Mailänder, V. & Landfester, K. Interaction of Nanoparticles with Cells. *Biomacromolecules* **10**, 2379–2400 (2009).

44. Hu, Y., Xie, J., Tong, Y. W. & Wang, C.-H. Effect of PEG conformation and particle size on the cellular uptake efficiency of nanoparticles with the HepG2 cells. *Journal of controlled Release* **118**, 7–17 (2007).

45. Chithrani, B. D., Ghazani, A. A. & Chan, W. C. W. Determining the size and shape dependence of gold nanoparticle uptake into mammalian cells. *Nano letters* **6**, 662–668 (2006).

46. Ferrari, M. Nanogeometry: Beyond drug delivery. *Nature nanotechnology* **3**, 131–132 (2008).

47. Decuzzi, P. & Ferrari, M. The adhesive strength of non-spherical particles mediated by specific interactions. *Biomaterials* **27**, 5307–5314 (2006).

48. Jain, R. K. Transport of Molecules, Particles, and Cells in Solid Tumors. *Annual Review of Biomedical Engineering* **01**, 241–263 (1999).

49. Yu, B., Tai, H. C., Xue, W., Lee, L. J. & Lee, R. J. Receptor-targeted nanocarriers for therapeutic delivery to cancer. *Mol Membr Biol* **27**, 286–298 (2010).

50. Bertrand, N., Wu, J., Xu, X., Kamaly, N. & Farokhzad, O. C. Cancer nanotechnology: The impact of passive and active targeting in the era of modern cancer biology. *Advanced Drug Delivery Reviews* 1–24 (2013).doi:10.1016/j.addr.2013.11.009

51. Koshkaryev, A., Sawant, R., Deshpande, M. & Torchilin, V. Immunoconjugates and long circulating systems: Origins, current state of the art and future directions. *Advanced Drug Delivery Reviews* **65**, 24–35 (2013).

52. Low, P. S., Henne, W. A. & Doorneweerd, D. D. Discovery and Development of Folic-Acid-Based Receptor Targeting for Imaging and Therapy of Cancer and Inflammatory Diseases. *Acc. Chem. Res.* **41**, 120–129 (2008).

53. Le Droumaguet, B. *et al.* Versatile and Efficient Targeting Using a Single Nanoparticulate Platform: Application to Cancer and Alzheimer's Disease. *ACS Nano* **6**, 5866–5879 (2012).

54. Bernkop-Schnürch, A., Schwarz, V. & Steininger, S. Polymers with Thiol groups: A new generation of mucoadhesive polymers? *Pharmaceutical research* **16**, (1999).

55. Perche, F. & Torchilin, V. P. Recent Trends in Multifunctional Liposomal Nanocarriers for Enhanced Tumor Targeting. *Journal of Drug Delivery* **2013**, 1–32 (2013).

56. Kummitha, C. M., Malamas, A. S., Lu, Z.-R. & (null) Albumin pre-coating enhances intracellular siRNA delivery of multifunctional amphiphile/siRNA nanoparticles. *International journal of nanomedicine* 5205 (2012).doi:10.2147/IJN.S34288

57. Torchilin, V. P. Multifunctional, stimuli-sensitive nanoparticulate systems for drug delivery. *Nature Publishing Group* 1–15 (2014).doi:10.1038/nrd4333

58. Ying, X. *et al.* Pharmacokinetics and Tissue Distribution of Dual-Targeting Daunorubicin Liposomes in Mice. *Pharmacology* **87**, 105–114 (2011).

59. Ying, X. *et al.* Dual-targeting daunorubicin liposomes improve the therapeutic efficacy of brain glioma in animals. *Journal of controlled release : official journal of the Controlled Release Society* **141**, 183–192 (2010).

60. Pang, Z., Feng, L., Hua, R., Chen, J. & Gao, H. Lactoferrin-conjugated bodegradable polymersome Holding Doxorubicin and Tetrandrine for Chemotherapy. *Molecular pharmaceutics* **7**, 1995–2005 (1995).

61. Fu, Y. & Kao, W. J. Drug release kinetics and transport mechanisms of non-degradable and degradable polymeric delivery systems. *Expert Opin. Drug Deliv.* **7**, 429–444 (2010).

62. Duncan, R. *et al.* Anticancer agents coupled to N-(2-hydroxypropyl)methacrylamide copolymers. I. Evaluation of daunomycin and puromycin conjugates in vitro. *British Journal of Cancer* **55**, 165–174 (1987).

63. Rejmanova, P., Kopecek, J., Duncan, R. & Lloyd, J. B. Stability in rat plasma and serum of lysosomally degradable oligopeptide sequences in N-(2-hydroxypropyl) methacrylamide copolymers. *Biomaterials* **6**, 45–48 (1985).

64. Duncan, R., Cable, H. C., Lloyd, J. B., Rejmanova, P. & Kopecek, J. Polymers containing enzymatically degradable bonds. Design of oligopeptide side-chains in poly[N-(2-ydroxypropyl)methacrylamide] copolymers to promote efficient degradation by lysosomal enzymes. *Macromolecular chemistry* **184**, 1997–2008 (1983).

65. de Las Heras Alarcon, C., Pennadam, S. & Alexander, C. Stimuli responsive polymers for biomedical applications. *Chemical Society reviews* **34**, 276–285 (2005).

66. Graziano, G. On the temperature-induced coil to globule transition of poly-N-isopropylacrylamide in dilute aqueous solutions. *International journal of biological macromolecules* **27**, 89–97 (2000).

67. Zhang, X.-Z., Wang, F.-J. & Chu, C.-C. Thermoresponsive hydrogel with rapid response dynamics. *Journal of materials science. Materials in medicine* **14**, 451–455 (2003).

68. Carter, S., Hunt, B. & Rimmer, S. Highly Branched Poly(N -isopropylacrylamide)s with Imidazole End Groups Prepared by Radical Polymerization in the Presence of a Styryl Monomer Containing a Dithioester Group. *Macromolecules* **38**, 4595–4603 (2005).

69. Rimmer, S., Carter, S., Rutkaite, R., Haycock, J. W. & Swanson, L. Highly branched poly-(N-isopropylacrylamide)s with arginine?glycine?aspartic acid (RGD)- or COOH-chain ends that form sub-micron stimulus-responsive particles above the critical solution temperature. *Soft Matter* **3**, 971 (2007).

70. Bawa, P., Pillay, V., Choonara, Y. E. & Toit, du, L. C. Stimuli-responsive polymers and their applications in drug delivery. *Biomedical materials* **4**, 022001 (2009).

71. Pua, M. L., Yoshitomi, T., Chonpathompikunlert, P., Hirayama, A. & Nagasaki, Y. Redox-active injectable gel using thermo-responsive nanoscale polyion complex flower micelle for noninvasive treatment of local inflammation. *Journal of controlled release : official journal of the Controlled Release Society* **172**, 914–920 (2013).

72. Abulateefeh, S. R. *et al.* Enhanced uptake of nanoparticle drug carriers via a thermoresponsive shell enhances cytotoxicity in a cancer cell line. *Biomater. Sci.* **1**, 434 (2013).

73. Chen, G., Ito, Y. & Imanishi, Y. Regulation of Growth and Adhesion of Cultured Cells by Insulin Conjugated with Thermoresponsive Polymers. *Biotechnology and bioengineering* **53**, 339–344 (1997).

74. Hatakeyama, H., Kikuchi, A., Yamato, M. & Okano, T. Influence of insulin immobilization to thermoresponsive culture surfaces on cell proliferation and thermally induced cell detachment. *Biomaterials* **26**, 5167–5176 (2005).

75. Qiu, Y. & Park, K. Environment-sensitive hydrogels for drug delivery. *Advanced Drug Delivery Reviews* **53**, 321–339 (2001).

Chapter 2

Thermosensitive polymers as drug carriers

2.1 Introduction

Taking into account the importance of targeting strategies in drug delivery to achieve more effective therapies, simple and fast methods must be designed to synthesize targeted drug delivery systems. Therefore, in this chapter, the synthesis of a thermo-responsive system is explored by means of classic chemistry through a core-shell approach in order to decorate their surface with a wide range of molecules.

2.1.1 Smart polymers for drug delivery

As mentioned in the previous chapter, stimuli-responsive or smart polymers that can undergo conformational or phase changes in response to variations of external stimuli are of special interest in order to enhance drug release at the target site. In fact, the functions of living cells are regulated by macromolecules that respond to a change in the local environment. Thus, many synthetic polymers that exhibit environmentally responsive behaviour can be considered as biomimetic[1]. To date these triggered mechanisms have been largely based on heat, light, chemical (pH) or biochemical (enzymes) routes[2]. Among these four types of responsive polymers, pH and thermo-sensitive are the most widely studied. In this chapter, attention will be focused on thermoresponsive polymers in order to design a versatile smart delivery system.

Interestingly, these thermosensitive polymers exhibit a coil-to-globule transition at a certain temperature, changing from a state of well solvated coils, at lower temperature, to a state of tightly packed globular particles, at higher temperature[3]. Below the transition temperature, known as Lower Critical Solution Temperature (LCST), the hydrogen bonds in the polymer act cooperatively to form a stable hydration shell around the hydrophobic groups, which leads to the high water-solubility polymer. However, as the temperature increases, the hydrogen bond interactions (monomer-solvent interaction) become weakened or destroyed, thus the hydrophobic interactions among the hydrophobic groups (monomer-monomer interactions) become stronger and subsequently induce the freeing of the entrapped water molecules from the polymer network[4] (Figure 2.1).

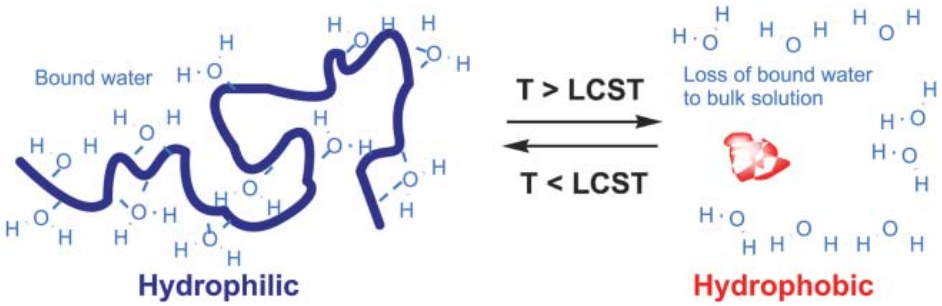

Figure 2.1: Diagram of polymer response to temperature[1]

In thermodynamic terms, the enthalpic contribution of water hydrogen-bonded to the polymer chain becomes lower than the entropic gain of the system as water molecules associated with the side-chain polymer are released into the bulk aqueous phase[1]. At this point, polymer chains collapse rapidly leading to a two-phases solution.

In the case of copolymers, LCST depends on the degree of polymerization, polydispersity, branching, monomer ratio and its hydrophilic or hydrophobic nature[5,6]. Therefore, the LCST of a polymer can be "tuned" as desired by varying these parameters[1]. In addition, LCST is also sensitive to the nature and concentration of certain salts present in the solution[7]. Consequently, thermosensitive polymers have been frequently evaluated in the past years as drug carriers thanks to this characteristic behaviour. It is taken advantage of the conformational change to entrap molecules present in the solution, simply by heating, at LCST, and cooling down, which lets the dissolved drug to diffuse into the polymer network as it absorbs water and re-swells. Drug release can be achieved by raising the temperature again as polymer expulse the water into the bulk solution, resulting in higher release rates above LCST and lower, below LCST[8].

Among the thermosensitive polymers known nowadays it can be found poly(N,N-diethylacrylamide) (DEAAm), poly(N,N'-dimethylacrylamide) (DMAAm), poly(N-vinylcaprolactam) (PVCL), poly(ethylene glycol) (PEG), poly(ethylene oxide) (PEO), poly(propylene oxide) (PPO) and poly(N-isopropylacrylamide)[1], being this last one the most widely studied for drug delivery applications[9]. The incorporation of ionisable monomer units, such as poly(acrylic acid) (PAAc) and poly(methacrylic acid) (PMAc), into polymer backbones enables phase transition and solubility changes depending on pH. Combination of both temperature and pH-responsive polymers offers further control over polymer phase behaviour.

Poly(N-isopropylacrylamide) (pNIPAAm) has attracted increasing attention due to the proximity of its LCST to human body temperature, which can be tuned above 37°C by the addition of comonomers[1]. Consequently, when injecting the drug carrier in the body, the release of the entrapped drug is supposed to occur when the system reaches a certain tissue where the temperature is slightly higher than the rest of the body and above the LCST of the thermoresponsive system. Therefore, these systems are useful in applications where the temperature is typically higher, such as in inflammations[10,11], tumours[12] or during digestion[13,14], allowing preferential release.

Thermo-responsive polymers are especially interesting for the development of new drug delivery systems for cancer therapy, since it has been widely demonstrated that temperature in solid tumours can be up to 1-2ºC higher than the surrounding healthy tissue due to higher cell metabolism[15,16]. Thermal abnormality in tumours may be related to blood flow, microvessel density, inflammation, cell distribution and cell viability[17]. In addition, it is well known that pH values in tumour tissue is often 0.5-1.0 units lower than in normal tissue[18], leading to the possible use of dual-responsive polymers, as mentioned previously.

The efficacy of thermoresponsive drug delivery systems can be further improved via combination with other therapies, such as local hyperthermia, which consists in the exposure of localized tissue areas to high temperatures, causing damage or kill cancer cells with minimal injury to normal tissues[19]. A combined therapy of thermoresponsive drug carriers and local hyperthermia has been reported by several authors[20,21], as the combination of both techniques provides synergistic advantages over either treatment modality used individually. The LCST of such systems must be above physiological temperature but below the hyperthermia temperature. Such combined treatments

have been shown to be more efficient in comparison to the same delivery system without hyperthermia or thermally unresponsive polymer of similar molecular weight and composition along with hyperthermia.

However, these systems can be used for other applications apart from cancer. As mentioned before, thermo-responsive drug delivery systems can also be useful for other typical situations where the physiological body temperature is raised, that is, digestion. During digestion, the metabolic rate rises due to the several chemical reactions associated to digestion, absorption and food storage, which is known as the food thermogenic effect. The spectacular increase of metabolic tax can reach between 20-40% the normal value (basal metabolic rate) one hour after eating, and it is maintained from three to twelve hours later. This metabolic rate increase involves the corresponding temperature rise[22]. Taking profit of this mechanism seems to be a good strategy to deliver drugs orally by means of a thermo-responsive system. This approach provides an alternative for all those drugs whose oral delivery is not feasible, such as peptides and proteins. A good example is insulin, as it is a massively consumed drug worldwide to treat diabetes. Due to the huge number of diabetic patients worldwide, supposed to reach 370 million people by 2030, many attempts have been made in the design of a pharmaceutical that allows oral delivery of insulin.

Summarizing, thermo-responsive polymers show multiple applications on the basis of a temperature increase. Therefore, they arise as promising candidates for the obtaining of versatile drug delivery systems.

2.1.2 Synthesis of thermoresponsive polymers

Owing to the need of a versatile thermoresponsive drug delivery system that can be employed for different applications, a simple and fast method of preparation was required.

The polymer–drug conjugates and polymer–based systems that have been clinically tested typically have a tripartite structure: the polymer, a linker and the bioactive. However, much more elaborate multicomponent compositions exist nowadays with additional features. Modern polymer chemistry is producing increasingly intricate polymer structures, including multivalent polymers, branched polymers, grafted polymers, dendrimers, dendronized polymers, block copolymers, stars and hybrid glycol- and peptide derivatives[23]. The synthesis methods of all this macromolecular structures is varied, ranging from free-radical polymerization, ring-opening polymerization (e.g. polyethylene glycol), polycondensations (e.g. polyesters), to more sophisticated “living” radical polymerizations, such as Reversible addition-fragmentation chain transfer (RAFT), atom transfer radical polymerization (ATRP) or nitroxide-mediated polymerization (NMP)[24]. However, random copolymers with a wide range of chemical functionalities and compositions are readily available through facile synthesis[25]. Concretely, free radical polymerization is of enormous industrial importance; hence approximately the 50% of all commercial polymers are produced by this method. The reason is a large list of advantages, such as compatibility with water, tolerance to impurities, versatility with respect to compatibility with functional monomers, easiness and speed[26].

Of special interest are water-based heterogeneous polymerizations, such as microemulsion polymerization, where the polymerization takes place in compartmentalized nanoscale micelles. The advantages these systems present over solution or bulk are the significantly faster rates of polymerization, the solvent, water, is both environmentally friendly and cheap, the use of a wide variety of monomers under a wide range of reaction conditions, high conversion of polymer with low monomer residuals and easiness to process because of its low viscosity[24]. Their unique physical properties have led to the development of methods for the polymerization of organic monomers in microemulsions, with the primary goal of producing stable latexes with particle sizes close to those of the parent microemulsion droplets. Such polymerizations typically show fast reaction rates and produce latex nanoparticles between 10 and 100 nm made of very high molecular weight polymers ($15x10^6$ Da) and broad molecular weight distributions[27].

Polymerization in microemulsions is compartmentalized, meaning that polymerization occurs in monomer-swollen micelles through a micellar nucleation mechanism[28]. This kind of polymerization uses a large amount of surfactant, compared to emulsion polymerization, and consequently the number of monomer-swollen micelles is much higher than the number of polymerizing particles. On average, there is only one radical entry per particles, in which case each entered radical is nearly perfectly segregated in well-separated polymerizing micelles that behave as nanoreactors[27] (Figure 2.2).

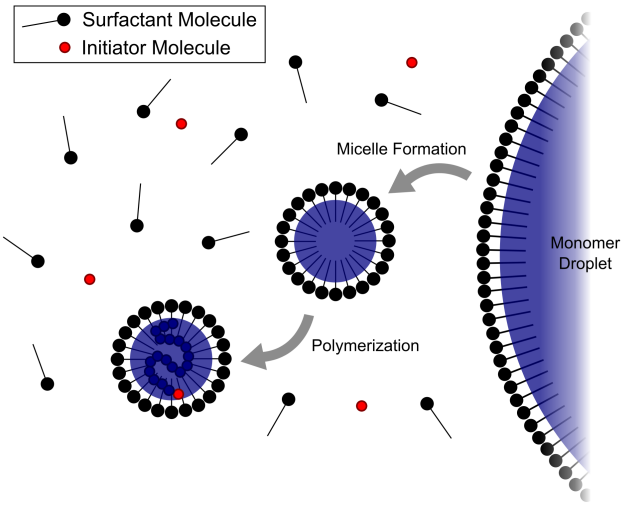

Figure 2.2: Diagram of a microemulsion polymerization, showing the formation of monomer micelles from monomer droplets and subsequent compartmentalized polymerization by entry of a radical molecule.

In contrast to ordinary emulsions, microemulsions form upon simple mixing of the components and do not require vigorous agitation, as they do not contain large monomer droplets[27,28]. It can also be divided in three stages. The first stage consists in the polymerization itself that occur when an initiator-derived radical reacts with the monomer in the water phase and propagates to a critical chain length whereby its solubility diminishes and it enters a monomer-swollen micelle. These oligomeric radicals are now located in a monomer-rich environment and rapidly propagates to form young “latex” particles. Second stage comprises particle growth via propagation with continuous replenishing of monomer from droplet reservoirs, maintaining

monomer concentration in the polymer particles high and constant. The third stage commences when there are no more monomer droplets present in the system, resulting in a concomitant decrease in monomer concentration in the growing particles with conversion. The polymeric radical can exit the particle, via diffusion, and either terminates in the water phase or enters another particle and terminates the propagating polymeric radical present in that particle via instantaneous termination[24].

Since microemulsion polymerization in three-component systems was first reported, the influence of different parameters on the polymerization kinetics and on the obtained latexes have been studied. Such parameters are initial monomer concentration, reaction temperature and initiator and surfactant concentration[29]. Polymerization and conversion rate increase with monomer concentration, due to the higher number and size of the drops being formed in the microemulsion, as well as with initiator concentration, because of the higher number of nuclei. Temperature has also influence on both parameters. Reaction rate rises with increasing temperature due to a quick increase in the initiator decomposition rate and conversion also, because of the increase in macromolecules mobility.

In conclusion, the combination of microemulsion systems with free radical polymerization seemed to be a good strategy to obtain a versatile nanoparticulate thermoresponsive systems due to the compatibility with water of both systems, the wide range of monomers to be used and the easiness and speed of the synthesis.

2.1.3 Targeted thermoresponsive systems through a core-shell approach

In order to obtain a truly versatile drug delivery system, not only the synthesis process but also the surface modification methodology must allow this variability, depending on the final application. As mentioned before, targeting is crucial to achieve more efficient therapies, and must be different and specific for each application. Therefore, in this thesis, different methods of surface modification have been developed for each nanocarrier studied in order to achieve versatile platforms easily targetable. In this chapter, the goal was to find a method that broadens the options of coating materials, such as thiol groups, peptides or fluorophors, in order to recognize a wider range of targets. Therefore, the strategy established in this chapter is the synthesis of polymeric nanoparticles by free-radical polymerization through a core-shell approach in microemulsion. Nanoparticles will consist of a cross-linked polymeric core and a shell formed by a linker, where coating moieties will be anchored. These coating moieties will vary depending on the final application of the delivery system (Figure 2.3).

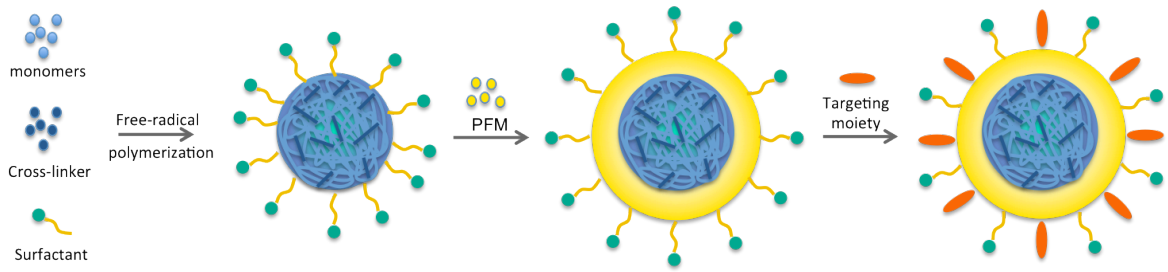

Figure 2.3: Scheme of the core-shell synthesis of nanoparticulate systems in microemulsion polymerization

As mentioned before, poly(N-isopropylacrylamide) hydrogels are one of the most extended studied thermo-responsive hydrogels for biomedical applications thanks to its LCST, which is close to body temperature. Over the past decade, considerable efforts have been devoted to design and prepare pNIPAAm-based thermo-sensitive polymeric micelles as delivery vehicles for controlled drug release[25]. In addition, the acrylic nature of pNIPAAm, allows its reaction with pentafluorophenyl methacrylate (PFM), which could serve as a linker between nanoparticles' core and targeting moieties.

In our group, there's an extensive experience on surface modification by plasma polymerization of pentafluorophenyl methacrylate (PFM), which offers a highly reactive ester group that can potentially react with amino groups, thus being able to react with a wide variety of molecules containing amino groups through a nucleophilic substitution[30,31]. Indeed, this click chemistry-like procedure has recently received intense interest as a well-established synthetic strategy to obtain tailor-made complex materials and has been exploited in many areas such as dendrimers, bioconjugates, therapeutics and functionalized polymers[32]. Therefore, this would be an easy and effective method to coat nanoparticles with any desired molecule containing a terminal amino group, such as fluorophores that allow the monitorization of nanoparticles uptake or any biomacromolecule, such as proteins and peptides, to address the system to a certain target through receptor-mediated interaction.

In following chapters, post-modification as a surface decoration method will be explored, as well as, multiple targeting through the same method.

2.1.4 Applications of core-shell thermoresponsive systems

An application of these thermoresponsive core-shell drug delivery systems could be some of the aforementioned situations where the temperature is higher in the tissue to be targeted. For instance, the oral delivery of insulin, which is still nowadays a pending challenge. These thermoresponsive particulate carrier systems meet all the requirements to protect insulin from degradation of proteolytic enzymes from the gastrointestinal (GI) tract[33,34], enhance its permeation across the intestinal mucosa[35], which is restricted to relatively small hydrophilic molecules that can fit the paracellular space[36,37], and release their payload when the temperature reaches the nanocarriers' LCST.

Strategies to improve oral bioavailability of biological drugs involving permeation enhancement or protease inhibitors as additives have already been employed. However, the use of enzyme inhibitors in long-term therapies remains questionable because of possible absorption of unwanted proteins, disturbance of the digestion of nutritive proteins and stimulation of protease secretion as a result of feedback regulation[38]. What seems to be a crucial factor for oral delivery is a good interaction between the drug delivery system and the intestinal mucosa, in order to guarantee drug absorption. So far the majority of polymers evaluated present insufficient affinity for this kind of membranes. However, a slight modification of their chemical structure can result in an improvement of their adhesive properties[39]. Thiolated polymers are mucoadhesive delivery systems, which adhere to the mucous gel layer covering mucosal membranes[35]. Such systems are expected to prolong the residence time at

the local site of absorption allowing a sustained drug release. Furthermore, mucoadhesive polymers can guarantee an intimate contact with the absorption membrane, providing the basis for a high concentration gradient as a driving force for passive drug uptake. The improved mucoadhesive properties of these polymers are explained by the formation of covalent bounds between thiol groups of the polymer and cysteine-rich subdomains from mucus glycoproteins, which constitute the mucus layer covering the GI-epithelia[39].

The application of this strategy to drug delivery systems is reflected in the results obtained by Calceti *et al.* that combined PEGylated insulin with a thiolated polymer used as a drug carrier matrix in a tablet formulation, which succeeded in reducing glucose levels in diabetic mice[40]. Other systems with mucoadhesive properties are currently under development such as BioOral^{TM}, based on calcium sulphate nanoparticles coated with casein, a mucoahseive agent, and loaded with PEGylated insulin. However, non-adhesive systems are also being developed, such as liposomal insulin, Orasome^{TM}, carbohydrate nanoparticles coated with B12 vitamin, Oraldel^{TM} or lipid-based microemulsions, Macrulin^{TM}, which reached phase II[41]. Therefore, the coating of the thermoresponsive core-shell system here presented with a molecule containing an amine group, able to react with the linker (PFM), and a thiol group, in order to increase the residence time in the intestinal tract, seems to be a feasible strategy to deliver insulin orally.

Although it is not trivial the way to cross the intestinal epithelia, it is not as difficult as crossing other biological barriers in the body, such as the blood-brain barrier (BBB). This barrier protects and isolates the CNS structures (i.e. the brain and spinal cord) from the rest of the body very efficiently, creating a unique biochemical and immunological environment[42]. It is mainly formed by a layer of brain capillary endothelial cells, which is closely sealed by tight junctions. In addition, brain capillaries also possess few fenestrae and few endocytic vesicles, compared with the capillaries of other organs[43]. The BBB restricts the diffusion of pathogens (e.g. bacteria) and large (or hydrophilic) molecules into the CSF to protect the brain from harmful agents, while allowing the diffusion of gases (O_2, CO_2), small hydrophobic molecules (e.g. hormones) or the active transport of metabolic products, such as glucose or aminoacids[44]. Its permeability is frequently a rate-limiting factor for the penetration of proteins and peptides or pharmacological agents into the brain. Circulating molecules can access the brain cells only via two processes: lipid-mediated transport of small molecules by diffusion or catalysed transport, which includes carrier-mediated transport for low molecular weight nutrients and water soluble vitamins, or receptor-mediated transport for circulating peptides (e.g. insulin), plasma proteins (e.g. transferrin) or viruses[45] (Figure 2.4).

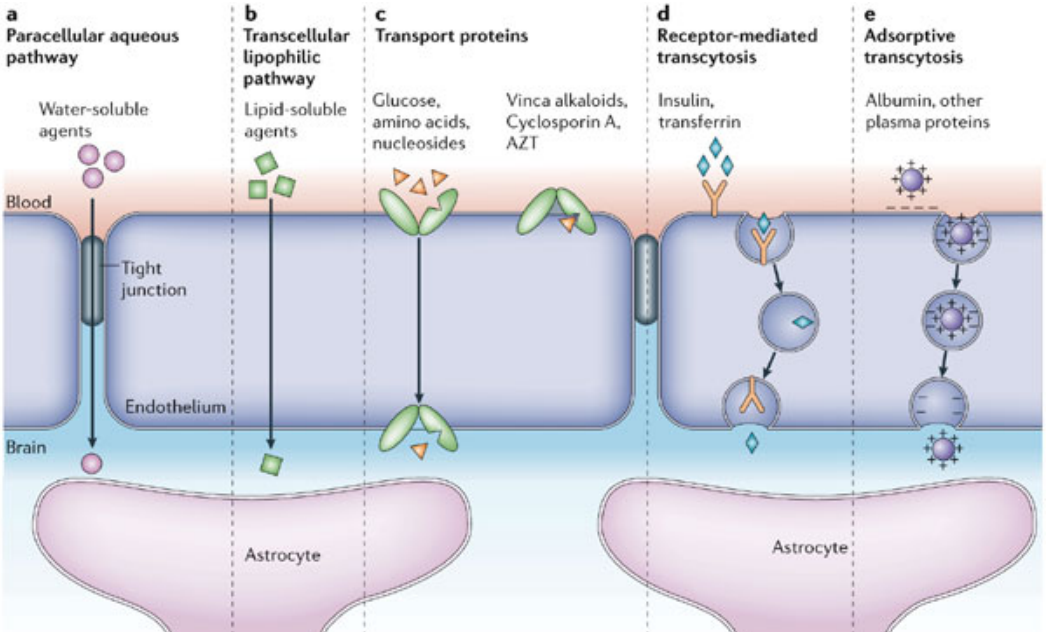

Figure 2.4: A scheme of the main routes for molecular traffic across the BBB are shown[46]

It has been estimated and reported that the transport of small molecules across the BBB is the exception rather than the rule and that 98% of all small molecules do not cross it[45]. Because most drugs do not cross the barrier, few treatments are available against most CNS disorders such as Parkinson's disease, Alzheimer's disease and brain cancers[45,47]. Overcoming the difficulty of delivering therapeutic agents to specific regions of the brain presents a major challenge to treat most of the aforementioned disorders, hence the BBB is the main bottleneck in brain drug development[45].

In the past, several mechanisms have been used to go through the blood-brain barrier such as disruption by osmotic means[45], the use of vasoactive substances[48], localized exposure to high-intensity focused ultrasound (HIFU)[49], or other less aggressive methods that entail the use of endogenous transport systems, including carrier-mediated transporters such as glucose and amino acid carriers and receptor-mediated transcytosis for insulin or transferrin[50]. Regarding receptor-mediated transcytosis, different transporters and receptors present at the BBB have been described as playing roles in maintaining the integrity of the BBB and brain homeostasis. Among them, the low-density lipoprotein receptor-related protein (LRP1 and LRP2) has been reported to possess the ability to mediate transport of ligands across endothelial cells of the BBB. A ligand of LRP and LRP2 is aprotinin, a 6500-Da protease inhibitor having Kunitz protease inhibitor (KPI) domain, whose presence has been demonstrated to play a key role in the recognition and internalisation by LRP[43].

The transcytosis ability of aprotinin and peptides derived from Kunitz domains has been demonstrated using an *in vitro* model of BBB and *in situ* brain perfusion. Alignment of the amino acid sequence of aprotinin with the Kunitz domains of human proteins allowed the identification and the design of a family of peptides, named Angiopeps. These peptides, and in particular Angiopep-2, exhibit higher transcytosis capacity and parenchyma accumulation than aprotinin. Overall, these results suggest that these Kunitz-derived peptides could be advantageously used as a new brain

delivery system for pharmaceutical agents that do not readily enter the brain[43]. For instance, paclitaxel-loaded angiopep-coated pegylated nanoparticles (ANG-PEG-NP) showed higher accumulation in *in vivo* glyoma than plain nanoparticles (PEG-NP) and their anti-glioblastoma efficacy was significantly enhanced compared to that of taxol or and PEG-NP[51].

Nowadays, nanotechnology plays an important role providing materials and devices that can potentially be designed to carry out multiple specific functions at once or in a predefined sequence, an important requirement for the clinically successful delivery and use of drugs and other molecules to the CNS[42]. The ability to cross the blood-brain barrier while potentialy targeting a specific group of cells requires several things to happen together. Ideally, a nanodelivery-drug complex would be administered systemically (e.g. intravenously) but would find the CNS while producing minimal systemic effects, be able to cross the BBB without compromising its integrity and correctly target cells in the CNS, and last but not least, carry out its primary active function, such as releasing a drug. Throughout this thesis, several peptides with affinity for LRP-1 have been tested with different drug delivery systems to obtain a system able to perform the aforementioned steps. In this chapter, two peptides are evaluted in terms of specificity towards the BBB, whereas in the chapter 4, the selected peptide will be used in a dual-target approach that enables crossing the BBB while adressing diseased cells inside the brain.

2.1.5 Biocompatibility

Despite all the advantages these systems may present, there are potential disadvantages in terms of safety that cannot be ignored, such as possible cytotoxicity, hemotoxicity, complement activation, immunogenicity, carcinogenicity and teratogenicity, among others[23]. An ideal drug delivery platform must be water-soluble, biodegradable and biocompatible[52], meaning by biocompatible all those substances that do not cause any of the adverse effects mentioned above. Several physicochemical parameters have been proposed to be critical determinants in nanomaterial's toxicity, such as chemical composition, size, shape, surface reactive groups or tendency to form aggregates[53].

Nowadays, testing the safety of a nanomaterial is easy, fast and economically affordable. The first step towards understanding how an agent will react in the body often involves cell-culture studies. Referring to cytotoxicity, tests ranges from a simple visual inspection of the cells with bright-field microscopy for changes in cellular or nuclear morphology to colorimetric methods to measure cell death, which can be categorized between those that measure mitochondrial activity and those that measure cell membrane integrity[54]. Therefore, while designing a drug delivery system, attention must be paid on the systems's biocompatibility as well as on its ability to carry out its function, this is, protecting the drug, deliver it to the target site and release their payload causing minimum harm to healthy tissues.

2.1.6 Aims of this chapter

The general purpose of this chapter was to develop a versatile thermoresponsive nanometric system suitable to deliver peptides, proteins or chemothereapeutic agents, for diverse applications, from oral delivery or cancer therapy to brain delivery. To achieve this goal, the specific challenges of this chapter are:

- Synthesis of thermo-responsive polymeric nanoparticles through a core-shell approach allowing simple surface functionalization for different targets.
- Characterization of this system to ensure it fulfils the requirements for being a drug delivery platform, according to size, surface charge and LCST
- Determination of drug loading efficiency and release of different model drugs
- Evaluation of nanoparticles' biocompatibility in terms of cytotoxicity and hemocompatibility.
- Specificity of *In vitro* cellular uptake evaluation of targeted nanoparticles in endothelial cells with different BBB-ligands.

2.2 Materials and methods

2.2.1 Materials

N-isopropylacrylamide (NIPAAm, 97%), N,N-dimethylacrylamide (DMAAm, 99%), acrylic acid (AAc, 99%), methylenebisacrylamide (MBAAm, 99%), Sodium dodecyl sulphate (SDS, ReagentPlus^{TM} $\geq$ 98.5%), ammonium persulphate (98+%, A.C.S reagent), Arg-Gly-Asp-Ser (RGDS, ≥95% HPLC) and methoxypolyethylene glycol amine (5000 g/mol, extent of labeling: ≥0.17 mmol/g NH_2 loading) were all purchased from Sigma-Aldrich, Germany, and used without further purification unless otherwise stated. Pentafluorophenyl methacrylate (PFM) was purchased from Apollo scientific, UK, cysteamine hydrochloride (purum ≥ 97.0%) and methoxypolyethylene glycol amine (5000, ≥ 0.17mmol/g NH_2) from Fluka, Germany, and Alexa Fluor 660 carboxylic acid succinimidyl ester from Invitrogen, US.

Solvents, such as dimethyl sulfoxide (DMSO, ≥ 99,5%) were purchased from Sigma-aldrich, Germany, ethanol (HPLC) from Panreac, Spain, and deuterium oxide (D_2O, 100%) from Eurisotop, France.

AGBBB015F, AGBBB015I and AGBBB05A were kindly donated from Aplagen, Germany, as well as RP3, from Regulon, Greece, and human insulin, from Novo Nordisk, Denmark, within Nanobiopharmaceutics project. Insulin from bovine pancreas was purchased from Sigma, Germany. ECM collagen booster was purchased from Infinitec activos S.L., Spain (Figure 2.5).

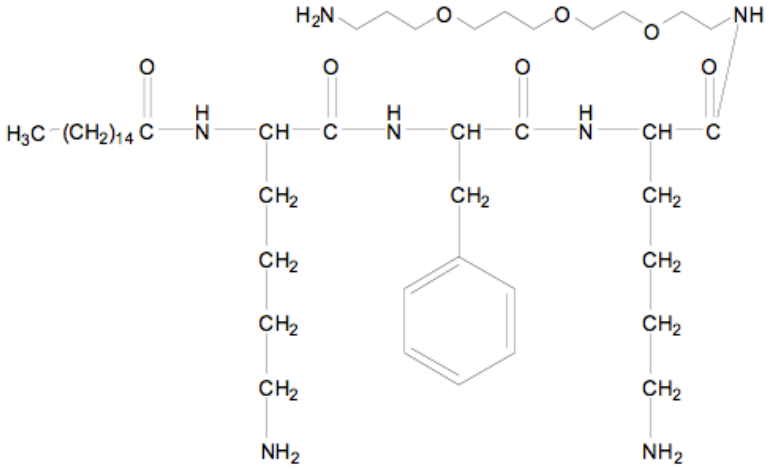

Figure 2.5: ECM collagen booster. Chemical formula: $C_{47}H_{87}N_7O_7$, MW: 862.24 g/mol.

Dialysis membranes (nominal MWCO 6000-8000) were purchased from Membrane filtration products Inc., US, and nylon syringe filters (0,2 µm) were purchased from Teknokroma.

For H^1-NMR studies, nanoparticles were lyophilized and dissolved in D_2O (20 mg/ml) and analyzed in a Varian 400 MHz MR spectrometer.

To perform the cytotoxicity assays, several assay kits were purchased from Promega, US. For MTS assay a CellTiter 96 Aqueous Non-Radioactive Cell Proliferation

Assay and for the ATP production assay a CellTiter-Glo Luminiscent Cell Viability Assay was used.

2.2.2 Synthesis of nanoparticles

A library of nanoparticles with different Critical Solution Tempreatures (CST), sizes and surface coatings, were synthesized by a free-radical polymerization method in a microemulsion system, where the monomers used were N-isopropylacrylamide, N,N-dimethylacrylamide and acrylic acid, the cross-linker was methylenebisacrylamide, the surfactant, sodium dodecyl sulphate, and the initiator ammonium persulphate.

For the synthesis of the nanoparticles a three-neck bottom-flask was charged with N-isopropylacrylamide (0.35 g, 3.09 mmol), N,N'-dimethylacrylamide (0.04 g, 4.5 mmol), acrylic acid (0.05 g, 3.6 mmol), methylenebisacrylamide (0.01 g, 1.54 mmol), sodium dodecyl sulphate (0.02 g, 5.76 mmol) and 117 ml of mili-Q water. The reaction mixture was heated at 70°C in a hot plate, under nitrogen atmosphere and stirring for four hours. After some minutes, when the reaction mixture was homogeneous, ammonium persulphate (0.036 g, 8.21 mols) was added.

2.2.3 Surface decoration

After 1 hour of reaction, pentafluorophenyl methacrylate (3,8 mmol) was added and the reaction mixture was further heated for 30 minutes. The obtained nanoparticles were further modified by the addition of the desired coating molecule. For thiolating, cysteamine hydrochloride (0.015g, 3.8 mmol) was added, for labelling, Alexa fluor 660 carboxylic acid succinimidyl ester (10 μg, 9 mmol) and for pegylation, methoxypolyethylene glycol amine (0.1g, 0.02 mmol). For small peptide coating, RGDS added was (0.3 mg, 0.69 μmol).

Nanoparticles for brain delivery were coated with three different peptides that present high affinity for specific BBB-receptors such as the low-density lipoprotein receptor-related protein (LRP) or ferroproteins (FP). Two different angiopep 2 derivates were used to coat the delivery system, AGBBB015F and AGBBB015I. Both peptides have the same peptidic chain with terminal thiol group and are labelled with carboxyfluorescein. The difference between them is that AGBBB015F is biotinylated and AGBBB015I has a terminal amine (Table 2.1). A third peptide belonging to a different peptide family was also used as targeting was Regulon peptide 3, a derivative of ferroproteins FP1 and FP2, that may have the potential to lead particles over the BBB. The existence of FP1 in the blood-brain barrier has been demonstrated as it plays an important role in exporting iron from BBB cells[55].

Table 2.1: BBB-passing peptides structure

Name	Peptide structure
AGBBB015F (MW = 3230 g/mol)	
AGBBB015I (MW = 2646 g/mol)	
Regulon peptide 3 (MW = 7295 g/mol)	(5-TAMRA)-HKKWQFNSPFVPRADEPARKGKVHIPFPLDNITCRVPMAREPTVIHGKREVTLHL HPDH(-COOH)

In this approach, NP's were first coated with cysteamine hydrochloride using the amino-reactive PFM groups, followed by thiol oxidative coupling between cysteamine hydrochloride and BBB-passing peptide. Therefore, after thiolating peptides AGBBB015I (1.055 mg, 0.39 μmol) or RP3 (1.1 mg, 119 μmol) were added.

Oxidative coupling of thiols to disulfides[56,57] was achieved by heating a mixture of 20 ml of the freshly synthesised nanoparticles solution and 10 ml of DMSO at 30°C, under nitrogen atmosphere and agitation. A peptide solution of AGBBB015F (1.045 mg, 0.32μmol) was added dropwise. In order to ensure disulfide bond formation between nanoparticles and the peptide a spectrophotometric assay to detect free thiol groups was performed with Ellman's reagent (DTNB)[58]. DTNB reacts with a free sulfhydryl group to yield a mixed disulfide and 2-nitro-5-thiobenzoic acid (TNB). The target of DTNB in this reaction is the conjugate base ($R\text{-}S^-$) of a free sulfhydryl group. TNB is the "coloured" specie produced in this reaction, which was monitored at 412 nm[59]. Sulfhydryl groups might be estimated in a sample by comparison to a standard curve composed of known concentrations of a sulfhydryl-containing compound such as cysteine.

2.2.4 Purification and sterilization

After synthesis, the reaction mixture is placed in a dialysis membrane and is dialyzed in mili-Q water with agitation for five days to eliminate the excess of reagents. When dialyzed, the nanoparticles solution is filtered through nylon syringe filters in a laminar flow hood. Nanoparticles were lyophilized and stored in the freezer.

2.2.5 Characterization of nanoparticles

Nanoparticles size and zeta potential was determined using dynamic light scattering in a Nano-ZS Nanosizer (Malvern Intruments Ltd., Worcestershire, UK) with a laser light wavelength of 632.8 nm and a scattering angle of 173 degrees. The analysis temperature was set at 25°C. Nanoparticles solutions were measured without previous dilution at an approximate final concentration of 4 mg/ml using

Smoluchowski approximation. To study their thermosensitive behaviour a temperature ramp cycle was performed ranging from 25°C to 55°C.

Nanoparticles were also visualized by AFM and SEM. Samples were previously prepared by fixing nanoparticles on a silicon wafer by covalent bonding. To achieve this, it was necessary to previously coat the wafer surface with allylamine by plasma polymerization. Plasma polymerization was carried out in a home-built 30 cm long cylindrical Pyrex reactor using an excitation frequency of 13,56 MHz for 4 minutes at 10 W with a pulsing of 100 ms. The coated wafer was added to a freshly synthesized nanoparticles solution. Samples were dried with an argon flow and were analysed in dry conditions.

AFM imaging was performed with a XE-100 Atomic Force microscope (Park Systems, Korea) with lateral and vertical resolution of 0.15 and 0.05 nm, respectively. Pyramidal cantilevers with silicon tip (ACTA) were purchased from Park Systems, Korea. AFM Images were collected using the non-contact mode. For the characterization of the thermo-responsive behaviour, the sample was placed on a gold support, which belongs to the dynamic liquid cell module, connected to a temperature controller but without connecting the water flow.

For SEM imaging, samples were previously prepared by fixing nanoparticles on a silicon wafer as explained before. Then, the prepared silicon wafer was coated with gold by low vacuum sputter coating technique. SEM images were obtained from a Hitachi H-4100FE scanning electronic microscope.

2.2.6 Drug loading

The solution containing the desired drug was added to a nanoparticles solution at room temperature. The resulting solution is stored in the fridge for three hours before drug loading. Then, the solution is heated in a water bath above the transition temperature for 30 minutes. After letting the sample to cool down, the percentage of non-entrapped drug (free drug) can be analysed using high performance liquid chromatography (HPLC).

Insulin was analysed using an HPLC system equipped with a Waters sunfire C18 column (150 mm, 4.6 mm and 5 μm). Samples were injected (20 μl) as obtained. The mobile phase consisted of 70% of 1 mmol sodium sulphate and 0.2% of triethylamine in water (pH adjusted to 3.2 by phosphoric acid) and 40% of acetonitrile[60] at a flow rate of 1 ml/min at 25°C. The elution products were monitored with UV detector set at 214 nm. Human insulin was analysed with the same method. Insulin standard solutions were prepared at concentrations of 20, 40, 60, 80 and 100 μg/ml.

ECM peptide was analysed using the same HPLC system and column. Samples were injected as obtained (10 μl). UV detection was performed at 220nm and linear gradients from 5 to 100% of CH_3CN (+0.036% TFA) into water (+0.045% TFA) were run at 1.0 mL/min flow rate over 20 minutes. Standard solutions of the peptide were prepared at concentrations of 0.1mg/ml, 0.5mg/ml and 1 mg/ml in ethanol.

2.2.7 Drug release

For the drug release determination, nanoparticles were loaded with an angiopep 2 derivative, AGBBB05A (Table 2.2), which was easily quantified by HPLC/MS in Joanneum Research, Graz, Austria.

Table 2.2: AGBBB05A structure

Name	Peptide structure
AGBBB05A (MW= 2065 g/mol)	

The peptide AGBBB05A was loaded following the same process detailed above and their release was further analysed. To evaluate their release aliquots of the loaded nanoparticles solution were pipetted into PCR Lobind tubes and heated at 45°C for different periods of time (0 min, 10 min, 30 min, 60 min). One aliquot of non-loaded nanoparticles solution was heated at 45°C for 60 min, to serve as a control.

Prior to HPLC/MS analysis, the solutions were diluted to a concentration of 700 ng/ml of AGBBB05A. In parallel, a solution with AGBBB05A corresponding to 700 ng/ml AGBBB05A was prepared to serve as a reference. TCEP (*tris*(2-carboxyethyl)phosphine) was added to all solutions and incubation at 60°C for 20 minutes was performed to ensure that AGBBB05A is in a reduce state until HPLC/MS analysis. In addition, an internal standard, AGBBB05D, which is a peptide of the same family, is added to all solutions.

2.2.8 Cytotoxicity

Cytotoxicity tests were performed in collaboration with the Centre for Medical Research (ZMF) at the Medical University of Graz (MUG), where a mitochondrial activity assay (MTS), membrane integrity assay and ATP assay tests were performed. The assays were performed with human umbilical vein endothelial cells, EAhy926, at a concentration of 14,000 cells/well.

Cells (100 μl) were grown in supplemented DMEM in 96-well plates from 16 to 24 hours before exposure in an incubator (37°C, 5 % CO_2, 95 % rH). Then, culture medium was removed carefully and 100 μl of nanoparticles suspension is added to each well. The nanoparticle concentrations tested were 12.5, 25, 50, 100 and 200 μg/ml. All concentrations were assayed in quadruplicate. The plate is again incubated at the same conditions for 4 and 24 hours. At this point the proper reagents of each assay can be added.

For the MTS assay, an MTS solution was prepared firstly, dissolving 42 mg of MTS in 21 ml of DPBS adjusting the pH at 6.5 with 1N HCl. The solution was filter-sterilized through a 0,2 μm filter. Then, 2 ml of this solution was mixed with 100 μl of PMS solution and 20 μl of the resulting solution was pipetted into each cultured well of a 96-well plate, containing 100 μl of culture medium. The plate was incubated for 4 and

24 hours at 37°C in a humidified, 5% CO_2 atmosphere. The absorbance was recorded at 490 nm using a microplate reader.

For the ATP assay, cells were grown in opaque-walled multiwall plate. For CellTiter-Glo reagent preparation, lyophilized luciferase was reconstituted in the entire volume of CellTiter-Glo buffer provided by the kit. Then, 100 μl of the resulting luciferase solution (CellTiter-Glo reagent) were added to each well of cultured cells containing 100 μl of DMEM. Plates were shaked for 2 minutes in an orbital shaker to induce cell lysis. Plates are stabilized at room temperature for 10 minutes before measuring luminescence in a multiplate reader.

2.2.9 Hemocompatibility

All hemocompatibility tests were performed in collaboration with the Centre Interfacultaire des Biomatériaux (CEIB) at Liège University, Belgium, where hemolysis test, counting and size distribution of red blood cells and platelets, complement activation test and coagulation test were performed.

Human blood was obtained from The Red Cross Transfusion at Central Hospital of the University of Liège. Blood was collected from healthy donors in 4.5 mL tubes containing 3.2% sodium citrate, 15 minutes before blood exposure. The hemocompatibility pre-screening tests have been carried out after blood exposure according to ISO 10993-4.

Once volume of nanoparticles' solution was diluted in nine volumes of whole blood. In all experiments, a rapid homogenization of the nanoparticle suspension with the whole blood was performed in order to avoid any high local concentration of nanoparticles. Samples were incubated during 15 minutes at 37°C under horizontal roller mixing (35 rpm).

2.2.9.1 Realization of blood smear for the control of the Red Blood cell morphology

After blood incubation, 5 μl of the solution were withdrawn and spread on a microscopy glass side. Blood cells were observed with Olympus Provis microscope at 20x and 50x magnification in transmission mode.

2.2.9.2 Haemolysis test

Haemolysis test was adapted from Standard Practice for Assessment of Haemolytic Properties of Materials (ASTM designation: F 756-00). Polymer solutions and blood were prepared and incubated as described above. After incubation samples were centrifuged during 5 minutes at 600 g at room temperature. Supernatants were collected and mixed with cyanmethemoglobin reagent. Hemoglobin released was measured at 540 nm in a microplate reader (Anthos HT III, type 12600). Calibration curve was established with bovine hemoglobin standard. Saponine (0.8 mg/mL) and PBS were used as positive and negative control respectively. Total hemoglobin released from whole blood diluted in cyanmethemoglobin reagent was determined as 100% hemoglobin release. Haemolysis was expressed as the percentage of hemoglobin released (% rHb) to total content. Tests were done in triplicate.

2.2.9.3 Counting and size distribution of red blood cells and platelets

Counting and size distribution of red blood cells and platelets were determined with a Coulter Multisizer IIS after blood dilution in Isoton II. For RBC's analysis the whole blood was totally diluted 4000x in isotonic medium. Platelets were analysed starting from a platelet rich fraction obtained by centrifugation blood samples diluted (24×) in isotonic solution performed at 850*g* for 90 sec at room temperature. Aliquots of 1 mL of supernatants were added to 40 mL isotonic solution.

Counting and size measurements were performed on a Coulter Multisizer II equipped with an orifice tube of 70 µm. RBC's were counted between 3.7 µm and 8 µm and platelets, between 1.0 and 3.7 µm. Samples incubated with PBS (pH 7.4) were adopted as negative control. Tests were done in duplicate.

2.2.9.4 Complement activation

After incubation of nanoparticles with blood, EDTA (1 mM) was added in order to stop any complement activation. Zymozan (final blood concentration of 2 mg/ml) was used as a positive control while PBS was used as a negative control. Non-incubated blood was added as an additional negative control.

Samples were centrifuged during 5 minutes at 200 g at room temperature. Supernatants were stored at -80°C until future analysis. Complement activation was estimated adopting the Human C3a ELISA kit for quantification of Human C3a-desArg (Beckton Dickinson). Absorbance was measured at 450 nm with a microplate reader (Anthos HT III, type 12600). Concentration of C3a was expressed in ng/mL and as percentage of activation to the blood control incubated and treated in the same manner. Measurements were conducted in duplicate.

2.2.9.5 Coagulation cascade activation

Quick test and ACT assays were performed on a Dade Behring instrument (Behring Coagulation Timer, or BCT) with commercial reagents, Tromborel S (Dade Behring/Siemens for Quick test and a C.K. PREST kit (Roche Diagnostic) for ACT.

For Quick test, calcium thromboplastin and excess calcium were added to citrated plasma to induce coagulation and the time of fibrin clot formation was measured. For ACT test, phospholipid suspension, an activator (kaolin), and calcium (to reverse the anticoagulant effect of citrate) were mixed into plasma sample. Time of clot formation was measured.

Whole blood and nanoparticle suspensions were mixed and incubated as described above. Samples were centrifuged during 5 minutes at 2000 g at room temperature. After supernatant collection prothrombin time (PT) and activated partial thromboplastin time (APTT) were measured directly with a Behring Coagulation Timer analyzer (BCT) (Dade Behring). Kaolin (0.5 mg/mL final blood concentration) was used as a positive control in ACT and PBS as negative control. Measurements were done in duplicate.

2.2.10 Cellular uptake

After ensuring nanoparticles biocompatibility, the cell uptake of nanoparticles was determined *in vitro*. Thanks to nanoparticle dual-coating with BBB-targeting peptides and a flurophore, nanoparticles uptake was monitored in three different endothelial cell lines. Nanoparticles were loaded with AGBBB005A, which is labelled with carboxyfluorescein.

Cellular uptake and the corresponding E-selectin expression and MTS test were performed in collaboration with the Institute for Pathology at Johannes-Gutemberg Universität in Mainz, Germany.

For the E-selectin expression test (CAM/EIA), 10,000 Huvec cells/well were seeded onto a fibronectin-coated 96-well plate. After reaching confluence, cells were treated with different concentrations of nanoparticles (35, 70, 350 µg/ml). The stimulation with lipopolysaccharide (1:8000, 1µg/ml) was used as positive control, while untreated cells were used as control. After the stimulation for 4 h and 24 h, cells were washed with HEPES buffer containing 0.2% bovine serum albumin. Cells were fixed with methanol/ethanol (2:1) for 15 minutes. Afterwards cells were stained with primary antibody (mouse anti-human E-selectin, 1:2000; BenderMedSystems, Austria) for 1 h. After 3 times of washing with PBS with 0.05% Tween20, cells were incubated with the corresponding secondary antibody, biotinalyted-coupled IgG (anti-mouse; SE Healthcare, USA) for 1 h. Cells were washed with PBS with 0.05% Tween20 and incubated with streptavidin coupled horseradish peroxidase. A substrate solution was added after an additional washing step. The enzymatic reaction was stopped with the addition of HCl 3M. The absorption was measured at λ = 450 nm in a plate reader (Genios Plus, Tecan, Germany). The positive control (LPS stimulated cells) was set to 100% (4 h).

For cellular uptake assay, the same amount of cells was incubated in 6-well culture plate. After reaching confluence, cells were incubated with nanoparticles at a concentration of 70 µg/ml at 37°C for 24 hours. After washing with PBS with 0.05% Tween20, cell nuclei were stained with Hoechst dye while cell membranes were stained with the antibody CD31 (mouse anti-human, DakoCytomation, Glostrup, Denmark) and the corresponding secondary antibody (goat anti-mouse Alexa Fluor 546, Molecular Probes, Carlsbad, USA) at room temperature for 1 hour each. Fluorescence in culture cells was observed with a fluorescence microscope (Olympus IX71 with Delta Vision system, Applied Precision, USA).

2.3 Results and discussion

2.3.1 Synthesis of nanoparticles via microemulsion polymerization

The first challenge was the synthesis of nanoparticles by free-radical polymerization in a microemulsion system, as discussed before. Technically, in the case of thermo-responsive acrylamides, such as NIPAAm, DEAAm or DMAAm, the terminology that should be employed would be precipitation polymerization as most acrylamides are soluble enough in water to consider the system as a continuous phase. On the other hand, regarding IUPAC terminology[61], the precipitation polymerization implies large and non-regular particles, as a result of little or no stabilizer present. It this case, the amount of colloid stabilizer (SDS) is much larger than in a precipitations polymerization, in order to obtain the gel nanoparticles. According to the IUPAC terminology, the methodology used is more similar to a dispersion polymerization where more surfactant is normally used. However, the fact that PFM is used as a linker for targeting moieties, which is an insoluble monomer, led to an emulsionated system in water. In addition, the amount of surfactant and the size of the nanoparticles obtained are similar to the ones used in a microemulsion polymerization.

Previously, in our group, a library of acrylamide-based nanoparticles was prepared to get a collection of thermosensitive nanoparticles with a wide range of critical solution temperatures. In this exploratory experiment, three main types of nanoparticles were studied. A first set of nanoparticles was obtained from N,N'-dimethylacrylamide (DMAAm) and N,N'-diethylacrylamide (DEAAm). Another two families were prepared by varying the ratios of N-isopropylacrylamide (NIPAAm), N,N'-dimethylacrylamide (DMAAm) and acrylic acid (Aac). All the reactions were performed in the presence of N,N'-methylenebisacrylamide (MBAAm) as a cross-linker and dodecyl sodium sulphate (SDS) as a surfactant. A summary of the obtained results is shown in Table 2.3.

PNIPAAm is one of the most widely studied thermosensitive polymers. It constitutes the base of the thermosensitive system while the addition of DMAAm[62] and Aac[63,64] resulted in an increase of the LCST. Moreover, Aac modifies swelling degrees[65], which has a high influence on the degree of drug encapsulation. The role of MBAAm is to preserve the nanoparticle structure, preventing the dissolution of the polymer chains below LCST[66].

Table 2.3: Characterization of nanoparticles depending on composition

Sample	Composition (%)						Size (nm)	Zeta potential (mV)	LCST (°C)
	NIPAAm	DMAAm	Aac	MBAAm	DEAAm	SDS			
DD 10		21		2	75	2	29	-0.8	34
ND 25 AA	77	8	6	3		5	90	-7.9	37
ND 29	84	11		2		3	89	-5	36

All three types of nanoparticles were characterized in terms of size, zeta potential and LCST. The use of different monomers and their proportion resulted in nanometric particles of different sizes, ranging from 29 nm to 89 nm. Particles prepared from DEAAm were significantly smaller in size than particles obtained containing NIPAAm.

All nanoparticles showed negative zeta potential values because of the presence of the anionic surfactant in their structure. Interestingly, DEAAm particles also showed a different behaviour of zeta potential (-0.8 vs -7.9 and -5 mV), when compared to NIPAAm particles, which suggests that NIPAAm colloidal systems possess higher potential stability as their zeta potential values are higher in absolute value. All three nanoparticles showed thermosensitive behaviour with a LCST comprised between 34 and 37°C.

In the light of the results, further experiments were based on NIPAAm systems due to their potential stability, the proximity of their LCST to body temperature and the small size range (between 30 and 100 nm), which are supposed to be less cytotoxic[67].

2.3.2 Nanoparticles characterization

2.3.2.1 Hydrodynamic radius. Zeta potential and Critical Solution Temperature

The second challenge to attempt, after having successfully synthesized nanoparticles with different core composition, was to modify their surface with different coating moieties to fulfil different types of delivery, such as oral delivery or brain delivery.

Needless to say, it is expected that the size of coated nanoparticles differs from uncoated nanoparticles, as they have a shell where coating molecules are added. The characteristics of these coating molecules will have a big influence on the final size of the nanoparticle, not only because of their molecular weight but also because of their hydrophilic or hydrophobic character, which will affect the final assembly of the nanoparticle.

Regarding LCST of thermosensitive polymers, many studies have been done to define the causes of its variation. It can be raised or lowered via introduction of hydrophilic or hydrophobic comonomers, respectively[68,69]. However, it has been demonstrated that not only depends on the number of hydrophobic incorporations and on its chemical structure, but also on its position on the chain[68].

Hydrophobic end groups decrease cloud points while hydrophilic end groups tend to increase them, with the magnitude of the effect depending on the nature of the end group. Hydrophobic end groups act by increasing the degree of ordering of solvating water while hydrophilic ones tend to decrease it. These effects are supposed to be greater when these groups are located at chain ends rather than in mid-chain[70]. A reasonable explanation for the decrease of the LCST with the incorporation of hydrophobic end groups is that the polymer might already form aggregates below its LCST due to its poor miscibility in water as a result of the direct interactions between water and the hydrophobic groups[68,71]. Consequently, the coil-to-globule transition occurs more rapidly, when raising the temperature.

The molecular weight (MW) dependence of cloud point has been an active controversial topic. The cloud point of NIPAAm has been reported to be inversely dependent[70,72,73], directly dependent[68,74] or independent[75] on the molecular weight. However, most of these studies were based on polydisperse polymers synthesised via

conventional polymerisation, which may have hindered precise examination of MW effect. Free radical polymerization is classified within this type of polymerisations; hence the difficulty to extract some conclusions from the above presented results.

Although the mentioned parameters affect directly the thermoresponsive polymer used in this work, it must be taken into consideration that in this case the polymer is forming a nanoparticle in conjunction with a surfactant and hence this supramolecular structure may vary its final behaviour. Therefore, polymer behaviour may not be comparable to nanoparticles behaviour.

Table 2.4 summarizes the results of the exploratory experiment where the influence of chemical nature of the coating moieties was evaluated. All coating molecules are linked to the core through pPFM shell as explained in Materials and methods section.

Table 2.4: Characterization of nanoparticles coated with small molecules

Sample	Surface group	PFM (mmol)	Coating molecule (CM)	CM (mmol)	Size (nm)	Zeta potential (mV)	LCST. (°C)
ND 25 AA PFM OH	OH	0.0269	Ethanolamine	0.2456	180	-15	29
ND 25 AA PFM CH_3	CH_3	0.0001	Butylamine	0.1390	200	-10	34
ND 25 AA PFM COOH	COOH	0.1191	γ-aminobutiric acid	0.1406	97	-9	33
ND 25 AA PFM SH	SH	0.3970	Cysteamine hydrochloride	0.4727	150	-6.4	34
ND 25 AA PFM AF488	AF488	0.3970	Alexa fluor cadaverine 488	4.5E-05	128	-5.5	35
ND 25 AA PFM AF660	AF660	0.1985	Alexa fluor 660 carboxylic acid, succinimidyl ester	2.3E-05	279	-18.3	34

The results are ordered by increasing molecular weight of the coating moiety. There is a 1:1 molar ratio of PFM to amines in the nucleophilic substitution. Amines were added in slight excess in order to ensure complete reaction with PFM groups. Regarding the last two samples, the amount of fluorphore was lower than PFM to obtain nanoparticles slightly coated of a reasonable size. In general, it is observed that the larger the coating molecule is, the larger will the nanoparticle be, which can be modulated by controlling the amount of pPFM added. Regarding zeta potential, all values are negative as expected and vary slightly depending on the nature and amount of the surface groups of the nanoparticle. Concerning LCST, values varied depending on the targeting moiety, suggesting that LCST can be fine-tuned according to the coating moiety.

Once demonstrated that nanoparticles can be coated with a wide variety of molecules, the next challenge to tackle is to coat them with different molecules, which will allow to decorate them with a targeting moiety and a fluorophore at the same time. This approach is of special interest to monitor the cellular uptake of targeted nanoparticles. Table 2.5 shows the properties of dual-coated nanoparticles with thiol groups and a fluorophore for oral delivery.

Table 2.5: Characterization of nanoparticles coated with two molecules

Sample	Surface groups	PFM (mmol)	Coating molecule (CM)	CM (mmol)		Size (nm)	Zeta potential (mV)	LCST. (°C)
				SH	AF			
ND 25 AA PFM SH AF488	SH/ AF488	0.0794	Cysteamine hydrochloride/ Alexa fluor 488	0.0555	9.1E-06	127	-8	34
ND 25 AA PFM SH AF660	SH/ AF660	0.0476	Cysteamine hydrochloride/ Alexa fluor 660	0.1373	9.1E-06	155	-6.7	40

Results (Table 2.5) demonstrate the ability to obtain dual-coated nanoparticles of reasonable size by controlling the amount of linker. Zeta potential values were kept in the normal range while LCST present considerable variability.

However, cysteamine hydrochloride is a relatively small molecule among the targeting molecules used in this work, thus further experiments on coating possibilities should be done with larger molecules. This is the case of poly(ethylene glycol). As mentioned in chapter 1, the use of polyethylene glycol (PEG) as a coating molecule is widely extended as it has shown a prolonged blood circulation leading to "passive" targeting of drug carriers to solid tumours through the enhanced permeability and retention (EPR) effect[76]. In addition, it is known as a FDA approved material for human use because of its low toxicity.

To further improve delivery efficiency and tissue specificity, a strong emphasis has been put on the development of nanocarrier systems that can actively target tumours through molecular recognition of unique cancer-specific markers. Integrin $\alpha_v\beta_3$ is such a molecular target that is highly expressed in angiogenic endothelial cells in many solid tumors. RGDS is a ligand that can target these receptors and subsequently induce receptor-mediated endocytosis for cell uptake[76]. In addition, the use of certain peptides can target specifically nanoparticles to receptors on the blood-brain barrier, as mentioned in previous sections.

Table 2.6 shows nanoparticles modified with two ligands, PEG, a fluorophore and a large peptide, which was used as a BBB-passing peptide.

Table 2.6: Characterization of nanoparticles coated with large molecules

Sample	Surface group	PFM (mmol)	Coating molecule (CM)	CM (mmol)		Size (nm)	Zeta potential (mV)	LCST (°C)
ND 25 AA PFM PEG	PEG	0.0397	Methoxypolyethyl eneglycol amine	0.02		103	-6	34
ND 25 AA PFM RP3	RP3	0.1191	Regulon peptide 3	0.0002		500	-13.06	38
ND 25 AA PFM RGDS AF660	RGDS/ AF660	0.397	RGDS/Alexa fluor 660	4E-04[a]	4E-05[b]	278	-18.55	33

[a]RGDS and [b]Alexa fluor 660 amount.

In the light of the results (Table 2.6), it can be said that the largest nanoparticles correspond to the largest coating molecule, RP3 (7265 g/mol), as it was expected. Although, RGDS is smaller than the poly(ethylene glycol) used in the experiment, with a molecular weight of 433 and 5,000 g/mol respectively, nanoparticles coated with RGDS are smaller. This is probably because the second ones are also labelled with

alexa fluor 660, which is a very voluminous substituent, and therefore are larger. In this case, the highest LCST belongs to the nanoparticles with the largest coating, suggesting that the larger coating moieties the polymer has, the more difficult is to expulse the water and collapse, hence the transition takes place at higher temperatures.

In order to analyse the effect of nanoparticles coating with BBB-passing peptides in depth, a detailed study was performed with the angiopep BBB-passing peptides. Table 2.7 shows characterization of nanoparticles before and after coating with AGBBB015F and AGBBB015I.

Table 2.7: Characterization of nanoparticles coated with BBB-passing peptide via thiol group coupling

	Sample	Size (nm)	Z-Pot (mV)	LCST (°C)	Coating molecule	CM (mmol)	Size (nm)	Z-Pot (mV)	LCST (°C)
1	ND 25 AA PFM SH AF660	104	-8.9	33	AGBBB015F	0.0003	682	-0.085	37
2	ND 25 AA PFM SH AF660	76	-4.97	35	AGBBB015F	0.0002	250	-0.0279	38
3	ND 25 AA PFM SH AF660	76	-4.97	35	AGBBB015F	7E-05	350	-0.0682	39
4	ND 25 AA PFM SH AF660	300	-7.76	33	AGBBB015I	0.0003	450	-14.26	33
5	ND 25 AA PFM SH AF660	11	-11.5	42	AGBBB015I	0.0003	145	-9.15	45

For all samples there is an increase in size after coating, which is reasonable in the case of AGBBB015F and AGBBB015I, as they have molecular weights of 3,576 and 3,135 g/mol. respectively. In addition, the difference in size between non-coated and coated nanoparticles, in the case of AGBBB015F, is higher as the coating of this peptide involves the use of cysteamine hydrochloride as a linker.

In the same way, LCST shows a clear increase comparing non-coated and coated nanoparticles. In this case it is clearly observed that LCST is higher for larger nanoparticles. This fact may suggest that polymer chains of the nanoparticle lose flexibility with large coating moieties, such as peptides, and cannot expulse water at the same temperature of non-coated nanoparticles. Therefore, a higher temperature will be required so that polymer chains gain mobility.

Regarding zeta potential, the trend is to decrease in absolute value, as in the beginning nanoparticles are negatively charged, because of thiol and surfactant groups, and then are coated with angiopep peptides, which both have positive net charge. The fact that all the values are close to zero indicates that they have a very high tendency to aggregate.

To sum up, it could be concluded that particle size can be tuned, by regulating the amount of linker (PFM) and coating molecule added. Moreover, the larger the coating particle is, the larger the whole nanoparticle will be. Generally, the larger the particle is, the higher the LCST will be. In the case of Zeta potential, it always depends on the nature of the surface groups.

Nanoparticles were characterized not only by DLS but also by SEM and AFM. Size values of three different NIPAAm-based nanoparticles obtained by these techniques are compared in Table 2.8.

Table 2.8: Size values measured by DLS, SEM and AFM.

	Size (nm)		
Sample	DLS	SEM	AFM
ND 29 PFM	739	683	790
ND 25 AA PFM SH F660	246	267	200
ND 25 AA PFM SH	223	205	300

Taking into account the experimental variability between techniques, results are in good agreement. Figure 2.6 shows SEM and AFM pictures of the nanoparticles mentioned in Table 2.8.

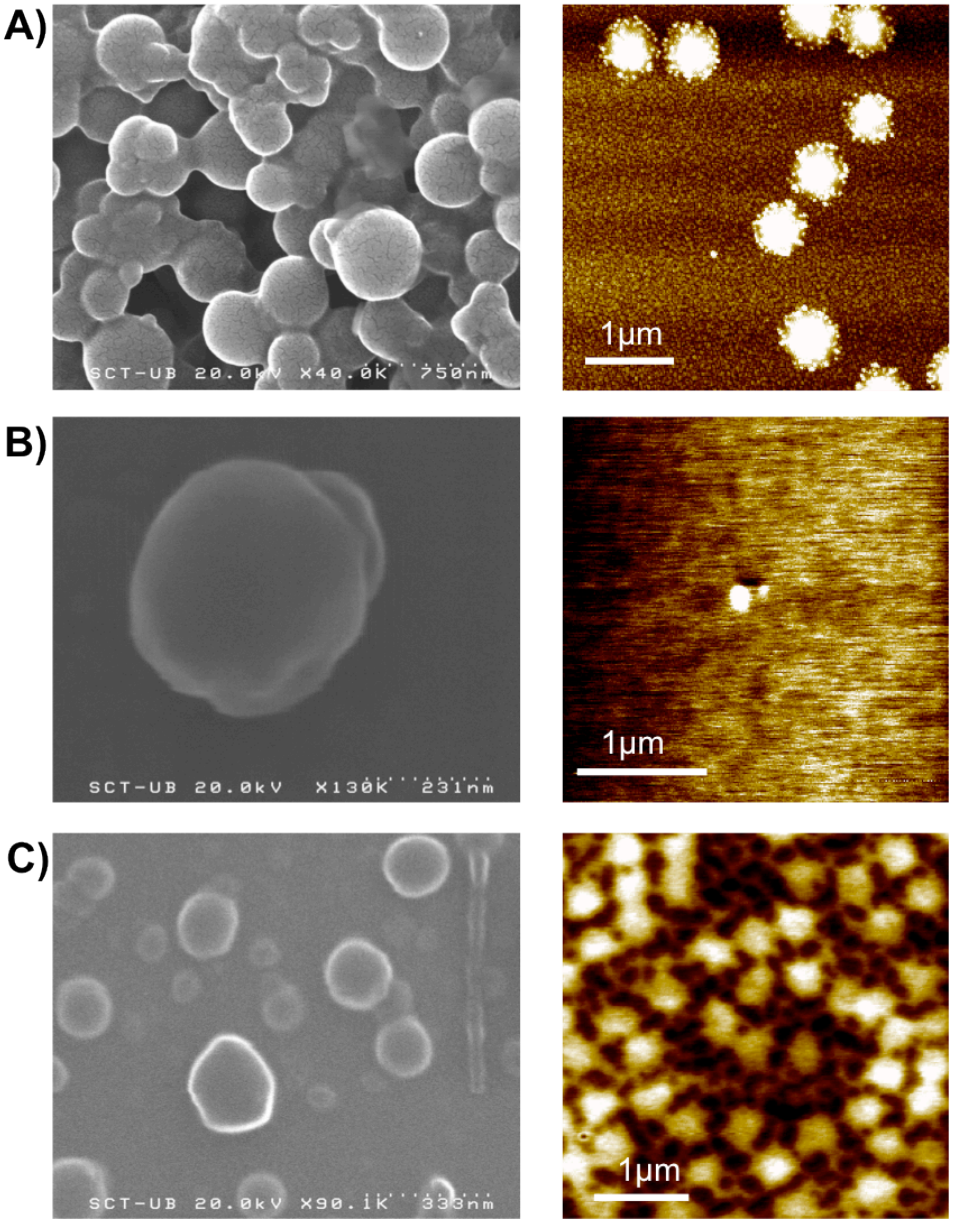

Figure 2.6: SEM and AFM images of nanoparticles from Table 2.8.A) ND 29 PFM, B) ND 25 AA PFM SH F660 and C) ND 25 AA PFM SH.

Discrete nanoparticles can be observed in all images, except in SEM Figure 2.6A, where some aggregation was observed. All nanoparticles were deposited on silicon wafers, but in Figure 2.6A the silicon wafer was added to a freshly synthesized

nanoparticles solution, while in Figure 2.6B and C, the solution of nanoparticles was deposited on the wafer with an spray.

2.3.3 Thermosensitive behaviour

The third challenge to overcome once the system is modified as desired is to characterize its thermosensitive behaviour in depth. As explained before, thermosensitive polymers shrink above LCST as they expel water to the bulk solution and diminish in size (Figure 2.7)[1].

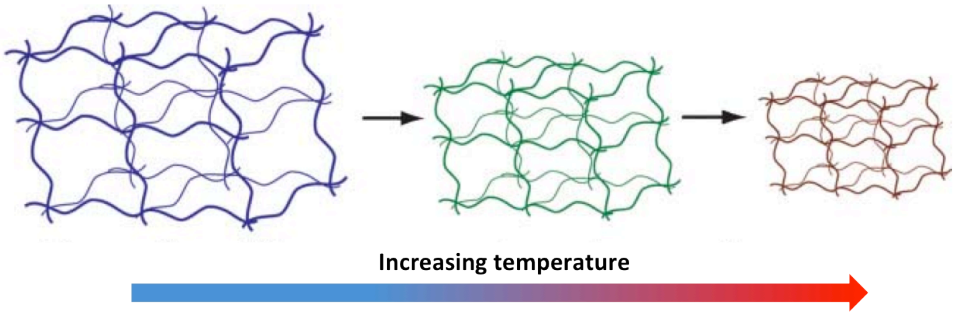

Figure 2.7: Shrinkage of thermo-responsive hydrogels with increasing temperature[9].

However, nanoparticles do not show the same behaviour when analysed by DLS. In contrast, they show an increase in size instead of a decrease, although cloudiness of the bulk solution is observed.

To make sure this behaviour is not an artificial result caused by the DLS equipment, thermosensitive behaviour was further analysed by AFM, to directly monitor the behaviour of nanoparticles. Nanoparticles size and shape was assessed by DLS and AFM between ranges of temperatures around the LCST. For DLS, samples were first examined at room temperature and changes in their nanoparticle size were monitored as temperature was increased at 1°C/min, as shown in Figure 2.8.

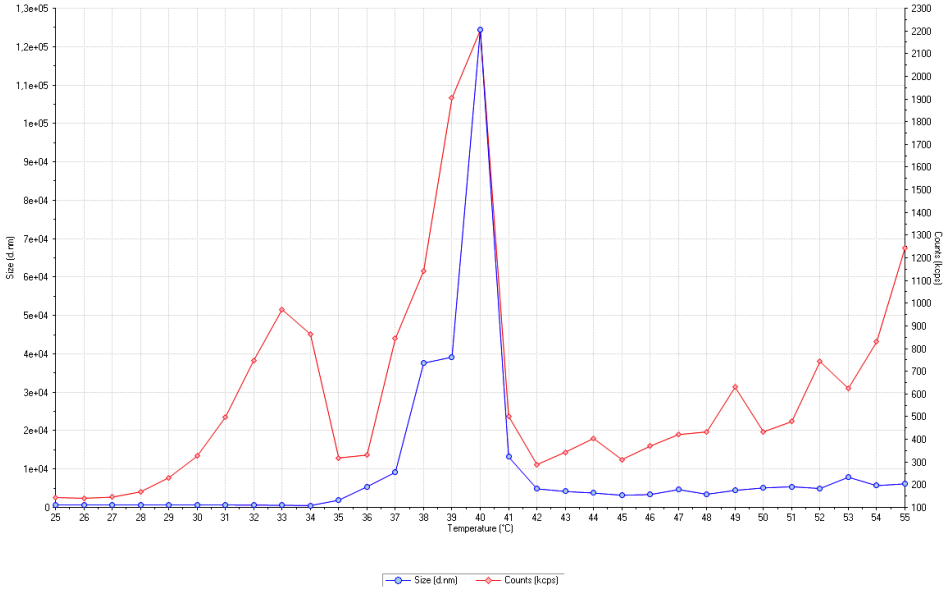

Figure 2.8: Variation of size with temperature of ND 29 PFM determined by DLS.

Results in Figure 2.8 show the change in nanoparticle size with the temperature. Nanoparticles show an excellent stability in terms of size in temperatures ranging from 25 to 34°C. At temperatures above 34°C, nanoparticles experienced a sudden increase in size reaching 125 μm. The inflection point of the curve is considered the LCST, which for these nanoparticles is 39°C. Interestingly, at temperatures above 42°C the size of the nanoparticles remained stable at around 5 μm.

The thermosensitivity of the synthesized nanoparticles was also studied using AFM (Figure 2.9) in order to confirm the changes in particle size observed in the DLS measurements. The same sample was placed on a silicon wafer as explained in materials and methods section for AFM imaging.

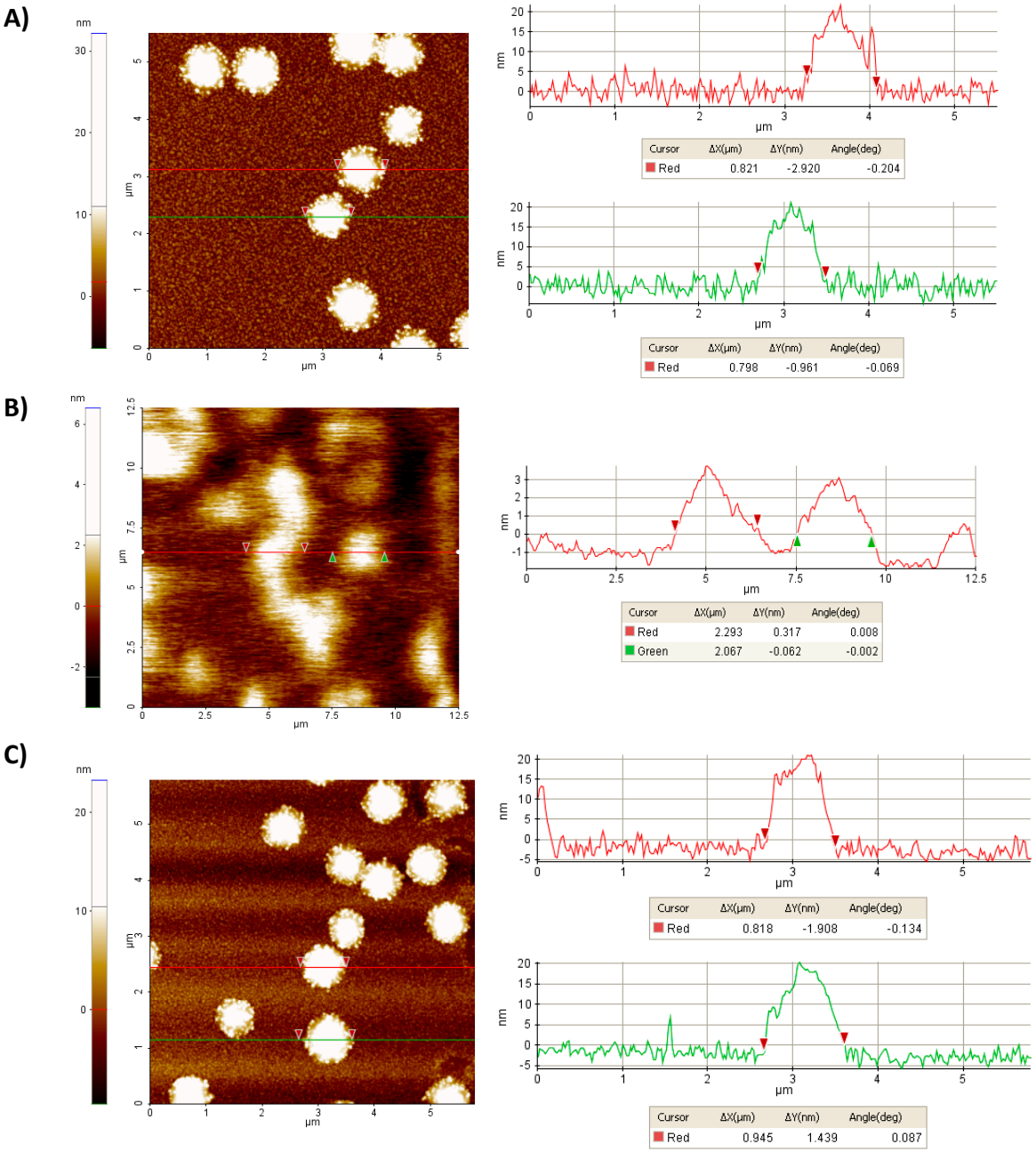

Figure 2.9: AFM image and surface profile of ND 29 PFM at different temperatures.A) at room temperature, B) at 45ºC and C) at room temperature, after being heated up to 45ºC.

Figure 2.9A shows a clear image of homogeneous round-shape nanoparticles about 800 nm big and 20 nm high at room temperature, which is in good agreement with the results obtained by DLS. When the temperature was raised up to 45°C (Figure 2.9B), the image became blurred and the particles expanded, up to 2 μm, and flattened (3 nm high), what some authors call a "mushroom-like" state[77]. The size increase of the nanoparticles reflects the behaviour monitored by DLS. When the sample was cooled down again at room temperature (Figure 2.9C), nanoparticles shrank to the same size confirming the reversibility of the process.

These results suggest that nanoparticles have an opposite behaviour to what was expected by observing the typical thermosensitive polymer behaviour. However, although most samples exhibited a sharp and reproducible LCST, the opposite behaviour was also observed in some cases, meaning that nanoparticles decreased in size when the temperature was raised above LCST, which is called UCST behaviour (Table 2.9).

Table 2.9: Nanoparticles showing UCST behaviour.

Sample	Size (nm)	Zeta potential (mV)	UCST (°C)
ND 25 AA	180	-4	36
ND 25 AA	190	-	34
ND 25 AA PFM	90	-7.29	43
ND 25 AA PFM SH	193	-	34
ND 25 AA PFM AF660	620	-	33
ND 25 AA PFM AF660	100	-10.4	37
ND 25 AA PFM PEG SH AF488	83	-5.3	33
ND 25 AA PFM RP3	500	-13.06	38
ND 25 AA PFM SH AF660 AGBBB015F	682	-0.085	37
ND 25 AA PFM SH AF660 AGBBB015F	350	-0.0682	39

In general, those nanoparticles showing a decrease in size above UCST, were larger than those showing a size increase, and exhibited a phase transition at higher temperatures (Table 2.9).

In order to further characterize the obtained nanoparticles and their behaviour in solution, the phase transition was also studied by AFM and ^{1}H-NMR. Additionally, NMR gives an accurate profile of LCST since it provides valuable information of this phenomenon at the molecular level. Two different samples, ND 25 AA and ND 25 AA PFM AF660, showing opposite behaviours, an increase and a decrease in size, respectively, were selected for this purpose (Figure 2.10).

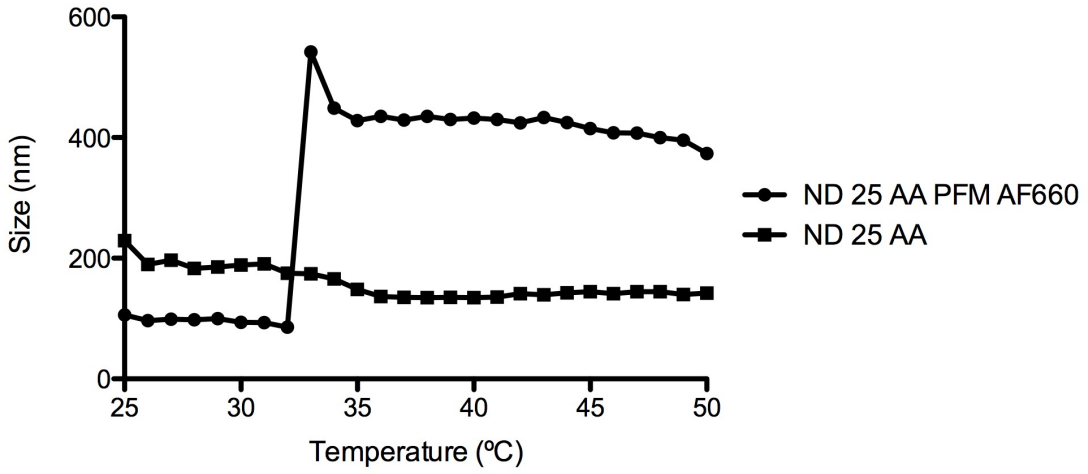

Figure 2.10: Samples showing LCST behaviour (ND 25 AA PFM AF660) and UCST behaviour (ND 25 AA), measured by DLS.

The first sample to study is ND 25 AA PFM AF660, which has a particle size of 106 nm, a zeta potential of -6.7 mV and an LCST of 33°C, measured by DLS (Figure 2.10). AFM images of the same sample (Figure 2.11) show nanoparticles between 417 and 585 nm, below LCST, and around 850 nm, above LCST. As seen before in the previous AFM study, it can be observed a reduction in height of the nanoparticle, from 20 to 2 nm. The difference here is that below LCST, nanoparticles are very sharp and above it, they become more flat.

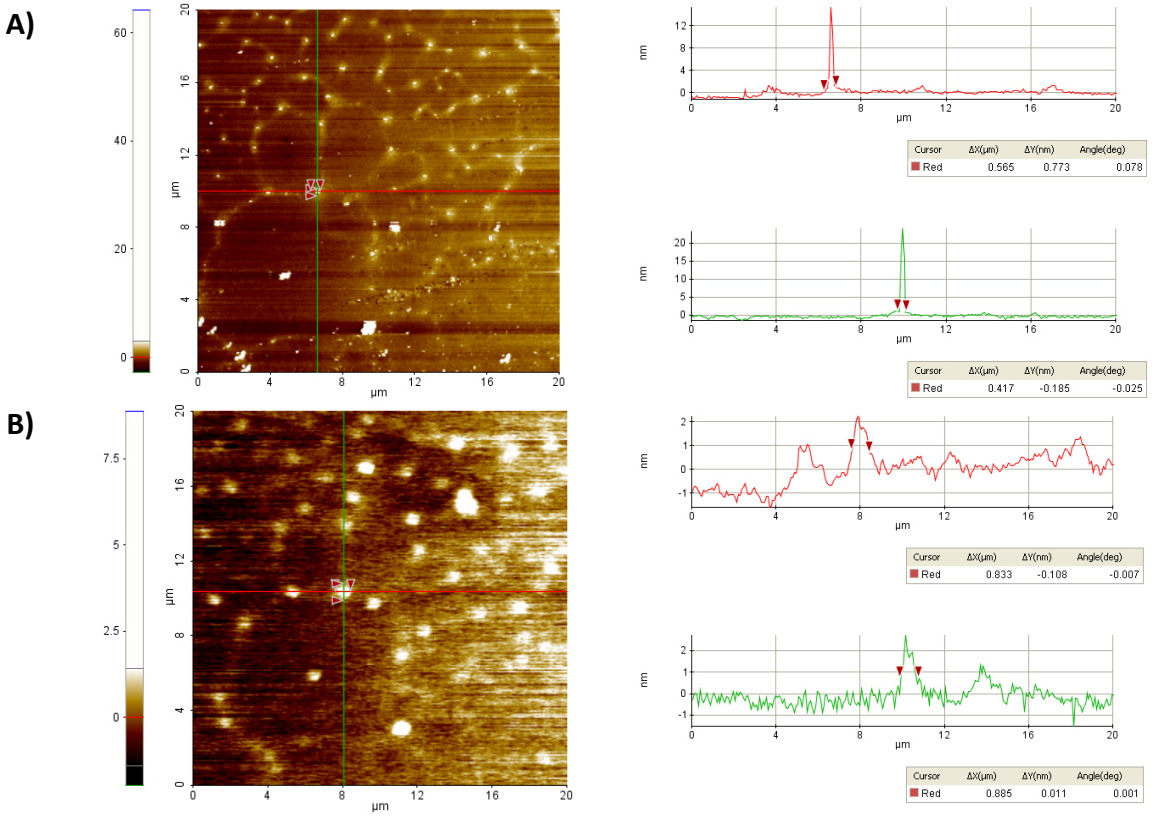

Figure 2.11: AFM images and surface profile of ND 25 AA PFM AF660 at different temperatures. A) at 32°C and B) at 47°C.

NMR spectroscopy has been used to study phase transitions in poly(acrylamide) hydrogels, in aqueous solutions and swollen networks of NIPAAm and its copolymers and in swollen networks of poly(N-isopropylacrylamide). In most of these studies, the changes in ^{1}H-NMR relaxation times (T_1 and T_2) and diffusion coefficients were employed to investigate the dynamics of both polymer segments and solvent molecules during the phase transition[78]. Thus, local segmental mobility information can be obtained.

^{1}H-NMR spectra measured under liquid conditions allow us differentiation between solid and liquid spins in the sample. “Solid” spins are restricted in mobility, so that the heterogeneity on the molecular level will, due to dipolar interactions, lead to a fast relaxation and a substantial decrease in intensity of all protons due to signal broadening such that it cannot be detected in a liquid type experiment. “Liquid” spins, however, show fast isotropic motion, which is averaging the dipolar interaction and leads to slow relaxation[79,80].

This phenomenon can be directly related with the coil-to-globule transition in thermosensitive polymers, such as NIPAAm. The temperature dependence of ^{1}H-NMR spectra showed a significant decrease of the intensity and a broadening of the signal above LCST[78,81]. This is due to the fact that at temperatures above the LCST, the mobility of most NIPAAm is reduced to such an extent that corresponding lines become too broad (and spin-spin relaxation times T_2 of respective protons become too short) to be detected in high-resolution spectra measured with a liquid-state NMR spectrometer. This mobility reduction can be attributed to the phase transition and the formation of rather compact solid-like globular structures[81].

In fact, at room temperature, the side-groups of a polymer have higher mobility than the backbone, so that the relaxation time of the nuclei in these side-groups is generally longer than interior backbone nuclei. Consequently, the peaks corresponding to side-groups nuclei are wider than the same peaks of its monomer, looking much more like a band rather than a peak. This causes a lost of resolution preventing to see the multiplicity of the signal[82].

Equally, the ^{1}H-NMR spectrum of the studied nanoparticles, which are a copolymer of NIPAAm-*co*-DMAAm-*co*-Aac, showed the same results (Figure 2.12). The typical signals of poly(N-isopropylacrylamide) are the following: at 1.14 ppm CH_3 (6H), at 1.60 ppm CH_2 (2H), at 2.01 ppm CH (1H) and at 3.88 ppm CH (1H). The proton of the amine group could not be identified, probably due to the fast exchange with the water deuterons, so that the signal is buried in the HDO resonance, around 4.5 ppm[79]. Above LCST, no significant reduction of the integrated intensity was observed for the HDO signal, indicating that all HDO molecules are directly detected in ^{1}H-NMR spectra in the whole range of temperatures[81]. For this reason, the integrated intensities were measured in relation to the HDO signal with the MestReNova® software. NIPAAm is known to interact strongly with surfactants, such as SDS, through hydrogen bonding. Therefore, the signals of sodium dodecyl sulphate can be identified at 0.88 ppm CH_3 (3H) and 1.28 ppm CH_2 (10H)[83].

At 30°C, below LCST, the broadening of the signals is hardly seen, while at 35°C, above LCST, it began to be clearly distinguished, at 55°C, the signal becomes too broad

that escapes the detection in high-resolution spectra due to the pronounced reduction in mobility of most NIPAAm units (Figure 2.12). These results are in good agreement with those obtained by DLS and AFM. The chemical shift of all signals remained constant except from HDO signal, which presented a linear trend with temperature, as it has been described in literature[84].

Temperature dependence of integrated intensities of the main protons of pNIPAAm is plotted in Figure 2.13.

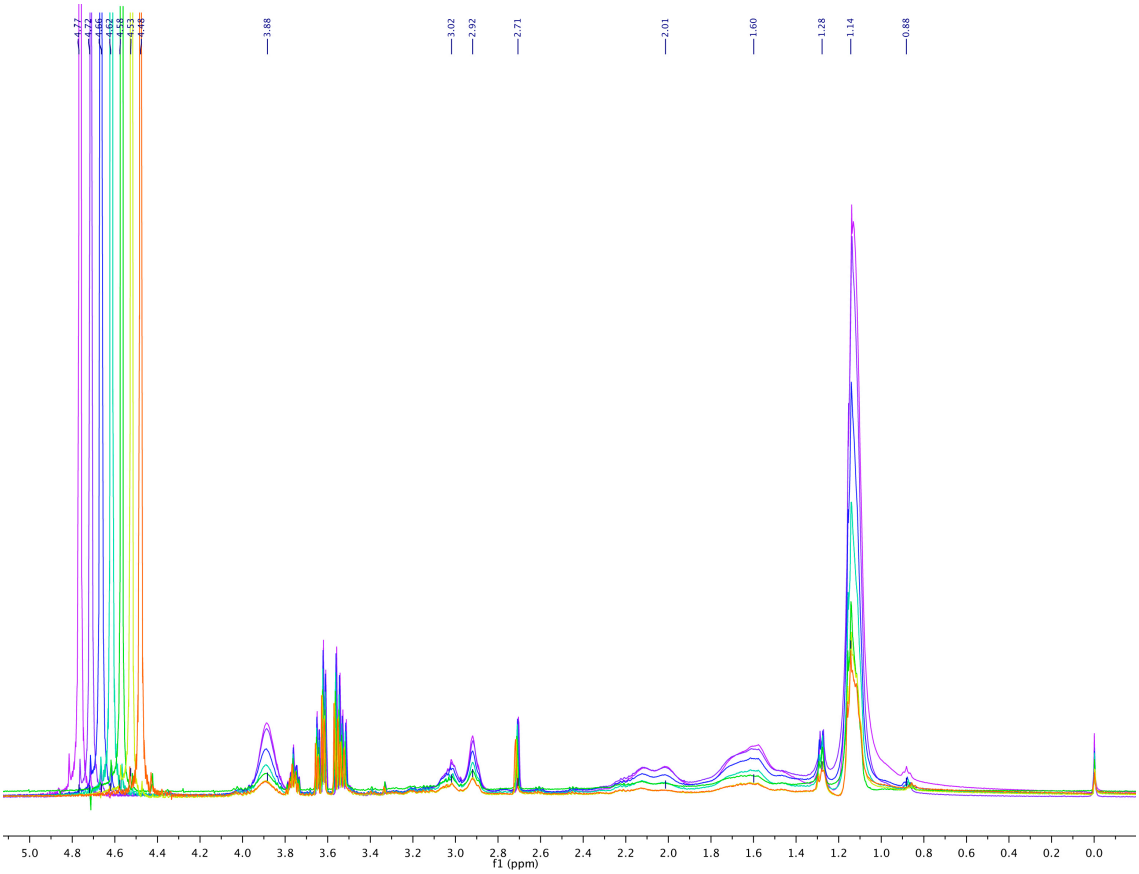

Figure 2.12: ^{1}H-NMR spectrum of ND 25 AA PFM AF660 at different temperatures: at 25°C (violet), at 30°C (lilac), at 35°C (dark blue), at 40°C (light blue), at 45°C (green), at 50°C (yellow) and at 55°C (orange). NIPAAm signals: 1.14 ppm CH_3 (6H), at 1.60 ppm CH_2 (2H), at 2.01 ppm CH (1H) and at 3.88 ppm CH (1H). SDS signals: 0.88 ppm CH_3 (3H) and 1.28 ppm CH_2 (10H). HDO signal at 4.5 ppm.

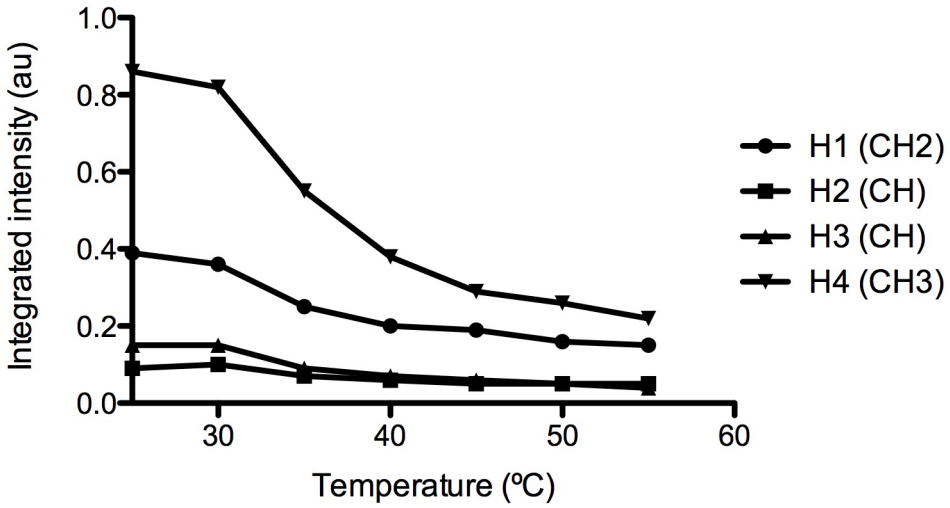

Figure 2.13: Temperature dependence of integrated intensities of the protons of poly(N-isopropylacrylamide) of sample ND 25 AA PFM AF660. The hydrogen nomenclature refers to Figure 2.14

As seen in the spectrum, the intensities of all signals diminish, but in a slightly different way. The methylic protons of the isopropyl group present the most pronounced decrease, followed by the protons of the methylene of the polymer backbone, the proton of the tertiary carbon of the isopropyl group and the proton of the tertiary carbon of the backbone. This makes clear that there is a higher loss of mobility of the methylic protons of the isopropyl group, followed by the others in the order previously mentioned. Interestingly, the highest decrease in intensity is observed for protons that are far away from the amide functionality, which confers the hydrophilic character. On the contrary, the intensity variation is reduced in signals of protons that are directly or closely situated to the amide functionality. These results indicate that parts of the polymer that are situated further from the amide group may experience a more pronounced hydrophobic collapse during phase transition than parts of the polymer that are more exposed to water (Figure 2.14).

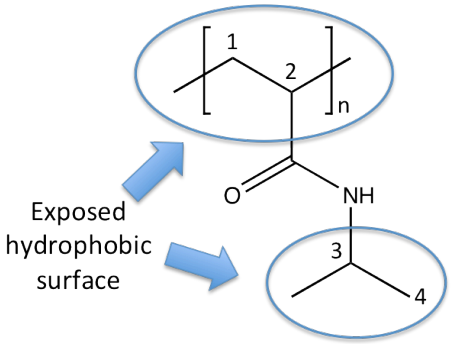

Figure 2.14: Hydrophobic exposed areas of pNIPAAm[7].

LCST transition zone is encompassed by two plateau regions in which the area under the signal practically remained constant (Figure 2.13). The inflection point corresponds to LCST. The signal area does not reach zero at temperatures above LCST, suggesting thereby that a small fraction of low molecular weight species still remains in solution. The same trend has also been reported by other authors[85].

The other sample of the study is ND 25 AA, which has a particle size of 230 nm and presents an inverse behaviour at 35°C, measured by DLS (Figure 2.10). AFM images show nanoparticles around 700 nm, below LCST, and around 600 nm, above LCST (Figure 2.15). Although. AFM results differ from DLS results; the size variation when heating is around 100 nm in both techniques. In this case, nanoparticles are also very sharp, below LCST, and acquire a rounded shape above it. The flattening of the nanoparticles is not as pronounced as in the other sample. A decrease in height is also observed at temperatures above LCST (Figure 2.15B).

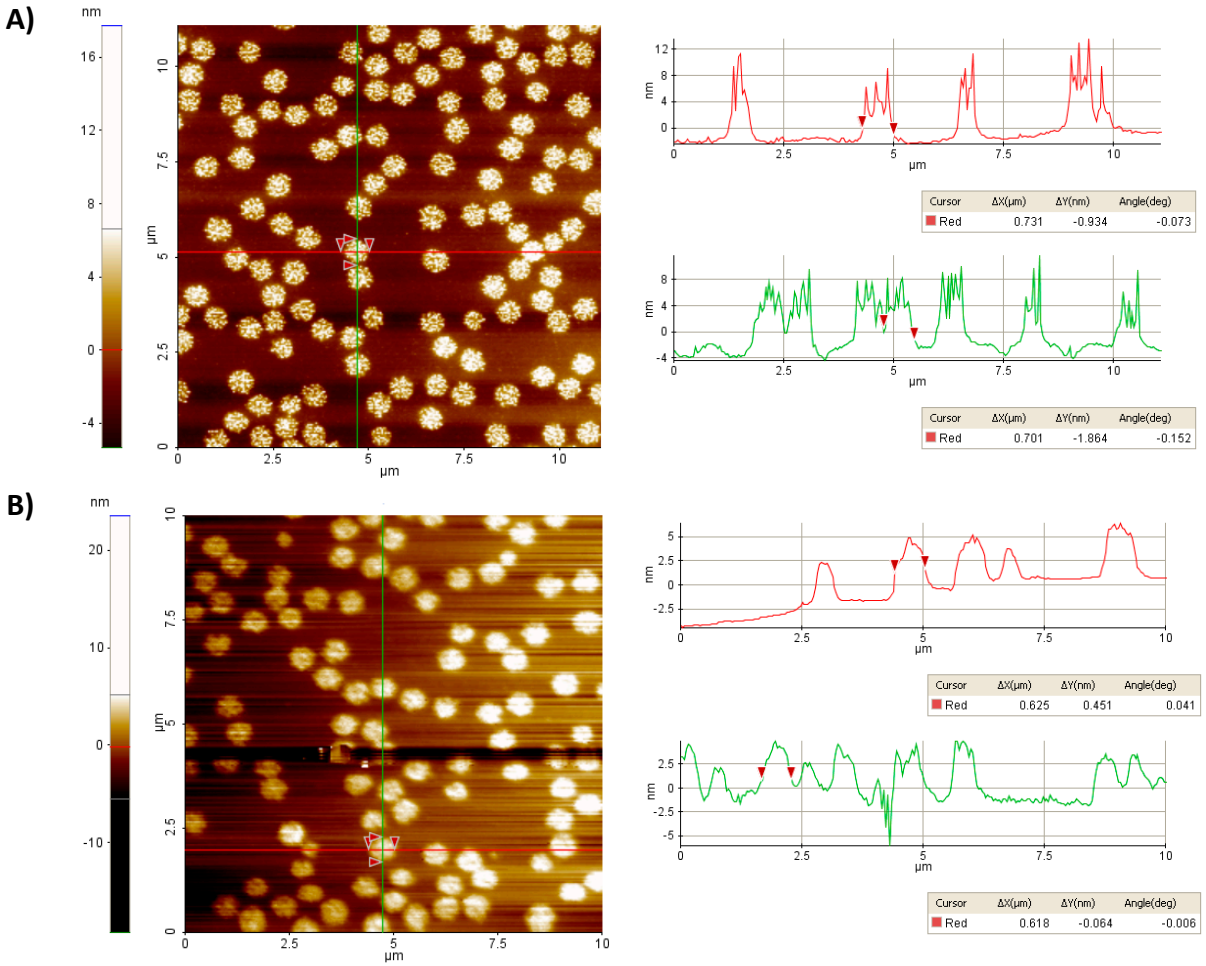

Figure 2.15: AFM images of ND 25 AA at different temperature.A) at room temperature and B) at 62°C.

However, no difference was observed between the ^{1}H-NMR spectra of both samples. Below LCST, at 25, 29, 32 and 34°C, signals are nearly superimposed. Above LCST, at 37°C, the broadening of the signals is already visible (Figure 2.16).

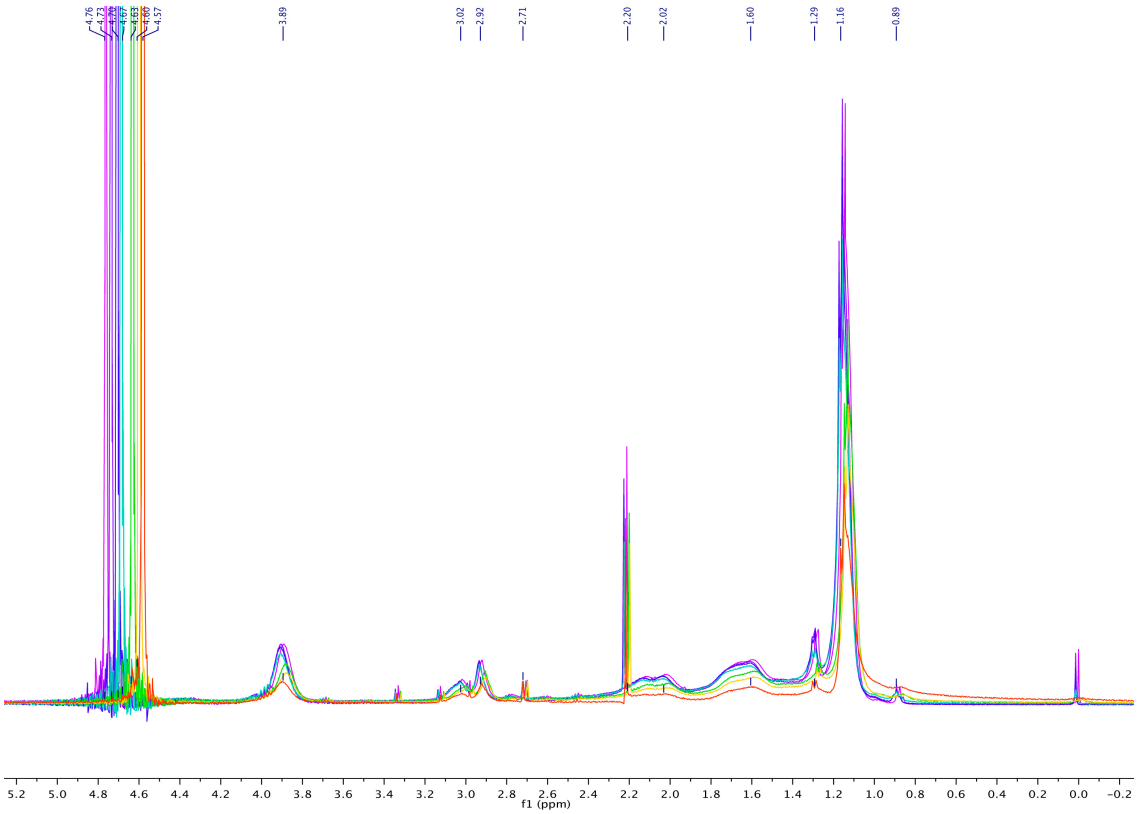

Figure 2.16: ^{1}H-NMR spectrum of ND 25 AA at different temperatures: at 25°C (violet), at 29°C (lilac), at 32°C (dark blue), at 34°C (light blue), at 37°C (green), at 40°C (yellow) and at 44°C (orange). NIPAAm signals: 1.14 ppm CH_3 (6H), at 1.60 ppm CH_2 (2H), at 2.01 ppm CH (1H) and at 3.88 ppm CH (1H). SDS signals: 0.88 ppm CH_3 (3H) and 1.28 ppm CH_2 (10H). HDO signal at 4.5 ppm.

The studied signals were also the characteristic signals of poly(N-isopropylacrylamide). Their intensity variation towards temperature is plotted in Figure 2.17. Similarly to the previous sample, the graph presents two plateau areas, before and after LCST transition zone. The inflection point at the transition area corresponds to LCST value, 35°C.

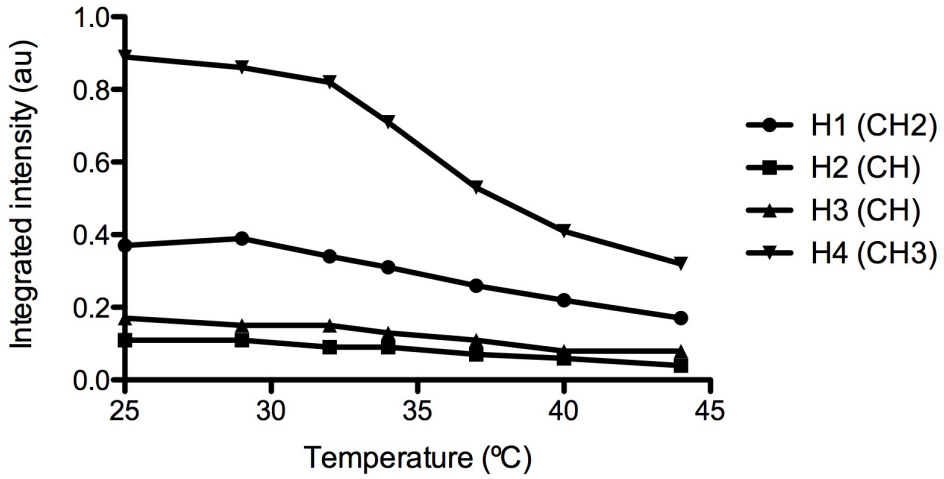

Figure 2.17: Temperature dependence of integrated intensities of the protons of poly(N-isopropylacrylamide) of sample ND 25 AA. The hydrogen nomenclature refers to Figure 2.14

The fact that ^{1}H-NMR spectra for both nanoparticles samples, the ones that increase in size and the ones that shrink when reaching the LCST, show the same behaviour suggest that the thermosensitive polymer is behaving in the same way in both samples, exhibiting an LCST. Therefore the change in size must be caused by the nanoparticles per se probably due to some change in their structure.

Further characterization of this behaviour was done by analysing phase AFM images (Figure 2.18). Figure 2.18A shows round shape nanoparticles presenting three regions of different composition, which suggest a differentiation between the core and the shell material. Above LCST (Figure 2.18B), nanoparticles increase in size and collapse presenting a hollow morphology, where three different regions still can be distinguished although it can be clearly observed that nanoparticles structure is not the same.

A) 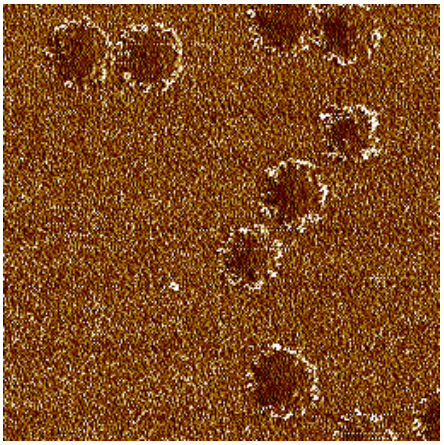 **B)** 

Figure 2.18: AFM phase image of sample ND 29 PFM (Figure 2.9) at room temperature (A) and at 45°C (B).

On the other hand, the results from the study of size transitions of nanoparticles as a function of composition (Table 2.9) show that temperature change varies with polymer composition. Hence, this variation is clearly related with the LCST expected for them.

These results suggest that the dramatic increase in size observed in small nanoparticles above LCST is directly related with a change in conformation from a micelle to a vesicle[86] (Figure 2.19). The formation of polymer vesicles from surfactant/polymer mixed micelles is based on surfactant removal from mixed micelles by dilution, dialysis or temperature increase of a polymer/surfactant mixture of an appropriate composition. Some authors have pointed out, that surfactants can be incorporated into polymer micelles up to a critical saturating surfactant/polymer ratio, which describes the effective surfactant concentration in the bilayer in relation to the total polymer concentration. Beyond this critical ratio, vesicles are destroyed leading to polymer saturated mixed micelles of a minimum effective surfactant/polymer ratio[87].

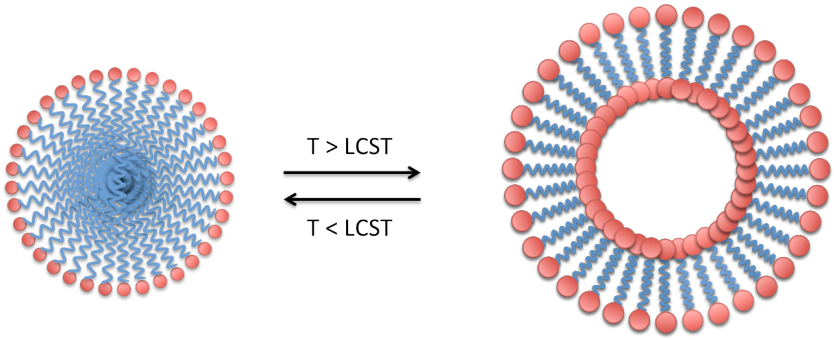

Figure 2.19: Conformational change of a nanoparticle from a micelle, below LCST, to a vesicle, above LCST.

This change in nanoparticles arrangement is related with the change in polymer conformation due to its thermosensitivity (Figure 2.1), promoting a change in the hydrophobic/hydrophilic interactions that lead to the formation of a defined bilayer structure. The result is a fusion-like behaviour between each other, observed by a size increase. The explanation for those nanoparticles, generally larger than usually, which exhibit a decrease in size above LCST, may be related with the critical surfactant/polymer ratio. Thus, in a solution of large nanoparticles with a low content of surfactant, vesicles cannot be formed and no increase in size is observed. Instead, a decrease in size of the micelles can be seen behaving in the same way of the polymer, showing shrinkage above LCST. This is in good agreement with the information described in literature for the morphology of self-assembled systems in surfactant solutions[88,89].

2.3.4 Drug loading and release

After full characterization of nanoparicles thermosensitive behaviour, the drug loading capacity of the synthesized nanoparticles was determined. As mentioned before, these thermo-responsive systems can be used not only for cancer therapy but also for oral delivery. In fact, acrylamide-based systems can encapsulate hydrophilic compounds, such as proteins or peptides, rather than chemotherapeutic agents, which are mainly hydrophobic. Therefore, to evaluate the loading efficiency of these systems, peptides and proteins will be used as model drugs. It has been previously shown that active principles, such as small drugs and peptides or proteins, can be encapsulated into thermosensitive nanoparticles via repeated thermal cycles[90]. In order to check that the synthesized nanoparticles can encapsulate drug, particles were stored at 4°C for a certain time period and then quickly incubated with a solution containing the drug, EMC collagen booster (Figure 2.5), insulin or AGBBB05A (Table 2.2), separately, at initial concentrations of 100 and 165 μg/ml for 30 minutes at a temperature slightly above the LCST. Samples were cooled down at room temperature before determining their loading efficiency.

Average loading efficiency for ECM at an initial concentration of 100 μg/ml was 33 % ± 3.58, while at 165 μg/ml the average loading efficiency reached 53 % ± 3.67. Regarding insulin loading, the average loading efficiency reached 6.8 % ± 3.11, at an initial concentration of human insulin of 100 μg/ml. When the initial concentration was raised up to 165 μg/ml, the loading efficiency average also rose up to to 41.5 % ± 8.52. These results suggest that the initial concentration has a strong effect on the loading efficiency of the nanoparticles, rising with increasing initial drug concentration.

Slight differences between ECM and insulin loading can also be observed at the same initial concentration (165 μg/ml). The loading efficiency average for ECM is 53% while it is 41.5% for insulin. This result is in good agreement with drug size, as ECM peptide (862.24 g/mol) is smaller than insulin (5808 Da), and thus, may diffuse easier into nanoparticles matrix.

To study the influence of the chemical composition of nanoparticles on the loading efficiency of human insulin, different types of nanoparticles were synthesized, having different composition, size, zeta potential and LCST, as shown in Table 2.10.

Table 2.10: Different types of nanoparticles with different composition, size, zeta potential, LCST and loading efficiency of insulin.

	Sample	Characteristics				
		Coating molecules	Size (nm)	Zeta potential (mV)	LCST (°C)	Loading efficiency (%)
1	ND 29	-	36	-1.57	47	46
2	ND 25 AA PFM SH	SH	55	-8	34	39
3	ND 29 PFM SH AF488	SH/AF488	81	-1.16	34	27
4	DD10 PFM AF488	AF488	23	-7	35	36

Interestingly, the nanoparticle that shows the highest loading efficiency is ND 29, which only consists of an acrylamide core without any shell, whereas for coated nanoparticles the loading is lower. Among coated nanoparticles, some differences can be observed. The next nanoparticle type with higher loading efficiency is the one with the less voluminous moiety (number 2), followed by number 4 that is coated with alexa fluor cadaverine 488, which is more voluminous than the thiolated moiety. Finally, the nanoparticle with lower loading efficiency is the one with the largest shell, number 3, which is thiolated and labelled. These results suggest that the bigger the coating moiety is, the lower the loading efficiency will be, regardless of the particle size. A reasonable explanation for this effect may be the difficulty that the drug has to diffuse through the polymeric network when coating moieties are very voluminous.

Regarding zeta potential, it can be observed that it may not play an important role in this aspect, as nanoparticles with the highest and the lowest loading efficiencies show the same values. It should be taken into account that nanoparticles suspension had an acidic pH, consequently insulin will be positively charged as it is below its isoelectric point, indicating that repulsive interactions will not be present between the drug and the negatively charged nanoparticle.

Contrary to loading, drug release is achieved by heating nanoparticles solution at the LCST and stirring. In this case, the whole process, loading and release, was accomplished by following AGBBB05A signal in HPLC/MS, as there was a well-established method to monitor its release. Nanoparticles (ND 25 AA PFM SH AF660 AGBBB015I; 145 nm and -9.15 mV) were loaded with an initial concentration of 316 ng/ml of AGBBB05A. Loading efficiency was determined by HPLC/MS. Figure 2.20 shows the percentage of AGBBB05A release as a function of incubation time at 45°C.

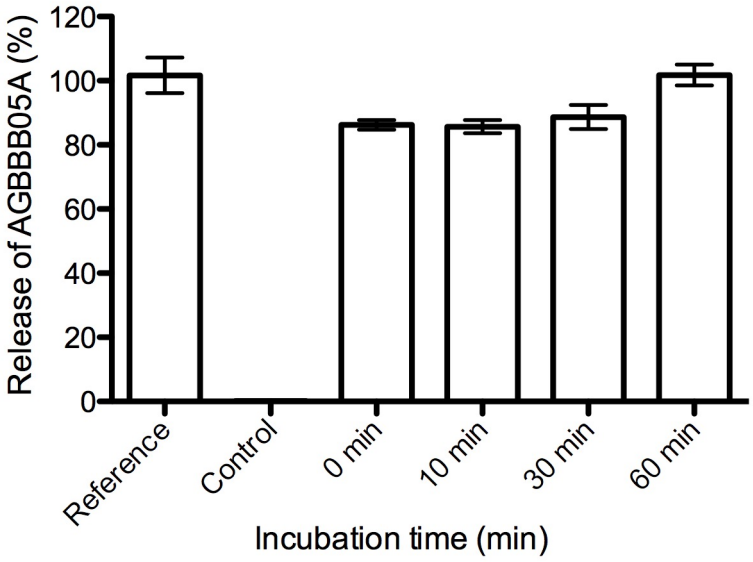

Figure 2.20: AGBBB05A release as a function of incubation time at 45°C. Pure AGBBB05A at initial concentration was used as a reference while non-loaded nanoparticles incubated for 60 minutes at 45°C served as a control.

It can be observed that non-incubated nanoparticles solution has a large amount of free peptide (85.7%) that was not entrapped inside the nanoparticles as the loading efficiency was 14.3%. This low loading efficiency may be attributed to the large nanoparticle shell as they are coated with AGBBB015I peptide.

Despite this fact, as incubation time is increased the amount of peptide in the solution is increased, thus showing the release of the entrapped peptide. The total amount of peptide loaded is completely released after 60 minutes at 45°C.

2.3.5 Nanoparticle-cell interaction

Although pNIPAAm and its copolymers have been good candidates for controlled drug release because of its thermosensitivity, biocompatibility is still a major concern in the use of pNIPAAm nanoparticles as drug carriers, due to the high toxicity of NIPAAm monomer. Some preliminary tests have been done on PEGylated NIPAAm nanoparticles, showing no toxicity at a concentration of 2mg/ml of nanoparticles for a time period of 24 hours. However, a 93% reduction in cell viability was observed when NIPAAm monomer was incubated at the same concentration[19]. In addition, there are many concerns regarding the effects of these nanoscale materials. Because of their nanometric dimension, the pharmacodynamic properties of nanoparticles may differ greatly from small drugs and unexpected adverse effects may arise. In principle, nanoparticles are small enough to resist cellular defence systems, but large enough to interfere with cell processes.

For this reason, after having fully characterized and loaded nanoparticles the next step is to evaluate the body response to them at a cellular level. Nanoparticles with different size and surface coatings were evaluated in terms of cytotoxicity and hemocompatibility to evaluate the influence of these parameters on their suitability.

2.3.6 Biocompatibility

2.3.6.1 Cytotoxicity

Cell damage can occur trough a diverse range of mechanisms that disrupt cellular integrity. Membrane-soluble or pore-forming compounds may act directly on the cytoplasmic membrane and prevent the cell maintaining homeostatic integrity, leading to cell lysis. Other compounds may act directly to disrupt cell's biochemical, synthetic or signalling pathways, leading to apoptosis.

For oral drug delivery route, the cell model chosen was caco-2 cell line, serving as a model for the epithelial intestine. Whereas for BBB delivery route, the selected cell line was human umbilical vein endothelial cells (HUVEC). Endothelial cells (cells that line the vascular system) form a physical barrier for particles, having very tight junctions, typically smaller than 2 nm. Nevertheless larger values, from 50 nm up to 100 nm have been reported, depending on the organ or tissue[53].

The results shown below correspond to cell viability determined by MTS for two samples of nanoparticles, one coated with RP3 peptide (ND 25 AA PFM RP3) and its blank, which consists of a sample of the same batch without targeting peptide (ND 25 AA PFM).

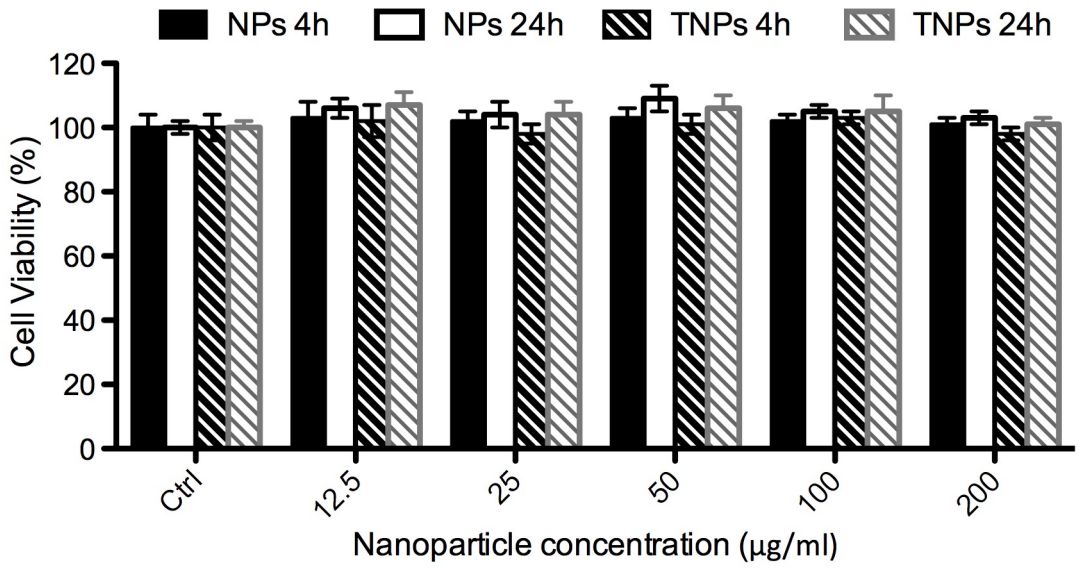

Figure 2.21: Cell viability in percentage of control at increasing nanoparticle concentration at 4 and 24 hours. NPs = ND 25 AA PFM and TNPs = ND 25 AA PFM RP3 (targeted nanoparticles). Bars = ± SD (n=4)

Figure 2.21 shows the effect of nanoparticles on cell viability, indicating no statistically significant differences at the concentrations tested, ranging from 12 to 200 µg/ml. Neither difference was observed between short-term (4 hours) and medium-term culture (24 hours). The difference between the blank nanoparticles and the targeted ones was negligible.

The quantification of the ATP present is a signal of the presence of metabolically active cells, that is, viable cells. Figure 2.22 shows the effect of nanoparticles on metabolically active cells, indicating a slightly decrease in the number of viable cells

towards concentration; this is, for higher nanoparticle concentration the number of viable cells is lower. The effect of nanoparticles for medium culture times (24 hours) is lower than at short time culture. In this case, there are also slightly differences between uncoated and targeted particles, but, in general, the nanoparticles are well tolerated.

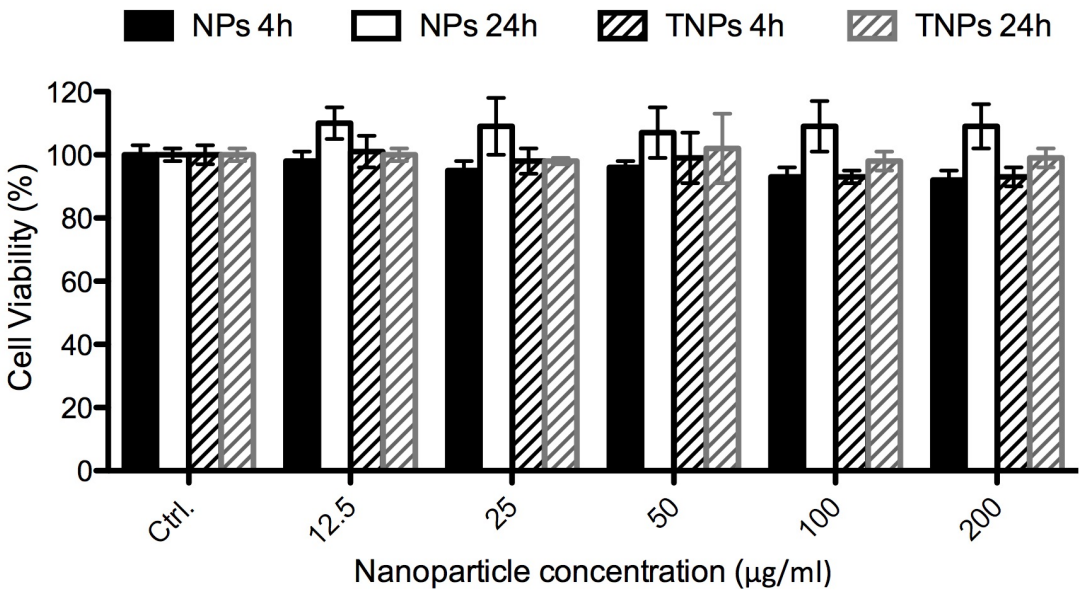

Figure 2.22: Cell viability in percentage of control at increasing nanoparticle concentration at 4 and 24 hours. NPs = ND 25 AA PFM and TNPs = ND 25 AA PFM RP3 (targeted nanoparticle). Bars = ± SD.

In summary, the MTS assay, the membrane integrity assay and the ATP quantification prove no influence of nanoparticles, at a maximum concentration tested of 200 μg/ml. on cell viability.

2.3.6.2 Hemocompatibility

Blood represents one of the most complex biochemical systems in living organisms, and its multiple components play integral roles in several life functions, including the transport of oxygen, destruction of pathogens and repair of damaged tissues. Because these functions are critical, drugs and medical devices that have to be frequently in contact with blood stream must be hemocompatible[91].

Therefore, it is a fundamental requirement to evaluate the hemocompatiblity of the nanoparticles, especially for those that are designed to cross the blood brain barrier. Indeed, they will be first dispersed in the blood stream and therefore will be able to cause several toxicological reactions, in particular: embolization, haemolysis, cellular activation, but also several well-known biological cascades such as coagulation, complement activation, kininogen and fibrinolysis.

In addition, it has to be kept in mind that when targeting nanoparticles to the CNS, the first barrier this nanomaterial will meet before the BBB is blood itself and the reticuloendothelial System (RES), which is directly connected to it. Indeed, the clearance system efficiency to eliminate foreign bodies from the circulating blood is so high that their blood lifetime does not exceed some minutes. To make sure the

suitability of a drug system delivered to the brain, hemocompatibility must be verified, both for toxicological reasons and efficiency of the targeting.

Firstly, as mentioned before for cytotoxicity tests, a visual examination of red blood cell's morphology was performed in a smear after exposure to nanoparticles at the highest concentration tested. Figure 2.23 shows no anomaly in red blood cells morphology incubated with nanoparticles. They are round-shaped and have a uniform cytoplasmatic membrane, when compared to untreated control cells.

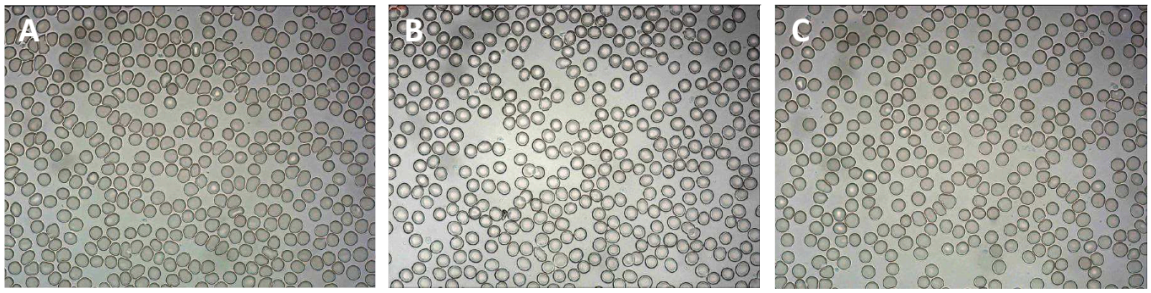

Figure 2.23: Optical miscrocope images of whole blood after material exposure (smear) at the highest concentration tested (350 μg/ml). A) Control incubated with PBS. B) ND 25 AA PFM. C) ND 25 AA PFM RP3 (magnification 50x).

Haemolysis is regarded as an especially significant screening test to perform in this category because of its measurement of red blood cell membrane fragility in contact with materials and devices[91]. Therefore, a haemolytic test is performed according to ASTM to determine the haemolytic potential of nanoparticles. This test is based on the quantification of plasma haemoglobin, released when lysis of red blood cells takes place.

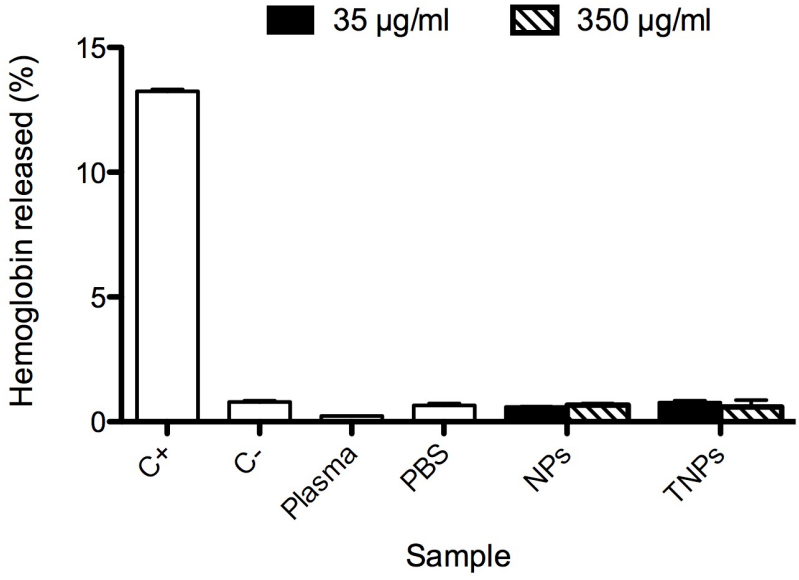

Figure 2.24: Percentage of haemoglobin released. C+=positive control, C-= negative control, NPs= ND 25 AA PFM and TNPs= ND 25 AA PFM RP3. Bars= ± SD

Figure 2.24 shows the percentage of released haemoglobin after incubation with the nanoparticles. It can be observed that both samples of nanoparticles do not cause an increase in the percentage of haemolysis according to negative control and PBS

values at the concentration tested. Typically, less than 5% haemolysis is considered acceptable for blood biocompatibility[19]. On increasing the concentration, no significant increase in haemolysis percentage was detected.

To discard any significant interaction of the nanoparticles with red blood cells and platelets, both cell types were counted and their size distributions analysed. Figure 2.25 shows red blood cell size distribution for controls and different nanoparticles concentrations. None of them show any anomaly.

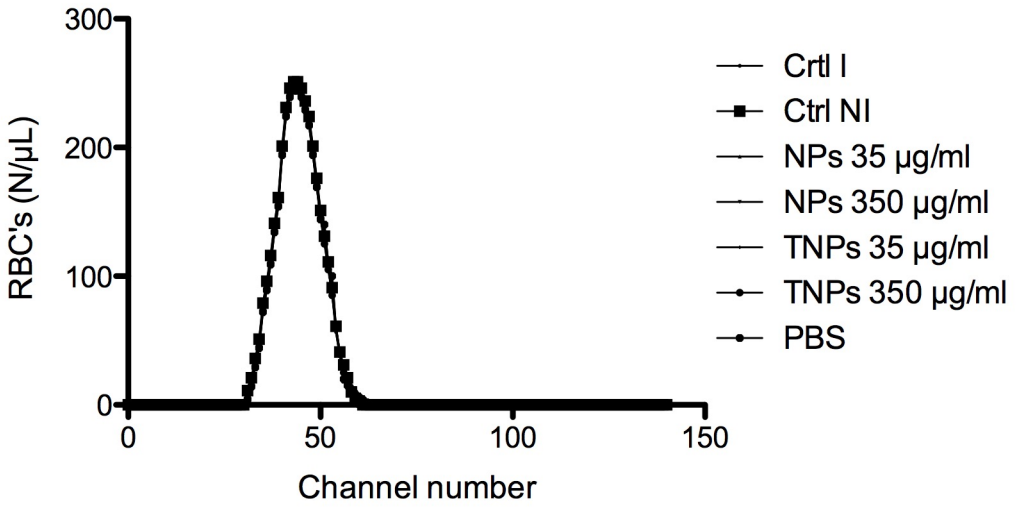

Figure 2.25: Size distribution of Red Blood Cells (RBC). Ctrl I= blood control incubated, Ctrl NI= blood control non-incubated, NPs= ND 25 AA PFM and TNPs= ND 25 AA PFM RP3

RBC count is shown Figure 2.26. No significant decrease in RBC concentration is observed for samples incubated with nanoparticles at both concentrations. All values are within the expected range, which is between 4 and 5 million of RBC/µL for an adult human[92].

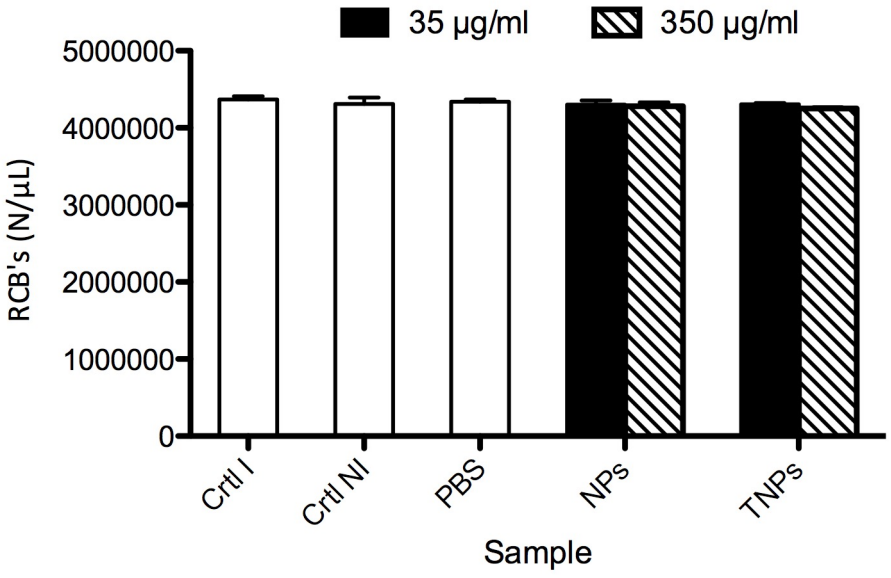

Figure 2.26: Red blood cells concentration. Ctrl I= blood control incubated, Ctrl NI= blood control non-incubated, NPs= ND 25 AA PFM and TNPs= ND 25 AA PFM RP3. Bars= ± SD

Similarly, the compatibility of the nanoparticles with platelets was evaluated by assessing the size distribution of platelets, as shown in Figure 2.27. Platelets keep their size when incubated with different concentrations of nanoparticles.

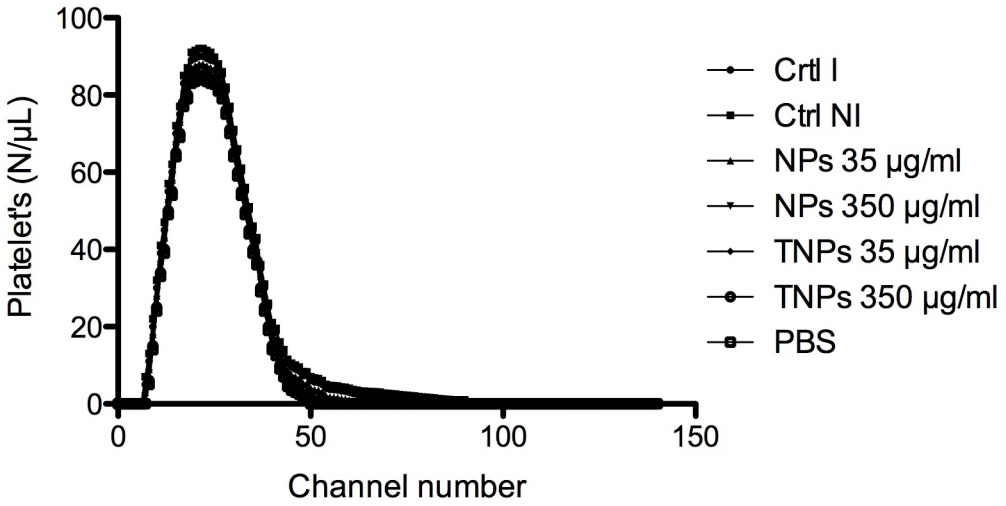

Figure 2.27: Size distribution of platelets. Ctrl I= blood control incubated, Ctrl NI= blood control non-incubated, NPs= ND 25 AA PFM and TNPs= ND 25 AA PFM RP3

Figure 2.28 shows platelets concentration for controls, PBS and different nanoparticles concentration. There is no variation of the platelets concentration between blood samples incubated with nanoparticles and blood incubated with control (Ctrl I). Moreover, there is no variation in platelet concentration when a higher concentration of nanoparticles was tested. All values are within the normal range for platelet count, which is between (150 - 400) x 10^3 N/µL[19].

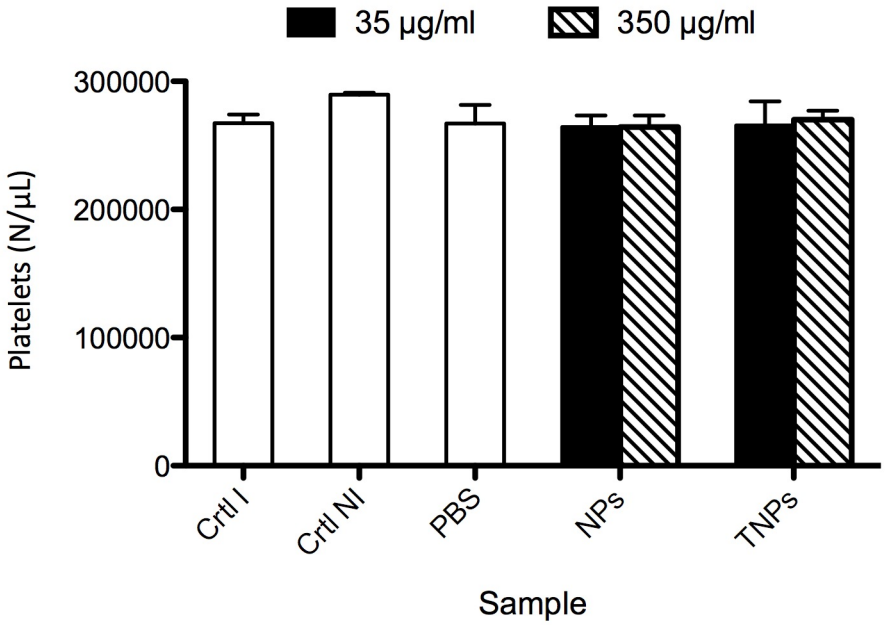

Figure 2.28: Platelet concentration. Ctrl I= blood control incubated, Ctrl NI= blood control non-incubated, NPs= ND 25 AA PFM and TNPs= ND 25 AA PFM RP3. Bars= ± SD

It should not be forgotten that blood plays an important role in the immune system. Complement system is a central part of the innate immune system, providing a

highly effective means for destruction of invading microorganisms, clearance of immune complexes and elimination of dead and apoptotic cells[93]. It consists in an enzyme cascade that facilitates the elimination not only of pathogens but also other foreign materials from our body.

Nanoparticles can be cleared from the blood circulation as a consequence of complement activation in particular via the alternative pathway, which arises from the C3 hydrolysis to form C3a and C3b. Due to the large surface exposed, nanoparticles in suspension within the blood could enhance the activation of the complement. They may adsorb serum proteins such as albumin, fibrinogen and XII factor, as well as C3. Therefore, interaction between nanoparticles and complement C3a must be tested, in order to ensure minimal activation of the complement system.

Figure 2.29 shows the percentage of activation of C3a. There is a slight increase of complement activation by nanoparticles compared to controls, but the difference is not statistically significant. For higher nanoparticle concentrations, there is a slight increase in complement activation that is not statistically significant.

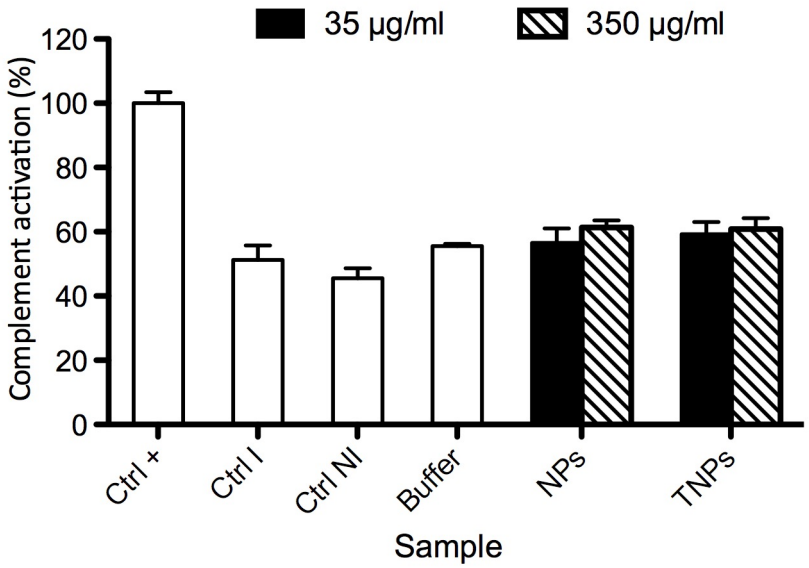

Figure 2.29: Percentage of complement C3a activation. Ctrl+= positive control, Ctrl I= blood control incubated, Ctrl NI= blood control non-incubated, NPs= ND 25 AA PFM and TNPs= ND 25 AA PFM RP3. Bars= ± SD

An artificial toxic material can activate the complement cascade as well as it can activate platelets and coagulation pathways. Therefore, an analysis of the activation of the coagulation cascade either by the intrinsic (ACT) or the extrinsic (PT) cascade was performed. The ACT assay (Activating Clotting Time)[94] measures the time required to form a clot when adding an activator of the coagulation, in this case, kaolin. Basically, it demonstrates if the factors associated with this cascade are adsorbed or denatured by foreign material, e.g. nanoparticles. A reduction of the percentage corresponds to an inactivation of this coagulation pathway.

The PT (prothrombine time) assay is used for the detection of inherited or acquired coagulation defects related to the extrinsic (tissue factor) pathway of coagulation[95]. In this case, the coagulation activator used is thromboplastin. In the same way as the ACT assay, it verifies if the factors associated to this cascade are

adsorbed or denatured by nanoparticles. A reduction of the percentage corresponds to an inactivation of this coagulation pathway. The results of ACT and PT assays are plotted in Figure 2.30.

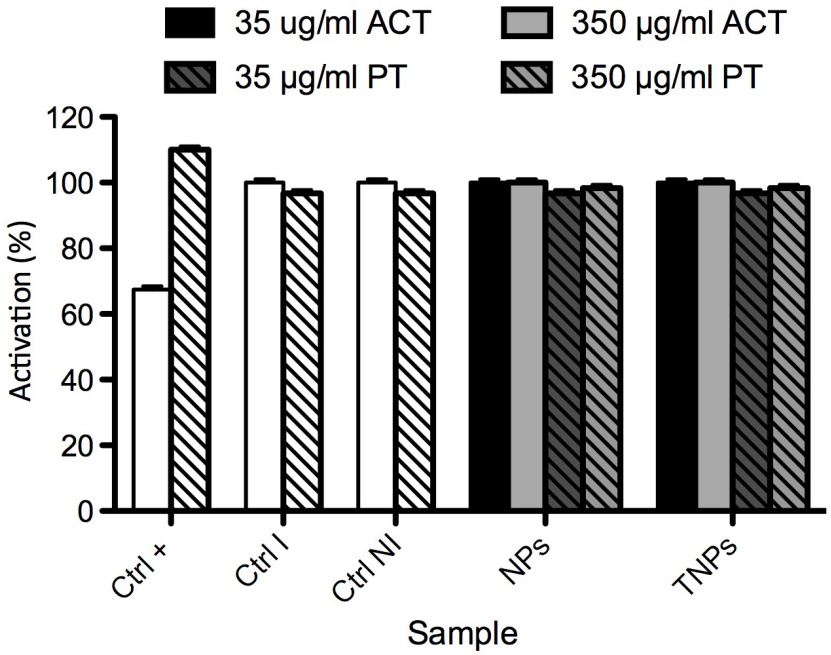

Figure 2.30: Percentage of activation of the intrinsic (ACT) and the extrinsic (PT) coagulation pathway.ACT in solid bars and PT in striped bars. Ctrl+= positive control, Ctrl I= blood control incubated, Ctrl NI= blood control non-incubated, NPs= ND 25 AA PFM and TNPs= ND 25 AA PFM RP3. Bars= ± SD

In the ACT assay, the percentage of activation of the coagulation of nanoparticles is essentially the same as the incubated control, meaning that both samples do not interfere at all in the coagulation process in any of the concentrations tested. Regarding the PT assay results, no inactivation of the coagulation pathway is observed for both samples at any of the tested concentrations.

In the light of the results, ND 25 AA PFM and ND 25 AA PFM RP3 are found to be hemocompatible in all the tested concentrations and did not show any significant interaction with RBCs, platelets, complements and coagulation factors.

Although, several authors have demonstrated that size and surface groups of nanoparticles are critical parameters that have a great influence on cytotoxicity and hemocompatibility, synthesized nanoparticles with different sizes and surface coatings (Table 2.11) presented no cytotoxic effects and were hemocompatible.

Table 2.11: Tested nanoparticles with different sizes and surface coatings.

Sample	Surface groups	Size (nm)	Zeta potential (mV)
ND 25 AA PFM	-	174	-5.89
ND 25 AA PFM RP3	RP3	500	-13.06
ND 25 AA PFM SH AF660 AGBBB015I	AGBBB015I	145	-9.15
ND 25 AA PFM SH AF660 AGBBB015F	AGBBB015F	375	-18.3
ND 25 AA PFM CH_3	CH_3	100	-10
ND 25 AA PFM PEG	PEG	111	-6.29
ND 25 AA PFM OH	OH	100	-20.16
ND 25 AA PFM AF660 RGDS	RGDS	211	-14.85

Table 2.11 shows the nanoparticles that have been tested in terms of cytotoxicity as well as hemocompatibility. Nanoparticles size ranged from 100 to 500 nm and surface coatings involved BBB-passing peptides, which are RP3, AGBBB015I and AGBBB015F, integrin ligands, such as RGDS, and other chemical species such as PEG, CH_3 and OH.

2.3.7 Cellular uptake

Once biocompatibility of acrylamide-based nanoparticulate systems has been demonstrated, the suitability of these systems can be tested *in vitro*. Firstly, as they are easily targetable systems, the specificity of this targeting strategy will be evaluated as a proof of concept.

The potential drug delivery of our nanoparticles was validated via the comparison of cellular uptake of two different nanoparticles in various cell lines. The cellular uptake assay was focused on the efficacy of two of the BBB-passing peptide used in this chapter, AGBBB015I and RP3. Therefore, the samples selected for this study were nanoparticles coated with RP3 (ND AA 25 PFM RP3), nanoparticles coated with AGBBB015I (ND 25 AA PFM SH AF660 AGBBB015I) and their respective blanks, taken as controls.

Three different endothelial cell lines, HCMEC, HDMEC and HUVEC, were chosen to assess the cellular uptake of targeted and non-targeted nanoparticles. HCMEC are brain microvascular endothelial cells, HDMEC are primary human microvascular endothelial cells and HUVEC are primary human macrovascular endothelial cells. The aim of this experiment was to determine if targeted nanoparticles were selectively taken up by brain endothelial cells (HCMEC), or if they were indistinctively taken up by other endothelial cells (HDMEC and HUVEC).

Previously, an MTS assay and an E-selectin expression assay (CAM-EIA) to determine the expression of E-selectin were performed. E-selectin is a endothelial cell surface adhesion molecules, also known as Endothelial Leucocyte adhesion molecules 1 (ELAM-1), that is expressed by cytokine-activated endothelium that mediates the adhesion of blood neutrophils[96].

Figure 2.31 shows the results of CAM-EIA assay. After 4 hours of treatment, a slight increase in E-selectin expression can be observed at a concentration of 350 μg/ml for all the samples tested. After 24 hours of treatment, an increase is also observed at all concentrations, being significant at the maximum one. The behaviour is very similar for all the samples.

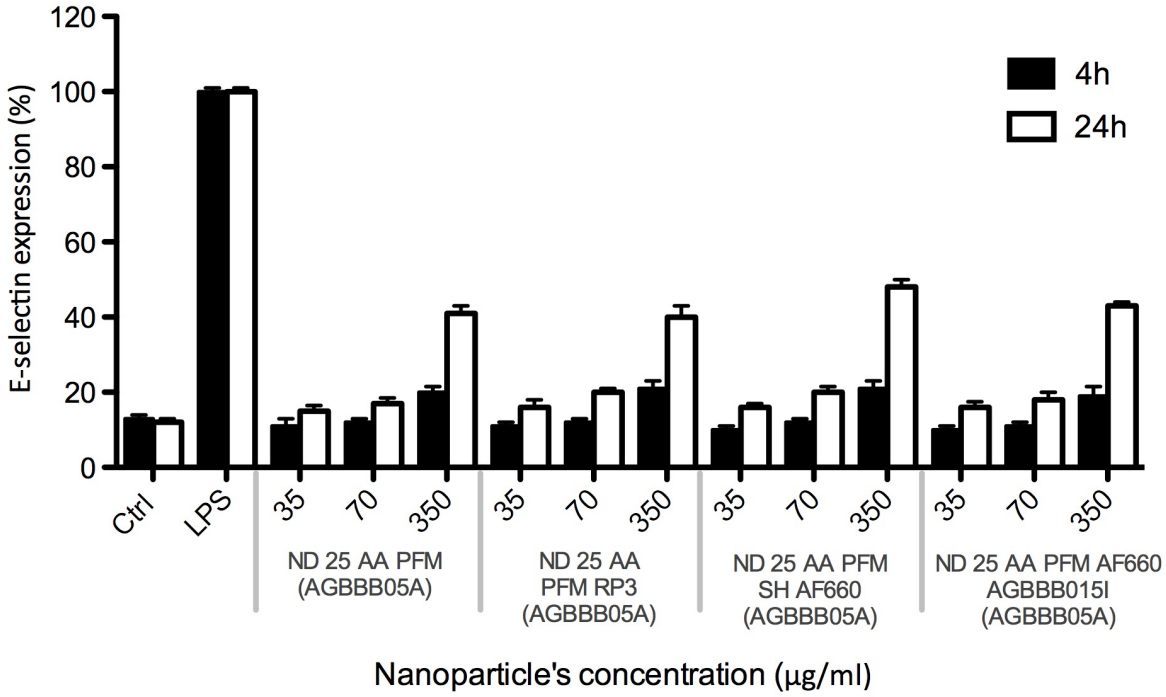

Figure 2.31: E-selectin expression in HUVEC after treatment with different samples for 4 and 24 hours. Ctrl= negative control and LPS= positive control.

All the samples used for this study were previously tested and were found to be non-cytotoxic, hemocompatible and endotoxin free. In addition, the fact that no considerable increase at a concentration of 70 μg/ml compared to 35 μg/ml can be seen, may suggest that none of the negative interactions seen in these results can be considered as a consequence of cytotoxicity or endotoxin contamination, but rather as an effect of the nanoparticles. However, in cells incubated with higher concentration of polymer, 350 μg/ml, a slight increase in E-selectin expression was observed.

On the other hand, the results of MTS assay show no influence of any of the nanoparticles on cell viability even at 24 hours (Figure 2.32). The slight decrease in cell viability for ND 25 AA PFM SH AF660 (AGBBB05A) and ND 25 AA PFM SH AF660 AGBBB015I (AGBBB05A) at 4 hours was considered statistically not significant.

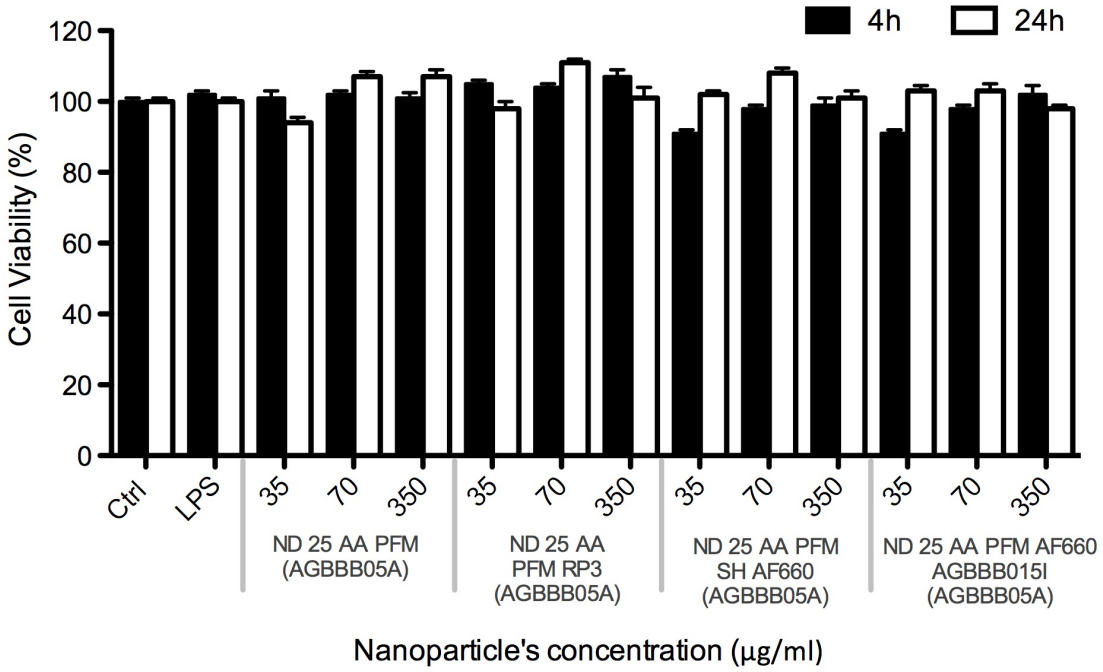

Figure 2.32: Cell viability of HUVEC after the treatment with different samples for 4 and 24 hours. Ctrl= negative control and LPS (lipopolysaccharide)= positive control.

In order to study the cellular uptake of the nanoparticles, they were loaded with a fluorescently labelled peptide. Targeted and non-targeted nanoparticles (both loaded with fluorescent peptide) were incubated with the three chosen cell lines and the resulting fluorescence was evaluated in a fluorescent microscope.

Figure 2.33 shows nanoparticle uptake in HUVEC, HDMEC and HCMEC at a concentration of 70 μg/ml. Irregular uptake of all nanoparticles were observed throughout the different cell lines. Slight differences between cell lines can also be observed. In the case of HCMEC, the uptake is lower than in the other cell lines, especially for non-targeted nanoparticles, which is almost negligible. However, no significant differences are observed for HDMEC and HUVEC. This fact seems to be reasonable as blood-brain barrier endothelial cells are much more selective than other endothelial cells from the rest of the body. Peptide specificity can be observed in HCMEC cells, as almost no fluorescence was observed in cells treated with non-targeted nanoparticles. In addition, cells incubated with targeted peptides showed fluorescent nanoparticles inside the cell, suggesting peptide-mediated internalization, for both RP3 and AGBBB015I.

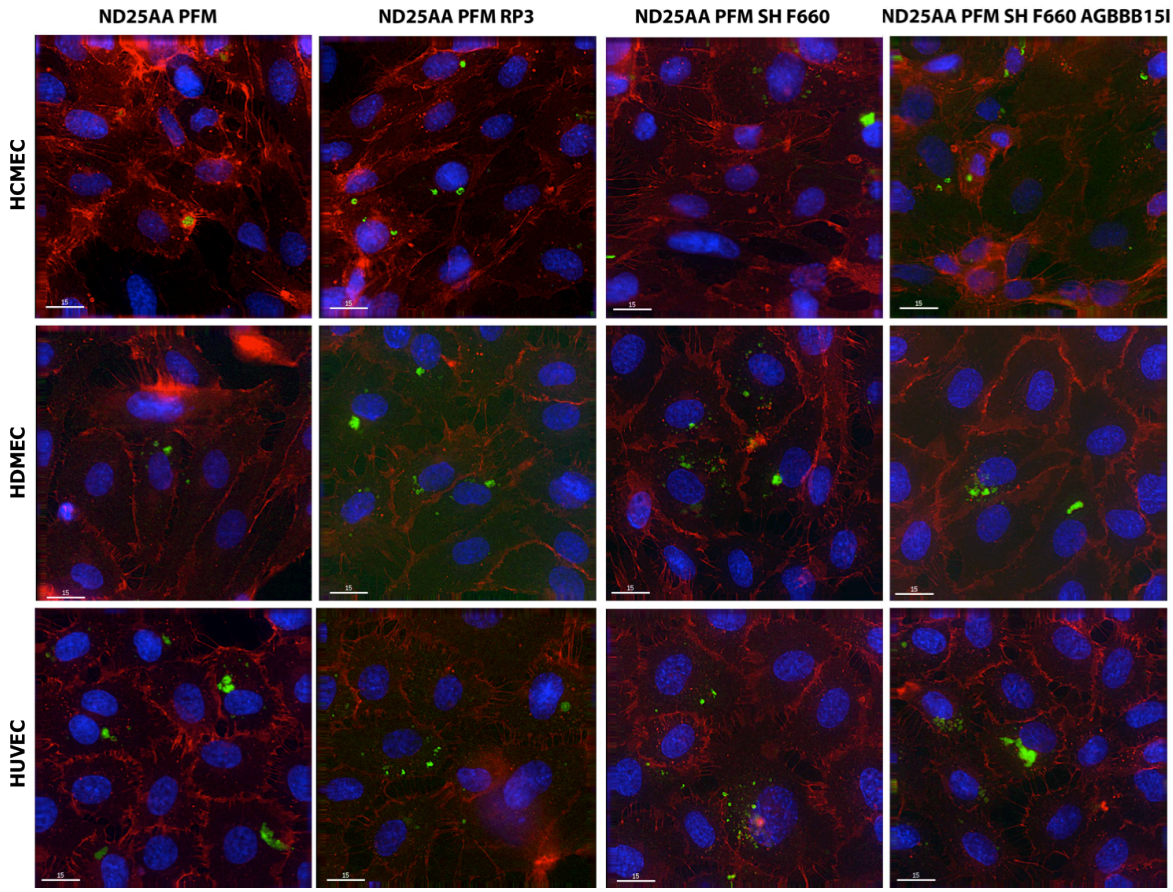

Figure 2.33: Nanoparticles uptake in HCMEC, HDMEC and HUVEC after 24 hours. Nuclei are stained in blue and cell membrane in red.

In the case of HDMEC, a slight difference in uptake of non-targeted and targeted nanoparticles is also visible. Suggesting also a higher affinity of this cell line towards peptide-targeted nanoparticles.

No significant difference in uptake is observed between targeted and non-targeted nanoparticles (both RP3 and AGBB015I) in the case of HUVEC, suggesting that signal peptide targeting does not provide higher specificity to the system compared to the non-targeted nanoparticles. A feasible explanation for the similarity in the uptake of non-targeted and targeted particles might be the high rate of non-specific endocytosis, which is typical of this cell line.

Interestingly, thiolated nanoparticles (ND 25 AA PFM SH F660) seem to be more favourably taken up by all cell lines in comparison to uncoated nanoparticles (ND 25 AA PFM).

A feasible explanation for the similarity in the uptake of non-targeted and targeted particles is the low targeting density, as it has been found to be a critical factor in cellular uptake, with higher densities providing greater uptake through cooperativism[67].

Although not conclusive, this assay shows differential uptake in all three cell lines, specially between HCMEC and the other lines, suggesting peptide specificity in

intracellular trafficking of nanoparticles. However, further experiments on nanoparticles uptake and peptide efficacy should be performed.

2.4 Concluding remarks

In this chapter it has been demonstrated that free-radical polymerization in microemulsion was a simple and fast method to synthesize acrylamide-based nanoparticles, ranging from 23 nm to 740 nm in size, presenting different Low Critical Solution Temperatures (LCST) ranging from 29 to 45°C, and negative zeta potential. Core-shell approach using poly(pentafluorophenyl methacrylate) (pPFM) as a linker has been found to be a good method to coat nanoparticles with a large variety of molecule containing amino groups with different molecular weights and structures. As it was expected, the final size of the nanoparticles depends on the size of the coating moieties added to the shell. Hence, the larger the coating moieties are, the larger the nanoparticle will be. Therefore, nanoparticles size can be tuned by regulating the amount of PFM added to the core, and thus controlling the amount of coating moieties. Regarding zeta potential, acrylamide-based nanoparticles showed negative values, which varied as a function of the targeting molecules' nature.

Characterization of the thermo-responsive behaviour of nanoparticles showed the reversibility of the process, as they increase in size above LCST and decrease to their initial size below LCST, shown by DLS and AFM. It has been suggested that this increase in size, in contrast to the characteristic shrinkage of thermosensitive polymers, is caused by a change in nanoparticles conformation from micelle to vesicle due to a change in hydrophobic/hydrophilic interactions that lead to the formation of a bilayer structure above LCST. In addition, it was observed that LCST could be tuned by modifying nanoparticles' core composition and varying comonomers ratio. Surface modification had also a significant effect on the transition temperature, causing its increase for larger coating moieties. This effect may suggest that polymer chains of he nanoparticle lose flexibility with large coating moieties, such as large peptides, and cannot expel water at the same temperature than non-coated nanoparticles. Therefore, higher temperatures may be required for these systems so that polymer chains gain mobility.

As shown by other authors, the loading of thermo-responsive drug delivery systems can be achieved via repeated thermal cycles at the LCST of the employed carrier. Regarding encapsulation of model peptides and proteins, such as ECM, AGBBB05A and Insulin, the highest loading efficiency achieved was 58.7%, 14% and 54.7%, respectively, being higher for higher initial drug concentration. Again, nanoparticle shell showed a strong effect on loading efficiency, being lower for nanoparticles coated with voluminous moieties as they make difficult the diffusion of the drug. In the same way of the encapsulation procedure, release of the entrapped drug, in this case AGBBB05A, by thermo-responsive systems can be achieved by rising temperature again, up to the LCST, as a function of time. Total release of AGBBB05A was achieved after 60 minutes of incubation at LCST.

Regarding the safety of this system, it can be concluded that acrylamide-based nanoparticles are suitable for drug delivery as all the nanoparticles here tested have been found to be non-cytotoxic and hemocompatible.

Finally, a preliminary experiment to evaluate targeting efficacy of these drug delivery systems was performed *in vitro*. Results showed that both coated and non-

coated nanoparticles were taken up by HUVEC and HDMEC because of the high-rate of non-specific endocytosis typical from endothelial cell lines. However, in the case of HCMEC, the uptake was restricted to targeted nanoparticles as brain endothelial cells are much more selective, suggesting peptide specificity for both RP3 and AGBBB015I. Therefore, thermosensitive acrylamide-based peptide-targeted nanoparticles seems to be a promising system to deliver drugs successfully to the brain.

In the light of the results, it can be concluded that the fabrication of thermoresponsive nanoparticles through a core-shell approach by free radical polymerization in microemulsion is an easy and fast method to obtain targeted stimuli-responsive nanoparticulate systems. In addition, this system allows the fine-tuning of nanoparticle's properties, such as size, zeta potential and LCST, by varying the nanoparticle's core composition and selecting different coating moieties. However, the high polydispersity in nanoparticle's size due tot the fast reaction rate typical from free radical polymerization and discrepancies in thermoreponsive behaviour depending on nanoparticles structure, may compromise their use in pharmaceutical applications, where this lack of homogeneity can have a strong influence on the biological activity of the system, showing irregular loading efficiency, release, interaction with cells or uptake. On the other hand, acrylamide-based systems do not appear to be feasible systems for the encapsulation of hydrophobic drugs, such as many chemotherapeutic agents, thus limiting their applicability in cancer therapy. In addition, despite their probed biocompatibility, pNIPAAm utilisation for pharmaceutical applications is still a major concern, although it is still widely used, due to the high toxicity of its monomer, NIPAAm.

Taking these limitations into account, other drug delivery systems are explored in the following chapters, in order to overcome high polydispersity, broaden loading options and avoid the use of acrylamides.

2.5 References

1. de Las Heras Alarcon, C., Pennadam, S. & Alexander, C. Stimuli responsive polymers for biomedical applications. *Chemical Society reviews* **34**, 276–285 (2005).

2. Alexander, C. Drugs take control. *Nature materials* **7**, 767–768 (2008).

3. Graziano, G. On the temperature-induced coil to globule transition of poly-N-isopropylacrylamide in dilute aqueous solutions. *International journal of biological macromolecules* **27**, 89–97 (2000).

4. Zhang, X.-Z., Wang, F.-J. & Chu, C.-C. Thermoresponsive hydrogel with rapid response dynamics. *Journal of materials science. Materials in medicine* **14**, 451–455 (2003).

5. Carter, S., Hunt, B. & Rimmer, S. Highly Branched Poly(N -isopropylacrylamide)s with Imidazole End Groups Prepared by Radical Polymerization in the Presence of a Styryl Monomer Containing a Dithioester Group. *Macromolecules* **38**, 4595–4603 (2005).

6. Rimmer, S., Carter, S., Rutkaite, R., Haycock, J. W. & Swanson, L. Highly branched poly-(N-isopropylacrylamide)s with arginine?glycine?aspartic acid (RGD)- or COOH-chain ends that form sub-micron stimulus-responsive particles above the critical solution temperature. *Soft Matter* **3**, 971 (2007).

7. Zhang, Y., Furyk, S., Bergbreiter, D. E. & Cremer, P. S. Specific ion effects on the water solubility of macromolecules: PNIPAM and the Hofmeister series. *Journal of the American Chemical Society* **127**, 14505–14510 (2005).

8. Purushotham, S. *et al.* Thermoresponsive core-shell magnetic nanoparticles for combined modalities of cancer therapy. *Nanotechnology* **20**, 305101 (2009).

9. Melendez-Ortiz, I. H. & Bucio, E. Stimuli-Sensitive Behaviour of Binary Graft Co-polymers (PP-g-DMAEMA)-g-NIPAAm and (PP-g-4VP)-g-NIPAAm in Acidic and Basic Medium. *Designed Monomers \& Polymers* **12**, 99–108 (2009).

10. Pua, M. L., Yoshitomi, T., Chonpathompikunlert, P., Hirayama, A. & Nagasaki, Y. Redox-active injectable gel using thermo-responsive nanoscale polyion complex flower micelle for noninvasive treatment of local inflammation. *Journal of controlled release : official journal of the Controlled Release Society* **172**, 914–920 (2013).

11. Abulateefeh, S. R. *et al.* Enhanced uptake of nanoparticle drug carriers via a thermoresponsive shell enhances cytotoxicity in a cancer cell line. *Biomater. Sci.* **1**, 434 (2013).

12. Bawa, P., Pillay, V., Choonara, Y. E. & Toit, du, L. C. Stimuli-responsive polymers and their applications in drug delivery. *Biomedical materials* **4**, 022001 (2009).

13. Chen, G., Ito, Y. & Imanishi, Y. Regulation of Growth and Adhesion of Cultured Cells by Insulin Conjugated with Thermoresponsive Polymers. *Biotechnology and bioengineering* **53**, 339–344 (1997).

14. Hatakeyama, H., Kikuchi, A., Yamato, M. & Okano, T. Influence of insulin immobilization to thermoresponsive culture surfaces on cell proliferation and thermally induced cell detachment. *Biomaterials* **26**, 5167–5176 (2005).

15. Soliman, M., Allen, S., Davies, M. C. & Alexander, C. Responsive polyelectrolyte complexes for triggered release of nucleic acid therapeutics. *Chemical communications (Cambridge, England)* **46**, 5421–5433 (2010).

16. Fan, L. *et al.* Novel super pH-sensitive nanoparticles responsive to tumor extracellular pH. *Carbohydrate Polymers* **73**, 390–400 (2008).

17. Yahara, T. *et al.* Relationship between microvessel density and thermographic hot areas in breast cancer. *Surgery today* **33**, 243–248 (2003).

18. Haag, R. & Kratz, F. Polymer therapeutics: concepts and applications. *Angewandte Chemie (International ed. in English)* **45**, 1198–1215 (2006).

19. Gulati, N., Rastogi, R., dINda, A. K., Saxena, R. & Koul, V. Characterization and cell material interactions of PEGylated PNIPAAM nanoparticles. *Colloids and surfaces. B, Biointerfaces* **79**, 164–173 (2010).

20. Meyer, D. E., Shin, B. C., Kong, G. A., Dewhirst, M. W. & Chilkoti, A. Drug targeting using thermally responsive polymers and local hyperthermia. *Journal of controlled release : official journal of the Controlled Release Society* **74**, 213–224 (2001).

21. Chilkoti, A., Dreher, M. R., Meyer, D. E. & Raucher, D. Targeted drug delivery by thermally responsive polymers. *Advanced Drug Delivery Reviews* **54**, 613–630 (2002).

22. Guyton, A. C. & Hall, J. E. *Tratado de fisiología médica*. (Elsevier Saunders, 2011).

23. Duncan, R. The dawning era of polymer therapeutics. *Nature reviews. Drug discovery* **2**, 347–360 (2003).

24. Monteiro, M. J. Nanoreactors for Polymerizations and Organic Reactions. *Macromolecules* **43**, 1159–1168 (2010).

25. Wei, H., Cheng, S.-X., Zhang, X.-Z. & Zhuo, R.-X. Thermo-sensitive polymeric micelles based on poly(N-isopropylacrylamide) as drug carriers. *Progress in Polymer Science* **34**, 893–910 (2009).

26. Zetterlund, P. B., Kagawa, Y. & Okubo, M. Controlled/living radical polymerization in dispersed systems. *Chemical reviews* **108**, 3747–3794 (2008).

27. Liu, S., Hermanson, K. D. & Kaler, E. W. Reversible Addition-Fragmentation Chain Transfer Polymerization in Microemulsion. *Macromolecules* **39**, 4345–4350 (2006).

28. Min, K. & Matyjaszewski, K. Atom Transfer Radical Polymerization in Microemulsion. *Macromolecules* **38**, 8131–8134 (2005).

29. Katime, I., Arellano, J. U. S., Mendiz a abal, E. & Flores, J. Cationic microemulsion polymerization of alkyl acrylates. *Materials science and applications* **1**, 292–300 (2010).

30. Francesch, L., Borros, S., Knoll, W. & F o rch, R. Surface reactivity of pulsed-plasma polymerized pentafluorophenyl methacrylate (PFM) toward amines and proteins in solution. *Langmuir* **23**, 3927–3931 (2007).
31. Cifuentes, A. Tailoring carbon nanotubes properties for gene delivery applications. (2013).
32. Nicolas, J. *et al.* Synthesis of Highly Functionalized Poly(alkyl cyanoacrylate) Nanoparticles by Means of Click Chemistry. *Macromolecules* **41**, 8418–8428 (2008).
33. Tozaki, H. *et al.* Use of protease inhibitors to improve calcitonin absorption from the small and large intestine in rats. *J Pharm Pharmacol* **50**, 913–920 (1998).
34. Morishita, M., Morishita, I., Takayama, K., Machida, I. & Nagai, T. Site-dependent effect of aprotinin, sodium caprate, Na2EDTA and sodium glycocholate on intestinal absorption of insulin. *Biological pharmaceutical bulletin* **16**, 68–72 (1993).
35. Morishita, M. & Peppas, N. A. Is the oral route possible for peptide and protein drug delivery? *Drug discovery today* **11**, 905–910 (2006).
36. Camenish, G., Alsenz, J., van der Waterbemmd, H. & Folkers, G. Estimation of permeability by passive diffusion through Caco-2 cell monolayers using the drugs' lipophilicity and molecular weight. *European journal of pharmaceutical sciences* **6**, 317–324 (1998).
37. Rubas, W. *et al.* Flux measurements across Caco-2 monolayers may predict transport in human large intestinal tissue. *Journal of pharmaceutical sciences* **85**, 165–169 (1996).
38. Shah, S. P. Drug delivery to the central nervous system: a review. *Journal of pharmaceutical sciences* **6**, 353–273 (2002).
39. Bernkop-Schnürch, A., Schwarz, V. & Steininger, S. Polymers with Thiol groups: A new generation of mucoadhesive polymers? *Pharmaceutical research* **16**, (1999).
40. Calceti, P., Salmaso, S., Walker, G. & Bernkop-Schn u rch, A. Development and in vivo evaluation of an oral insulin-PEG delivery system. *European journal of pharmaceutical sciences : official journal of the European Federation for Pharmaceutical Sciences* **22**, 315–323 (2004).
41. Park, K., Kwon, I. C. & Park, K. Oral protein delivery: Current status and future prospect. *Reactive and Functional Polymers* **71**, 280–287 (2011).
42. Silva, G. A. Nanotechnology approaches to crossing the blood-brain barrier and drug delivery to the CNS. *BMC neuroscience* **9 Suppl 3**, S4 (2008).
43. Demeule, M. *et al.* Identification and Design of Peptides as a New Drug Delivery System for the Brain. *Journal of Pharmacology and experimental therapeutics* **324**, 1064–1072 (2008).
44. Kim, H. R. *et al.* Translocation of poly(ethylene glycol-co-hexadecyl)cyanoacrylate nanoparticles into rat brain endothelial cells: role of apolipoproteins in receptor-mediated endocytosis. *Biomacromolecules* **8**, 793–799 (2007).

45. Pardridge, W. M. The blood-brain barrier: bottleneck in brain drug development. *NeuroRx : the journal of the American Society for Experimental NeuroTherapeutics* **2**, 3–14 (2005).

46. Abbott, N. J., Rönnbäck, L. & Hansson, E. Astrocyte-endothelial interactions at the blood-brain barrier. *Nat Rev Neurosci* **7**, 41–53 (2006).

47. Pardridge, W. M. Brain Drug Targeting and Gene Technologies. *Japanese journal of pharmacology* **103**, 97–103 (2001).

48. Black, K. L. & Ningaraj, N. S. Modulation of brain tumor capillaries for enhanced drug delivery selectively to brain tumor. *Cancer Control* **11**, 165–173 (2004).

49. Blakeley, J. Drug delivery to brain tumors. *Current neurology and neuroscience reports* **8**, 235–241 (2008).

50. Rautio, J. & Chikhale, P. J. Drug delivery systems for brain tumor therapy. *Current pharmaceutical design* **10**, 1341–1353 (2004).

51. Xin, H. *et al.* Anti-glioblastoma efficacy and safety of paclitaxel-loading Angiopep-conjugated dual targeting PEG-PCL nanoparticles. *Biomaterials* **33**, 8167–8176 (2012).

52. Bisht, S. *et al.* Polymeric nanoparticle-encapsulated curcumin ('nanocurcumin'): a novel strategy for human cancer therapy. *Journal of nanobiotechnology* **5**, 3 (2007).

53. Buzea, C., Pacheco, I. I. & Robbie, K. Nanomaterials and nanoparticles: sources and toxicity. *Biointerphases* **2**, MR17–71 (2007).

54. Lewinski, N., Colvin, V. & Drezek, R. Cytotoxicity of nanoparticles. *Small (Weinheim an der Bergstrasse, Germany)* **4**, 26–49 (2008).

55. Qian, Z.-M. *et al.* Development and iron-dependent expression of hephaestin in different brain regions of rats. *Journal of cellular biochemistry* **102**, 1225–1233 (2007).

56. Tam, J. P., Wu, C. R., Liu, W. & Zhang, J. W. Disulfide bond formation in peptides by dimethyl sulfoxide. Scope and applications. *Journal of the American Chemical Society* **113**, 6657–6662 (1991).

57. Wallace, T. J. & Mahon, J. J. Reactions of Thiols with Sulfoxides. III. Catalysis by Acids and Bases. *The Journal of Organic Chemistry* **30**, 1502–1506 (1965).

58. Ellman, G. L. Tissue sulfhydryl groups. *Arch. Biochem. Biophys.* **82**, 70–77 (1959).

59. et al Riddles, P. W. Reassessment of Ellman's reagent. *Meth. Enzymol.* **91**, 49–60 (1983).

60. Rajan, D. S. *et al.* Development of RP-HPLC for analysis of human insulin. *Indian journal of Pharmaceutical Sciences* **68**, 662–665 (2006).

61. Slomkowki, S. Terminology of polymer and polymer processes in dispersed systems (IUPAC Recommendation 2011). *Pure and Applied Chemistry* **83**, 2229–2259 (2011).

62. Ueki, T. *et al.* Thermodynamic study on phase transitions of poly(benzyl methacrylate) in ionic liquid solvents. *Pure and Applied Chemistry* **81**, 1829–1841 (2009).

63. Aoki, T. *et al.* Temperature-Responsive Interpenetrating Polymer Networks Constructed with Poly(acrylic acid) and Poly(N,N-dimethylacrylamide). *Macromolecules* **27**, 947–952 (1994).

64. Shibanuma, T., Aoki, T., Sanui, K. & Ogata, N. Thermosensitive Phase-Separation Behavior of Poly (acrylic acid) - gra f t -poly (N , N -dimethylacrylamide) Aqueous Solution. *Macromolecules* **33**, 444–450 (2000).

65. Byun, J., Lee, Y. M., Cho, C.-S. & Sung, Y.-K. Thermosensitive interpenetrating polymer networks omposed of poly(acrylamide-co-dimethylacrylamide) and poly(acrylic acid). *Korea polymer journal* **3**, 1–6 (1995).

66. He, J., Tong, X., Tremblay, L. & Zhao, Y. Corona-Cross-Linked Polymer Vesicles Displaying a Large and Reversible Temperature-Responsive Volume Transition. *Macromolecules* **42**, 7267–7270 (2009).

67. Verma, A. & Stellacci, F. Effect of surface properties on nanoparticle-cell interactions. *Small (Weinheim an der Bergstrasse, Germany)* **6**, 12–21 (2010).

68. Kujawa, P. *et al.* Impact of End-Group Association and Main-Chain Hydration on the Thermosensitive Properties of Hydrophobically Modified Telechelic Poly(N -isopropylacrylamides) in Water. *Macromolecules* **39**, 341–348 (2006).

69. Qiu, Y. & Park, K. Environment-sensitive hydrogels for drug delivery. *Advanced Drug Delivery Reviews* **53**, 321–339 (2001).

70. Xia, Y., Burke, N. A. D. & St o ver, H. D. H. End Group Effect on the Thermal Response of Narrow-Disperse Poly(N -isopropylacrylamide) Prepared by Atom Transfer Radical Polymerization. *Macromolecules* **39**, 2275–2283 (2006).

71. Duan, Q. *et al.* Synthesis and thermoresponsive property of end-functionalized poly(N-isopropylacrylamide) with pyrenyl group. *Journal of Polymer Science Part A: Polymer Chemistry* **44**, 1117–1124 (2006).

72. Lessard, D. G., Ousalem, M. & Zhu, X. X. Effect of the molecular weight on the lower critical solution temperature of poly(N,N-diethylacrylamide) in aqueous solutions. *Canadian Journal of Chemistry* **79**, 1870–1874 (2001).

73. Tong, Z., Zeng, F., Zheng, X. & Sato, T. Inverse Molecular Weight Dependence of Cloud Points for Aqueous Poly(. *Macromolecules* **32**, 4488–4490 (1999).

74. Plunkett, K. N., Zhu, X., Moore, J. S. & Leckband, D. E. PNIPAM chain collapse depends on the molecular weight and grafting density. *Langmuir* **22**, 4259–4266 (2006).

75. Tiktopulo, E. I. *et al.* 'Domain' Coil-Globule Transition in Homopolymers. *Macromolecules* **28**, 7519–7524 (1995).

76. Nasongkla, N. *et al.* Multifunctional Polymeric Micelles as Cancer-Targeted, MRI-Ultrasensitive Drug Delivery Systems. *Nano letters* **6**, 2427–2430 (2006).

77. Ishida, N. & Biggs, S. Direct observation of the phase transition for a poly(N-isopropylacryamide) layer grafted onto a solid surface by AFM and QCM-D. *Langmuir* **23**, 11083–11088 (2007).

78. Hanykova, L., Spevacek, J. & Ilavsky, M. 1H NMR study of thermotropic phase transition of linear and crosslinked poly(vinyl methyl ether) in D2O. *Polymer* **42**, 8607–8612 (2001).

79. Larsson, A. 1H NMR of thermoreversible polymers in solution and at interfaces: the influence of charged groups on the phase transition. *Colloids and Surfaces A: Physicochemical and Engineering Aspects* **190**, 185–192 (2001).

80. Badiger, M. V., Rajamohanan, P. R., Kulkarni, M. G., Ganapathy, S. & Mashelkar, R. A. Proton MASS-NMR: a new tool to study thermoreversible transition in hydrogels. *Macromolecules* **24**, 106–111 (1991).

81. Spevacek, J. I. NMR investigations of phase transition in aqueous polymer solutions and gels. *Current opinion in Colloid \& Interface Science* **14**, 184–191 (2009).

82. Heatley, F. *Introduction to NMR and its use in the study of polymer stereochemistry. In NMR spectroscopy of polymers*. (1993).

83. Badiger, M. V., Lele, A. K., Bhalerao, V. S., Varghese, S. & Mashelkar, R. A. Molecular tailoring of thermoreversible copolymer gels: Some new mechanistic insights. *The Journal of Chemical Physics* **109**, 1175 (1998).

84. Gottlieb, H. E., Kotlyar, V. & Nudelman, A. NMR Chemical Shifts of Common Laboratory Solvents as Trace Impurities In the course of the routine use of NMR as an aid for organic chemistry , a day-to-day problem is the identifica- tion of signals deriving from common contaminants literature , but the. *Journal of Organic Chemistry* **62**, 7512–7515 (1997).

85. Deshmukh, M. V., Vaidya, A. A., Kulkarni, M. G., Rajamohanan, P. R. & Ganapathy, S. LCST in poly(N-isopropylacrylamide) copolymers: high resolution proton NMR investigations. *Polymer* **41**, 7951–7960 (2000).

86. Moughton, A. O. & O'Reilly, R. K. Thermally induced micelle to vesicle morphology transition for a charged chain end diblock copolymer. *Chemical communications (Cambridge, England)* **46**, 1091–1093 (2010).

87. Majhi, P. R. & Blume, A. Temperature-Induced Micelle-Vesicle Transitions in DMPC−SDS and DMPC−DTAB Mixtures Studied by Calorimetry and Dynamic Light Scattering. *The journal of physical chemistry. B* **106**, 10753–10763 (2002).

88. Nagarajan, R. Molecular Packing Parameter and Surfactant Self-Assembly: The Neglected Role of the Surfactant Tail †. *Langmuir : the ACS journal of surfaces and colloids* **18**, 31–38 (2002).

89. Lee, J. S. Biodegradable Polymersomes for Drug Delivery. 1–172 (2011).

90. Leobandung, W., Ichikawa, H., Fukumori, Y. & Peppas, N. A. Preparation of stable insulin-loaded nanospheres of poly(ethylene glycol) macromers and N-isopropyl acrylamide. *Journal of controlled release : official journal of the Controlled Release Society* **80**, 357–363 (2002).

91. Wallin, R. F. A Practical Guide to ISO 10993-4: Hemocompatibility. *Medical device and diagnostic industry magazine* (1998).

92. Dean, L. *Blood groups and red cells antigens*. (NCBI).

93. Pio, R. Revision Control of complement activation by cancer cells and its implications in antibody-mediated cancer immunotherapy. *Inmunologia* **25**, 173–187 (2006).
94. Hattersley, P. G. Activated Coagulation Time of Whole Blood as a Routine Pre-Operative Screening Test. *California Medicine* **114**, (1971).
95. Riley, R. S., Carr, M. E., Tidwell, A. R., Williams, D. & Bode, A. P. Laboratory evaluation of homeostasis. *pathology.vcu.edu*
96. Collins, T. *et al.* Structure and chromosomal location of the gene for endothelial-leukocyte adhesion molecule 1. *Journal of biological chemistry* **266**, 2466–2473 (1991).

Chapter 3

Self-assembling amphiphilic multiblock copolymers for drug delivery

3.1 Introduction

After being able to synthesize biocompatible and non-cytotoxic thermosensitive nanocarriers, study their thermosensitive behaviour, modify their surface with diverse targeting moieties and load hydrophilic drugs, a further step towards the design of more robust systems capable of overcoming the limitations of free-radical polymerization, the ambiguity of vesicle-micelle transition and broadening the loading options to hydrophobic drugs as well was sought.

Although free-radical polymerization is of enormous industrial importance because a large list of advantages mentioned in the previous chapter, its major drawback is that it proceeds with very limited control. Therefore, it is not possible to obtain polymers with controlled architecture and narrow molecular weight distributions, due to the high reactivity of the propagating radicals and their tendency to undergo bimolecular termination, transfer and other side reactions[1].

Polymer architecture and weight distribution may not be a critical point in bulk materials industry; however, it becomes a major concern when designing polymers for drug delivery applications, as it can affect their interaction with the body[2]. Due to increasing utility of polymers in different areas of biomedicine and (nano)biotechnology, research has been driven into generating homogeneous and well-defined polymeric structures manifesting uniformity in physicochemical properties and reproducible biological activity. Molecular weight and its distribution, molecular architecture, solubility, chemical and biological functionality of these biomolecule-polymer platforms need to be well-controlled to establish a solid correlation between the performance and the platform design[3].

Therefore, it has been a long-standing goal in the field of polymer chemistry to develop a process that combines the advantages of radical polymerization with an additional control and precision on molecular weight and architecture, typical from more traditional living techniques, such as anionic polymerization. This challenge has lead to the discovery and development of controlled/living radical polymerization techniques (CRP)[1]. CRP enables preparation of polymers with predetermined molecular weight and narrow molecular weight distribution, as well as block copolymers, and more complex macromolecular architectures, such as stars, combs and brushes[1]. These well-defined complex macromolecules can be used to build nanostructures such as micelles, vesicles and nanoparticles, which can be combined with biomolecules or inorganic nanoparticles to address problems in medicine and bio- or nanotechnology[4,5]

The three most well known CRP techniques are Nitroxide-Mediated Radical Polymerization (NMP), Atom Transfer Radical Polymerization (ATRP) and Reversible Addition-fragmentation Chain Transfer Polymerization (RAFT). These systems operate on the basic principle of propagating radicals being reversibly deactivated, thus alternating between active and dormant states. The differences among them are dormant state's nature, being a polymeric alkoxyamine in NMP, a polymeric alkyl halide in ATRP and a polymer chain with a Chain Transfer Agent (CTA) end group, in RAFT[1].

Reversible Addition-fragmentation Chain Transfer (RAFT) polymerization was first reported in 1998 by Moad *et al.* at CSIRO (Commonwealth Scientific and Industrial Research Organisation)[6] and is the CRP technique that has attracted more attention as it is currently the most versatile[7], thanks to mild reaction conditions in both water and organic media, an infinite number of RAFT mediating agents, compatibility with a broad range of monomers[8] and introduction of end group functionality (CTA) allowing facile transformation of terminal groups[3,7]. This last characteristic is an especially valuable tool in the fabrication of polymer conjugates as it allows the transformation of polymer end groups to introduce additional and specific chain-end functionality, such as fluorophors and biomolecules, for targeted delivery purposes[9].

To better understand all the advantages this technique offers and explore the possibilities that provides in the preparation of drug delivery systems, a further insight in RAFT mechanism will be presented.

3.1.1 RAFT mechanism

In controlled/living radical polymerizations, the term livingness refers to the number fraction of polymer chains that are dormant and can be chain extended if more monomer is available. Control, on the other hand, refers to M_n increasing linearly with conversion and M_w/M_n decreasing with increasing conversion to approach unity[1].

In the case of RAFT, the key to successful controlled/living polymerization is the appropriate choice of the RAFT agent or Chain Transfer Agent (CTA). These are thiocarbonylthio compounds and have the general structure of RS-C(=S)-Z. Examples of RAFT agents span all thiocarbonylthio families including dithioesters, xanthates, dithiocarbamates and trithiocarbonates[7] (Figure 3.1). The key structural features of these RAFT agents are the Z and R groups[7,8].

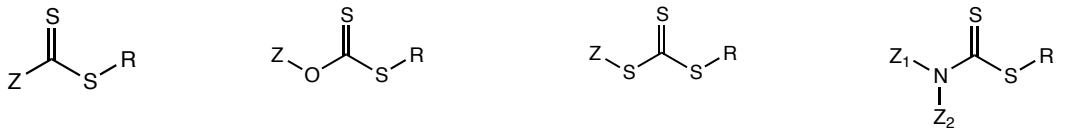

Figure 3.1: Generic structures of RAFT chain transfer agents[6].

The Z group controls the "bulk" reactivity of the RAFT-agent and serves two fundamental roles: it determines the general reactivity of the C=S bond towards radical addition and it is the major influencing factor affecting the lifetime of the intermediate radical resulting from the addition of radical species across the C=S bond in the pre- and main-equilibrium in the RAFT process (Figure 3.2). Increased activation of the thiocarbonyl double bond increases the likelihood of propagating chains will add to the CTA, allowing fewer monomers to add to the growing polymer chains between transfer events. Over-stabilization of the intermediate radicals, however, can lead to slow fragmentation resulting in retardation of the polymerization and a higher probability of intermediate radical termination[7].

Initiation:

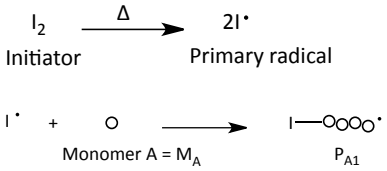

Pre-equilibrium:

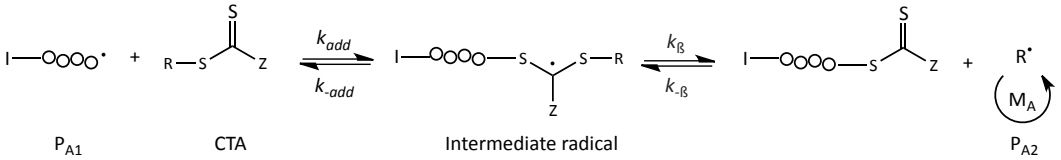

Main equilibrium/Homopolymer formation:

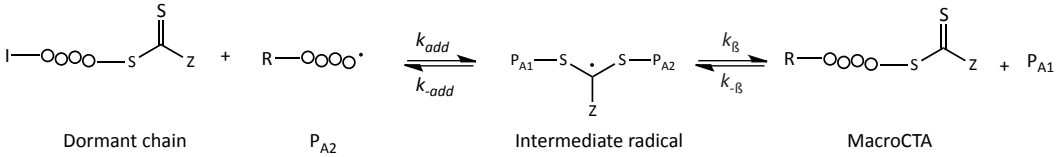

Reinitiation/Monomer addition:

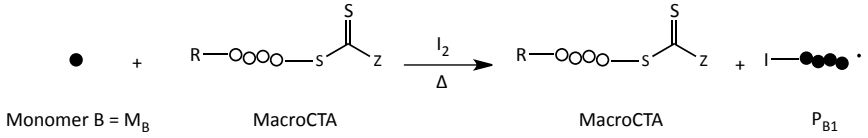

Pre-equilibrium:

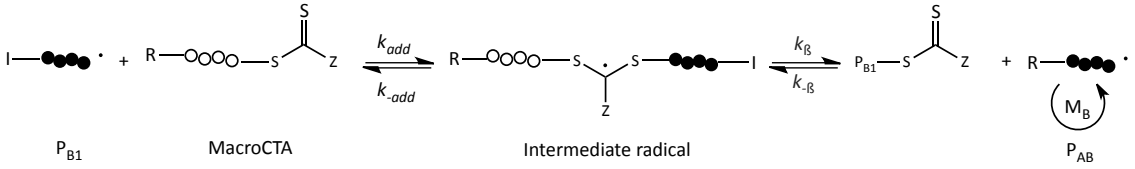

Main equilibrium/Block copolymer formation:

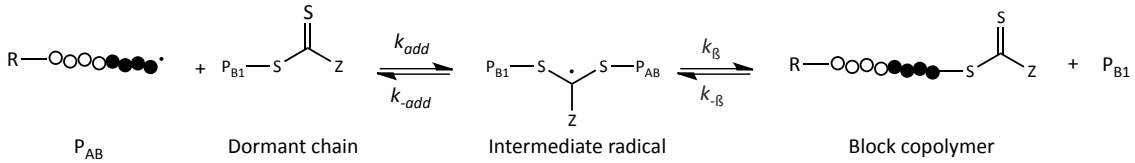

Termination:

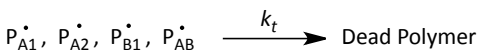

Figure 3.2: RAFT mechanism for the formation of block copolymers[1,7,10]

While Z group controls the "bulk" reactivity, R group allows for the fine tuning of the overall reactivity, and thus the ability for these species to effectively mediate

polymerization in a controlled fashion. R group has two key roles too. First, it must be a good free radical (homolytic) leaving group, and second, the radical that is generated from the homolytic dissociation must be able to initiate polymerization or simply add to monomer (propagate). The stability of the expelled $R^{\bullet}$ must be greater than or equal to the oligomeric radical $P_{A1}^{\bullet}$ to allow for fragmentation from the intermediate radical; however, the reactivity of $R^{\bullet}$ must be high enough to rapidly reinitiate polymerization of monomer[7].

Overall control in RAFT polymerization is a result of a fine balance among the addition (Z-group controlled), lifetime of the intermediate radical (predominantly Z-group controlled, but also R-group influenced), the fragmentation steps(s) (R-group controlled) and propagation, and their associated rate constants[8]. Improper CTA selection can cause a loss of control, significant retardation, a prolonged induction period and/or complete inhibition of polymerization[7].

Since RAFT is essentially a conventional radical polymerization conducted in the presence of a CTA, initiation can be accomplished with traditional initiators such as azo compounds, peroxides, redox initiating systems, photo-initiators and γ-radiation. The primary radical, $I^{\bullet}$, is generally believed to add to monomer prior to addition to the CTA due to the high relative concentration of monomer to CTA. Normally, the concentration of initiator relative to CTA is kept low to ensure that majority of the chains are initiated by CTA fragments ($R^{\bullet}$) as initiator-derived chains have a negative effect on the control of the molecular weight of the resulting polymer. Additionally, due to the exponential decomposition of conventional thermal initiators, primary radicals are continuously produced throughout the polymerization possibly leading to bimolecular termination. The continuous production of radicals also has the beneficial effect of replenishing any radicals lost to termination events and aids in maintaining reasonable polymerization rates. After reaction of the primary radical $I^{\bullet}$ with monomer to give a propagating oligomeric chain ($P_{A1}^{\bullet}$), the CTA reacts with $P_{A1}^{\bullet}$ to give an intermediate radical. This intermediate radical can fragment to yield the CTA and $P_{A1}^{\bullet}$, or, if the correct CTA is chosen, fragmentation to form a polymeric macroCTA ($P_{A1}SC(=S)Z$) and a new radial specie $R^{\bullet}$.

The pre-equilibrium is defined as the time required for all $R^{\bullet}$ fragments to add monomer units to form propagating chains, $P_{A2}^{\bullet}$, and is governed by the four rate constants k_{add}, k_{-add}, $k_{ß}$ and $k_{-ß}$. In order to achieve narrow molecular weight distributions, the pre-equilibrium must be completed early in the reaction for all the chains to enter the main equilibrium at the same time.

Once the pre-equilibrium is complete, the polymerization enters the main equilibrium. This stage involves the degenerative transfer of the thiocarbonylthio end group between propagating chains through the formation and fragmentation of an intermediate radical. The exchange between active and dormant chains is established by the rapid fragmentation of the intermediate radical in both directions allowing for the controlled, intermittent addition of monomer to each chain with equal probability.

As in all “living” polymerization techniques, RAFT works to limit the number of irreversible termination events by minimizing the instantaneous concentration of radicals available for termination. As in all free radical processes, however, termination

events occur through radical coupling and disproportionation and can be directly related to the starting initiator concentration. The RAFT process effectively limits the number of termination events thanks to the high $[CTA]_0/[I]_0$ commonly used, which prevents the number of dead chains from exceeding 5%.[3,7]

The polymer product of a RAFT polymerization contains in very high percentage the CTA-moiety in its structure. Therefore it is also called macroCTA and can be reactivated again for further growth as expected in any living polymerization process. This property of the macroCTA can be exploited for chain extension with a different monomer opening the door for block copolymer synthesis, which are polymers consisting of several covalently interconnected polymer segments based on two or more different homopolymers[11]. However, pursuing block copolymers by using any living polymerization method sequentially requires adjustment of polymerization conditions in each step. It is easy to predict that this will not work for any desired combination of monomers; specially if reactive functional groups are present and also if the polymerization rate of both monomers is very different[10].

Several conditions must be met in order to control molecular weight, which are a sufficiently high ratio of CTA to initiator and proper CTA selection for the monomer of choice. According to the reaction mechanism, there are two sources where polymer chains can come from: initiator fragments and the CTA leaving group ($R^{\bullet}$). Thus, the theoretical number-averaged molecular weight (M_n) can be defined as follows:

$$M_n = \frac{[M]_0 M_{MW} \rho}{[CTA]_0 + 2f[I]_0(1 - e^{-k_d t})} + CTA_{MW} \qquad \textbf{Equation (1)}$$

where $[M]_0$ is the initial monomer concentration, M_{MW} is the molecular weight of the monomer, ρ is the monomer conversion, $[CTA]_0$ is the initial CTA concentration, ƒ is the initiator efficiency, $[I]_0$ is the starting initiator concentration, k_d is the initiator decomposition rate constant and CTA_{MW} is the CTA molecular weight. In a well-designed RAFT polymerization with a high CTA to initiator ratio, the fraction of initiator-derived chains will be less than 5% and the term for such chains can be neglected. This allows to simplify Equation (1) into Equation (2).

$$M_n = \frac{[M]_0 M_{MW} \rho}{[CTA]_0} + CTA_{MW} \qquad \textbf{Equation (2)}$$

Thus, molecular weight increases linearly with conversion allowing for the synthesis of tailored polymers with predetermined molecular weights and low polydispersities (PDIs)[7].

Summarizing, the key to ensure controlled/living polymerization conditions is based on a thorough selection of the chain transfer agent, which depends at the same time on the monomers to be used. Modification of Z and R groups allow fine tuning of the reactivity of this RAFT agent broadening the range of thiocarbonylthio compounds that can be used.

3.1.2 Amphiphilic multiblock copolymers

With the ability to synthesize various architectures of a wide variety of polymers with defined structures, controlled molecular weights and narrow polydispersities, the RAFT technique appears to be one of the most flexible techniques to the generation of nanoscale polymeric systems for drug delivery[12]. For instance, micelles and polymer vesicles (polymersomes) from self-assembly of amphiphilic block copolymers have been investigated in recent years as potential carriers for therapeutic and diagnostic agents. What makes polymersomes interesting is their ability to entrap simultaneously hydrophobic and hydrophilic species due to the presence of a hydrophobic lamellar wall and an internal aqueous compartment of these synthetic vesicles[4].

Multiblock copolymers have been known and studied, but less than their lower homologues, i.e., diblock and ABA triblock copolymers, with which they share many properties and applications. Taking into account the potential of amphiphilic multiblock copolymers synthesized by RAFT polymerization for drug delivery applications, a new strategy was designed. Multiblock copolymers, from two up to five blocks, of two alternating monomers, were synthesized by RAFT polymerization (Figure 3.3). In order to get an amphiphilic block copolymer capable of building nanostructures, a hydrophilic and a hydrophobic monomer were chosen. In addition, total copolymer molecular weight should not exceed 30-50 KDa, so that it could avoid the typical renal threshold[13,14].

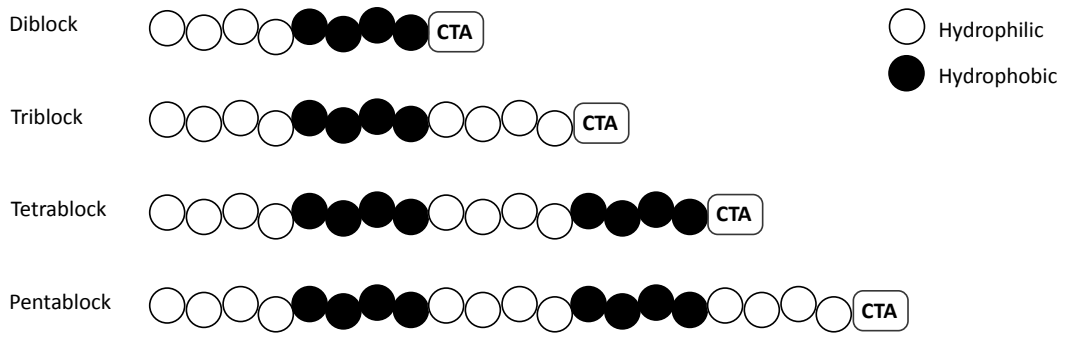

Figure 3.3: Scheme of alternating amphiphilic multiblock copolymers synthesized by RAFT polymerization.

Although pNIPAM has been used in the previous chapter and its combination with diverse monomers to obtain amphiphilic block copolymers has been widely used in drug delivery[7,10,15-18], its degradation into NIPAM monomers is still a major concern due to its high toxicity[19,20]. In addition, the vesicle-micelle duality of NIPAM copolymers adds an extra factor of complexity to the system. Therefore, the goal at this stage of the thesis was to substitute acrylamide monomers, NIPAM and DMAM, by non-cytotoxic hydrophilic monomer.

Owing to its biocompatibility, hemocompatibility[21], biodegradability[22,23] and lack of toxicity[24], 2-hydroxyethyl methacrylate (HEMA), has been one of the most extensively used polymers in biomedical applications, such as in contact lenses, scaffolds and hydrogels for drug delivery systems since 1960's. All along with the aforementioned characteristics, the fact that it is an uncharged monomer, which improves colloidal stability[25], makes it a promising monomer for this application.

Regarding the hydrophobic block, an in-house synthesized methacryloylated cholesterol derivative, which was previously used for obtaining amphiphilic polymers[26], was selected. Cholesterol is well-known for its ability to drive the self-assembly of cholesterol-containing materials[27], arising from its strong tendency for hydrophobic interactions. Studies suggest that, because of this behaviour, as well as its structural rigidity, a polyelectrolyte may be modified into a strongly associative polymer by covalently incorporating a small amount of cholesterol moieties into the polymer chain[28]. On the other hand, combining biocompatibility and ability to enhance directed cell growth, polymers bearing cholesterol mesogens are viable candidates for materials used in tissue engineering and implanted artificial organs[29].

In the light of their ability to drive self-assembling, their biocompatibility and their capability to polymerize by RAFT technique thanks to their acrylic nature, both monomers arose as a promising combination to build amphiphilic block copolymers able to self-assemble.

3.1.3 Number and length of blocks

Length and number of the blocks are determining parameters of the architecture of an amphiphilic multiblock copolymer and its interaction with the body. Therefore, once the monomers to be used are established, length and number of the blocks must be defined.

Differences in chemical nature of the blocks forming the copolymer make them interact very differently with the environment and behave distinctly in solution[30]. Amphiphilic block copolymers (ABCs) undergo phase separation as a result in chain association in solvents that selectively dissolve one of the blocks, resulting in the formation of nanoscopic supramolecular core-shell structures. The soluble block will be oriented towards the continuous solvent medium and become the “corona”, whereas the insoluble part will be shielded from the solvent in the “core” of the structure[31]. Self-assembly of ABCs leads to a rich variety of microstructures in solution, from spherical micelles and vesicles, to rods or cylinders and lamellar structures[32], depending on copolymer’s composition, structure, molecular weight, concentration, solvent composition, temperature or the presence of additives in the solvent[33-35].

Intense efforts have been dedicated to try to establish a general correlation between the aforementioned characteristics and final conformation of the copolymer in solution. A crucial factor in the micellization process is the weight fraction or ratio[36] of hydrophilic to hydrophobic segments, which defines the curvature between hydrophilic-hydrophobic interface. Its mean curvature (*H*) and its Gaussian curvature (*K*) are related by the packing parameter (ρ) (Equation (3)), where v is the volume of the hydrophobic part, a the interfacial area per molecule and l the chain length of the hydrophobic part[37].

$$\rho = \frac{v}{al} = 1 - Hl + \frac{Kl^2}{3} \qquad \textbf{Equation (3)}$$

As a general rule, spherical micelles are favoured when $\rho \leq 1/3$, cylindrical micelles when $1/3 \leq \rho \leq 1/2$, and vesicles for $1/2 \leq \rho \leq 1$ values (Figure 3.4).

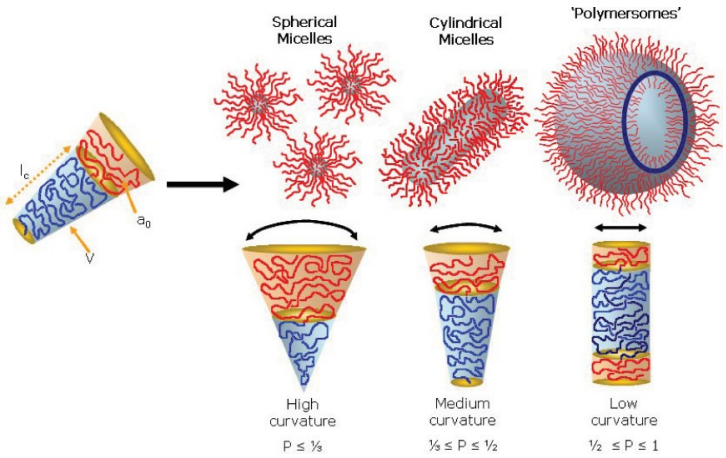

Figure 3.4: Schematic self-assembled structures in selective solvent depending on the packing parameter (ρ)[38]

However, this method, where pure geometrical considerations are taken into account, was originally established considering liposomal structures and may not be adequate to describe the self-assembly of amphiphilic macromolecules, where polymer chains entropy and entropy loss during vesicle formation can have a considerable effect on the resultant structure at the thermodynamic equilibrium[39]. Therefore, the length of the blocks is not the only factor to consider, as the interaction and compacting of polymer chains with themselves and adjacent chains may have a strong influence on the final self-assembly. The possible bilayer assemblies in an aqueous environment for AB diblock, ABA and BAB triblocks, ABAB tetrablock and ABABA pentablock copolymers are schematically illustrated in Figure 3.5.

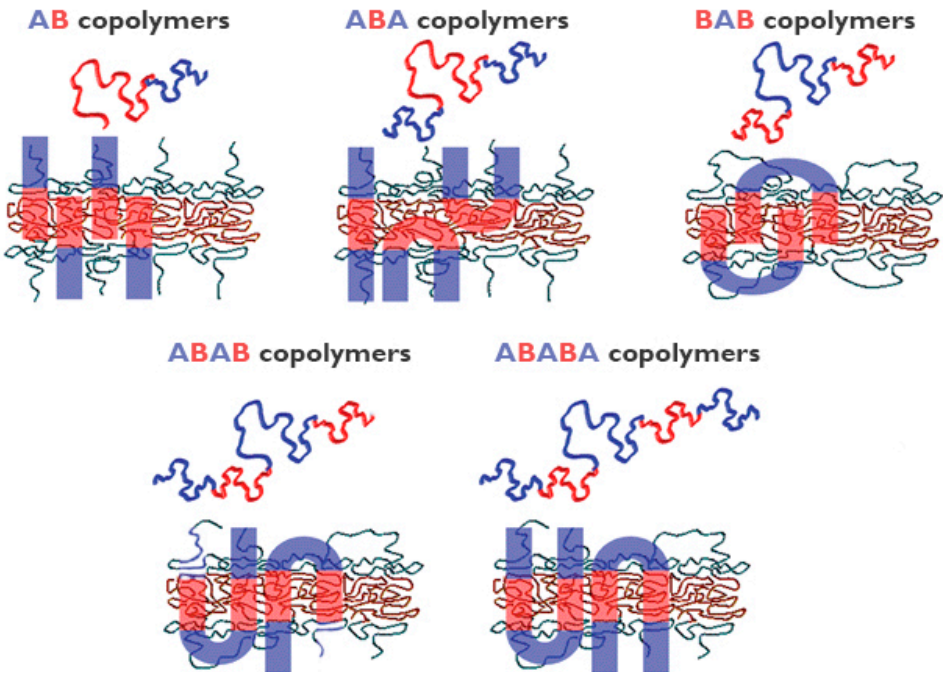

Figure 3.5: Hypothetical membrane conformation of polymersomes formed by amphiphilic diblock, triblock, tetrablock and pentablock copolymers[37]. Where A is the hydrophilic block and B the hydrophobic.

The hydrophobic chains would be entangled in the middle of the membrane to minimize the interfacial area with water and the hydrophilic block should be positioned to the outer side of the membranes. In the case of ABA copolymers, two

possible conformations may exist. The hydrophobic block can either form a curved loop, in such a way that both hydrophilic chains are exposed toward the outside of the membrane, or they can stretch forming a cylindrical shape with the two hydrophilic blocks at the opposite sides of the membrane. Thus, geometric conformations of the amphiphiles in an aqueous environment are driven by complementary hydrophobic/hydrophobic interactions between the polymer chains and the flexibility of blocks that permit their folding or bending[37].

Especially in the amphiphilic multiblock copolymers designed in this work, the hydrophobic block used has very special characteristics in terms of spatial distribution because of the molecular architecture of cholesterol. As mentioned before, some cholesterol derivatives are known to form ordered supramolecular structures in aqueous media such as lyotropic liquid crystalline (LC) phases, liposomes, micelles and ordered monolayers[40]. These LC domains observed in cholesterol polymers can function as a physical crosslinker making the self-assembled structures soft and tenacious. The orientational order arises from parallel arrangement of cholesterol, while positional order is obtained from attractive forces that hold the assembly together[41]. For instance, polymethacrylates bearing cholesterol side-chains have been found to self-assemble to form layered smectic mesophases, a type of liquid-crystal phase (Figure 3.6).

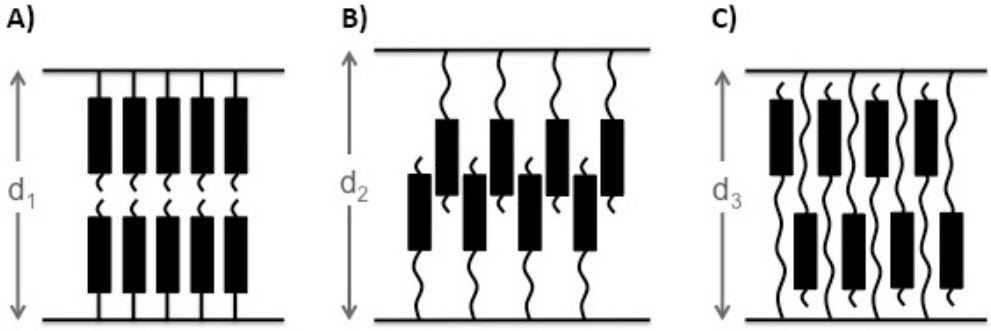

Figure 3.6: Scheme of smectic packing cholesterol side-chain polymers.A) Bilayer structure. B) and C) Interdigitated structure. *d* represents membrane thickness.

The smectic or layered arrangement of cholesterol can be bilayered, partially interdigitated, or completely interdigitated single layered packing with increasing spacer length between mesogens and polymer backbones[41], thus leading to vesicles with thicker walls.

Summarizing, a large list of factors are involved in the final conformation of self-assembled nanostructures from amphiphilic multiblock copolymers, thus it is very difficult to predict the final state of these structures in solution. Therefore, to determine how monomer's nature, number and length of blocks and other aspects influence the assembling process, it must be figured out experimentally.

In parallel, in order to help to understand what takes place in solution and to provide support to experimental studies, some authors have tried to simulate how these factors influence the spontaneous self-assembly of amphiphilic block copolymers. Results from a Coarse-Grain model have shown that diblock polymers of

PEE-PEO with random configuration spontaneously self-assembled into a bilayer, while larger hydrophilic fractions, close to lipid-like hydrophilic/hydrophobic ratios (60% hydrophilic fraction), facilitated the formation of a stable spherical micelle configuration after 20 ns[42]. After this first approach, research has gone further into the study of polymer micelles interactions with lipid vesicles in water, in order to model loaded polymer assisted drug transportation across a cell membrane[43]. A Coarse-Grain model showed that micelles of a binary diblock copolymer (PEG and a hydrocarbonate chain) interacted with DPPC lipid vesicles, getting fully absorbed without destroying lipid vesicle's structure. In addition, nearly the 50% of the loaded hydrophilic contents quickly diffused out of the lipid bilayer region and moved into the inner core of the lipid vesicle, where the confined water existed.

3.1.4 Preparation method

In order to determine experimentally the conformation adopted by these structures, self-assembled structures must be obtained. There are many techniques to prepare nanostructures by self-assembly of amphiphilic block copolymers. The most important preparation methods are generally classified into two groups: solvent-switching techniques or phase inversion and polymer rehydration technique[44]. In the first case, nanostructures are formed by dissolving block copolymers in an organic solvent suitable for all blocks, followed by the hydration of the solution. This hydration can be achieved by either adding water to the organic polymer solution (inverse precipitation) or by injecting the dissolved polymer into water (direct precipitation). In this new polar environment, hydrophobic blocks tend to minimize their contact with water and, therefore, hydrophobic chains associate together, while hydrophilic parts prefer the contact with water and repel each other, forming an outer shell and rendering self-assembled structures[45]. Size and size distributions can be tuned by modifying the initial polymer concentration, the stirring speed, the rate of addition[46] or by selecting the proper organic solvent, however the remaining amount of this solvent in nanostructures' membrane, despite solvent evaporation, is a limiting factor in their application for biomedical purposes[47].

However, the real mechanism of polymer vesicles formation through phase inversion technique is not clear yet. Polymer vesicles are considered to form in a two-step process, where firstly the polymer chains formed a bilayer-type membrane, which then subsequently closed to form a hollow structure[48]. Theoretical calculations based on particle models have revealed that some vesicles formation process may be more complicated than the mentioned "two-step" process. The results of these calculations can be summarized in to proposed mechanisms (Figure 3.7).

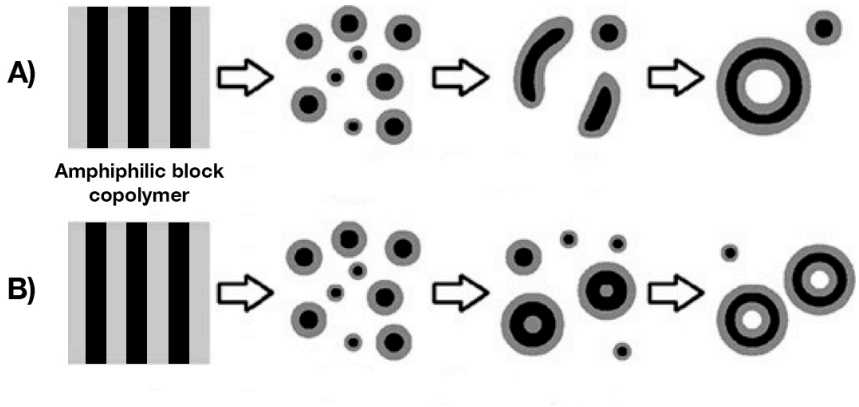

Figure 3.7: Schematic representation of two vesicle formation mechanisms.[48]Black and grey correspond to hydrophilic and hydrophobic blocks, respectively.

In the first mechanism (Figure 3.7A), the homogeneous amphiphilic block copolymer self-assemble into small spherical micelles rapidly, which slowly evolve into larger cylindrical or open disc-like micelles by collision. Then, these large disc-like micelles slowly close up to form vesicles. In the second mechanism (Figure 3.7B), small spherical micelles are formed rapidly as well, but finally they grow up to large spherical micelles by an evaporation-condensation-like process[49]. In 2004, Du and Chen[50] experimentally trapped the transition states in the evolution of spherical micelles to vesicles by gradually increasing the polarity of the solvent mixture, showing a transition from predominant spherical micelles with some rod-like micelles to rods along with some vesicles as water content increased, to finally obtain a solution of mainly vesicles with some rods at a 50% of water. These experimental results showed by TEM, support the first mechanism aforementioned as the mechanism of vesicle formation (Figure 3.7A).

On the other hand, polymer hydration techniques are based on the hydration of amphiphilic block copolymers films to induce self-assembly (Figure 3.8).

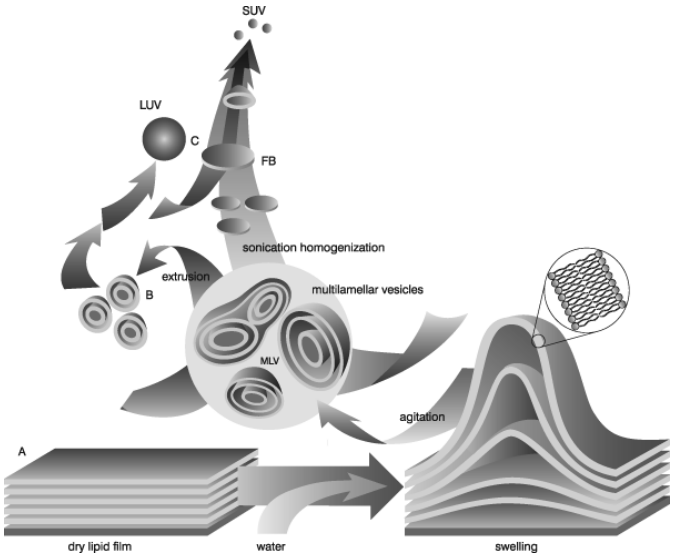

Figure 3.8: Schematic mechanism of the self-assembly of nanostructures by lipid hydration technique[51].

Firstly, polymers are dissolved in an organic solvent as well, and then a thin film is prepared by evaporation of the solvent. Subsequently, the polymer film is hydrated by the addition of water, which leads to the permeation of water through defects in polymer layers driven by hydration forces, inflation of these layers and formation of bulges, which finally yield multilamellar vesicles upon detachment from the film's surface[37]. Typically, this process produces large spread of vesicle sizes in the micron range, therefore, subsequent sizing through extrusion or sonication is required to promote the formation of narrower distributions of smaller vesicles and also reducing their lamellarity[46]. Size changes considerably from one technique to another. For instance, phase inversion method renders usually micrometer-sized vesicles as size cannot be efficiently controlled, whereas rehydration techniques followed by extrusion or sonication have been reported to give nanometer-sized structures[45,47].

3.1.5 Drug loading

As mentioned before, nanostructures formed from the self-assembly of amphiphilic triblock copolymers are highly attractive candidates for drug delivery of both hydrophilic and hydrophobic drugs. However, in order to truly reach their potential as delivery vehicles, these platforms must be able to entrap drugs at high encapsulation efficiencies to reach therapeutic concentrations[52]. Encapsulation efficiency of these systems depends on a number of factors, such as the nanostructures' preparation method (solvent switch, rehydration, etc.), the structure of the self-assembly (vesicles, micelles, etc.), polymer structure (flexibility, charge, length of the block that will entrap the drug)[53] as well as the encapsulation procedure (*in situ* or post loading)[48,54,55]. Regarding the encapsulation procedure, *in situ* loading is referred to the procedure when drugs are loaded at the same time that nanostructures are being formed, this is during self-assembly, while post loading referred to the encapsulation of drugs after nanostructures have self-assembled. In addition, the substances to be encapsulated can either be incorporated in the organic solvent by co-dissolving it with the block copolymer solution, or it can be added to the rehydrating aqueous solution, therefore both hydrophobic and hydrophilic substances can be loaded through both techniques[46].

This ability to entrap both hydrophilic and hydrophobic substances provides the system with a high versatility to transport a wide range of drugs, thus being appropriate for different therapies, or even suitable for combination therapy[56], where two or more drugs are simultaneously administered to improve therapy efficacy. In particular, it has been reported that highly lipophilic anticancer drugs like Paclitaxel, dyes and quantum dots as well as membrane proteins[57,58] can be integrated within the membrane of polymersomes while maintaining their functionality[44]. On the other hand, hydrophilic anticancer drugs like Doxorubicin[59], proteins like Hemoglobin[60] or fluorphores[61] can be entrapped in the internal aqueous cavity of vesicles[62]. As mentioned, these systems are highly interesting for combination therapy, as "cocktails" of drugs are routinely used in cancer treatment and indeed the combination of different therapeutic agents often improves therapeutic profile. Unlike single-agent therapy, multi-agent therapy can modulate different signalling pathways in diseased cells, maximising the therapeutic effect and, possibly, overcoming mechanisms of resistance, thus the chances of success are higher. For example, in

acute nonlymphocytic leukaemia, the use of the anthracycline daunorubicin (DNA intercalator) with ara-C (inhibitor of DNA polymerase) is a successful example of complementary inhibition as this combination interferes with DNA repair as well as its synthesis. Another good example of biochemical synergy is the administration of leucovorin (LV) prior to 5-fluorouracil (5-FU) in colorectal cancer as LV markedly enhance the ability of 5-FU to bind and consequently block the action of thymidilate synthetase[56]. The application of this strategy to the polymeric systems here described has resulted in diverse drug delivery systems (DDS). For instance, biodegradable polymersomes loaded with doxorubicin and tetrandrine, a potent hydrophobic multidrug resistance (MDR) inhibitor, demonstrated an enhanced efficacy compared to loaded doxorubicin alone to treat glioma rats[63], whereas another therapy combining paclitaxel and endostatin, a hydrosoluble peptide that targets angiogenesis regulatory genes, co-loaded in polymeric nanospheres showed a synergetic anti-angiogenic effect in HUVEC[64].

The characteristics here exposed explain the reasons why self-assembling amphiphilic multiblock copolymers have attracted enormous interest[65,66] in the past decade[67] as potential drug delivery systems. The discovery of RAFT polymerization and its application in the synthesis of multiblock copolymers allow the preparation of amphiphilic copolymers with controlled molecular weight and narrow molecular weight distributions, which is crucial for the achievement of self-assembled nanostructures with low polydispersities that have uniform physicochemical properties and biologic activity. As stated before, an accurate design of this multiblock copolymers allow a fine tuning of important properties of the final self-assembled nanostructures such as their conformation in solution or their loading capacity. However, other factors that are independent from polymers' structure can also have a big influence on these properties, for instance, the preparation method. In addition, the amphipathic nature of these systems make them very versatile regarding the amphipathicity of the loaded drugs, permitting the encapsulation of both hydrophilic and hydrophobic drugs. Therefore, in this chapter, preparation and characterization of these systems will be performed.

3.1.6 Aims of this chapter

Considering amphiphilic multiblock copolymers as a promising platform for drug delivery and the versatility of RAFT polymerization to accurately synthesize these platforms, the aims of this chapter are as follows:

- The substitution of acrylamide monomers for a hydrophilic monomer, HEMA, and a hydrophobic monomer, a methacryloylated cholesterol derivative.
- The synthesis of an amphiphilic multiblock copolymer with predetermined molecular weight through RAFT polymerization
- The optimization of the length and number of blocks of an amphiphilic block copolymer to obtain self-assembled nanostructures
- The study of the influence of nanostructures' preparation technique on their final characteristics

- The study of drug loading versatility, capacity and efficiency of the obtained nanostructures and their physical characterization

3.2 Material and Methods

3.2.1 Materials and reagents

For the synthesis of Ma-acap-Chol, cholesterol, Dicyclohexylcarbodiimide (DCC), 4-(dimethylamino)pyridine (DMAP), anhydrous THF and magnesium sulphate were purchased from Sigma-Aldrich (Germany), whereas, EtOAc, glacial acetic acid and sodium bicarbonate were purchased from Panreac.

For HEMA protection and deprotection, the monomer 2-hydroxyethyl methacrylate (HEMA), t-butyldimethylsilyl chloride (TBDMS) and imidazole were purchased from Aldrich (Germany) while CH_2Cl_2 and HCl were purchased from Panreac.

For the synthesis of multiblock copolymers, the initiator 2-azobis(isobutyronitrile) (AIBN), which was purified by recrystallization in MeOH at -20°C overnight, the solvent 1,4-dioxane, the CTAs, 4-cyano-4-(phenylcarbonylthioylthio)pentanoic acid (PHPA), 4-cyano-4-[(dodecylsulfanylthiocarbonyl)sulfanyl]pentanoic acid (DSPA) and 2-(dodecylthiocarbonothioylthio)-2-methylpropionic acid (DCMA), and $CDCl_3$ were purchased from Sigma-Aldrich, Germany. THF (HPLC grade), MeOH and ACN (HPLC grade) were purchased from Merck. Polystyrene Standards Kit low MW was supplied by Supelco.

For drug loading, Doxorubicin hydrochloride was purchased from Abcam Biochemicals, UK, whereas Paclitaxel, Docetaxel, citric acid, sodium citrate, Nile red, fluorescein, HEPES and sodium chloride from Sigma-Aldrich, Germany. NaOH was purchased from Panreac and dialysis tubing from Spectrum Labs, US.

3.2.2 Synthesis of Ma-acap-Chol

For the synthesis of Ma-acap-Chol, a cold solution (-20°C) of DCC (3.09 g, 0.0149 mol) in 7 ml of anhydrous THF was added to a cold solution (-20°C) of cholesterol (5.15g, 0.013 mol) and Ma-acap-OH (2.92g, 0.0146 mol) in 40 ml of anhydrous THF. Several crystals of DMAP were added to the mixture, which was kept at -20°C for one hour and left, afterwards, at 4°C overnight. Then, 100 µL of glacial acetic acid was added to the previous mixture and stirred for one hour at room temperature. The white precipitate of N,N'-dicyclohexylurea that appeared, was filtrated under vacuum and discarded. THF of the filtrate was removed by rotary evaporation and the remaining oil was dissolved again in 40 ml of ethyl acetate. The solution was washed with sodium bicarbonate (2%, 2 x 20 ml) to remove unreacted Ma-acap-OH. The organic fraction was dried over magnesium sulphate and the solvent eliminated by rotary evaporation. The resultant oil was dissolved in 45 ml of acetone and kept at -20°C overnight. The purity of the recrystallized monomer was ensured by TLC analysis and ^{1}H-NMR.

^{1}H-NMR (400 MHz, $CDCl_3$, TMS) (ppm): δ = 7.19 (s, 1H, NH), 5.66 (s, 1H, H^1), 5.39 (d, 1H, H^{11}), 5.27 (t, 1H, H^2), 4.53 (m, 1H, H^9), 3.23 (q, 2H, H^4), 2.29, (t, 2H, H^8), 2.0 - 0.8 (methylene envelope), 1.96 (s, 3H, H^3), 0.95 (d, 3H,H^{13}), 0.88 (d, 6H, H^{14}), 0.73 (s, 3H, H^{12}). (Numeration referred to Figure 3.9)

3.2.3 Protection and deprotection of 2-Hydroxyethyl Methacrylate

To protect the hydroxyl group of HEMA with t-butyldimethylsilyl chloride (TBDMS), a mixture of HEMA (1g, 7.7 mmol) and imidazole (0.58g, 8.5 mmol) in CH_2Cl_2 was cooled at 0°C. A solution of TBDMS (1.28g, 8.5 mmol) in 10 ml of CH_2Cl_2 was added dropwise to the previous mixture. The reaction was stirred for 2 hours at 0°C and afterwards at room temperature overnight. HEMA-TBDMS formation and complete reaction was confirmed by TLC analysis. The white solid was filtered off and the filtrate was washed with water (2 x 20 ml). The organic fraction was dried over $MgSO_4$ and the solvent removed under vacuum. The final product was dried under vacuum as well. ^{1}H-NMR spectrum in CH_2Cl_2 confirmed the structure of the synthesized product.

^{1}H-NMR (400 MHz, $CDCl_3$, TMS) (ppm): δ = 6.08 and 5.5 (m, 2H, C*H*$_2$=C(CH$_3$)COO-), 4.2 (m, 2H, -C*H*$_2$CH$_2$-), 3.8 (m, 2H, -CH$_2$C*H*$_2$-), 1.89 (s, 3H, CH$_2$=C(C*H*$_3$)COO-), 0.8 (s, 9H, -Si(CH$_2$)$_2$(C*H*$_3$)$_3$) and 0.03 (s, 6H, -Si(C*H*$_3$)$_2$(CH$_3$)$_3$).

To deprotect HEMA, HCl 37% was added dropwise (0.01 ml) to a solution of the copolymer in 1,4-Dioxane (0.5 ml). The reaction mixture was stirred overnight at room temperature. Depending on the multiblock copolymer, the deprotected form may precipitate, if not the solution was added over diethylether to obtain a precipitate, which was centrifuged at 5500 rpm for 20 min and dried under vacuum.

3.2.4 Polymerization of multiblock copolymer

Amphiphilic block copolymers were accomplished by sequential RAFT polymerization of the previously synthesized HEMA-TBDMS, as the hydrophilic block, and Ma-acap-Chol, as the hydrophobic block.

For the synthesis of pHEMA-TBDMS homopolymer, a polymerization tube equipped with a screw cap was charged with HEMA-TBDMS (2.5 g, 0.01 mol), AIBN (7 mg, 4.1 x 10^{-5} mol), 1,4-dioxane (3.5 ml) and 4.1 x 10^{-4} mol of the corresponding CTA, which were PHPA (0.11 g), DCMA (0.15 g) or DSPA (0.16 g). The reaction mixture was deoxygenated with argon for 20 min and then placed in a heated oil bath at 70°C under stirring for 24 hours. The mixture was vacuum-dried and the resulting oil was dissolved in 1,4-dioxane for the synthesis of the copolymer, as pHEMA-TBDMS did not precipitate in any solvent. For further reaction with pHEMA-TBDMS, its molecular weight was analysed by GPC.

For the synthesis of the copolymers, a similar procedure was followed, and instead of dissolving CTA in the polymerization flask, a calculated amount of polymer in which CTA was incorporated (macroCTA) was dissolved. In particular, for the synthesis of the diblock copolymer, pHEMA-TBMDS macroCTA (2.42 g, 3.3 x 10^{-4} mol), Ma-acap-Chol (4.68 g, 8.28 x 10^{-3} mol) and AIBN (5.4 mg, 3.3 x 10^{-5} mol) were dissolved in 1,4-dioxane (7 ml). The reaction mixture was deoxygenated with argon for 20 min and then placed in an oil bath at 70°C under stirring for 2 hours. The diblock copolymer was precipitated in acetone, washed three times with acetone (3 x 40ml), centrifuged at 5500 rpm for 20 min and vacuum-dried overnight after solvent removal.

Characterization of pHEMA-TBDMS-*co*-pCHOL:

^{1}H-NMR (400 MHz, THF-d_8, TMS) (ppm): δ= 5.38 (s, 1H, H^7), 4.55 (s, 1H, H^6), 4.03 (s, 2H, H^2), 3.75 (s, 2H, H^3), 3.09 (s, 2H, H^4), 2.3 (s, 2H, H^5), 2.05 (s, 6H, H^1), 0.8 (d, 6H, H^{10}), 0.74 (s, 3H, H^8). (Numeration referred to Figure 3.13)

^{13}C-NMR (400 MHz, THF-d_8, TMS) (ppm): δ= 205.4 (C^a), 173.59 (C^b), 141.77 (C^e), 123.91 (C^f), 74.95 (C^c), 68.82 (C^g), 61.34 (C^h), 29.82 (-C^jH_2- from CTA), 28.72, 25.9 (C^i).

IR (ATIR): ν = 525, 959, 1028, 1082, 1162, 1256, 1383, 1466, 1521, 1649, 1732, 2867, 2945, 3426 cm^{-1}.

The synthesis of the triblock copolymer was accomplished by dissolving diblock copolymer (2 g, 1.25 x 10^{-5} mol), HEMA-TBDMS (0.76 g, 3.13 x 10^{-3} mol) and AIBN (2 mg, 1.25 x 10^{-5} mol) in 1,4-dioxane (4 ml) and methanol (4 ml). The mixture was degassed and incubated at 70°C for 24 hours. The triblock copolymer was purified by precipitation in acetone, washed with acetone (3 x 40 ml) and vacuum-dried. For the synthesis of the tetrablock copolymer, triblock (0.96 g, 0.025 mmol), Ma-acap-Chol (0.35 g, 0.63 mmol) and AIBN (0.8 mg, 0.0048 mmol) were dissolved in 1,4-dioxane (3 ml) and methanol (3 ml). The reaction mixture was deoxygenated with argon for 20 min and then heated in an oil bath at 70°C under stirring for 2 hours. The tetrablock copolymer was precipitated in acetone, washed with acetone (3 x 40ml) and vacuum-dried. For the synthesis of the pentablock copolymer, tetrablock copolymer (0.35 g, 8.1 x 10^{-3} mmol), HEMA-TBDMS (0.03 g, 0.00012 mmol) and AIBN (0.6 mg, 0.0037 mmol) were dissolved in 1,4-dioxane (1 ml) and methanol (1 ml). The reaction mixture was deoxygenated with argon for 20 min and then heated in an oil bath at 70°C under stirring for 24 hours. The pentablock copolymer was precipitated in acetone, washed with acetone (3 x 40ml) and vacuum-dried

3.2.5 Amphiphilic multiblock copolymer characterization

All the synthesized polymers were characterized in terms of their molecular weight and composition by GPC and ^{1}H-NMR. GPC was performed on a LabChrome Elite HPLC system from Hitachi equipped with a Shodex KF-603 column and a refractive index (RI) detector. The eluent was THF pumped at 0.5 ml/min. Calibration was performed using Polystyrene Standards Kit low MW.

Diblock copolymer was also characterized by ^{13}C-NMR and IR. ^{1}H-NMR and ^{13}C-NMR spectra were recorded in a Varian 400 MHz MR spectrometer (Varian NMR Instruments, IL, US) in $CDCl_3$. IR spectra were obtained using Nicolet Magna 560 (Thermo Fisher Scientific, MA, US) with a KBr beam splitter.

3.2.6 Nanostructures formation

3.2.6.1 Nanoprecipitation

In direct nanoprecipitation, 20 mg of copolymer were dissolved in 1ml of THF and added dropwise over 10 ml of PBS with a 8 mm syringe using a syringe pump at a rate of 50 µL/min and stirring at 1000 rpm. In inverse nanoprecipitation, 10 ml of mili-Q water were added dropwise over a solution of 20 mg of copolymer in 1 ml of THF with

a 14.3 mm syringe, using a syringe pump at a rate of 50 µL/min and stirring at 1000 rpm. The sample was transferred to a dialysis tube (MWCO 100 KDa) and dialyzed against 4L of PBS for 5 hours at 4°C to remove free polymer.

3.2.6.2 Film hydration technique

Nanostructures from amphiphilic block copolymers obtained through the lipid film hydration technique[68], were prepared as follows. A dry film of polymer was prepared by rotary evaporation of a chloroform solution of copolymer (10 mg/ml) followed by freeze-drying for 4 hours. The film was hydrated with 1ml of PBS to render a final polymer concentration of 10 mg/ml. The hydrated mixture was vortexed vigorously for 5 min to form multilamelar vesicles and then sonicated with a probe sonicator at 35% amplitude, with pulsed frequency, 2 s on and 2 s off, for 8 minutes. The probe sonicator used was VC-505 (500 W) Vibra-cell™ ultrasonic processor from Sonics and materials, Inc. (US) equipped with a 5 mm tapered microtip. The sample was transferred to a dialysis tube (MWCO 100 KDa) and dialyzed against 4L of PBS for 5 hours at 4°C to remove free polymer.

The nanostructures obtained were characterized in terms of size distribution and zeta potential by Dynamic Light Scattering (DLS) and Nanoparticle Track Analysis (NTA). Size and zeta potential values were both determined by DLS in a Zetasizer Nano ZS90 (Malvern Instruments, Ltd., UK). Correlation functions were collected at a laser wavelength of 632.8 nm and scattering angle of 173 degrees. Size was determined using Malvern sizing software (DTS v5.03) by intensity, volume and number analysis, as the mean of three measurements; each of them was recorded as an average of 10 runs of 10 scans in a disposable plastic cuvette. Nanostructure's size was also characterized by NTA using a NanoSight LM10 (Malvern Instruments, Ltd., UK) recording 10s videos. Samples were analysed with no further dilution and temperature was set at 22°C in both equipment.

3.2.7 Transmission electronic microscopy (TEM)

Samples were prepared as described above and diluted to 1:10 in Mili-Q water. Then, 1 µl of this sample was deposited onto a copper grid and allowed to air dry. 1% uranyl acetate was used as a negative stain, 5 µl was applied to the grid, left for 5 seconds, blotted off and left to air dry. The microscope used to monitor the images was a Hitachi H-7000.

3.2.8 Fluorescence microscopy

Nanostructures were prepared by the film hydration technique and loaded with 2% (wt/wt) of Nile red and fluorescein. *In situ* loading was achieved by dissolving the polymer (20 mg) and nile red in THF, followed by freeze-drying to obtain the film, and further hydrated with 1 ml of PBS and fluorescein. The solution was sonicated as explained before and further dialyzed in a dialysis tube (MWCO 100 KDa) against 50 ml of PBS for 2 hours protected from light. 2 µl of the loaded samples without dilution are placed on a glass slide, covered with a coverslip and sealed. Samples were visualized with a Zeiss Axiovert inverted fluorescence microscope (Axiovert 200M; Carl Zeiss Inc.) equipped with Zeiss ApoTome system at 400 X magnification with FITC and TRITC filters.

3.2.9 Drug loading

3.2.9.1 Paclitaxel loading (in situ loading)

A dry film of polymer and paclitaxel was prepared by rotary evaporation of a chloroform solution of copolymer (10 mg/ml) and Paclitaxel (1 mg/ml) followed by freeze-drying for 4 hours. The film was hydrated with PBS to render a final polymer concentration of 10 mg/ml. The hydrated mixture was vortexed vigorously for 5 min to form multilamelar vesicles and then sonicated with a probe sonicator at 35% amplitude, with pulsed frequency, 2 s on and 2 s off, for 8 minutes. Free paclitaxel and remaining free polymer were removed by dialysis in a dialysis bag (MWCO 100 KDa) against 4L of PBS for 5 hours at 4°C. Paclitaxel's concentration was determined by HPLC after liquid-liquid extraction using docetaxel as an internal standard. Docetaxel was added to each sample to render a solution of 10 µg/ml of docetaxel. Then, 1 ml of the sample was lyophilized and resuspended in 1ml of MeOH to dissolve the copolymer and release Paclitaxel. Afterwards, MeOH was evaporated with N_2 stream. Once dried, 1 ml of CH_2Cl_2 was added to the sample. After agitation, supernatant was moved to an HPLC vial and CH_2Cl_2 was evaporated again with N_2 stream. The remaining solid was resuspended in 1ml of ACN and analysed in a Hitachi LabChrome Elite chromatograph at a flow rate of 1 ml/min, at 30°C, using a mixture of mili-Q water and ACN (40:60) as eluent for 10 min. DAD detector was set at 227 nm.

3.2.9.2 Doxorubicin loading (post loading)

Doxorubicin was entrapped by remote loading driven by a transmembrane pH gradient[69]. To achieve this gradient, polymeric films were previously rehydrated in $300\ \mathrm{mM}$ ammonium citrate buffer (pH 4) at a concentration of $10\ \mathrm{mg/ml}$. The hydrated mixture was vortexed vigorously for 5 min to form multilamelar vesicles and then sonicated with a probe sonicator at 35% amplitude, with pulsed frequency, 2s on and 2s off, for 8 minutes. The solution was dialyzed in a dialysis bag (MWCO 100 KDa) for 4 hours against 1L HEPES buffered saline (HBS), 150 mM NaCl, 20 mM HEPES at pH 7.4 to replace the extraliposomal solution. Subsequently, doxorubicin HCl was added to the liposomal dispersion at a concentration of 1 mg/ml and incubated for 1 hour at 65°C. Free doxorubicin was removed by dialysis in a dialysis bag (MWCO 100 KDa) against 4L of HBS for 5 hours at 4°C. Doxorubicin's concentration was determined in triplicate by spectrophotometry at 485 nm using a multidetection microplate reader (Bio-Tek, Winooski, VT) after lysis of polymersomes with Triton X-100 at 1% (v/v).

Loading efficiency or encapsulation efficiency (EE) was calculated as drug percentage in nanostructures relative to the initial amount as indicated in Equation (4), whereas loading capacity or encapsulation capacity (EC) was calculated as a weight percentage of loaded drug relative to polymer (w/w) as indicated in Equation (5)[70].

$$EE\ (\%) = \left(\frac{loaded\ drug}{initial\ amount\ of\ drug}\right) \times 100 \qquad \textbf{Equation (4)}$$

$$EC(\%) = \left(\frac{weight\ of\ loaded\ drug}{weight\ of\ polymer}\right) \times 100 \qquad \textbf{Equation (5)}$$

3.3 Results and Discussion

3.3.1 Synthesis of monomers

Prior to synthesize the different block copolymers by RAFT polymerization, the selected monomers were prepared. HEMA, chosen to synthesize the hydrophilic blocks, was commercially acquired and its hydroxyl group was protected, whereas the methacryloylated cholesterol derivative used to obtain the hydrophobic blocks was synthesized from scratch.

Regarding the hydrophilic monomer, HEMA was typically protected with trimethylsilyl (TMS) prior to its copolymerization to form block copolymers[29,71], in order to avoid undesired secondary reactions of its hydroxyl group and solubility incompatibilities between the two monomers that could complicate polymerization handling due to their opposite nature in solution. In addition, it has been reported that synthesis of high molecular weight pHEMA with polydispersities below 1.2 can only be achieved by protecting the hydroxyl groups[72,73].

In this work, HEMA was successfully protected with TMS, however it became hydrolyzed and deprotected during further polymerization of copolymers. Other authors also observed irregularities when protecting HEMA with TMS, such as gradual deactivation of propagating chain end with no chain end surviving after 1 hour[74]. They presented, as an alternative, the use of a more stable protecting group, which was tert-butyldimethylsilyl (TBDMS). By using TBDMS, the protected functional groups of both monomer and the resulting polymers were stable and intact during experimental operations under basic and neutral conditions, but were cleaved readily under acidic conditions. Therefore, commercially available HEMA was protected with t-butyldimethylsilyl chloride (TBDMS-Cl).

On the other hand, the synthesis of the methacryloylated cholesterol derivative, that is known as Ma-acap-Chol, consisted in a two-step synthesis[26] beginning with the acylation of aminocaproic acid with methacryloyl chloride in aqueous NaOH, known as Schotten-Baumann reaction(Figure 3.9).

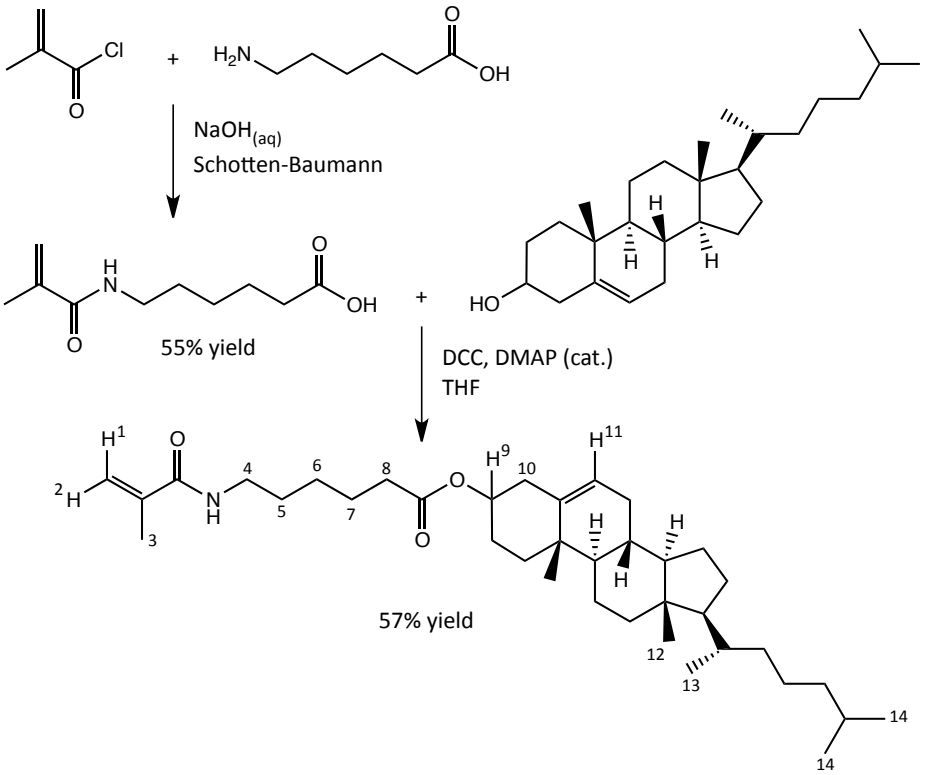

Figure 3.9: Synthesis of methacryloylated monomer.

The yield of the reaction was 55% and the purity of the obtained N-methacryloyl-6-aminohexanoic acid (Ma-acap-OH) was confirmed by TLC analysis, which only showed one spot on the TLC plate. Afterwards, Ma-acap-OH is esterified with cholesterol using dicyclohexylcarbodiimide (DCC) and a catalytic amount of 4-dimethyl-aminopyridine (DMAP) in THF to obtain Ma-acap-CHOL, in 57% yield.

The ^{1}H-NMR spectrum of the synthesized compound showed a complex area between 2.0 and 0.0 ppm, which included the signals of the aliphatic protons belonging to the cholesterol structure and the aminocaproic acid linker. Usually, in these relatively large and complex molecules, this region is known as methylene envelope and assignment of these signals is generally a complicated task due to high overlapping of the signals. Therefore, analysis of selected signals outside that area was used to successfully confirm the structure of the synthesized compound. Esterification of the 3β hydroxyl group from the cholesterol structure was confirmed by a chemical shift to lower fields of its adjacent proton (H-3α), from 3.47 to 4.53 ppm[75]. ^{1}H-NMR spectrum also showed the characteristic signals of the Ma-acap-OH protons discussed above, except that corresponding to the carboxylic acid proton (10.50 ppm), which confirmed the formation of the ester. No impurities of cholesterol were observed between 3.26 and 4.4 ppm.

3.3.2 Chain Transfer Agent (CTA) selection

Once the monomers were successfully synthesized, the next step consisted in the identification of a suitable chain transfer agent capable of controlling the polymerization of both monomers. As mentioned before, the selection of the optimum CTA is the key point in the design of the polymerization, to ensure the control of the

molecular weight and its narrow distribution. It has been earlier described that dithioesters and trithiocarbonates are capable of mediating the polymerization of both methacrylates and methacrylamides[5,6]. For the polymerization of HEMA and Ma-acap-chol, three CTAs compatible for both methacrylates and methacrylamide were chosen from CSIRO's Raft agent Monomer matching guide[76] (Figure 3.10).

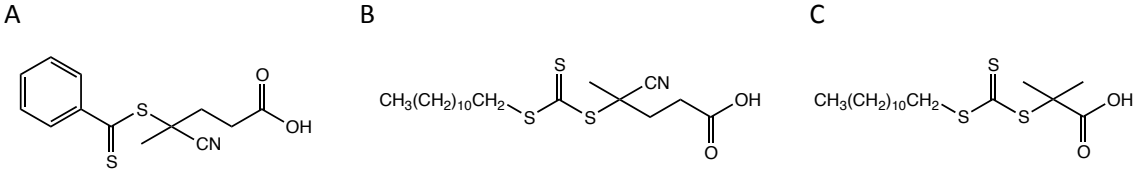

Figure 3.10: RAFT agents compatible with methacrylates and methacrylamides.A) 4-cyano-4-(phenylcarbonylthioylthio) pentanoic acid (PHPA) B) 4-cyano-4-[(dodecylsulfanylthiocarbonyl)sulfanyl] pentanoic acid (DSPA). C) 2-(dodecylthiocarbonothioylthio)-2-methylpropionic acid (DCMA). (Sigma-Aldrich® Materials Science)

Following the presented strategy, it was considered to begin the copolymerization with the hydrophilic block for two reasons. On one hand, the nanostructures to be formed from the self-assembly of the polymers were conceived for therapeutic reasons so that they would be mainly in aqueous environment. Having a hydrophilic shell stabilizes drug-loaded nanostructures in the bloodstream contributing to a longer circulation in the body[54]. Therefore, for instance, in the case of a triblock copolymer, it was preferred to have an ABA structure, where A is the hydrophilic block, instead of BAB, with hydrophobic blocks on both extremes. On the other hand, HEMA was commercially available, being easier and faster to obtain and having standardized specifications.

As it has been stated before, one requirement for forming a narrow polydisperse multiblock copolymer in a sequential polymerization is, for example in the case of an AB diblock, that the first-formed polymeric thiocarbonylthio compound (macroCTA) should have a higher transfer constant in the subsequent polymerization step to allow the growth of the B block[10]. Therefore, synthesis of the homopolymer must be checked for both monomers with the three CTAs selected, as well as further polymerization of the AB diblock copolymer with homopolymer A and B.

Needless to say that the proper selection of the CTA is not enough to ensure a controlled/living radical polymerization, appropriate ratio of monomer to CTA and CTA to initiator must be considered to achieve a good control over molecular weight and polydispersity. Both ratios depend on the monomer type and desired molecular weight[10]. On one hand, monomer concentration has to be much higher than the concentration of CTA to increase the probability of initiator's addition to the monomer prior to the addition to the CTA[7]. In addition, RAFT concentration must be kept low to prevent substantial retardation[77]. Adjusting monomer to RAFT ratio allows control over the desired molecular weight as indicated by **¡Error! No se encuentra el origen de la referencia.**)[78].

On the other hand, the ratio of CTA to initiator has to be high as well in order to minimize termination events[7]. As shown by several authors, control over

polymerization increases with increasing ratio of [CTA]/[I], leading to a decrease in M_n and PDI, due to a polymerization rate decrease as more chain transfer reactions occur via the reversible addition-fragmentation mechanism[7,79,80]. Vega-Rios *et al.* polymerized HEMA with PHPA (Figure 3.10A) at a [CTA]/[I] ratios between 25:1 and 50:1 and [HEMA]/[CTA] ratio around 300-400:1, whereas Zhou *et al.* copolymerized HEMA and cholesteroyl methacrylate (CMA) with DCMA at a [CTA]/[I] of 33:1 and a [CMA]/[CTA] ratio between 5:1 and 20:1. Therefore, as ratios varies for each monomer-CTA couple, for the copolymerization of HEMA and Ma-acap-CHOL the ratios were initially fixed at 25:1 for [M]/[CTA] and at 10:1 for [CTA]/[I].

Since RAFT is a conventional radical polymerization conducted in the presence of a CTA agent, traditional methods for radical generation can be used. The most commonly employed method is the application of azo compounds, such as azobisisobutyronitrile (AIBN), as they can be used over a wide range of temperatures[8]. Either way, in RAFT polymerization, the initiator is a minor component of the reaction mixture, thus the consequences of a poor initiator selection may not be detectable[81].

Taking all the aforementioned factors, homopolymers of poly(2-hydroxyethyl methacrylate) (pHEMA) and poly(Ma-acap-Chol) (pCHOL) were synthesized with the three selected CTAs, PHPA, DSPA and DCMA, using AIBN as an initiator in a ratio of [M]/[CTA] of 25:1 and [CTA]/[AIBN] of 10:1, at 70° for 24 hours. Table 3.1 shows the characterization by NMR and GPC in terms of monomer conversion, molecular weight (M_n) and polydispersity (PDI) of both homopolymers.

Table 3.1: Characterization of hydrophilic block (HEMA) and hydrophobic block (CHOL) polymerized with different CTAs.

Sample	$[CTA]_0:[I]_0$	$[M]_0:[CTA]_0:[I]_0$	Monomer conversion[a] (%)	M_n H^1-NMR[a] (g/mol)	M_n GPC (g/mol)	M_w GPC (g/mol)	PDI[b]
pHEMA PHPA	10:1	25:1:0.1	50	668	n.d.	n.d.	n.d.
pHEMA DSPA			94	5634	3451	4414	1.28
pHEMA DCMA			95	6518	16039	25400	1.58
pCHOL PHPA			25	2140	n.d.	n.d.	n.d.
pCHOL DSPA			43	2610	n.d.	n.d.	n.d.
pCHOL DCMA			92	12312	9200	12622	1.37

[a] As determined by ^{1}H-NMR; [b] PDI=Mw/Mn

The first RAFT agent tested, PHPA, was found to be not suitable as a chain transfer agent for none of the monomers as the conversion percentages were below de 50% and M_n could not be measured by GPC because no peak was detected, suggesting that polymerization proceeded to a very limited extent. Regarding HEMA polymerization, conversion percentages were closer to 100% when using DSPA and DCMA as CTAs. Polymerization in the presence of DSPA rendered an average molecular weight (M_n) similar to RAFT theoretical value calculated using **¡Error! No se encuentra el origen de la referencia.**, which was 6528 g/mol, with a polydispersity index of 1.28, typical from trithiocarbonates[12]. On the contrary, DCMA produced polymers with higher polydispersity index (1.58) than what would be expected for living polymerizations (PDI<1.4)[6] and a dramatic increase in M_n, suggesting that probably, in this case, the polymerization approached a free radical mechanism rather than being controlled via a RAFT mechanism.

A similar trend was observed regarding pCHOL polymerization (Table 3.1). DCMA

A similar trend was observed regarding pCHOL polymerization (Table 3.1). DCMA provided large polymers (large M_n) with high PDI as well. Although a fraction of CHOL monomer polymerized, as indicated by monomer conversion observed in ^{1}H-NMR, molecular weight could not be measured in GPC when using DSPA and PHPA as chain transfer agents because the absence of peaks, probably indicating that polymerization proceeded to a very limited extent. However, these results were not determining as CHOL was not the initial block to polymerize, therefore its polymerization would be controlled by the macroCTA of the previous block, pHEMA-CTA, whose effect on the polymerization would vary from the CTA itself. Hence, polymerization of CHOL monomer will be later studied with pHEMA-CTA.

Discrepancies observed between molecular weights calculated by GPC and ^{1}H-NMR were probably related to the limitations of both techniques. On one hand, in GPC, polymers can adopt more compact structures in solution and can interact with the stationary phase. Therefore, polymers with higher molecular weights could become absorbed onto the surface of the matrix and exhibit an inhibited flow through the porous media[82], showing molecular weights smaller that the real value. On the other hand, the molecular weight calculated from ^{1}H-NMR is based on the ratio of CTA to polymer signals. Taking into account that there is one molecule of CTA per chain of polymer, the number of monomer units per chain of polymer can be calculated.

To further understand the differences between DCMA and DSPA in the polymerization kinetics of pHEMA and determine which CTA should be selected, samples were collected and analysed at different time points during 24 hours of polymerization (Figure 3.11).

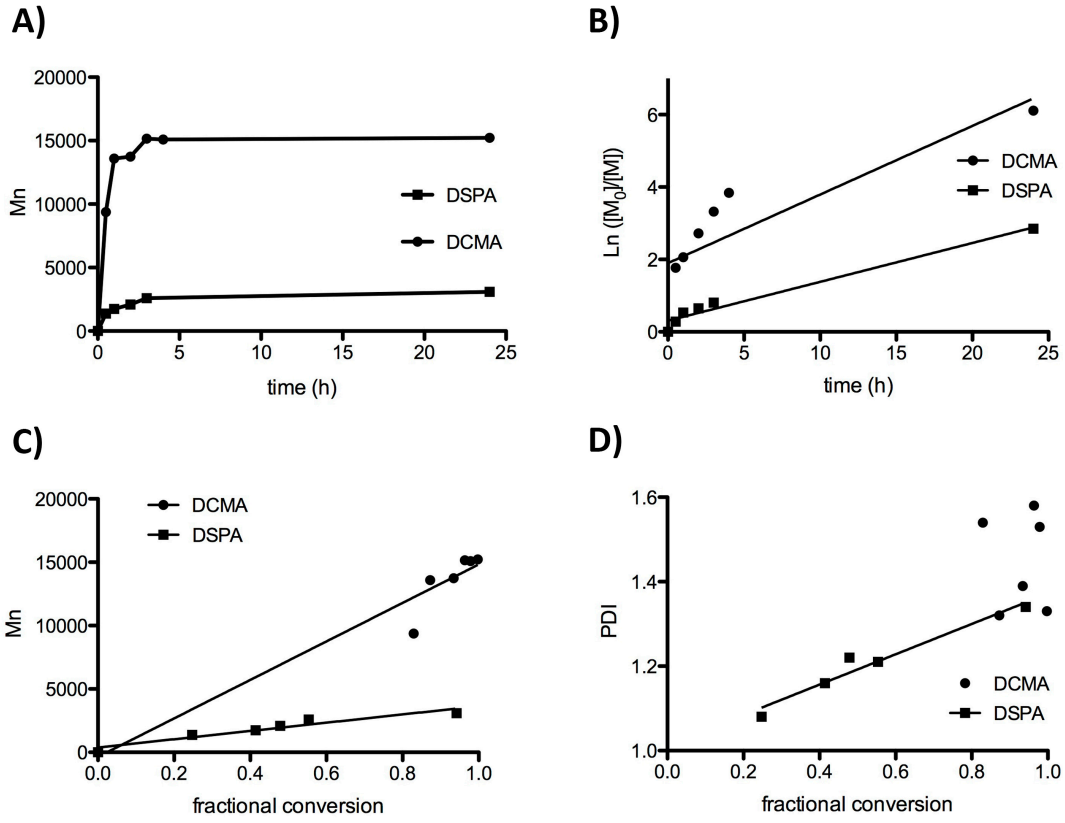

Figure 3.11: Polymerization kinetics of HEMA polymerization comparing the efficacy of DCMA and DSPA as RAFT agents. A) Evolution of M_n through polymerization. B) Ln([M_0]/[M]) vs polymerization time. C) Number average molecular weight (M_n) *vs* monomer conversion. D) Polydispersity index (PDI) *vs* monomer conversion.

Figure 3.11A shows the molecular weight evolution of pHEMA during polymerization making clear that the polymerization rate was much higher in the presence of DCMA as M_n was 5 times larger from the very beginning of polymerization, compared to DSPA. The linearity of Ln([M_0]/[M]) vs polymerization time indicates that the system obeys a living radical polymerization mechanism, explaining that the concentration of the growing radicals was constant during the polymerization[83]. In Figure 3.11B, a pseudo-first order kinetic was observed for the polymerization in the presence of DSPA, confirming that polymerization followed a living radical polymerization process. However, for the polymerization using DCMA, the plot lost linearity, reminding of a typical free radical polymerization that did not proceed in a controlled fashion. In addition, both plots (A and B) showed a lower polymerization rate in the case of DSPA, demonstrating that more chain transfer reactions occurred via the reversible addition fragmentation mechanism in this case. The number-average molecular weight (M_n) increased in a linear fashion with respect to monomer conversion in the presence of DSPA, while a typical free radical growth was observed when using DCMA (Figure 3.11C). PDI was well controlled during polymerization and was kept around 1.2 in the case of DSPA, however, when using DCMA as a CTA, PDI did not follow any defined trend and was always above 1.3 (Figure 3.11D).

In the light of these results, it can be concluded that DSPA acted controlling the polymerization of pHEMA yielding polymers with reasonable molecular weight and polydispersity index, typical from living radical polymerizations. On the other hand, DCMA was found to be unable to control HEMA polymerization, showing typical behaviours of free radical polymerizations with a fast increase of molecular weights and high polydispersity, thus not being efficient as a chain transfer agent for the polymerization of HEMA. Taking this fact into account and in the light of these results, the CTA selected, a priori, to perform the multiblock copolymer polymerization was DPSA, as it allows the synthesis of the first block (HEMA) in a controlled manner.

3.3.3 Length of hydrophobic block

After choosing the most convenient CTA for the polymerization of pHEMA, polymerization of the hydrophobic block, pCHOL, was performed with pHEMA macroCTA to make sure it was able to polymerize to render the diblock copolymer. Once synthesized, the precursor of the diblock copolymer was deprotected to render the diblock copolymer (Figure 3.12).

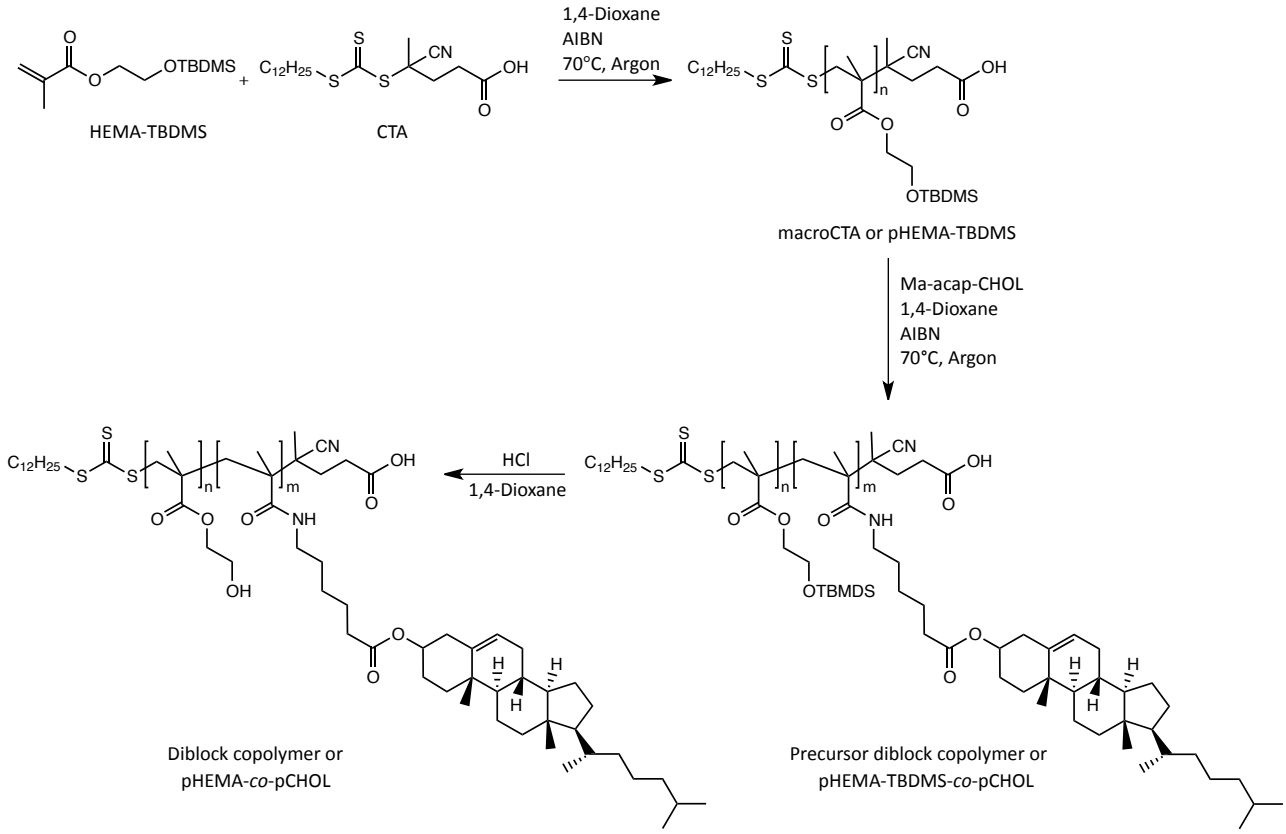

Figure 3.12: Synthesis route of diblock copolymer (pHEMA-*co*-pCHOL).

As mentioned before, the length of the hydrophobic block is an important factor to control the following self-assembly of the multiblock copolymer[84]. Therefore, pHEMA macroCTA was polymerized with CHOL at different polymerization times to obtain different pCHOL lengths. Nanostructures were obtained from the self-assembly of diblock copolymers in water through the film hydration technique, which were characterized by DLS. Table 3.2 shows the characterization of diblock copolymers in terms of monomer ratio, molecular weight (M_n), polydisperstity index (PDI) and nanostructures' size, at three different polymerization times, ranging from 1 to 6 hours of CHOL's polymerization.

Table 3.2: Characterization of diblocks with different pCHOL lengths synthesized using DSPA as CTA.

Sample	Time (h)	[HEMA]:[CHOL][a]	M_n H^1-NMR[a] (g/mol)	M_n GPC (g/mol)	M_w GPC (g/mol)	PDI[b]	NPs Size[c] (nm)
pHEMA-pCHOL	1	1:0.9	18265	9853	12027	1.22	133 ± 45.2
pHEMA-pCHOL	2	1:1.2	19058	13694	17335	1.27	98 ± 31
pHEMA-pCHOL	6	1:1.3	21175	10446	14333	1.43	71 ± 5.8

[a] As determined by ^{1}H-NMR; [b] PDI=Mw/Mn; [c] Measured by DLS.

It was demonstrated that it was possible to polymerize CHOL with pHEMA macroCTA to render a diblock copolymer of p(HEMA-co-CHOL), although CHOL's homopolymer polymerization did not work very well with DSPA as a chain transfer agent (Table 3.2). As expected, monomer ratio, molecular weight, calculated by ^{1}H-NMR, and polydispersity index increased with polymerization time. The first two diblocks were very similar in terms of M_n and polydispersity, which was kept below

1.3, indicating the control in their radical polymerizations. Regarding molecular weight, measured by GPC, an initial increase was observed from 1 to 2 hours of polymerization, followed by a decrease after 6 hours. As mentioned before, this final decrease in M_n can be attributed to a higher packing of diblock copolymer with longer hydrophobic block, thus being more retained in the pores of the stationary phase showing a lower apparent molecular value[82].

Interestingly, it was also proved that amphiphilic diblock copolymers of pHEMA and pCHOL were able to self-assemble and form nanostructures in water for any length of the hydrophobic block that were tested. Although no significant difference was observed among size values of the first two diblocks, a decrease in size was observed for the longest hydrophobic block. This decreasing trend seen is in good correlation with hypothesis presented by other authors, which suggest that longer hydrophobic blocks provided a stronger driving force for micellization[11].

Taking into account that it was sought to keep the total molecular weight of the multiblock below 30-50 KDa, molecular weight of the diblock could not be very high considering that the polymerization of the three remaining blocks would increase M_n as well and there would be a risk of exceeding the renal threshold. Therefore, to proceed with the following blocks, CHOL was polymerized for two hours to obtain diblocks below 20,000 g/mol, with acceptable polydispersity indexes and particles size.

3.3.4 Block copolymer characterization

Once the length of the hydrophobic block had been fixed, the diblock copolymer was fully characterized by ^{1}H-NNMR, ^{13}C-NMR and IR, which confirmed the proper synthesis of pHEMA-TBDMS-*co*-pCHOL (Figure 3.13).

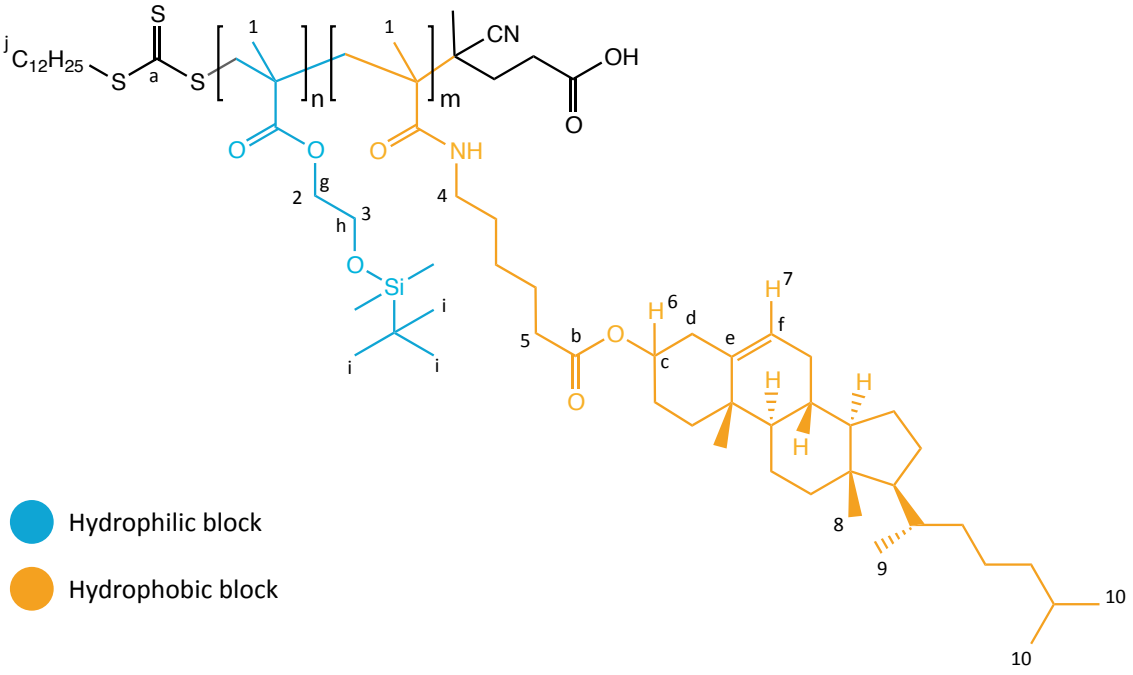

Figure 3.13: Scheme of the diblock copolymer (pHEMA-TBDMS-*co*-pCHOL) synthesized using DSPA as CTA.

Regarding ^{1}H-NMR analysis, broadening of the signals that belonged to the side chain of the polymer were observed as expected, due to missing isotropic molecular tumbling in solid state NMR[85]. The ^{1}H-NMR spectrum (400 MHz, THF-d_8, TMS, δ in ppm) of the synthesized pHEMA-TBDMS-*co*-pCHOL showed typical signals of cholesterol at 5.38 (s, 1H, H^7) and 4.55 (s, 1H, H^6), Ma-acap-CHOL methylenes at 3.09 (s, 2H, H^4) and 2.3 (s, 2H, H^5), and methyls at 0.74 (s, 3H, H^8) and 0.8 (d, 6H, H^{10}). Typical signals of HEMA methylenes were observed at 4.03 (s, 2H, H^2) and 3.75 (s, 2H, H^3), while methyls from polymer backbone were shown at 2.05 (s, 6H, H^1) ppm.

The addition of more blocks to the diblock copolymer analysed did not modify NMR or IR signals of the copolymer, but results in an increase of signal intensity of the added block. Therefore the characterization of the further multiblock copolymers was performed by GPC and ^{1}H-NMR, which allowed the measurement of the block ratio (pHEMA:pCHOL).

3.3.5 Number of blocks

After having completely characterized the first block copolymer, multiblock copolymers, ranging from diblock to pentablock, were synthesized by subsequent RAFT polymerization with purification of every block. Table 3.3 shows the characterization of all blocks in terms of total molecular weight and preliminary size and zeta potential values of the self-assembled nanostructures in water.

Table 3.3: Characterization of consecutive multiblock copolymers synthesized with DSPA as CTA

Sample	[HEMA]:[CHOL][a]	M_n H^1-NMR[a] (g/mol)	M_n GPC (g/mol)	M_w GPC (g/mol)	PDI[b]
Diblock	1:1.2	19058	13694	17335	1.27
Triblock	1.9:1.6	35490	12841	16501	1.29
Tetrablock	1.8:2.3	46434	18526	33796	1.82
Pentablock	2.9:2.3	52462	18701	36848	1.97

[a] As determined by 1H-NMR; [b] PDI=Mw/Mn; [c] Measured by DLS.

As shown in Table 3.3, molecular weight, calculated by ^{1}H-NMR, increased with number of blocks, which confirms block extension. In addition, the HEMA:CHOL ratio varied according to the expected composition of the different blocks. Although an increase in M_n was also observed in GPC values, it was not as clearly observed in ^{1}H-NMR values. As already observed in the analysis of diblock formation, this phenomenon might suggest that as block number increased, multiblock copolymers could adopt more compacted conformations, which could modify copolymer-matrix interaction[82], showing an apparent molecular weight smaller than the real M_n value.

Molecular weight distributions were relatively narrow, around 1.2, but broadened with increasing number of blocks, up to 1.97. This increase in PDI may indicate that the polydispersity of each block is accumulated and added up in the final multiblock, resulting in higher PDIs for the largest multiblocks, as shown by other authors[11]. In addition, it must be taken into account that CTA may degrade after subsequent polymerizations due to hydrolysis of the trithiocarbonate group, thus having a mixture of polymeric chains without CTA and chains with CTA that keep polymerizing.

Similarly to diblock copolymers, all multiblock copolymers, ranging from triblock to pentablock, were able to self-assemble in water and form nanostructures through

direct nanoprecipitation technique. Characterization of these nanostructures in terms of size and zeta potential was performed by DLS and NTA (Table 3.4).

Table 3.4: Characterization of self-assembled nanostructures from multiblock copolymers with DLS and NTA

Sample	NPs Size[a] (nm)	NPs Size[b] (nm)	Zeta potential[c] (mV)
Diblock	98 ± 31	95 ± 15	-49.3 ± 9.4
Triblock	114 ± 9	109.8 ± 3.5	-41.8 ± 7.8
Tetrablock	33 ± 1,6	142.7 ± 4.7	-16.2 ± 2.1
Pentablock	30 ± 4.4	157.8 ± 7.4	-14.4 ± 4.4

[a,c] Measured by DLS (by intensity and number); [b] Measured by NTA.

Regarding size of the nanostructures formed in water, a general decreasing trend was observed with increasing number of blocks, from tri- to pentablock copolymers, in DLS (Table 3.4). This decrease in the hydrodynamic radius is in good correlation with the phenomenon exhibited in GPC (Table 3.3), suggesting that copolymers with higher number of blocks would be able to form more compacted nanostructures with smaller hydrodynamic radius showing lower molecular weights than expected. The formation of these higher compacted conformations may be related to the higher bending modulus of higher molecular weight polymers, such as tetra- and pentablock, thus longer copolymers could bend easily and possibly pack better[33].

Regarding zeta potential, a decrease in absolute value was observed as number of blocks increased. As mentioned in previous chapters, zeta potential can be related to the potential stability of the colloidal system, being more stable those systems with larger zeta potential in absolute value. Thus, in this case, multiblock with higher number of blocks were supposed to be less stable as they showed lower zeta potential values, suggesting a lower repulsion between particles which could favour their aggregation.

Comparing size measurements between different techniques, such as DLS and NTA, values showed good correlation for di- and triblock. However, larger sizes were observed for larger copolymers, tetra- and pentablocks, when measured by NTA. In addition, the decrease in size of larger copolymers observed by DLS, was inverted in NTA results. In order to clarify these discrepancies between techniques and gain a further insight into size and morphology, nanostructures were further analyed by Transmission electronic microscopy (TEM) (Figure 3.14).

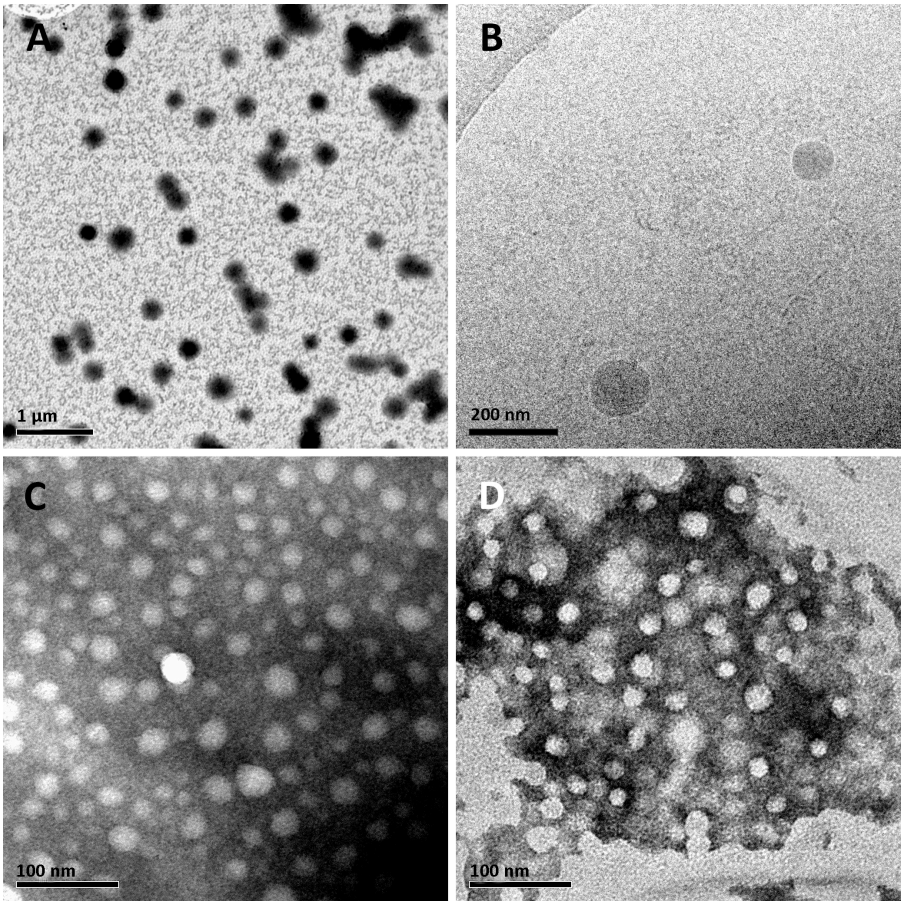

Figure 3.14: TEM images of self-assembled multiblock copolymers.(A) Diblock, (B) Triblock , (C) Tetrablock and (D) Pentablock copolymer. A, C and D were performed with uracil staining, whereas B was performed by cryoTEM.

TEM images of self-assembled multiblock copolymers confirmed the formation of the nanostructures already analysed by DLS and NTA. All multiblock copolymers showed round-shape, uniform and monodisperse nanostructures (Figure 3.14). These round-shape nanostructures discarded the formation of rods or lamellar structures, demonstrating the formation of micelles or vesicles. Regarding sizes, values of all multiblock copolymers are in good correlation with DLS results. The discrepancy between DLS and NTA values may be attributed to the fact that NTA was working at its optimum lower limit, which is 30 nm.

In the light of the results, it can be concluded that self-assembly of amphiphilic multiblock copolymers with narrow molecular weight distribution render round-shape nanostructures with low polydispersity, with smaller hydrodynamic radius for copolymers with higher number of blocks.

3.3.6 Preparation method

Although it has been demonstrated that round-shaped nanostructures with low polydispersity and an acceptable size were obtained through direct nanoprecipitation technique, the influence of the preparation method on the resulting nanostructures' size was studied. Self-assembly of multiblock copolymers, ranging from diblock to pentablock, was achieved through direct and inverse nanoprecipitation and film

hydration technique, with additional sonication in the last method, at the same initial copolymer concentration. Characterization of the obtained nanostructures in terms of size and zeta potential is shown in Table 3.5, measured by DLS.

Table 3.5: Characterization of nanostructures depending on the preparation method

Sample	Method	Size (nm)	Zeta potential (mV)
Diblock	DP	98 ± 31	-46 ± 0.8
	IP	87.8 ± 1.4	-60 ± 5.7
	Sonication	104 ± 8.3	-49 ± 3.6
Triblock	DP	107 ± 5.7	-40 ± 3.7
	IP	113 ± 3.9	-32 ± 2.7
	Sonication	110 ± 3.5	-37.8 ± 4.1
Tetrablock	DP	33 ± 1.6	-16.2 ± 2.1
	IP	35 ± 0.1	-9.7 ± 1.89
	Sonication	99.7 ± 11.9	-17.12 ± 3.7
Pentablock	DP	31.3 ± 0.18	-14.4 ± 4.44
	IP	27.5 ± 0.4	-18.06 ± 0.9
	Sonication	95.9 ± 9.6	- 17.96 ± 3.9

DP is Direct nanoprecipitation and IP is Inverse Nanoprecipitation

As a general trend, nanostructures obtained through direct and inverse nanoprecipitation showed the same size for each multiblock (Table 3.5), preserving the decreasing trend as number of blocks increase, observed in Table 3.4. The film hydration technique followed by sonication rendered nanostructures with the same size than precipitation for triblock copolymers. However, in the case of larger multiblocks, tetra- and pentablock, this technique produced nanostructures much larger than nanoprecipitation. This fact could be explained because of the principle of nanostructures' formation through this technique. As exposed before, water must penetrate into the pores and imperfections of the polymer's film to finally detach hydrated lipid sheets from the surface to render multilamelar vesicles (Figure 3.8). Therefore, in the case of larger polymers, it might be more difficult for water to penetrate into deeper layers properly, thus generating larger multilamelar vesicles. This may suggest that these larger multiblock copolymers could require higher hydration time or more vigorous stirring, as these parameters differ among different polymer's nature or structure[86].

Regarding zeta potential, values were similar for each copolymer between different techniques. Again, showing lower values for larger multiblocks, indicating a possible greater tendency to aggregation.

3.3.7 Drug loading

Once it has been demonstrated the possibility of obtaining nanostructures from all the studied multiblock copolymers trough three different techniques, their ability to encapsulate drugs at high concentration will determine weather they are suitable for drug delivery. Micelles[54] and vesicles[87,88] have shown their capability to encapsulate hydrophobic drugs, thanks to the hydrophobic core, in the case of micelles, and to the hydrophobic membrane, in the case of vesicles. Paclitaxel has been one of the most widely used hydrophobic drug in drug delivery systems thanks to its potent anti-angiogenic effect[89] and its traceability by HPLC[90]. Therefore, paclitaxel loading efficiency and capacity of nanostructures from multiblock copolymers were evaluated.

Taking into account that encapsulation efficiencies are lower for bulk methods compared to rehydration technique[46,91], nanoprecipitation was discarded for loading purposes and substituted by the film hydration techniques. Therefore, paclitaxel was loaded *in situ* by co-dissolving it with the copolymer and preparing the film by solvent evaporation to proceed with the film's rehydration in aqueous media. Table 3.6 shows loading efficiency and capacity, and physical characterization of paclitaxel-loaded nanostructures from triblock, tetrablock and pentablock copolymers. Loading of nanostructures was measured by HPLC, while physical characterization was performed by DLS.

Table 3.6: Characterization of paclitaxel-loaded self-assembled nanostructures from multiblock copolymers

Sample	Size (nm)	Zeta potential (mV)	Loading efficiency (%)	Loading capacity (%)
Triblock	148 ± 18.13	-47 ± 1.84	40.16 ± 6.7	3.06 ± 1.28
Tetrablock	117.2 ± 9.12	-17.43 ± 0.45	62.95 ± 5.01	7.19 ± 0.6
Pentablock	158.8 ± 10.11	-22.6 ± 1.04	72.3 ± 0.08	7.16 ± 0.01

As expected, size of nanostructures of all multiblocks increased when they were loaded (Table 3.6) compared to non-loaded nanostructures obtained by the film rehydration technique (Table 3.5). This increase in size might be due to the space that the loaded drug occupies, which might also interfere in block interactions leading to less compacted nanostructures. The decreasing trend in size observed in previous sections is kept between triblock and tetrablock nanostructures, but not for pentablock ones.

Regarding zeta potential, paclitaxel-loaded nanostructures showed negative values keeping the decreasing trend as block number increased, as already observed in Table 3.5. Thus, incorporation of paclitaxel did not alter the zeta potential value of the nanostructures as non-loaded formulations showed similar values, which can be explained by the lack of ionisable functional groups in the paclitaxel molecule[92].

In terms of loading, efficiency reached the 40% for triblock copolymer, which is slightly higher than what has been described for block polymersomes of PEG-Polycarbonate[70], whereas a 3% of loading capacity is comparable to the capacity of this PEG-Polycarbonate polymersomes, but lower than the 11% reached by Polybutadiene-PEO diblock copolymers[87]. Both loading efficiency and capacity increased with increasing number of blocks. This difference in loading capacity is in good agreement with the different hydrophobic ratio between triblock and the larger multiblocks, tetra and penta, as the second ones contain an additional hydrophobic block. This fact suggests that loading capacity is higher when drug-polymer interactions are maximized[93], thus larger amounts of hydrophobic substances can be encapsulated by raising the molecular weight of the hydrophobic block[87,91]. In the light of the results, it has been demonstrated that nanostructures from multiblock copolymers of an acceptable size, are able to load paclitaxel at high loading efficiency and capacity being suitable for therapeutic delivery of drugs.

Because their higher structural complexity, homogeneous multiblock copolymers (tetra- and pentablock) are more difficult to synthesize than diblocks and ABA triblocks. Thus, multiblocks are used only when they provide a clear advantage over

their lower homologues[11]. Consequently, the existing literature about amphiphilic block copolymers is mostly focused on di- and triblocks. In this work, larger multiblock copolymers have shown the ability to form smaller nanostructures and possess higher loading efficiency and capacity. However, they showed a higher tendency to aggregation compared to their lower homologues. Therefore, amphiphilic triblock copolymers were selected as reasonable candidates to perform further experiments, as they were able to form nanostructures of acceptable size, showed lower tendency to aggregation and presented an intermediate loading efficiency and capacity compared to what has been published[70,87].

3.3.8 Study of loading versatility of self-assembled nanostructures from triblock copolymer

As mentioned before, an attractive characteristic of polymersomes (vesicles) obtained from the self-assembly of amphiphilic block copolymers is their ability to entrap both hydrophilic and hydrophobic substances simultaneously. However, at this point, the exact conformation adopted in solution by the nanostructures here presented, was still unknown. Although TEM images showed round-shape nanostructures, it is usually difficult to distinguish the existence of a bilayer structure in the case of plain vesicles with this technique[94]. Therefore, in order to discern whether they are micelles or vesicles, an easy and fast assay was performed by fluorescence microscopy. Taking advantage of the ability of polymersomes to entrap simultaneously hydrophilic and hydrophobic compounds, the assay consisted in the simultaneous encapsulation of a hydrophilic (fluorescein) and a hydrophobic (nile red) fluorescent probe, so that it would result in the encapsulation of each fluorophor in separated compartments, fluorescein in the core and nile red in polymersomes' wall[59,95].

Figure 3.15 shows confocal microscopy images of simultaneously nile red and fluorescein-loaded nanostructures formed with an amphiphilic triblock copolymer.

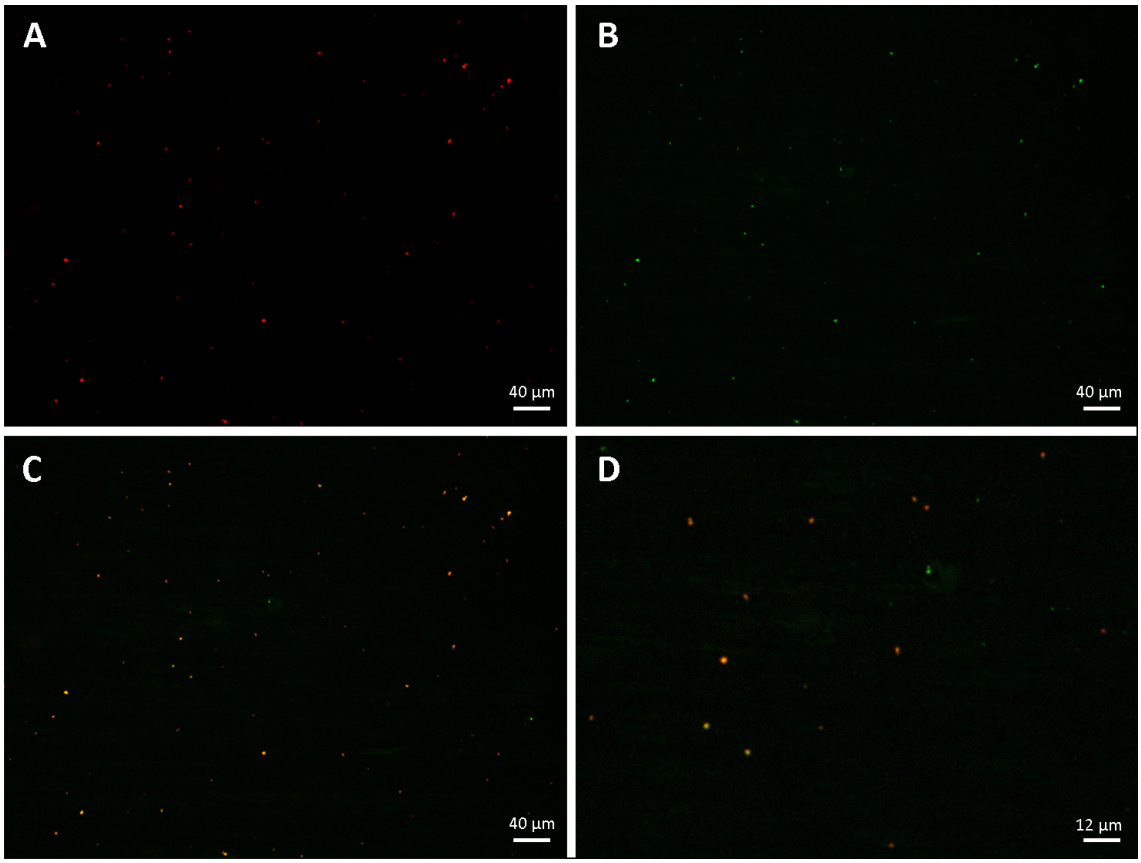

Figure 3.15: Confocal microscopy images of Nile Red and Fluorescein-loaded nanostructures. A) Nile Red-loaded nanostructures. B) Fluorescein-loaded nanostructures. C) Colocalization of Nile red and fluorescein-loaded nanostructures. D) Amplification of image C.

Confocal microscopy images showed round-shape monodisperse nanostructures loaded with Nile red (Figure 3.15A) and fluorescein (Figure 3.15B). Colocalization of Nile red and fluorescein in round-shape particles was observed in Figure 3.15C and D, with a Pearson's coefficient of 0.797, suggesting that the same nanostructure was able to entrap hydrophilic and hydrophobic substances. Due to the nanometric size of these nanostructures, it was not able to visualize distinguished compartments of the nanostructures, such as a wall and a core, which could be observed in experiments performed with giant polymersomes[61,96].

At the same time, the same nanostructures were loaded with just a hydrophobic substance (Nile red) in order to increase contrast in TEM images and allow to distinguish polymersomes wall[94]. Figure 3.16 revealed round-shape nanostructures of 200 nm with two distinguished compartment, a darker core and a lighter wall. The difference between nanostructures observed in Figure 3.14 and in Figure 3.16, was attributed to the loading of a hydrophobic substance that would be located in the hydrophobic region of the nanocarrier, thus allowing nanostructure's wall visualization due to a change in contrast.

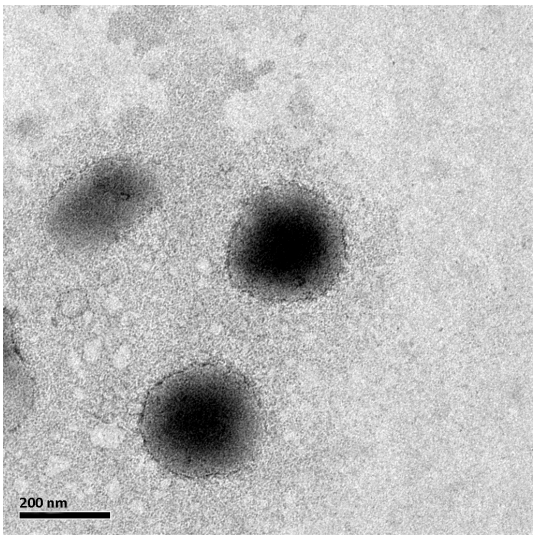

Figure 3.16: TEM images of Nile red-loaded nanostructures from triblock copolymer. Staining used was uranyl acetate.

In the light of these preliminary results, it seemed that nanostructures formed from the self-assembly of the presented triblock copolymers were able to encapsulate both hydrophilic and hydrophobic substances in separated compartments, being the hydrophobic substances entrapped in nanostructure's wall. However, loading capability of these nanostructures had to be determined qualitatively and quantitatively as well, as the loading efficiency and capacity of these systems are critical in order to reach therapeutic amounts of the entrapped drug to make them suitable for drug delivery. Therefore, encapsulation was performed with paclitaxel (hydrophobic), as shown previously, and doxorubicin (hydrophilic), which shows excellent anti-neoplastic activity against a multitude of human cancer diseases[97].

As mentioned before, paclitaxel was loaded *in situ* by the film rehydration technique. However, doxorubicin loading, was performed on preformed vesicles by a remote loading technique that has become very popular for liposomes' loading[69]. This technique consists in the generation of a pH gradient between the external physiologic medium (pH=7.4) and the acidic interior of vesicles rehydrated with citrate buffer (pH=4), which allows the drug to diffuse inside the vesicles where is protonated being unable to permeate through the bilayer to the outside and remain entrapped inside. Therefore, pH remote loading technique has been widely used in doxorubicin's loading as it achieves high loading efficiencies[98,99]. The physical characterization of paclitaxel and doxorubicin-loaded nanostructures as well as their loading efficiency and capacity (also known as drug content) is shown in Table 3.7.

Table 3.7: Characterization of loaded nanostructures from triblock copolymer

Sample	Size (nm)	Zeta potential (mV)	Loading efficiency (%)	Loading capacity (%)	Loaded Drug
Triblock	160.2 ± 26.5	13.2 ± 1.14	51.97 ± 8.4	3.96 ± 1.7	Doxorubicin
Triblock	148 ± 18.13	-47 ± 1.84	40.16 ± 6.7	3.06 ± 1.28	Paclitaxel

Results from Table 3.7 demonstrate the ability of nanostructures from triblock copolymers to load both paclitaxel and doxorubicin. As already shown for paclitaxel

loading, size of doxorubicin-loading nanostructures also increased compared to non-loaded nanostructures obtained by the film rehydration technique (Table 3.5). No significant difference in size was observed between paclitaxel and doxorubicin-loaded nanostructures. Regarding zeta potential, doxorubicin-loaded nanostructures changed substantially to positives values, compared to paclitaxel. This difference may be due to the positively charged amine groups of doxorubicin, which is a monocationic base[100,101].

In terms of doxorubicin loading, nanostructures from triblock copolymers showed an acceptable loading capacity around 4% and a loading efficiency around 50%, similar to the results described for biodegradable polymersomes of MPEG-Polycaprolactone loaded through the pH gradient technique, which achieved a 4.4% of loading capacity[63].

These results demonstrate the ability of the self-assembled triblock copolymer nanostructures to encapsulate both hydrophilic and hydrophobic drugs, reinforcing fluorescent microscopy results (Figure 3.15) and suggesting the formation of a compartmentalized nanostructure. It has been described that this dual capacity in terms of loading is typical for polymersomes, thanks to their compartmentalized structure with a hyprophobic membrane physically separated from the hydrophobic core. In contrast, micelles mostly encapsulate hydrophobic compounds[67] as a result of their inner hydrophobic core protected from the outside by a hydrophilic shell, whose function is basically to provide colloidal stability in an aqueous environment rather than being able to allocate hydrophilic substances like polymersomes' hydrophilic inner core[102] . To probe this, some authors have tried to load paclitaxel and doxorubicin in micelles and polymersomes, revealing that polymersomes were able to load both drugs, whereas micelles loaded only paclitaxel at higher loading efficiency and capacity compared to polyersomes[70].

In the light of the results, it has been demonstrated that nanostructures from multiblock copolymers of an acceptable size, are able to load both paclitaxel and doxorubicin at high loading efficiency and capacity, suggesting a polymersomal structure and being suitable for therapeutic delivery of drugs. Interestingly, polymersomes from amphiphilic triblock copolymers are the systems that resemble the most to liposomal structure because their assembly mimics a bilayer membrane with hydrophilic blocks on the opposite sites separated by a hydrophobic block. Therefore, liposomes, which are widely studied platforms, may serve as a reference to determine the suitability as a drug delivery system (DDS) of their polymeric equivalent, polymersomes from triblock copolymers.

3.4 Concluding remarks

In this chapter, the preparation of self-assembling amphiphilic multiblock copolymers as potential drug delivery systems has been demonstrated.

Acrylamide monomers have been substituted for two biocompatible and non-cytotoxic monomers, such as HEMA, as the hydrophilic one, and Ma-acap-CHOL, as the hydrophobic one. RAFT polymerization has allowed the subsequent synthesis of multiblocks copolymer, ranging from the diblok to the pentablock copolymer. DSPA was selected as the proper CTA for the polymerization of HEMA's homopolymer in a controlled manner to obtain predetermined molecular weight polymers with narrow molecular weight distributions (PDI < 1.3). In addition, the macroCTA formed by pHEMA and DSPA was able to polymerize Ma-acap-CHOL rendering multiblock copolymers up to pentablock with polydispersity indexes below 2. The regulation of polymerization time of the second block allowed the control of the hydrophobic block length, which influenced the final size of the self-assembled nanostructures, being two hours the ideal time to obtain diblock copolymers below 20 KDa of and acceptable size and polydispersity. Once the reaction conditions were optimized, multiblock copolymers were synthesized, ranging from triblock to pentablock. Polydispersity index increased with the number of blocks, indicating that the polydispersity of each block is accumulated and added up in the final multiblock. However, the polydispersity index of the highest multiblock did not exceed 2.

It has been demonstrated that amphiphilic multiblock copolymer, ranging from diblock to pentablock copoymers, self-assembled into round-shape nanostructures with low polydispersity in water as shown by DLS, NTA, TEM and fluorescence microscopy. Increasing number of blocks rendered smaller nanostructures but with higher tendency to aggregate. This trend was kept through all techniques employed, nanoprecipitation and film hydration. For lower copolymers, such as diblock and triblock, nanostructures formed showed the same size with all the techniques tested, whereas for higher copolymers, tetra- and pentablock, nanostructures obtained by film hydration technique were larger than those obtained by nanoprecipitation. It has been hypothesized, that this slight increase in size may suggest that is more difficult for the rehydrating solution to penetrate through the polymeric film's pores in the case of larger copolymers, thus larger vesicles are formed.

Nanostructures obtained through the film rehydration method showed the ability to encapsulate paclitaxel at high loading efficiency and capacity, for multiblocks ranging from triblock to pentablock, suggesting that higher loading of hydrophobic substances can be achieved by raising the ratio of hydrophobic blocks of the copolymer. In addition, nanostructures from triblock copolymers showed the ability to encapsulate both hydrophilic and hydrophobic substances with high loading efficiencies and drug content of paclitaxel and doxorubicin, suggesting the existence of a compartmentalized structure, typical from polymersomes, which is supported by TEM images as well.

In the light of the results presented in this chapter, it can be concluded that nanostructures obtained from the self-assembly of amphiphilic triblock copolymers, pHEMA-*co*-pCHOL-*co*-pHEMA, through the film hydration technique, arise as promising

platforms for the delivery of both hydrophilic and hydrophobic drugs at high loading efficiency and capacity.

3.5 References

1. Zetterlund, P. B.; Kagawa, Y.; Okubo, M. Controlled/Living Radical Polymerization in Dispersed Systems. *Chemical reviews* **2008**, *108*, 3747–3794.

2. Duncan, R. The Dawning Era of Polymer Therapeutics. *Nature reviews. Drug discovery* **2003**, *2*, 347–360.

3. Bulmus, V. RAFT Polymerization Mediated Bioconjugation Strategies. *Polymer Chemistry* **2011**, *2*, 1463.

4. Smith, A. E.; Xu, X.; Kirkland-York, S. E.; Savin, D. A.; McCormick, C. L. "Schizophrenic" Self-Assembly of Block Copolymers Synthesized via Aqueous RAFT Polymerization: From Micelles to Vesicles. *Macromolecules* **2010**, *43*, 1210–1217.

5. Boyer, C.; Stenzel, M. H.; Davis, T. P. Building Nanostructures Using RAFT Polymerization. *Journal of Polymer Science Part A: Polymer Chemistry* **2011**, *49*, 551–595.

6. Moad, G.; Rizzardo, E.; Thang, S. H. Living Radical Polymerization by the RAFT Process—a First Update. *Australian journal of chemistry* **2006**, *59*, 669.

7. Smith, A. E.; Xu, X.; McCormick, C. L. Stimuli-Responsive Amphiphilic (Co)Polymers via RAFT Polymerization. *Progress in Polymer Science* **2010**, *35*, 45–93.

8. Lowe, A. B.; McCormick, C. L. Reversible Addition–Fragmentation Chain Transfer (RAFT) Radical Polymerization and the Synthesis of Water-Soluble (Co)Polymers Under Homogeneous Conditions in Organic and Aqueous Media. *Progress in Polymer Science* **2007**, *32*, 283–351.

9. McCormick, C. L.; Sumerlin, B. S.; Lokitz, B. S.; Stempka, J. E. RAFT-Synthesized Diblock and Triblock Copolymers: Thermally-Induced Supramolecular Assembly in Aqueous Media. *Soft Matter* **2008**, *4*, 1760.

10. Vega-rios, A.; Licea-Claveríe, A. Controlled Synthesis of Block Copolymers Containing N-Isopropylacrylamide by Reversible Addition-Fragmentation Chain-Transfer (RAFT) Polymerization. *Journal of Mexican Chemical Society* **2011**, *55*, 21–32.

11. Hadjiantoniou, N. A.; Krasia-Christoforou, T.; Loizou, E.; Porcar, L.; Patrickios, C. S. Alternating Amphiphilic Multiblock Copolymers: Controlled Synthesis via RAFT Polymerization and Aqueous Solution Characterization. *Macromolecules* **2010**, *43*, 2713–2720.

12. Boyer, C.; Bulmus, V.; Davis, T. P.; Ladmiral, V.; Liu, J.; Perrier, S. E. B. Bioapplications of RAFT Polymerization. *Chemical reviews* **2009**, *109*, 5402–5436.

13. Fox, M. E.; Szoka, F. C.; Fréchet, J. M. J. Soluble Polymer Carriers for the Treatment of Cancer: the Importance of Molecular Architecture. *Acc. Chem. Res.* **2009**, *42*, 1141–1151.

14. Gormley, A. J.; Ghandehari, H. Evaluation of Toxicity of Nanostructures in Biological Systems. In *Nanotoxicity: From in vivo and in vitro models to health risks*; Sahu, S. C.; Casciano, D. A., Eds. John Wiley & Sons, Ltd., 2009; pp. 115–159.

15. Ge, Z.; Xie, D.; Chen, D.; Jiang, X.; Zhang, Y.; Liu, H.; Liu, S. Stimuli-Responsive Double Hydrophilic Block Copolymer Micelles with Switchable Catalytic Activity. *Macromolecules* **2007**, *40*, 3538–3546.

16. Kirkland-York, S.; Gallow, K.; Ray, J.; Loo, Y.-L.; McCormick, C. Temperature-Induced Ordering and Gelation of Star Micelles Based on ABA Triblocks Synthesized via Aqueous RAFT Polymerization. *Soft Matter* **2009**, *5*, 2179.

17. Schilli, C. M.; Zhang, M.; Rizzardo, E.; Thang, S. H.; Chong, B. Y. K.; Edwards, K.; Karlsson, G. O. R.; M u uller, A. H. E. A New Double-Responsive Block Copolymer Synthesized via RAFT Polymerization: Poly(N-Isopropylacrylamide)-Block-Poly(Acrylic Acid). *Macromolecules* **2004**, *37*, 7861–7866.

18. Mortisen, D.; Peroglio, M.; Alini, M.; Eglin, D. Tailoring Thermoreversible Hyaluronan Hydrogels by “Click” Chemistry and RAFT Polymerization for Cell and Drug Therapy. *Biomacromolecules* **2010**, *11*, 1261–1272.

19. Wadajkar, A. S.; Koppolu, B.; Rahimi, M.; Nguyen, K. T. Cytotoxic Evaluation of N-Isopropylacrylamide Monomers and Temperature-Sensitive Poly(N-Isopropylacrylamide) Nanoparticles. *Journal of Nanoparticle Research* **2008**, *11*, 1375–1382.

20. Fan, L.; Wu, H.; Zhang, H.; Li, F.; Yang, T.-H.; Gu, C.-H.; Yang, Q. Novel Super pH-Sensitive Nanoparticles Responsive to Tumor Extracellular pH. *Carbohydrate Polymers* **2008**, *73*, 390–400.

21. Wolf, F. F.; Friedemann, N.; Frey, H. Poly(Lactide)- Block -Poly(HEMA) Block Copolymers: an Orthogonal One-Pot Combination of ROP and ATRP, Using a Bifunctional Initiator. *Macromolecules* **2009**, *42*, 5622–5628.

22. Vert, M.; Li, S. M.; Spenlehauer, G.; Guerin, P. Bioresorbability and Biocompatibility of Aliphatic Polyesters. *Journal of materials science. Materials in medicine* **2014**, *3*, 432–446.

23. Mabilleau, G.; Moreau, M. F.; Filmon, R.; Baslé, M. F.; Chappard, D. Biodegradability of Poly (2-Hydroxyethyl Methacrylate) in the Presence of the J774.2 Macrophage Cell Line. *Biomaterials* **2004**, *25*, 5155–5162.

24. Kakwere, H.; Perrier, S. E. B. Design of Complex Polymeric Architectures and Nanostructured Materials/Hybrids by Living Radical Polymerization of Hydroxylated Monomers. *Polymer Chemistry* **2011**, *2*, 270.

25. Samsonova, O.; Pfeiffer, C.; Hellmund, M.; Merkel, O. M.; Kissel, T. Low Molecular Weight pDMAEMA-Block-pHEMA Block-Copolymers Synthesized via RAFT-Polymerization: Potential Non-Viral Gene Delivery Agents? *Polymers* **2011**, *3*, 693–718.

26. Ramos, V. Development of Cloaking Strategies for Lipid Membranes Using Amphiphilic Polymers, Univeristy of Oxford, 2007, pp. 1–247.

27. Chaw, C.-S.; Chooi, K.-W.; Liu, X.-M.; Tan, C.-W.; Wang, L.; Yang, Y.-Y. Thermally Responsive Core-Shell Nanoparticles Self-Assembled From Cholesteryl End-Capped and Grafted Polyacrylamides:; Drug Incorporation and in Vitro Release. *Biomaterials* **2004**, *25*, 4297–4308.

28. Yusa, S.-I. Self-Assembly of Cholesterol-Containing Water-Soluble Polymers. *International Journal of Polymer Science* **2012**, *2012*, 1–10.

29. Zhou, Y.; Kasi, R. M. Synthesis and Characterization of Polycholesteryl Methacrylate – Polyhydroxyethyl Methyacrylate Block Copolymers. *Journal of Polymer Science Part A: Polymer Chemistryer* **2008**, 6801–6809.

30. Rodríguez-Hernández, J.; Checot, F.; Gnanou, Y.; Lecommandoux, S. Toward "Smart" Nano-Objects by Self-Assembly of Block Copolymers in Solution. *Progress in Polymer Science* **2005**, *30*, 691–724.

31. Adams, M. L.; Lavasanifar, A.; Kwon, G. S. Amphiphilic Block Copolymers for Drug Delivery. *Journal of pharmaceutical sciences* **2003**, *92*, 1343–1355.

32. Harada, A.; Kataoka, K. Supramolecular Assemblies of Block Copolymers in Aqueous Media as Nanocontainers Relevant to Biological Applications. *Progress in Polymer Science* **2006**, *31*, 949–982.

33. Opsteen, J. A.; Cornelissen, J. J. L. M.; van Hest, J. C. M. Block Copolymer Vesicles*. *Pure and Applied Chemistry* **2004**, *76*, 1309–1319.

34. Onaca, O.; Enea, R.; Hughes, D. W.; Meier, W. Stimuli-Responsive Polymersomes as Nanocarriers for Drug and Gene Delivery. *Macromolecular bioscience* **2009**, *9*, 129–139.

35. Hadjichristidis, N.; Iatrou, H.; Pitsikalis, M.; Pispas, S.; Avgeropoulos, A. Linear and Non-Linear Triblock Terpolymers. Synthesis, Self-Assembly in Selective Solvents and in Bulk. *Progress in Polymer Science* **2005**, *30*, 725–782.

36. Discher, D. E. Polymer Vesicles. *Science* **2002**, *297*, 967–973.

37. Lee, J. S. Biodegradable Polymersomes for Drug Delivery, University of Twente, 2011, pp. 1–172.

38. Blanazs, A.; Armes, S. P.; Ryan, A. J. Self-Assembled Block Copolymer Aggregates: From Micelles to Vesicles and Their Biological Applications. *Macromolecular Rapid Communications* **2009**, *30*, 267–277.

39. Le Meins, J. F.; Sandre, O.; Lecommandoux, S. Recent Trends in the Tuning of Polymersomes' Membrane Properties. *Eur. Phys. J. E* **2011**, *34*, 14.

40. Ringsdorf, H.; Schlarb, B.; Venzmer, J. Molecular Architecture and Function of Polymeric Oriented Systems: Models for the Study of Organization, Surface Recognition and Dynamics of Niomembranes. *Angewandte Chemie (International ed. in English)* **2003**, *27*, 113–158.

41. Zhou, Y.; Briand, V. A.; Sharma, N.; Ahn, S.-K.; Kasi, R. M. Polymers Comprising Cholesterol: Synthesis, Self-Assembly, and Applications. *Materials* **2009**, *2*, 636–660.

42. Srinivas, G.; Shelley, J. C.; Nielsen, S. O.; Discher, D. E.; Klein, M. L. Simulation of Diblock Copolymer Self-Assembly, Using a Coarse-Grain Model. *The journal of physical chemistry. B* **2004**, *108*, 8153–8160.

43. Srinivas, G.; Mohan, R. V.; Kelkar, A. D. Polymer Micelle Assisted Transport and Delivery of Model Hydrophilic Components Inside a Biological Lipid Vesicle: a Coarse-Grain Simulation Study. *The journal of physical chemistry. B* **2013**, *117*, 12095–12104.

44. Lee, J. S.; Feijen, J. Polymersomes for Drug Delivery: Design, Formation and Characterization. *Journal of controlled release : official journal of the Controlled Release Society* **2012**, *161*, 473–483.

45. LoPresti, C.; Lomas, H.; Massignani, M.; Smart, T.; Battaglia, G. Polymersomes: Nature Inspired Nanometer Sized Compartments. *Journal of Materials Chemistry* **2009**, *19*, 3576.

46. Parnell, A. J.; Tzokova, N.; Topham, P. D.; Adams, D. J.; Adams, S.; Fernyhough, C. M.; Ryan, A. J.; Jones, R. A. L. The Efficiency of Encapsulation Within Surface Rehydrated Polymersomes. *Faraday Discussions* **2009**, *143*, 29.

47. Howse, J. R.; Jones, R. A. L.; Battaglia, G.; Ducker, R. E.; Leggett, G. J.; Ryan, A. J. Templated Formation of Giant Polymer Vesicles with Controlled Size Distributions. *Nature materials* **2009**, *8*, 507–511.

48. Du, J.; Lu, W.-L.; Ying, X.; Liu, Y.; Du, P.; Tian, W.; Men, Y.; Guo, J.; Zhang, Y.; Li, R.-J.; *et al.* Dual-Targeting Topotecan Liposomes Modified with Tamoxifen and Wheat Germ Agglutinin Significantly Improve Drug Transport Across the Blood-Brain Barrier and Survival of Brain Tumor-Bearing Animals. *Molecular pharmaceutics* **2009**, *6*, 905–917.

49. Uneyama, T. Density Functional Simulation of Spontaneous Formation of Vesicle in Block Copolymer Solutions. *The Journal of Chemical Physics* **2007**, *126*, 114902.

50. Du, J.; Chen, Y. Preparation of Organic/Inorganic Hybrid Hollow Particles Based on Gelation of Polymer Vesicles. *Macromolecules* **2004**, *37*, 5710–5716.

51. Lasic, D. D. *Liposomes in Drug Delivery*; CRC Press, 1997.

52. Adams, D. J.; Adams, S.; Atkins, D.; Butler, M. F.; Furzeland, S. Impact of Mechanism of Formation on Encapsulation in Block Copolymer Vesicles. *Journal of controlled Release* **2008**, *128*, 165–170.

53. Pang, Z.; Lu, W.; Gao, H.; Hu, K.; Chen, J.; Zhang, C.; Gao, X.; Jiang, X.; Zhu, C. Preparation and Brain Delivery Property of Biodegradable Polymersomes Conjugated with OX26. *Journal of controlled Release* **2008**, *128*, 120–127.

54. Wei, H.; Cheng, S.-X.; Zhang, X.-Z.; Zhuo, R.-X. Thermo-Sensitive Polymeric Micelles Based on Poly(N-Isopropylacrylamide) as Drug Carriers. *Progress in Polymer Science* **2009**, *34*, 893–910.

55. Judefeind, A.; de Villiers, M. M. Drug Loading into and In Vitro Release from Nanosized Drug Delivery Systems. In *Nanotechnology in Drug Delivery*
; de Villiers, M. M.; Aramwit, P.; Kwon, G. S., Eds. Springer; pp. 129–162.

56. Greco, F.; Vicent, M. J. Combination Therapy: Opportunities and Challenges for Polymer–Drug Conjugates as Anticancer Nanomedicines. *Advanced Drug Delivery Reviews* **2009**, *61*, 1203–1213.

57. Tanner, P.; Baumann, P.; Enea, R.; Onaca, O.; Palivan, C.; Meier, W. Polymeric Vesicles: From Drug Carriers to Nanoreactors and Artificial Organelles. *Acc. Chem. Res.* **2011**, *44*, 1039–1049.

58. Noor, M.; Dworeck, T.; Schenk, A.; Shinde, P.; Fioroni, M.; Schwaneberg, U. Polymersome Surface Decoration by an EGFP Fusion Protein Employing Cecropin a as Peptide "Anchor." *Journal of Biotechnology* **2012**, *157*, 31–37.

59. Marguet, M.; Edembe, L.; Lecommandoux, S. Polymersomes in Polymersomes: Multiple Loading and Permeability Control. *Angew. Chem. Int. Ed.* **2011**, *51*, 1173–1176.

60. Rameez, S.; Alosta, H.; Palmer, A. F. Biocompatible and Biodegradable Polymersome Encapsulated Hemoglobin: a Potential Oxygen Carrier. *Bioconjugate chemistry* **2008**, *19*, 1025–1032.

61. Kim, S.-H.; Shum, H. C.; Kim, J.-W.; Cho, J.-C.; Weitz, D. A. Multiple Polymersomes for Programmed Release of Multiple Components. *Journal of the American Chemical Society* **2011**, *133*, 15165–15171.

62. Levine, D. H.; Ghoroghchian, P. P.; Freudenberg, J.; Zhang, G.; Therien, M. J.; Greene, M. I.; Hammer, D. A.; Murali, R. Polymersomes: a New Multi-Functional Tool for Cancer Diagnosis and Therapy. *Methods* **2008**, *46*, 25–32.

63. Pang, Z.; Feng, L.; Hua, R.; Chen, J.; Gao, H. Lactoferrin-Conjugated Bodegradable Polymersome Holding Doxorubicin and Tetrandrine for Chemotherapy. *Molecular pharmaceutics* **1995**, *7*, 1995–2005.

64. Hammady, T.; Rabanel, J.-M.; Dhanikula, R. S.; Leclair, G.; Hildgen, P. Functionalized Nanospheres Loaded with Anti-Angiogenic Drugs: Cellular Uptake and Angiosuppressive Efficacy. *European Journal of Pharmaceutics and Biopharmaceutics* **2009**, *72*, 418–427.

65. Meng, F.; Zhong, Z. Polymersomes Spanning From Nano- to Microscales: Advanced Vehicles for Controlled Drug Delivery and Robust Vesicles for Virus and Cell Mimicking. *J. Phys. Chem. Lett.* **2011**, *2*, 1533–1539.

66. Hickey, R. J.; Koski, J.; Meng, X.; Riggleman, R. A.; Zhang, P.; Park, S.-J. Size-Controlled Self-Assembly of Superparamagnetic Polymersomes. *ACS Nano* **2014**, *8*, 495–502.

67. Meng, F.; Zhong, Z.; Feijen, J. Stimuli-Responsive Polymersomes for Programmed Drug Delivery. *Biomacromolecules* **2009**, *10*, 197–209.

68. Letchford, K.; Burt, H. A Review of the Formation and Classification of Amphiphilic Block Copolymer Nanoparticulate Structures: Micelles, Nanospheres, Nanocapsules and Polymersomes. *European Journal of Pharmaceutics and Biopharmaceutics* **2007**, *65*, 259–269.

69. Barenholz, Y.; Haran, G. Method of Amphipatic Drug Loading in Liposomes by pH Gradient **1993**, 1–16.

70. Chen, W.; Meng, F.; Cheng, R.; Zhong, Z. pH-Sensitive Degradable Polymersomes for Triggered Release of Anticancer Drugs: a Comparative Study with Micelles. *Journal of controlled release : official journal of the Controlled Release Society* **2010**, *142*, 40–46.

71. Beers, K. L. Atom Transfer Radical Polymerization of 2-Hydroxyethyl Methacrylate. *Macromolecules* **1999**, *32*, 5772–5776.

72. Coessens, V.; Pintauer, T.; Matyjaszewski, K. Functional Polymers by Atom Transfer Radical Polymerization. *Progress in Polymer Science* **2001**, *26*, 337–377.

73. Nguyen, N. H.; Leng, X.; Percec, V. Synthesis of Ultrahigh Molar Mass Poly(2-Hydroxyethyl Methacrylate) by Single-Electron Transfer Living Radical Polymerization. *Polymer Chemistry* **2013**, *4*, 2760–2766.

74. Mori, H.; Wakisaka, O.; Hirao, A.; Nakahama, S. Protection and Polymerization of Functional Monomers, 23. Synthesis of Well-Defined Poly(2-Hydroxyethyl Methacrylate) by Means of Anionic Living Polymerization of Protected Monomers. *Macromolecular chemistry and Physics* **1994**, *195*, 3213–3224.

75. Muhr, P.; Likussar, W.; Schubert-Zsilavecz, M. Structure Investigation and Proton and Carbon-13 Assignments of Digitonin and Cholesterol Using Multidimensional NMR Techniques. *Magnetic Resonance in Chemistry* **1996**, *34*, 137–142.

76. Moad, G.; Rizzardo, E.; Thang, S. H. Living Radical Polymerization by the RAFT Process. *Australian journal of chemistry* **2005**, 379–410.

77. Chong, Y. K.; Krstina, J.; Le, T. P. T.; Moad, G.; Postma, A.; Rizzardo, E.; Thang, S. H. Thiocarbonylthio Compounds [SC(Ph)S−R] in Free Radical Polymerization with Reversible Addition-Fragmentation Chain Transfer (RAFT Polymerization). Role of the Free-Radical Leaving Group (R). *Macromolecules* **2003**, *36*, 2256–2272.

78. Sumerlin, B. S.; Donovan, M. S.; Mitsukami, Y.; Lowe, A. B.; McCormick, C. L. Water-Soluble Polymers. 84. Controlled Polymerization in Aqueous Media of Anionic Acrylamido Monomers via RAFT. *Macromolecules* **2001**, *34*, 6561–6564.

79. Shim, S. E.; Lee, H.; Choe, S. Synthesis of Functionalized Monodisperse Poly (Methyl Methacrylate) Nanoparticles by a RAFT Agent Carrying Carboxyl End Group. *Macromolecules* **2004**, *37*, 5565–5571.

80. Lee, H.; Lee, J.; Shim, S.; Lee, B.; Choe, S. Synthesis of Carboxylic Acid Functionalized Nanoparticles by Reversible Addition?Fragmentation Chain Transfer (RAFT) Miniemulsion Polymerization of Styrene. *Polymer* **2005**, *46*, 3661–3668.

81. Barner-Kowollik, C. *Handbook ofRAFT Polymerization*; 2008(null) ed. Wiley-VCH: Weinheim, 2014; pp. 1–558.

82. Guttman, C. M.; Di Marzio, E. A.; Douglas, J. F. Influence of Polymer Architecture and Polymer-Surface Interaction on the Elution Chromatography of Macromolecules Through a Microporous Media. *Macromolecules* **1997**, *29*, 5723–5733.

83. Shim, S. E.; Shin, Y.; Jun, J. W.; Lee, K.; Jung, H.; Choe, S. Living-Free-Radical Emulsion Photopolymerization of Methyl Methacrylate by a Surface Active Iniferter (Suriniferter). *Macromolecules* **2003**, *36*, 7994–8000.

84. Alexandridis, P.; Holzwarth, J. F.; Hatton, T. A. Micellization of Poly(Ethylene Oxide)-Poly(Propylene Oxide)-Poly(Ethylene Oxide) Triblock Copolymers in Aqueous

Solutions: Thermodynamics of Copolymer Association. *Macromolecules* **1994**, *27*, 2414–2425.

85. Larsson, A. 1H NMR of Thermoreversible Polymers in Solution and at Interfaces: the Influence of Charged Groups on the Phase Transition. *Colloids and Surfaces A: Physicochemical and Engineering Aspects* **2001**, *190*, 185–192.

86. Morrissey, J. H. *Lab Protocol for Preparing Phospholipid Vesicles (SUV) by Sonication*; Avanti Polar Lipids Inc.; pp. 8–10.

87. Li, S.; Welsh, J.; Byrne, B.; Palmer, A. F. Self-Assembled Poly(Butadiene)-B-Poly(Ethylene Oxide) Polymersomes as Paclitxael Carriers. *Biotechnology Progress* **2008**, *23*, 278–285.

88. Cavaletti, G.; Cassetti, A.; Canta, A.; Galbiati, S.; Gilardini, A.; Oggioni, N.; Rodriguez-Menendez, V.; Fasano, A.; Liuzzi, G. M.; Fattler, U.; *et al.* Cationic Liposomes Target Sites of Acute Neuroinflammation in Experimental Autoimmune Encephalomyelitis. *Molecular pharmaceutics* **2009**, *6*, 1363–1370.

89. Loo, W. T. Y.; Fong, J. H. M.; Cheung, M. N. B.; Chow, L. W. C. The Efficacy of Paclitaxel on Solid Tumour Analysed by ATP Bioluminescence Assay and VEGF Expression: a Translational Research Study. *Biomedicine and pharmacotherapy* **2005**, *59*, 337–339.

90. Nussbaumer, S.; Bonnabry, P.; Veuthey, J.-L.; Fleury-Souverain, S. Analysis of Anticancer Drugs: a Review. *Talanta* **2011**, *85*, 2265–2289.

91. Budhian, A.; Siegel, S. J.; Winey, K. I. Haloperidol-Loaded PLGA Nanoparticles: Systematic Study of Particle Size and Drug Content. *International journal of pharmaceutics* **2007**, *336*, 367–375.

92. Tiwari, S. B.; Amiji, M. M. Improved Oral Delivery of Paclitaxel Following Administration in Nanoemulsion Formulations. *J. Nanosci. Nanotech.* **2006**, *6*, 3215–3221.

93. Massignani, M.; Lomas, H.; Battaglia, G. Polymersomes: a Synthetic Biological Approach to Encapsulation and Delivery. *Advances in Polymer Science* **2010**, *229*, 115–154.

94. Johnston, A. H.; Dalton, P. D.; Newman, T. A. Polymersomes, Smaller Than You Think: Ferrocene as a TEM Probe to Determine Core Structure. **2010**, 1–9.

95. Meng, F. Artificial Cells Based on Biodegradable Polymersomes, University of Twente, 2003, pp. 1–111.

96. Chandrawati, R.; Caruso, F. Biomimetic Liposome- and Polymersome-Based Multicompartmentalized Assemblies. *Langmuir : the ACS journal of surfaces and colloids* **2012**, *28*, 13798–13807.

97. Fritze, A.; Hens, F.; Kimpfler, A.; Schubert, R.; Peschkasuss, R. Remote Loading of Doxorubicin Into Liposomes Driven by a Transmembrane Phosphate Gradient. *Biochimica et Biophysica Acta (BBA) - Biomembranes* **2006**, *1758*, 1633–1640.

98. Li, X.; Hirsh, D. J.; Cabral-Lilly, D.; Perkins, W. R. Doxorubicin Physical State in Solution and Inside Liposomes Loaded via pH Gradient. *Biochimica et biophysica acta* **1998**, 23–40.

99. Mayer, L. D.; Tai, L. C. L.; Bally, M. B.; Mitilenes, G. N.; Ginsberg, R. S.; Cullis, P. R. Characterization of Liposomal Systems Containing Doxorubicin Entrapped in Response to pH Gradients. *Biochimica et biophysica acta* **1990**, *1025*, 143–151.

100. Tian, Y.; Tam, K. C.; Hatton, T. A.; Bromberg, L. Titration Microcalorimetry Study: Interaction of Drug and Ionic Microgel System. *MIT Libraries* **2003**, 1–5.

101. Manocha, B.; Margaritis, A. Controlled Release of Doxorubicin From Doxorubicin/ Γ-Polyglutamic Acid Ionic Complex. *Journal of Nanomaterials* **2010**, *2010*, 1–9.

102. Takahashi, A.; Ozaki, Y.; Kuzuya, A.; Ohya, Y. Impact of Core-Forming Segment Structure on Drug Loading in Biodegradable Polymeric Micelles Using PEG-B-Poly(Lactide-Co-Depsipeptide) Block Copolymers. *BioMed Research International* **2014**, *2014*, 1–10.

Chapter 4.

Comparative study of Polymersomes and Liposomes as potential Drug Delivery Systems to Breast Cancer Metastasis in the Brain

4.1 Introduction

As shown in the previous chapter, the nanostructures obtained from amphiphilic triblock copolymer have demonstrated their ability to encapsulate both hydrophilic and hydrophobic substances at high loading efficiency and capacity, making them suitable for combination therapy of different drugs, a commonly used strategy in malignancies like cancer.

As mentioned in the introduction of this thesis, cancer remains as one of the leading causes of death worldwide[1]. Although traditionally the treatment of primary tumours attracted much of the attention, the vast majority of deaths from cancer are due to metastatic disease[2]. For instance, the incidence of metastatic brain tumours is 200,000 cases per year in the United States, which is 10 times higher than the incidence of primary brain tumours[3]. In addition, malignant primary tumours can often be surgically resected, but the cells that gain the ability to migrate throughout the body, seeding and proliferating in distant organs, are often the cells that cause the most harmful effects and may become more difficult to target therapeutically[2].

Metastasis is the spread of cancer from the site of primary tumour to adjacent or distant organs[4] through a very complex process, called angiogenesis, which requires invasion from the primary tumour, intravasation, survival and dissemination, arrest in the capillary bed, extravasation of the circulatory system and colonization of a distant site[5,6] (Figure 4.1). In addition, tumour cells may acquire the ability to preferentially colonize certain organs due to molecular factors that may contribute to organ-specific metastasis[6].

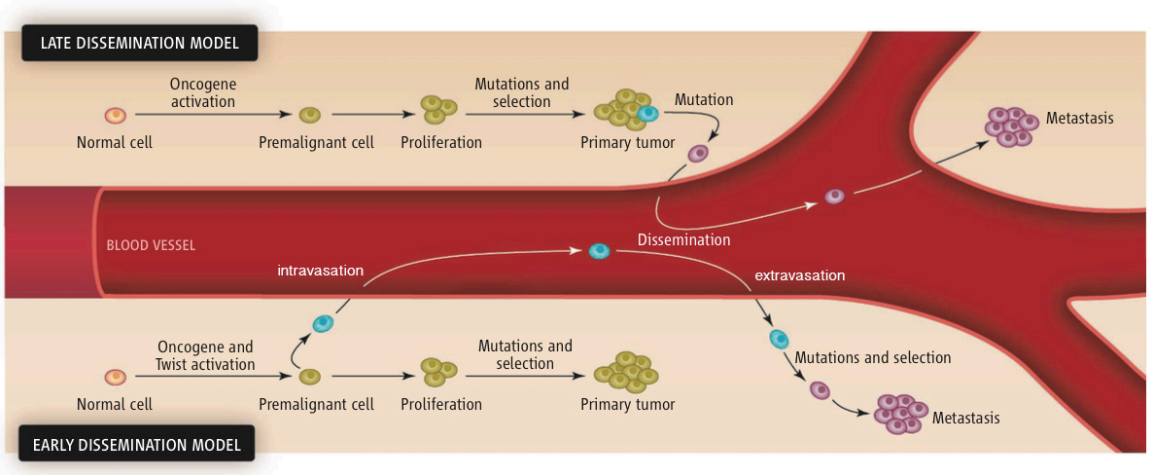

Figure 4.1: Evolution of tumour malignancy (adapted from Klein *et al.*[7])

Due to the molecular complexity of this malignancy, combination therapy for cancer treatment is well established, which generally refers to either the simultaneous administration of two or more pharmacologically active agents or to the combination of different types of therapy (e.g. two different chemotherapeutics or chemotherapy and radiotherapy). Unlike single-agent therapy, multi-agent therapy can modulate different signalling pathways in diseased cells, maximizing the therapeutic effect and overcoming mechanisms of resistance[8]. Traditional drug combinations for cancer therapy involve anthracycline-based combinations[8], such as AC (adryamicin and

cyclophosphamide) or combinations of anthracycline with taxanes[9], such as paclitaxel, among others, both for the treatment of metastatic breast cancer.

Current common practice for treating cancer with "cocktails" of small-molecule inhibitors is to administer the agents sequentially, starting with a "first-line" drug and switching to "second-line" therapies when tumour relapses[10]. However, the effectiveness of this approach was assessed by a mathematical model based on the data obtained from 20 melanoma patients, which revealed that combination therapy with two drugs given simultaneously is far more effective than sequential therapy where the drugs are used one after the other[11]. Therefore, drug delivery systems become appealing again as a way to encapsulate multiple active pharmaceutical ingredients (API) in a single platform that could potentially offer synergistic effects to promote the efficacy of therapies, while limiting the risk of resistance and cytotoxicity to healthy adjacent tissue[12]. As previously mentioned, this ability to simultaneously entrap several drugs is typical from polymer-drug conjugates[13], liposomes[14] and polymersomes[15]. Among these drug delivery systems, liposomes and polymersomes are of especial interest because of their capability to encapsulate both hydrophilic and hydrophobic compounds at different concentrations through a simple loading procedure[16].

Liposomes have been widely used during the past 40 years[17] as pharmaceutical carriers for cancer therapy or imaging. Owing to the amphiphilic characters of lipids, liposomes possess unique properties that make them attractive for drug delivery. On one hand, this compartmentalized structure that mimics cell membrane provides them the capability to encapsulate both hydrophilic and hydrophobic compounds[16] while facilitating membrane fusion and fission[18]. On the other hand, the low molecular weight of their phospholipids[18] confers to the bilayer lateral fluidity, allowing the permeation of substances, thus being able to encapsulate and release drugs[19]. A proof of the suitability of these systems as drug delivery agents are the amount of approved liposomal drugs and in clinical trials as a result of the breakthrough developments achieved in the past 25 years, already mentioned in chapter 1. Combination therapies have also been carried out in the field of liposomes, although none of them are commercially approved yet. For instance, combination of two traditional chemotherapeutic drugs, such as vincristine and topotecan, in PEGylated liposomes leaded to a superior therapeutic efficacy over free drug combination or single-drug loaded liposomes[14]. A further step in combination was recently achieved by encapsulating an antineoplastic agent with modulation of drug resistance in a formulation of peptide-targeted liposomes containing doxorubicin or cisplatin together with oligonucleotides against the two main drug resistance mechanisms Bcl-2 and MDR1, leading to a inhibition of tumour growth[20].

However, despite the goals achieved by liposomal drugs, these systems suffer from a lack of mechanical and chemical stability[18], therefore their polymeric equivalents, polymersomes, have arisen in the past decade[21] as a powerful alternative to minimize these drawbacks. The advantage and versatility that polymersomes provide over liposomes is the possibility to tune and control their properties at a molecular level[22], as it has been shown in chapter 3. For instance, membrane thickness can be controlled by varying the molecular weight of the hydrophobic blocks[23],

whereas fluidity and permeability of the membrane can be adjusted by changing the glass transition temperature of the hydrophobic block[24]. Thus, the control over polymersomes' membrane thickness allows the modulation of drug loading capacity, as shown in the previous chapter regarding paclitaxel loading, while adjustment of their fluidity influences both drug loading and release[22]. Nevertheless, due to higher molecular weight of polymers as compared to lipids, the membrane of polymersomes is generally thicker and tougher and, thus, are inherently more stable than conventional liposomes[21].

Owing to the versatility presented by this system, polymersomes have attracted an increasing interest in the past years. To this date, no polymersome-based formulations have been approved for therapeutic purposes yet due to their shorter history compared to liposomes, however, some of these drug delivery systems are in advanced clinical trials, as already mentioned in chapter 1. In addition, the application of these polymeric systems to combination therapy strategies has resulted in diverse approaches. For instance, biodegradable polymersomes loaded with doxorubicin and tetrandrine, a potent hydrophobic multidrug resistance (MDR) inhibitor, demonstrated an enhanced efficacy compared to loaded-doxorubicin alone to treat glioma rats[25], whereas another therapy combining paclitaxel and endostatin, a hydrosoluble peptide that targets angiogenesis regulatory genes, co-loaded in polymeric nanospheres showed a synergetic anti-angiogenic effect in HUVEC cells[26].

In order to achieve efficient therapies through combination therapy, targeting is sought for these drug delivery systems to be able to reach the tumour site at a sufficient concentration. Inherent tumour characteristics, such as their leaky vasculature and poor lymphatic drainage that allows an enhanced permeation and retention effect (EPR), and the overexpression of several receptors, makes them ideal targets for drug delivery[27]. For instance, antibody-conjugated[28] systems can target receptors involved in the angiogenesis process such as vascular endothelial growth factor (VEGF) or human epidermal growth factor 2 (HER2). Smaller molecules, such as folate, have been also widely used, owing to their easy conjugation to nanocarriers and their overexpression in several types of cancer[29].

However, before reaching their targets, nanocarriers must face other obstacles, such as physical barriers between the bloodstream and cells[30]. Overcoming these obstacles becomes particularly challenging when it comes to the blood-brain barrier (BBB), which is the most restrictive biological barrier in the body as it protects the CNS structures from intrusion of pathogens and large molecules, as already exposed in chapter 2. Therefore, the BBB becomes the bottleneck in cancer metastasis treatment when it is located in the brain[31].

The brain is regarded as a sanctuary site for metastatic tumor cells where they exist partially protected from drugs by the blood-brain barrier[6]. Brain metastases (BM) occur late in the progression of multiple types of solid tumors and are associated with poor patient survival[6]. It has been estimated that they can occur in up to 30% of patients[32] and strongly depend on the tumor type and molecular subtype, arising from primary tumors such as lung (40-50%), breast (15-25%), melanoma (5-20%), renal and gastrointestinal (4-6%)[5]. Thus, the brain is not only a site for primary tumorogenesis but increasingly a site of cancer metastasis[33]. Because of this high incidence of brain

metastases in systemic malignancies and their inaccessibility, metastasis to the Central Nervous System (CNS) remains a major cause of morbidity and mortality in patients with advanced cancer[3,34].

Current therapeutic approaches for BM include surgery, radiotherapy, chemotherapy or a combination of these therapies, which have to be tailored to each individual patient, resulting in patient survival between 4 and 24 months[5]. Recently, molecular targeted therapies have gained increasing interest because of the elevated expression or mutation of several receptors in metastatic progression that could serve as targets for BM treatment[5]. Several monoclonal antibodies and small molecules that inhibit key receptors involved in angiogenic pathways of neoplasms, such as the human epidermal growth factor receptor-2 (HER-2) or the family of vascular endothelial growth factors (VEGFR) [4,35], have demonstrated improvement in clinical trials delaying BM progression. In the treatment of metastatic breast cancer, bevacizumab (Avastin®) was the first monoclonal antibody (anti-VEGF antibody) approved by the FDA on 2008, as a result of the improvement showed in the median PFS (Progression-free survival) of patients treated with a combination of Bevacizumab and Paclitaxel in a phase III trial[36].

Approximately a 25% of human breast cancers demonstrate amplification of the HER-2. Patients with HER-2 positive breast cancer are at a high risk of developing brain metastasis, with a frequency as high as 50% in patients succumbing to advance disease[37]. Therefore, monoclonal antibodies that target the extracellular domain of HER2, such as trastuzumab (Herceptin®), have been the most widely used therapy, alone or in combination with chemotherapy, in the treatment of HER2-positive breast cancers, showing increasing overall survival[5]. However, no clear benefits for patients have been reported regarding the use of a single antiangiogenic drugs. Considering the multitude of molecular entities and signalling pathways regulating the proliferation and cellular survival, the inhibition of a singular target may not be sufficient to suppress neoplastic progression[5]. This lead to multiple-drug combination therapies, such as trastuzumab with bevacizumab, which have shown promising results in phase II trials, or trastuzumab and lapatinib in combination with an antimurine VEGFR2 antibody (DC101), which achieved significant reduction of tumor microvessel density and increased tumor necrosis *in vivo*, although their potential for increased toxicity is a major concern[37].

Although systemic disease is under control in many patients treated with the aforementioned therapies, their associated brain metastases appear resistant to the employed drugs, as they were not conceived to treat brain metastases but breast cancer primary tumor. The problem is that most of these drugs are not able to cross the BBB, like trastuzumab, or can cross it modestly, like lapatinib[5]. In addition, although generally tolerated, anti-VEGF agents can have adverse effects in the CNS and elsewhere. A major concern using agents targeting CNS vasculature is haemorrhage. Intracerebral haemorrhages were observed in patients treated with bevacizumab, and arterial thromboembolic events, including cerebral infarction, occurred at a higher incidence in patients receiving bevacizumab in combination with chemotherapy than in those receiving chemotherapy alone[35].

To overcome the drawbacks that these current therapies present, drug delivery arises again as a powerful tool providing a single platform that could allow multiple-targeting to reach the disease in several sites and simultaneous loading of several therapeutic agents that could treat different processes of the same illness. Targeted drug delivery plays an important role providing materials that can potentially be designed to carry out multiple specific functions at once, an important requirement for the clinically succesful delivery of drugs to the CNS. The ability to cross the blood-brain barrier while potentially targeting a specific group of cells requires several conditions to occur, this means being able to find the CNS, to cross the BBB without harming its integrity, to target cancer cells inside the brain and to release the therapeutic agent[31]. Therefore, there is a need of a functional carrier that is able to cross the BBB and then target the tumour inside, while allowing to apply combinated therapies to address several molecular targets of the diseased cells. Thus, dual-targeting of vesicular systems, such as polymersomes, represents an attractive approach that may provide the ability to cross the BBB, target tumour cells and release co-encapsulated drugs to treat metastatic malignancies in the brain.

As introduce in chapter 2, the BBB expresses a high level of proteins that pump foreign molecules away from the brain, while allowing others that are necessary to the function of the brain cells to cross the barrier[38]. One of the most recurrent mechanisms to go through the BBB is receptor-mediated transcytosis, taking advantage of different transporters and receptors present at the BBB. This is the case of low-density lipoprotein receptor-related protein (LRP-1), a multifunctional endocytic receptor that mediates the internalization and degradation of multiple ligands involved in diverse metabolic pathways[39], or lactoferrin receptor, which has been demonstrated that is involved in lactoferrin transport across the BBB *in vitro* and *in vivo*[40]. Both receptors have been widely used in drug delivery receptor-mediated approaches to cross the BBB[25,41-43], but probably the most popular one has been LRP-1 thanks to the discovery of angiopep-2[44]. Since then, other peptides have been developed to target this receptor, like a 59-residue novel peptide ligand of LRP-1, developed by Regulon Inc., whose conjugation to liposomal formulations resulted in higher concentrations in the brain rather than in the liver, when administered intravenously in animals[45].

Recently, some dual-targeted approaches to overcome the BBB have shown promising results. This is the case of PEGylated topotecan-loaded liposomes with both wheat germ agglutinin for brain capillary targeting and tamoxifen to decrease drug efflux, which crossed a BBB model *in vitro* and increased the survival of brain tumour-bearing rats over free topotecan or untargeted topotecan-loaded liposomes[46]. Taking advantage of other receptors expressed in the BBB endothelial cells, such as glucose transporter 1 and transferrin receptor, mannose and transferrin dual-targeted daunorubicin-loaded liposomes were used for the treatment of intracranial glyoma in mice, leading to superior tumour growth inhibition and increased survival over untargeted or single-targeted daunorubicin-loaded liposomes[47].

After being able to cross the BBB, the system should be able to target tumour cells inside the brain and overcome the barrier of the cell membrane to deliver their payload into specific organelles within the cytoplasm[29]. An approach that has demonstrated its ability to provide both tasks, especially in breast cancer, is the use of

cancer-specific peptide/phage fusion coat protein pVIII[27]. Membranophilic major phage coat protein pVIII fused with a breast cancer-specific targeting peptide identified by phage display can target a breast cancer cell line while enhancing endosomal escape of nanocarriers thanks to their buffering capacity[28]. The acid groups present in its N-terminus, aspartic and glutamic acid, act by absorbing protons like a "proton sponge" in an acidic environment, which results in a swelling and rupture of the endosomal membrane. In addition, phage protein amphiphilic characteristics allows it to spontaneously insert into bacterial membranes and lipid bilayers of liposomes[48]. It has been proved that hybrid phage VIII coat protein fused to a tumor-specific peptide incorporates into liposomes membrane via its C-terminal hydrophobic segment, while its water-exposed N-terminus is exposed on the surface to serve as a targeting moiety[49] (Figure 4.2).

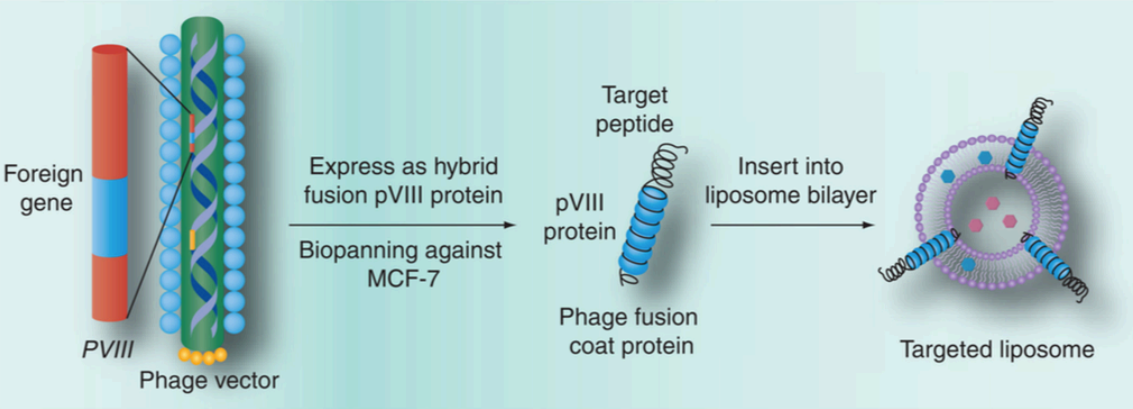

Figure 4.2: Production of hybrid phage fusion coat protein with genetically fused target peptide and its incorporation into liposomes[49]

The use of phage fusion coat protein pVIII bearing DMPGTVLP peptide as targeted delivery ligand in doxorubicin-loaded PEGylated liposomes[49] and in paclitaxel-loaded polymeric micelles[50] has shown an increase in binding and enhanced cytotoxicity in MCF-7[51], thanks to its specificity for this cell line and endosomal escape ability[52]. Thus, phage protein is supposed to not only mediate specific recognition and targeting of nanocarriers, but also facilitates its cytoplasmatic delivery via endosomal membrane destabilization[52].

Aiming to design a more effective therapy for a breast cancer metastasis scenario in the brain, a new drug delivery approach is engineered in this chapter, willing to provide the ability to cross the BBB via receptor-mediated strategy, target breast cancer cells in the brain and deliver its payload inside the tumour cell. The combination of an MCF-7-specific phage fusion pVIII coat protein and a BBB-specific peptide in a dual-targeted nanocarrier may provide the system the ability to cross the blood-brain barrier, address breast cancer cells (MCF-7) in a metastasis scenario in the brain and release the loaded chemotherapeutic agent to carry out its function (Figure 4.3). In order to achieve this strategy, there are several requirements that a nanocarrier shall meet. This is, the ability to load a wide range of drugs, both hydrophilic and hydrophobic, at high loading capacity to achieve therapeutic levels, and a simple way to modify its surface with biomolecules for specific targeting.

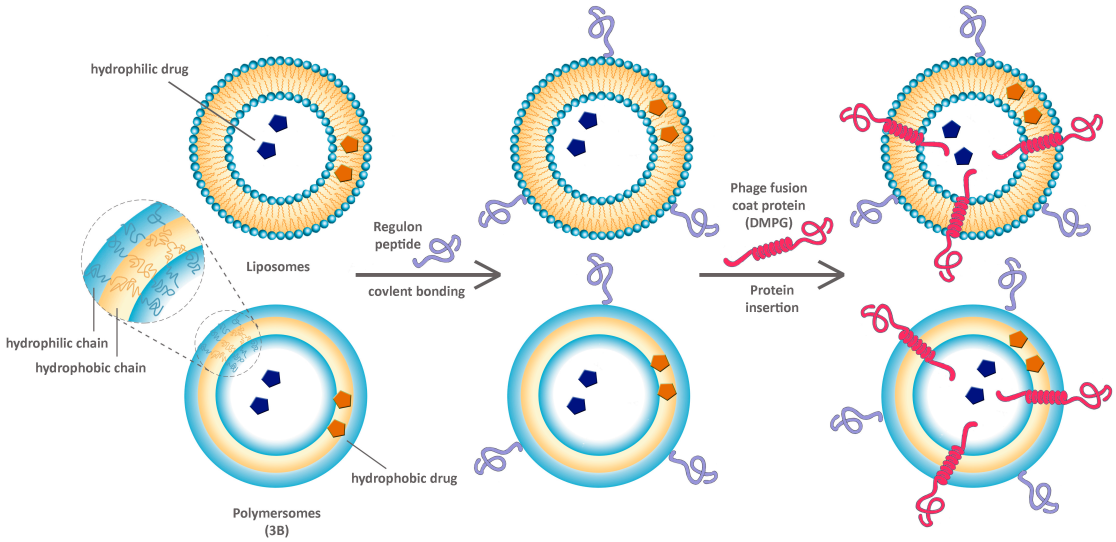

Figure 4.3: Scheme of the approach in this chapter presented. Both liposomes and polymersomes are firstly functionalized with a BBB-specific peptide (REG) through different chemical routes. Phage fusion pIII coat protein is inserted afterwards to achieve the dual-targeted delivery system.

Similarly to liposomes, the surface of the polymeric systems, as the one presented in the previous chapter, can be also easily functionalized with biomolecules to obtain bioconjugates. A simple and commonly used approach to form bioconjugates is the post-polymerization conjugation of functionalized polymers and biomolecules[53]. Thus, the selection of monomers or polymers with functional groups suitable for the conjugation of biomolecules under mild conditions is required[54]. As mentioned previously, RAFT agents present at both ends of each polymer chain in amphiphilic block copolymers synthesized via RAFT polymerization, are amenable to a wide range of simple transformation procedures to achieve reactive groups towards peptides and proteins. Among the most commonly used there is aminolysis followed by thiol coupling[54], carboxylic acid activation using N-hydroxysuccinimide (NHS) to perform carboxyl-to-amine crosslinking[55], or “click” chemistry, the most notable of which is the copper(I)-catalyzed azide-alkyne cycloaddition (CuAAC)[56]. In addition, we hypothesize that amphiphilic transmembrane proteins, such as phage fusion coat protein, could be internalized in polymersomes as well thanks to their similar structure to liposomes, as it has already been shown by other authors[57].

In the light of the background knowledge generated in the field of liposomes and the potential of their polymeric equivalents, it is interesting to compare the polymeric platform described in this thesis with a widely studied liposomal system that could serve as a reference to determine the suitability of this new system in a breast cancer metastasis in the brain.

4.1.1 Aims of this chapter

In this chapter, a comparative study between polymersomes and liposomes was performed in terms of targeting, drug loading, release, tumor cell killing capacity and crossing of a blood-brain barrier model. To accomplish this study, the aims of this chapter are as follows:

- Covalent binding of a thiolated BBB-specific peptide to liposomes and polymersomes' surface
- Insertion of a phage fusion coat protein into liposomes and polymersomes' membrane
- Remote loading and release of doxorubicin into liposomes and polymersomes through the pH gradient technique
- Evaluation of enhanced binding, uptake and cytotoxicity of phage-bearing liposomes and polymersomes in MCF-7 and U87MG by flow cytometry
- Evaluation of the intracellular uptake and pathway followed by targeted and non-targeted liposomes and polymersomes by fluorescence microscopy
- Evaluation of endosomal escape potential of phage-bearing polymersomes in MCF-7
- Evaluation of permeation through a BBB model, BBMVECs uptake and abluminal cell killing of non-targeted, single-targeted and dual-targeted liposomes and polymersomes

4.2 Methods

4.2.1 Materials and Reagents

For the attachment of Regulon peptide to triblock copolymer, ethanolamine (ETA), DTDP (dithiodipyridine) and DMF were purchased from Sigma-Aldrich, Germany. Anhydrous THF and acetone were purchased from Merck, whereas diethyl ether from Panreac. Regulon peptide was purchased from Regulon AE, Greece. Phage fusion coat protein was provided by the Department of Pathobiology, at the College of Veterinary Medicine of Auburn University, AL (US).

N-(Carbonyl-methoxypolyethyleneglycol 2000)-1,2-distearoyl-*sn*-glycero-3-phosphoethanolamine sodium salt was purchased from Corden Pharma, Switzerland, and 1,2-dipalmitoyl-*sn*-glycero-3-phosphothioethanol was purchased from Avanti Polar Lipids, US. $CDCl_3$ was purchased from Sigma-Aldrich, Germany.

For SDS-PAGE, acrylamide/bis-acrylamide, glycerol, 1,4-dithioerythritol (DTT), TEMED, ammonium persulfate (APS) and brilliant blue were purchased from Sigma-Aldrich, whereas resolving buffer, concentration buffer, polypeptide SDS-PAGE standards and silver staining kit were purchased from Bio Rad.

MCF-7, U87MG and C166 cells were purchased from ATCC, VA (US). Cell culture media and reagents, such as MEM, DMEM, FBS and PBS were all purchased from CellGro, NY (US). Fibronectin, Lucifer Yellow, dexamethasone, Ringer tablets, sodium cholate, chloroquine and bafilomycin A1 were purchased from Sigma-Aldrich, Germany. Transferrin Alexa Fluor 488 was purchased from Invitrogen, RO-20-1724 from Calbiochem, 8-(4-CPT) from Santa Cruz Biotechnology and Cell Titer Blue assay reagent from Promega, WI (US). Bovine brain microvasular endothelial cells (BBMVECs), Bovine brain endothelial growth media and Attachment Factor Solution (AFS) were all purchased from Cell Applications, CA (US).

4.2.2 Cytotoxicity of plain polymersomes in C166 and U87MG

C166 and U87MG were incubated 24 hours in 96-well plates at 10.000 cells/well in DMEM and MEM, respectively. Afterwards, cells were treated with polymersomes sample at 5 mg/ml for 24 hours. Cell viability was evaluated with the Cell Titer Blue kit, therefore cells were washed twice and incubated with 50 μl/well of fresh DMEM or MEM along with 10 μl/well of Cell Titer Blue assay reagent for 2 hours at 37°C. Fluorescence intensity was measured using a multidetection microplate reader (Bio-Tek, Winooski, VT) with 525/590 nm excitation/emission wavelengths.

4.2.3 Conjugation of Regulon peptide to macro-3B

Prior to attach Regulon peptide to the triblock copolymer (3B), the trithiocarbonate end group of DSPA (CTA) was cleaved by aminolysis, further activated with dithiodipyridine (DTDP) and finally reacted with the sulfhydryl group[58] of Regulon peptide (Figure 4.4).

For aminolysis of trithiocarbonate end group, a single-neck round-bottom cylindrical flask was charged with triblock copolymer (1) (48 mg, 3.8×10^{-6} mol),

ethanolamine (100 µL, 1.65 mmol) and 5 ml of anhydrous THF. The reaction mixture was deoxygenated with argon for 20 min and then stirred overnight at room temperature. The mixture was concentrated to 0.5 ml by rotary evaporation and precipitated in 45 ml of cold acetone (-20°C). The precipitate was washed with cold acetone (-20°C) 3x20 ml and centrifuged at 6000 rpm for 15 minutes. The supernatant was removed and the solid dried under vacuum.

For the reaction with DTDP, a single-neck round-bottom cylindrical flask was charged with 3B-Ethanolamine (25 mg, $1.95x10^{-6}$ mol), DTDP (55 mg, $2.5x10^{-4}$ mol) and 5 ml of anhydrous THF. The reaction mixture was deoxygenated with argon for 20 min and then stirred overnight at room temperature. The mixture was concentrated up to 0.5 ml by rotary evaporation and precipitated in 45 ml of cold diethyl ether (-20°C). The precipitate was washed with cold diethyl ether (-20°C) 3x20 ml and centrifuged at 6000 rpm for 15 minutes. The supernatant was removed and the solid dried under vacuum.

For the conjugation of Regulon peptide, a single-neck round-bottom cylindrical flask was charged with 3B-PDS (2) (19 mg, $1.55x10^{-6}$ mol), regulon peptide (23 mg, $3.1x10^{-6}$ mol) and 5 ml of DMF. The mixture was stirred at room temperature overnight. Then, it was concentrated to 0.5 ml by rotary evaporation and precipitated in 45 ml of cold diethyl ether (-20°C). The precipitate was washed with cold diethyl ether (-20°C) 2x25 ml and centrifuged at 6000 rpm for 15 minutes. 5 ml milli-Q water was added to the mixture to solubilize the unreacted peptide, which was then centrifuged at 6000 rpm for 20 min. Then, the supernatant was removed and the solid vacuum-dried (3).

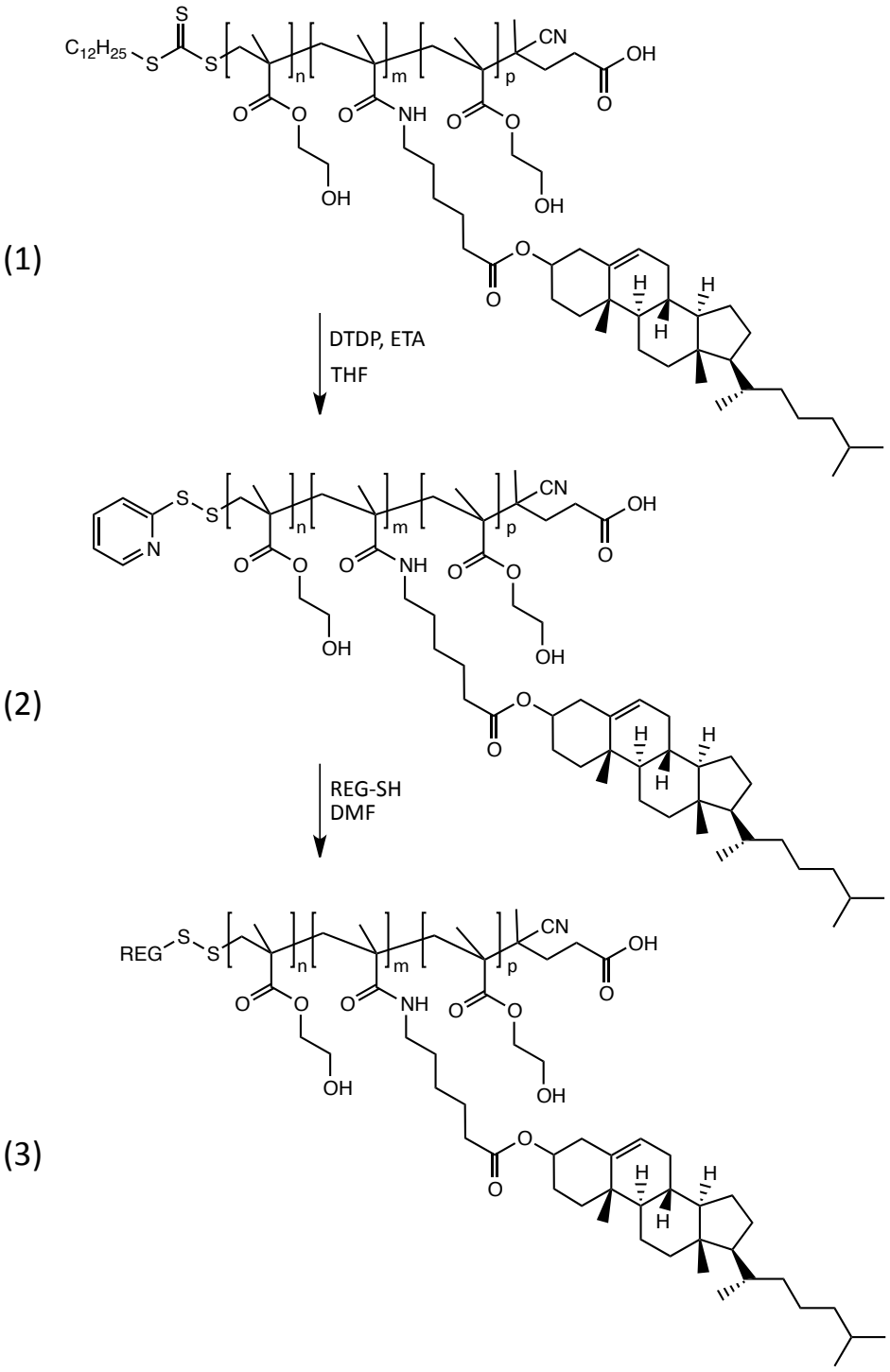

Figure 4.4: Attachment of Regulon peptide to triblock copolymer (3B)

4.2.4 Liposomes and Polymersomes preparation

Both formulations were obtained by the lipid film hydration technique followed by sonication. For plain formulations, a dry film of lipid or triblock was prepared by rotary evaporation of a chloroform solution of $MPEG_{2k}$-DSPE or 3B, respectively, followed by freeze-drying for 4 hours. The films were hydrated in 300 mM ammonium citrate buffer (pH 4) at a concentration of 10 mg/ml. The hydrated mixtures were vortexed vigorously for 10 min and further sonicated with a probe sonicator at 35% amplitude, with pulsed frequency, 2 s on and 2 s off, for 8 minutes. For thiolated

liposomes, films were prepared by mixing $MPEG_{2k}$-DSPE with 1,2-dipalmitoyl-*sn*-glycero-3-phosphothioethanol at 85% and 15% (w/w) and dissolving them in chloroform to render a final concentration of lipid of 10 mg/ml. For obtaining BBB-targeted polymersomes (3B-REG), films were prepared by mixing triblock copolymer (3B) and 3B-REG at 85% and 15% (w/w) to render a final concentration of polymer of 10 mg/ml.

The nanostructures obtained were characterized in terms of size distribution and zeta potential by Dynamic Light Scattering (DLS). Size and zeta potential were both determined by DLS in a Zetasizer Nano ZS90 (Malvern Instruments, Ltd., UK). Correlation functions were collected at a laser wavelength of 632.8 nm and scattering angle of 173 degrees. Size was calculated using Malvern sizing software (DTS v5.03) as the mean of three measurements determined by intensity, volume, number analysis; each of them was recorded as an average of 10 runs of 10 scans in a disposable plastic cuvette.

4.2.5 Phage protein insertion in Liposomes and Polymersomes

A landscape phage bearing breast cancer cell-specific peptide DMPGTVLP was selected from the 8-mer landscape library f8/8[59] using biopanning against MCF-7 cells. Phage fusion 55-mer coat protein ADMPGTVLPDPAKAAFDSLQASATEYIGYAWAMVVVIVGATIGIKLFKKFTSKAS (MW 5747.72 Da) was propagated and purified as described[60].

Both DMPG-liposomes and polymersomes were prepared by incubating doxorubicin-loaded liposomes or polymersomes with cholate-stabilized phage fusion pVIII coat protein (DMPG) at the matrix-to-protein ratio of 200:1. After overnight incubation at 37°C, the crude formulation was dialyzed at 4°C overnight against cholate-free phosphate-buffered saline (PBS) to remove cholate.

The presence of phage protein was monitored by SDS electrophoresis gel. A 16% non-gradient acrylamide/bisacrylamide gel was prepared by mixing 2.2 ml of acrylamide/bis-acrylamide, 2.93 ml of resolving buffer, 2.2 ml of distilled water, 13.3 µL TEMED and 200 µL of APS 15%. Then, stacking gel was prepared by mixing 210 µL acrylamide/bis-acrylamide, 540 µL of concentration buffer, 860 µL of distilled water, 5 µL TEMED and 15 µL APS 15%. Samples were mixed with an equal volume of Tricine sample buffer (8% SDS, 24% glycerol, 0.1 M Tris pH 6.8, 4% DTT, 0.01% Brilliant blue) and heated at 95°C for 40 minutes. Denaturated samples of 25 µL volume were loaded onto the prepared gel. Electrophoresis was carried out at 140 V for 1 hour. The resulting blots were developed with the Bio-Rad Silver Stain Kit.

4.2.6 Remote loading of doxorubicin into liposomes and polymersomes

Doxorubicin was entrapped by remote loading driven by a transmembrane pH gradient. To achieve this gradient, formulations were dialyzed for 4 hours against 1L HEPES buffered saline (HBS), 150 mM NaCl, 20 mM HEPES at pH 7.4 to replace the extraliposomal solution. Subsequently, doxorubicin HCl was added to the liposomal dispersion at a concentration of 1 mg/ml an incubated for 1 hour at 65°C.

4.2.7 Determination of doxorubicin's encapsulation efficiency

Free doxorubicin was removed by dialysis against 4L of HBS for 5 hours at 4°C. Doxorubicin's concentration was determined by spectrophotometry at 485 nm after lysis of both liposomes and polymersomes with Triton X-100 at 1% (v/v). Absorbance intensity was measured using a multidetection microplate reader equipped with a single-cuvette holder (Bio-Tek, Winooski, VT).

4.2.8 Doxorubicin's release from Liposomes and Polymersomes

Doxorubicin-loaded liposomes and polymersomes were dispersed in 1.5 ml of PBS (0.5 mg/ml) and then placed in a dialysis bag (MWCO 50KDa). The dialysis bag was then immersed in 50 ml PBS (pH 7.4) and incubated at 37°C. At specific time intervals, sample was taken from the drug-released solution (outside the bag) and doxorubicin concentration was analysed by UV spectrophotometry at 485 nm. The removed solution was replaced by equal volume of fresh PBS.

4.2.9 MCF-7-targeted and non-targeted liposomes and polymersomes uptake

To visualize the cellular uptake of doxorubicin-loaded liposomes and polymersomes in MCF-7, cells were seeded on coverslips at a concentration of 20000 cells/well and incubated in MEM supplemented with 10% FBS and 1% antibiotics, at 37°C and 5% CO_2. After 24 hours, cells were treated with doxorubicin-loaded liposomes and polymersomes at an equivalent concentration of doxorubicin of 10 µM for 1.5 hours. Cells were then washed with PBS four times and incubated with transferrin alexa fluor 488 at 10 µg/ml for 20 min at 37°C. Then, media was replaced for Hoechst 33324 at 5 µg/ml and cells were further incubated for 5 min at 37°C. Cells were washed with PBS four times and fixed with 4% of paraformaldehyde. Coverslips were mounted on microscope glass slides with fluorescent mounting medium. Images were acquired by a fluorescent microscope (Zeiss Co. Ltd., Germany) at x100 magnification.

4.2.10 MCF-7-targeted liposomes and polymersomes binding specificity

Both MCF-7 and U87MG were seeded on 12-well plates in MEM at 300000 and 200000 cells/well, respectively, and incubated for 24 hours at 37°C. Cells were treated with doxorubicin-loaded liposomes and polyersomes at an equivalent concentration of doxorubicin of 10 µM for 4 hours. Then, cells were washed with PBS three times, detached and collected by centrifugation. Cell pellets were resuspended in 200 µL of PBS with 4% paraformaldehyde, followed by flow cytometry analysis. Liposomes and polymersomes uptake was measured as doxorubicin fluorescence (FL2-H). Each sample was run in triplicate and 1000 events were acquired per sample with BD FACScailbur Flow cytometer (Becton Dickinson Company).

4.2.11 Cytotoxicity of doxorubicin-loaded liposomes and polymersomes in tumor cells

For cytotoxicity experiments cells (MCF-7, U87MG and C166) were seeded onto 96-well plates at a density of 5000 cells/well in supplemented MEM and incubated for 24 hours at 37°C. Cells were treated with free doxorubicin (control) and targeted and non-targeted liposomes and polymersomes at an equivalent doxorubicin concentration of 5 μM for 4, 24 and 48 hours. After 4 and 24 hours treatment, cells were washed with MEM and further incubated with fresh media till 48 hours. Then, all plates were washed again and incubated with 50 μl/well fresh MEM along with 10 μl/well of Cell Titer Blue assay reagent for 2 hours at 37°C. Fluorescence intensity was measured using a multidetection microplate reader (Bio-Tek, Winooski, VT) with 525/590 nm excitation/emission wavelengths.

4.2.12 Evaluation of endosomal escape ability of DMPG-bearing polymersomes

MCF-7 cells were seeded into 96-well microplates at a density of 5000 cells/well in supplemented MEM and growed until cells reached 40−50% confluence. For bafilomycin A1 (BFA) inhibition studies, MCF-7 cells were treated with 0.1 μM of BFA for 2 h in a serum-free medium and then incubated with 3B-Dox and 3B-Dox-DMPG separately at an equivalent doxorubicin concentration of 0.6 μM in supplemented MEM containing 0.1 μM of BFA for 24 h. For chloroquine inhibition, MCF-7 cells were treated with 50 of μM chloroquine for 2 h in a serum-free medium and then incubated with 3B-Dox and 3B-Dox-DMPG separately at an equivalent doxorubicin concentration of 0.6 μM in supplemented MEM containing 50 μM of chloroquine. As a control, MCF-7 cells were treated with free dox, 3B-Dox or 3B-Dox-DMPG, 0.1 μM of BFA or 50 of μM chloroquine in a serum-free MEM for 2 h and in supplemented MEM for 24 h. After treatment, cells were washed 3 times with PBS at pH 7.4, and cell viability was evaluated by the CellTiter-Blue Assay kit. Briefly, cells were incubated with 50 μl/well of fresh MEM along with 10 μl/well of Cell Titer Blue assay reagent for 2 hours at 37°C. Fluorescence intensity was measured using a multidetection microplate reader (Bio-Tek, Winooski, VT) with 525/590 nm excitation/emission wavelengths. The percentage of cell viability was calculated by dividing the treated sample value by the value for the untreated cell sample. The percentage of cell viability upon the treatment with 3B-REG or 3B-Dox-DMPG and BFA or chloroquine inhibitior was normalized to that with BFA or chloroquine treatment alone.

4.2.13 Evaluation of BBB model penetration of targeted and non-targeted doxorubicin-loaded formulations

4.2.13.1 Preparation of BBB model

BBMVECs were seeded in 6-well plate inserts at a concentration of 90,000 cells/insert and incubated in Bovine brain endothelial growth media for three days at 37°C. Inserts were previously coated with 1 ml of attachment factor solution (AFS) for

30 min at 37°C and with 1 ml of fibronectin for 10 min at 37°C. Inserts were placed in 6-well plates with 2 ml of the same media per well. After three days of incubation, inserts and wells media was changed for differentiation media (DMEM supplemented with 10% FBS, 1% penicillin/streptomycin, 312.5 µM of 8-(4-CPT) cAMP, 0.5 µM of Dexamethasone, 17.5 µM RO-20-1724, 50 mM HEPES pH 7.4) and further incubated for 3 days[61].

4.2.13.2 Transepithelial Electric Resistance (TEER) measurement

Plates were kept under the hood for few minutes till temperature was stable. Then, TEER of the BBMVECs monolayer was measured with an Electrical Resistance System (Mililcell-ERS, Millipore, Germany). Coated inserts with the same media and without cells were used as TEER blanks.

4.2.13.3 Permeability coefficient (P_e) measurement

Media from the inserts was replaced with 1.5 ml/insert of a 20 µM Lucifer Yellow solution in Ringer's HEPES. The insert to be tested was transferred to the first well of an empty 6-well plate with 2 ml/well of Ringer's solution. Every 15 min inserts were transferred from one well to another. After 45 min, samples were taken from upper (inserts) and lower compartments (wells) at each time point, and their fluorescence was measured in triplicate using a multidetection microplate reader (Bio-Tek, Winooski, VT) with 428/540 nm excitation/emission wavelengths.

Permeability calculations were performed as described by Siflinger-Birnboim[62]. To obtain a concentration-independent transport parameter, the clearance principle was used. Cleared volume was calculated by dividing the amount of compound in the receiver compartment (X) by the drug concentration in the donor (C_d) compartment at each time point.

$$Clearance\ (ml) = X/C_d$$

During the 45-min experiment, the clearance volumes increase linearly with time. The average volume cleared was plotted versus time, and the slope estimated by linear regression analysis. The slope of the clearance curves for the culture was denoted PS_t, where *PS* is the permeability x surface area product (in ml per min). The slope of the clearance curve with the control filter coated only with AFS and fibronectin was denoted PS_f. The PS value for the endothelial monolayer (PS_e) was calculated from:

$$1/PS_e = 1/PS_t - 1/PS_f$$

The PS_e values were divided by the surface area of the insert to generate the endothelial permeability coefficient (P_e, in cm per min).

4.2.13.4 Cytotoxicity of doxorubicin-loaded formulations in BBMVECs

For the evaluation of cell viability in BBMVECs, 96-well plates were precoated with 50 µL/well of ASF for 30 min at 37°C. After removing ASF, wells were further incubated with 50 µL/well of fibronectin for 10 min more at 37°. BBMVECs were seeded at a

concentration of 8000 cells/well in Bovine brain endothelial cell growth media (GM) till 100% confluence was reached (48 hours). Cells were treated with liposomes and polymersomes formulations at an equivalent doxorubicin concentration of 8 µM for 18 hours. Afterwards, cells were washed twice with fresh GM and incubated with 50 µl/well of GM along with 10 µl/well of Cell Titer Blue assay reagent for 2 hours at 37°C. Fluorescence intensity was measured using a multidetection microplate reader (Bio-Tek, Winooski, VT) with 525/590 nm excitation/emission wavelengths.

4.2.13.5 Transport experiment across the BBB model

While preparing the BBMVECs monolayer, U87MG were seeded onto a 6-well plate at a concentration of 50,000 cells/well and incubated in MEM at 37°C, 24 hours before the BBMVECs monolayer was ready. Then, U87MG media was replaced with 2 ml of fresh differentiation media, and BBMVECs inserts were placed on 6-well plates seeded with U87MG. Nanoparticle samples were added to the inserts at an equivalent doxorubicin concentration of 10 µM and the co-culture was incubated for 5 hours at 37°C. Samples were collected from upper and lower compartment and doxorubicin's fluorescence was measured in triplicate using multidetection microplate reader (Bio-Tek, Winooski, VT) with 485/590 nm excitation/emission wavelengths. BBMVECs were washed were washed with endothelial growth media, detached and collected by centrifugation. Cell pellets were resuspended in 200 µL of PBS with 4% paraformaldehyde, and flow cytometry analysis was performed. U87MG were further incubated for 24 hours. Then, media was changed for fresh MEM and further incubated for 24 hours at 37°C. Afterwards, cells were washed and incubated with a mixture of 4.8 ml of fresh MEM along with 1.2 ml of Cell Titer Blue assay reagent (1 ml/well) for 2 hours at 37°C. Fluorescence intensity was measured using a multidetection microplate reader (Bio-Tek, Winooski, VT) with 525/590 nm excitation/emission wavelengths.

4.3 Results and Discussion

Once the molecular target was identified, surfaces of both liposomes and polymersomes were decorated with targeting moieties to address the DDS to the BBB. Therefore, both systems were covalently bound to Regulon peptide to be able to cross the BBB, whereas phage protein (DMPG) was inserted into liposomes and polymersomes' membrane, as a MCF-7-specific targeting moiety.

4.3.1 Polymersomes surface modification with Regulon peptide

As mentioned before, end group modification of polymers prepared by RAFT polymerization can be accomplished by conversion of trithiocarbonate into suitable functional groups capable of undergoing conjugation with biomolecules or bioactive functionality[54]. The straightforward approach is to convert thiocarbonate functionality of RAFT-synthesized polymers to thiol functionality via reduction/ aminolysis[63].

To avoid side-reactions, such as interchain oxidations and intrachain additions[54], the reaction was carried out by simultaneously performing aminolysis and thiol–disulfide exchange reaction using an amine compound and 2,2-dithiodipyridine (DTDP) together to yield pyridyldisulfide (PDS)- functionalized polymers (3B-PDS), that can be further reacted with sulfhydryl-terminated biomolecules, such as Regulon peptide, under mild conditions[58]. The reaction was once performed step by step to monitor the CTA end group conversion. Conversion of the trithiocarbonate to PDS end groups was verified by ultraviolet-visible spectroscopy (UV-vis)[64,65]. Figure 4.5 shows the UV-vis spectrum of the polymer's end group modification after each reaction.

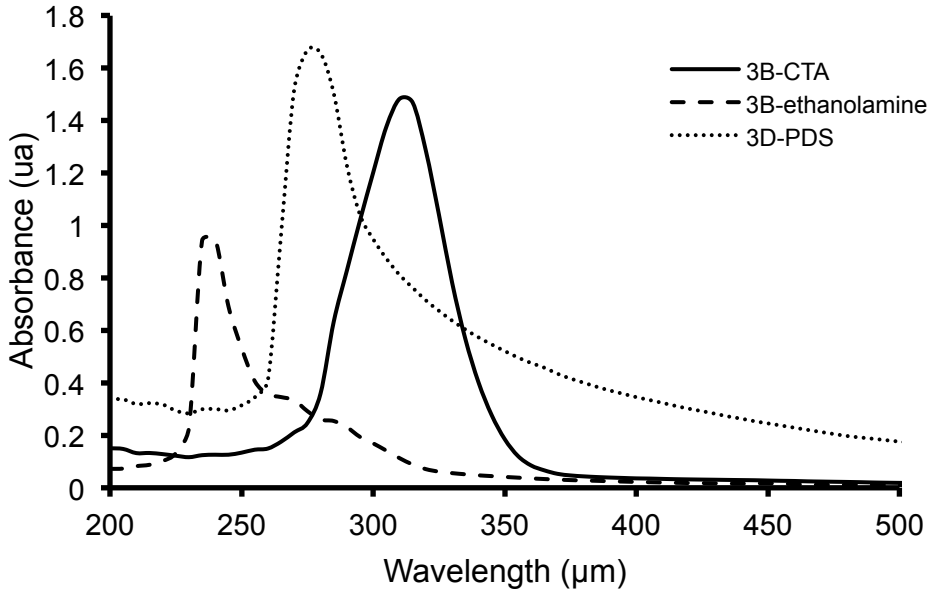

Figure 4.5: Uv-vis spectra of polymer's end-group modifications. Initial macroCTA of 3B-CTA (solid line), aminolysis with ethanolamine (dashed) and further reaction with DTDP (dotted).

As shown in Figure 4.5, the presence of trithiocarbonate group in the initial macroCTA (3B-CTA) was confirmed by a peak with maximum absorbance at 315 nm[66], indicating no degradation of the CTA. Upon aminolysis with ethanolamine, UV-Vis spectrum verified the consumption of the CTA group by reduction of the absorption at

310 nm and the appearance of a new product with a maximum at 235 nm, similar to dithiocarbamates absorbance around 230 nm[67]. After aminolysis, reaction between 3B-ethanolamine and DTDP showed a new shift in the absorbance spectrum. A new peak appeared at 275 nm, close to the described pyridyl disulphide-containing molecules absorbance (280 nm)[68].

Once CTA was successfully modified by aminolysis and further reaction with DTDP, Regulon peptide was attached to triblock copolymer by thiol-disulfide exchange[69]. In this case, confirmation of the coupling between the copolymer and the peptide was performed by ^{1}H-NMR. The cleavage of the pyridyldisulfide group was verified by the absence of pyridine ring signals at 8.47, 7.62 and 7.11 ppm in $CDCl_3$. The presence of characteristic peaks of the peptide was observed at 4.73 ppm, which corresponds to the α-carbon, indicating the obtention of the polymer-peptide conjugate (3B-REG)[70].

4.3.2 Preparation of plain liposomes and polymersomes

Both liposomes and polymersomes were prepared by the self-assembly of either a mixture of phospholipids ($MPEG_{2k}$-DSPE and DSPE-SH) or an amphiphilic triblock copolymer (pHEMA-*co*-pCHOL-*co*-pHEMA), respectively, via the film hydration technique followed by sonication.

Size of plain liposomes measured by DLS was 146 ± 43 nm, similarly to what has been already described[71], whereas polymersomes showed an average hydrodynamic diameter of 128 ± 48 nm, as determined in the previous chapter.

4.3.3 Cytotoxicity of plain polymersomes

First of all, the cytotoxicity of newly prepared polymersomes was assessed. For this purpose, two cell lines were selected, an endothelial cell line, C166, and a tumour epithelial cell line, U87MG. Polymersomes were incubated in both cells lines at a maximum concentration of 5 mg/ml for 48 hours (Figure 4.6).

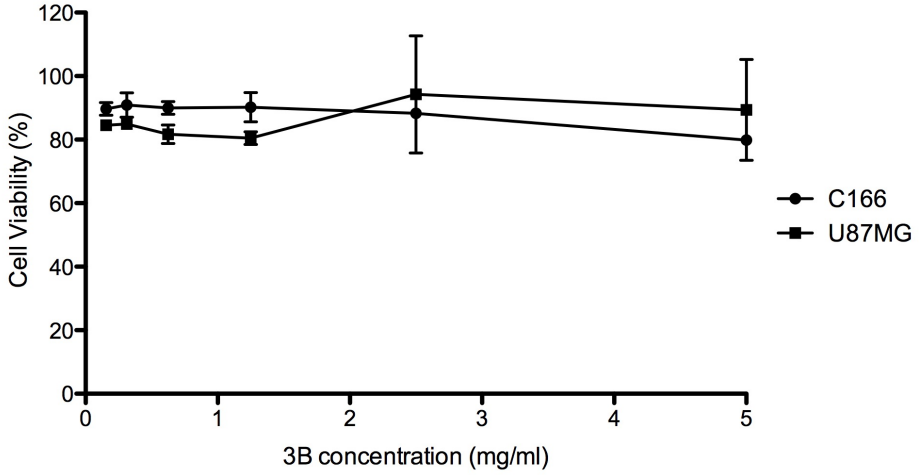

Figure 4.6: Cytotoxicity of plain polymersomes in C166 and U87MG after 24h of treatment, (n=3; mean SD).

Figure 4.6 shows that polymersomes themselves did not cause any cytotoxic effect in C166 and U87MG at the concentration tested, making them suitable for drug delivery.

4.3.4 Preparation of BBB-targeted liposomes and polymersomes

Targeted formulations, such as Regulon peptide-bearing liposomes and polymersomes, were prepared by the film hydration technique, following a slightly different approach. In order to partially decorate liposomes' surface with Regulon peptide, liposomes were obtained by the film hydration technique mixing $MPEG_{2k}$-DSPE with a thiolated phospholipid, 1,2-dipalmitoyl-*sn*-glycero-3-phosphothioethanol, which allows further thiol coupling with Regulon peptide, at a ratio of 85% and 15% (w/w), respectively. In the case of polymersomes, Regulon peptide was conjugated to the triblock copolymer before nanostructures formation. Afterwards, polymersomes were prepared by the film hydration technique mixing triblock copolymer with the conjugate of triblock copolymer-regulon at a ratio of 85% and 15%, respectively.

4.3.5 Phage fusion coat protein insertion into liposomes and polymersomes bilayers

After having achieved the preparation of peptide-bearing formulations, phage fusion coat protein (DMPG) was inserted into liposomes' and polymersomes' membranes thanks to its amphiphilic nature. In order to ensure that phage protein was inserted into liposomes' bilayer, an SDS-PAGE gel was performed (Figure 4.7). The percentage of phage protein inserted was around 74%, calculated with ImajeJ software. It was hypothesized that, similarly to liposomes, phage proteins could also get inserted into polymersomes thanks to their amphiphilic characteristics. Polymersomes attached to phage protein, 3B-DMPG, were prepared following the same procedure and analysed by SDS-PAGE, which showed the presence of phage protein in 3B-DMPG, achieving a 47% of insertion efficiency.

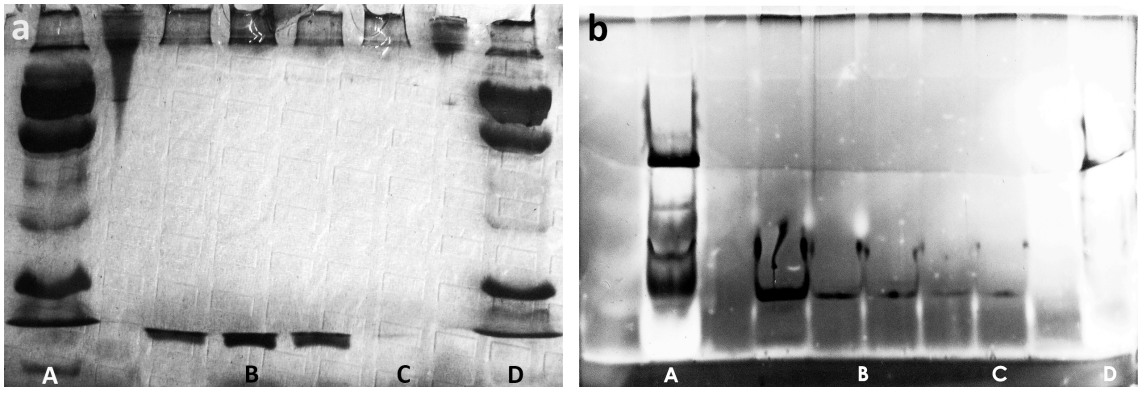

Figure 4.7: Phage protein (DMPG) insertion into liposomes and polymersomes membranes.16% acrylamide/bis-acrylamide SDS-PAGE gels of Lipo-DMPG (a) and 3B-DMPG (b). In (a): polypeptide marker 5 μg/ml (A) and 2 μg/ml (D), Phage protein standard curve (B) (100, 50, and 25 μg/ml) and Lipo-DMPG sample (C). In (b): polypeptide marker 5 μg/ml (A) and 2 μg/ml (D), Phage protein standard curve (B) (100, 80, 60 and 40 μg/ml) and 3B-DMPG sample (C).

Authors working in transmembrane protein insertion into polymersomes, suggested that high flexibility and conformational freedom of polymer molecules may allow a block copolymer membrane to adapt to the specific geometric and dynamic requirements of membrane proteins without considerable loss of free energy, even better that liposomes[18,57]. However, they based their work on poly(2-

methyloxazoline)-*b*-poly(methylsiloxane)-*b*-poly(2-methyloxazoline), PMOXA-PDMS-PMOXA, triblock copolymer, whose hydrophobic block flexibility (PDMS) is expected to be higher than the methacryloylated cholesterol derivative of 3B. Therefore, differences in flexibility constraints may be responsible for the different degree of phage insertion observed in polymersomes compared to liposomes.

In summary, the insertion efficiency here achieved seemed to be acceptable for an amphiphilic system containing a more rigid block such as cholesterol. In addition, cholesterol has been widely used in the preparation of drug delivery vehicles because of its well-known ability to drive self-assembly of cholesterol-containing materials[72,73] and his ability to interact with cellular membranes[74].

4.3.6 Characterization of targeted liposomes and polymersomes

After decoration of liposomes and polymersomes with targeting moieties, characterization of non-loaded formulations was performed by DLS. Table 4.1 shows size measurements of plain (Lipo and 3B), MCF-7-targeted (Lipo-DMPG and 3B-DMPG), BBB-targeted (Lipo-REG and 3B-REG) and dual-targeted (Lipo-DMPG-REG and 3B-DMPG-REG) liposomes and polymersomes.

Table 4.1: Size measurements of targeted liposomes and polymersomes by DLS.

Sample	Size (nm)
3B	128 ± 48
3B-DPMG	206 ± 80
3B-REG	214 ± 69
3B-DMPG-REG	236 ± 47
Lipo	146 ± 43
Lipo-DMPG	132 ± 61
Lipo-REG	227 ± 53
Lipo-DMPG-REG	231 ± 46

A new batch of plain polymersomes was prepared showing similar size values to those achieved in the previous chapter, whereas thiolated liposomes showed slightly larger nanostructures, 128 ± 48 nm and 146 ± 43 nm, respectively (Table 4.1). The insertion of phage protein (DMPG) contributed distinctly to nanostructures size. In the case of polymersomes, 3B-DPMG's size was larger than plain polymersomes, while Lipo-DMPG's size slightly decreased compared to plain liposomes. This shrinkage of liposomes is consistent with results shown by other authors after insertion of an transmembrane protein[50], indicating that lipids forming the liposome are flexible enough to adopt protein's dimension in its immediate neighbouring[18], leading to a more efficiently embedded structure. Regarding polymersomes, it must be taken into account that block copolymer membranes are considerably thicker than conventional lipid bilayers due to higher molecular weight of the hydrophobic block. Therefore, the hydrophobic part of transmembrane proteins may be too small to fit through polymer membranes as the hydrophilic-hydrophobic pattern of these proteins is naturally optimized with respect to thinner biological membranes[57]. This difference in membrane thickness and the presence of a rigid molecule, such as cholesterol, into

polymersomes structure may complicate the proper embedding of phage protein into polymersomes leading to larger nanostructures.

On the other hand, the attachment of Regulon peptide implied an increase in size for both formulations compared to plain and phage-bearing formulations, as Regulon peptide is a voluminous targeting moiety and in this case it was not inserted into the membrane. Consequently, when both targeting moieties were conjugated in the same carrier, both liposomes and polymersomes' size was larger, probably due to the steric hindrance between phage and Regulon peptide.

4.3.7 Doxorubicin loading into liposomes and polymersomes

Once single-targeted (3B-DMPG and 3B-REG) and dual-targeted (3B-DMPG-REG) formulations had been successfully prepared and characterized, plain and targeted formulations were loaded with doxorubicin through the remote loading method[75]. Doxorubicin's loading efficiency and capacity of liposomes and polymersomes are shown in Table 4.2.

Table 4.2: Doxorubicin's loading efficiency and capacity of liposomes and polymersomes

Samples	Loading efficiency (%)	Loading capacity (%)
3B-Dox	47.89 ± 2.5	4.8 ± 0.2
3B-Dox-DPMG	40.81 ± 0.7	2.2 ± 0.2
3B-Dox-REG	34.15 ± 1.8	1.2 ± 0.06
3B-Dox-DMPG-REG	36.59 ± 6.4	1.42 ± 0.25
Lipo-Dox	69.92 ± 7.9	7.1 ± 0.9
Lipo-Dox-DMPG	47.3 ± 4.7	3.8 ± 0.9
Lipo-Dox-REG	29 ± 5.3	2.89 ± 0.7
Lipo-Dox-DMPG REG	18 ± 2.7	1.5 ± 0.3

Plain liposomes showed higher loading efficiency and capacity than polymersomes (Table 4.2). This result is consistent with the higher fluidity of liposomes membrane, which allows easier diffusion of substances, compared to polymersomes. This difference between liposomes and polymersomes is extensible to all targeted formulations. It was also observed that both liposomes and polymersomes presented a decrease in loading when they were conjugated with targeting moieties. This fact corroborates that in the presence of ligands on the surface, loading capacity of the system is lower as it is more difficult for the drug to diffuse into the vesicles, as it has been stated in chapter 2. In addition, loading capacity is lower for larger ligands, as it can be observed in this case, as phage proteins has a MW of 5,747 Da, whereas Regulon peptide has MW of 7,295 Da. In addition, phage protein is inserted into the membrane so it does not represent such a steric hindrance for the drug to be encapsulated as Regulon peptide, which is attached on the outer layers of both nanostructures. Therefore, encapsulation is lower for peptide-conjugated vesicles than for phage-conjugated ones. However, loading capacity of phage-bearing formulations does not correspond to the real loading capacity of the system. During formulation preparation, doxorubicin was loaded before phage protein insertion; therefore significant drug leaking occurred during dialysis required for purification after phage insertion. The combination of both ligands in one vehicle implies much higher steric hindrance, leading to the lowest encapsulation levels for both formulations.

It must be said that size of doxorubicin-loaded formulations could not be measured neither by DLS nor by NTA as both techniques use a 633 and 638 nm-lasers, which interfere with doxorubicin fluorescence emission, whose maximum emission wavelength is around 580 nm.

4.3.8 Doxorubicin release from liposomes and polymersomes

Once both systems have demonstrated their ability to encapsulate doxorubicin, the next step consisted in determining their release profiles. Depending on the carrier's nature and the loading method, the release profile can vary significantly[76]. Stability and drug release of doxorubicin-loaded liposomes and polymersomes was examined under conditions approaching those that the delivery vehicle would encounter in his way to the site of action. These include contact with physiological fluids at pH 7.4, pH 6.5 of tumor tissue and pH 5.5 after uptake in endosomal compartments[77].

To evaluate formulations behaviour at different pH, doxorubicin-loaded liposomes and polymersomes were placed into dialysis tubes and dialyzed against different phosphate buffer solutions at pH 7.4, 6.5 and 5.5 for 4 days at 37°C (Figure 4.8). Doxorubicin's concentration outside the dialysis tube was measured by spectrophotometry at 480 nm at each time point.

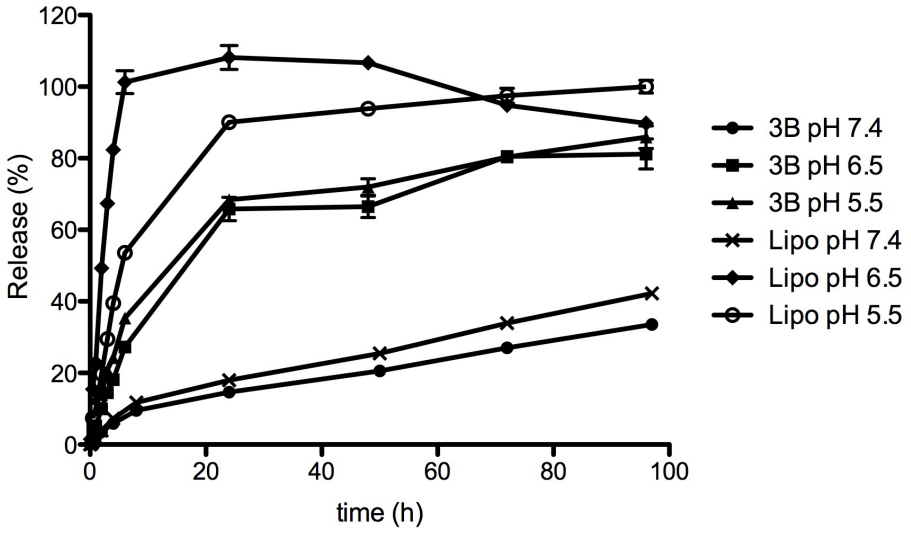

Figure 4.8: Release of doxorubicin from liposomes and polymersomes at pH 7.4, 6.5 and 5.5 at 37°C (n=3; mean SD).

Figure 4.8 shows the percentage of release of both formulations after 100 hours of dialysis at different pH. Stability profiles of both formulations at pH 7.4 was very similar although liposomes showed a slightly higher leaking, losing up to 40% of their loading, while polymersomes lost around 30% of it. At lower pH, the previous inward pH-gradient required for doxorubicin's remote loading nearly disappears, leading to the release of the entrapped uncharged doxorubicin[77-79]. Therefore, doxorubicin's release rose up to the 80% for both liposomes and polymersomes at pH 6.5. No significant differences were observed between the release at pH 6.5 and 5.5 in the case of polymersomes. On the other hand, liposomes achieved the 100% of release of their payload at pH 5.5.

It can be observed that release of doxorubicin that was loaded through the pH-gradient of a weak acid, such as citric acid, is highly dependent on the extraliposomal pH value, as already shown by other authors[77]. For instance, doxorubicin-loaded block copolymer vesicles of poly(trimethylene carbonate)-b-poly(L-glutamic acid)[80] showed a release of 25% at 7.4 pH and 55% at pH 5.5 after 24 hours at 37°C, while EPC/Chol liposomes released the 10% of entrapped doxorubicin at pH 7.4 and the 30% at pH 5.5 only after 2 hours[77], which is in good agreement with the results here presented.

Both the lower loading and release of polymersomes might be related to the structural differences between liposomes and polymersomes' membranes. The lower permeability of polymesomes' membranes can be attributed to the increased length of the amphiphile and its conformational freedom, which allows for greater toughness and reduced permeability, as opposed to natural amphiphiles, such as liposomes[81]. In addition, the presence of cholesterol in their structure may have an strong influence as well, as cholesterol's rigidity modifies membrane fluidity of polymersomes similarly to liposomes[28]. In fact, the first generation of liposomes was improved in terms of stability in blood and drug release by incorporating cholesterol intro their structures, which was shown to 'tighten' fluid bilayers and reduce the leakage of contents from liposomes[19].

These results suggested that both formulations are promising platforms for drug delivery, as they would keep much of their content until they reach the target site, taking into account that the elimination half-life of doxorubicin-loaded pegylated liposomes, such as Doxil, is approximately 45 hours in humans[82].

4.3.9 MCF-7-targeted liposomes and polymersomes binding specificity and uptake in MCF-7 and U87MG

The binding activity and selectivity of phage fusion pVIII coat protein after its incorporation into liposomes and polymersomes was investigated incubating doxorubicin-loaded formulations with specifically targeted MCF-7 cells and non-targeted U87MG cells, separately, followed by flow cytometry analysis based on doxorubicin fluorescence.

Figure 4.9 showed the binding selectivity of 3B-Dox, 3B-Dox-DMPG, Lipo-Dox and Lipo-Dox-DMPG in MCF-7 and U87MG cells after 4 hours of incubation at 37°C.

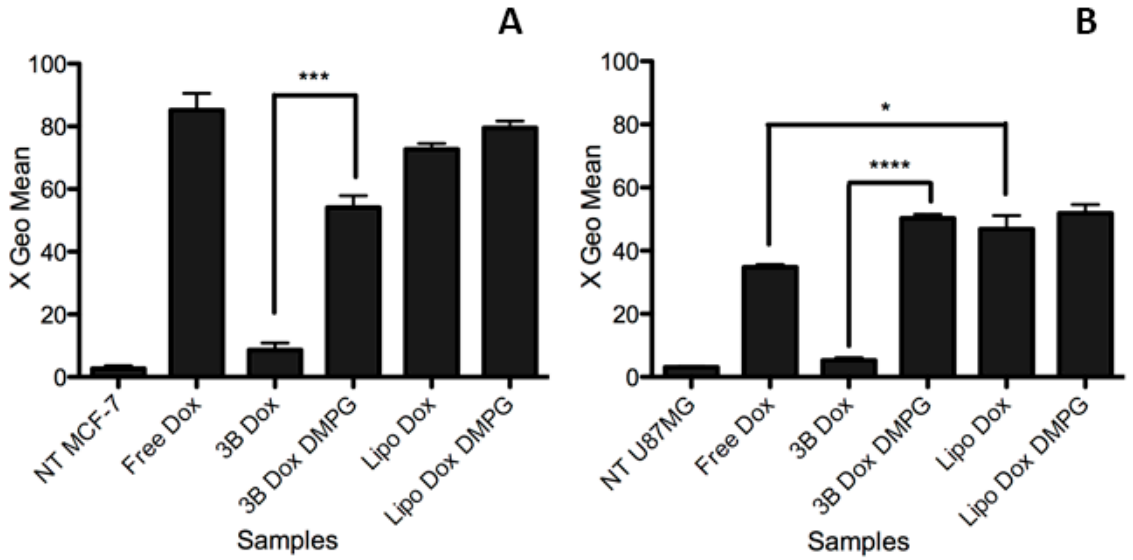

Figure 4.9: Flow cytometry analysis on uptake of doxorubicin and doxorubicin-loaded liposomes and polymersomes in MCF-7 (A) and U87MG (B) after 4 hours of treatment at 10 µM of doxorubicin (n=3; mean SD). (*p < 0.05, ***p < 0.001, ****p < 0.0001)

The general trend observed in flow cytometry results (Figure 4.9) was that the uptake of free and encapsulated doxorubicin was higher in MCF-7 cells rather than in U87MG cells, which is in good agreement with data shown by other authors[32,83], who suggested that the presence of p-glycoprotein pump (P-gp) in U87MG expelled doxorubicin from cells at higher rate than MCF-7. Regarding targeted formulations (DMPG), an increase in uptake was measured compared to non-targeted ones in both cell lines, which was significantly higher for polymersomes (3B-Dox-DMPG) ($p<0.001$). Phage protein bearing DMPGTVLP is known to interact with a cellular surface protein, nucleolin[5,51], which is overexpressed on the surface of activated endothelial cells and many cancer cells with high proliferative rates including breast cancer cells (MCF-7)[6,84], prostate carcinoma or lymphocytic leukemia, as well as glioblastoma (U87MG)[3,34,85], in considerable amount. However, nucleolin expression depends on each cancer type as it interacts with various regulatory pathways[5,86]. This explains the higher uptake of targeted formulations (DMPG) in MCF-7 as this cell line exhibits a higher expression of nucleolin rather than U87MG cells.

Both targeted formulations (3B Dox DMPG and Lipo Dox DMPG) represent a remarkable improvement in uptake compared to free doxorubicin in U87MG cells, while in MCF-7 cells only liposomal targeted formulation (Lipo Dox DMPG) is able to reach free doxorubicin's uptake.

These results confirmed what had been previously reported that phage fusion VIII coat protein bearing DMPGTVLP peptide has higher affinity for MCF-7 cells rather than other tumour cell lines, such as U87MG, and its insertion into different drug delivery vehicles improves their uptake through selective binding[5,37,49], which is specially remarkable in the case of polymersomes.

4.3.10 MCF-7-targeted and non-targeted liposomes and polymersomes uptake in MCF-7

The uptake and localization of MCF-7-targeted liposomes and polymersomes was investigated incubating the two doxorubicin-loaded delivery systems with organelle stained MCF-7 cells and followed by fluorescence microscopy. Early endosomes were labelled with a Transferrin alexa fluor conjugate to study the possible involvement of endocytic pathway in phage formulations uptake[52].

Uptake patterns of MCF-7-targeted and non-targeted doxorubicin-loaded liposomes and polymersomes is shown in Figure 4.10.

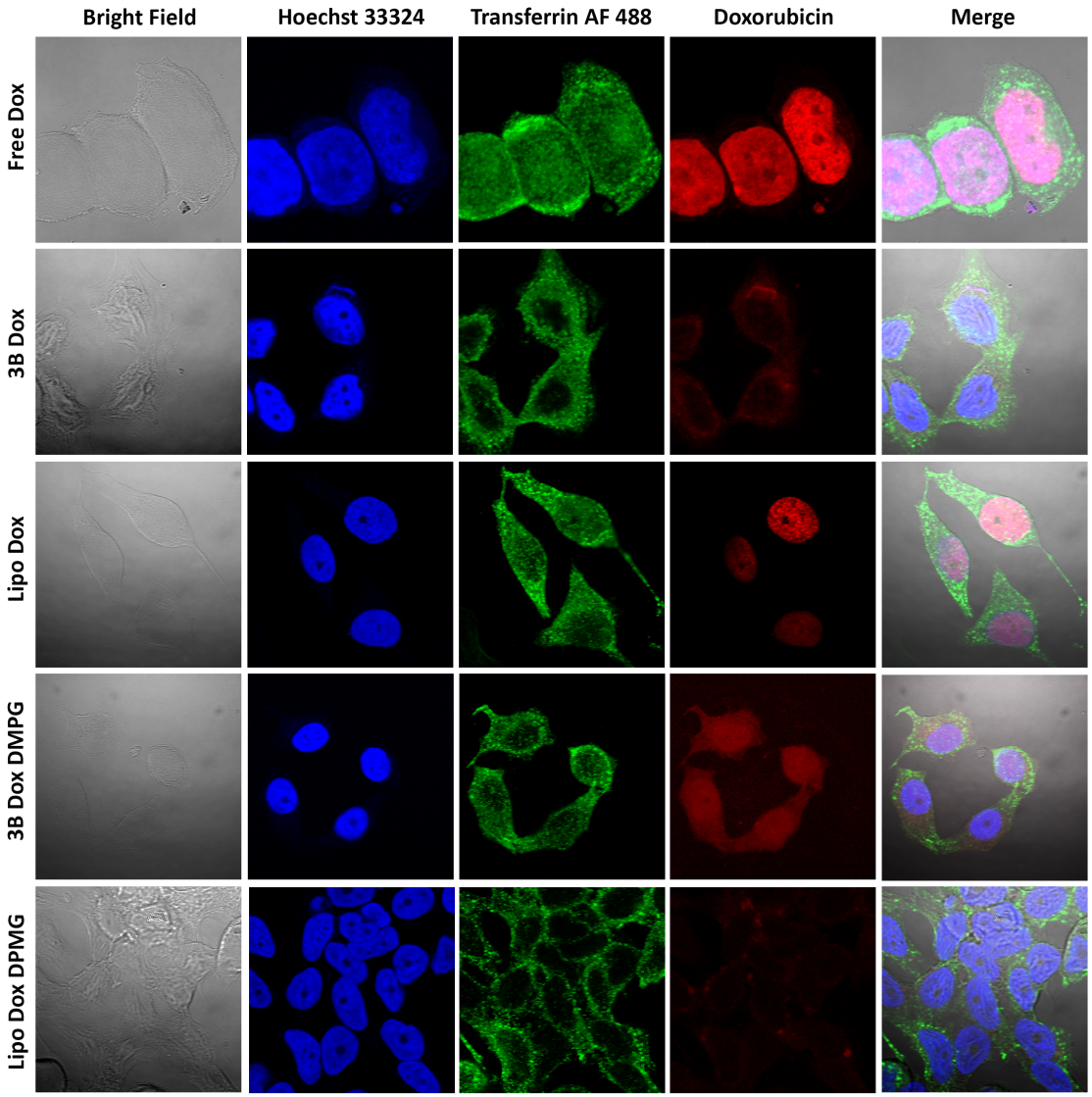

Figure 4.10: Uptake of free doxorubicin and MCF-7-targeted and non-targeted doxorubicin-loaded polymersomes and liposomes by MCF-7, visualized by fluorescence microscopy after 2-hours treatment at 40 µM of doxorubicin. Nuclei were stained with Hoechst 33324 and early endosomes with transferrin alexa fluor 488.

After 2 h of incubation with free doxorubicin, strong fluorescence was observed in cell nuclei, suggesting rapid intercalation of intracellular doxorubicin to the

chromosomal DNA after passive diffusion into the cells[83] (Figure 4.10). Similarly, it was seen that Lipo-Dox was mainly located in the nucleus, suggesting that entrapped doxorubicin was released from liposomes and uptaken as a free drug, as shown by cells incubated with free doxorubicin. This could be explained as liposomes have the ability to fuse with cell membranes thanks to their membrane mimic, so that they could release their payload when they are brought into contact with cells[18]. Contrarily, 3B-Dox showed much lower uptake than Lipo-Dox, as previously observed in flow cytometry assay (Figure 4.9). In addition, its distribution was mainly localized in the cytoplasm. This difference might suggest a different uptake pathway of polymersomes compared to liposomes. As mentioned before, the presence of cholesterol in polymersomes' structure give them more rigidity, which may complicate their fusion with cellular membrane that has also been described, although it takes place at a lower time scale[18]. Therefore, polymersomes uptake might follow other routes to enter the cell in endocytic vesicles, which could probably be clathrin-dependent endocytosis, as it is known that this is the classical route for the uptake of essential nutrients such as cholesterol carried into cells by LRP-1[87], which is expressed at low levels in MCF-7 cells[39,88,89].

Regarding MCF-7-targeted formulations, a considerable increase in uptake was observed in the case of targeted polymersomes, as already observed in flow cytometry analysis (Figure 4.9). Doxorubicin was observed in nuclei and cytoplasm equally, indicating that it has been released from endosomes compared to 3B-Dox. In the case of Lipo-Dox-DPMG, doxorubicin is not observed in the nuclei anymore, but in the cytoplasm. It seems that the presence of phage protein drove the uptake to the endosomes, preventing liposomes to fuse with cell membrane and release their content. These differences in DMPG contribution to doxorubicin's release from the endosomes between Lipo-Dox-DMPG and 3B-Dox-DMPG may suggest that DMPG presented a synergetic effect with polymersomes but not with liposomes. We hypothesized that the swelling of phage protein due to its buffering capacity[52] at endosomal pH may have led to the disruption of polymersomes as well, thus releasing their payload to the nucleus.

In the light of the results, it can be said that MCF-7-targeted and non-targeted formulations showed different uptake patterns, suggesting that the presence of phage fusion coat protein guided the uptake mainly through an endocytic pathway[6,52,83]. In the case of polymersomes, is where this difference was more evident, as non-target polymersomes are hardly uptaken by MCF-7 cells, whereas phage protein remarkably improved their overall uptake. In addition, it has been demonstrated that polymersomes had less fusogenic capacity than liposomes.

4.3.11 Tumor cell killing of doxorubicin-loaded liposomes and polymersomes

In order to test the killing improvement of MCF-7-targeted formulations, MCF-7 cells were incubated with MCF-7 targeted and non-targeted formulations and free doxorubicin, in MCF-7 and U87MG cells.

Enhanced tumor cell killing capacity of DMPG-bearing formulations was investigated through a CellTiter-Blue assay of incubated MCF-7 cells with doxorubicin-loaded non-targeted, MCF-7-targeted, BBB-targeted (REG) and dual-targeted (DMPG and REG) liposomes and polymersomes at an equivalent doxorubicin concentration of 10 µM for 48 hours (Figure 4.11).

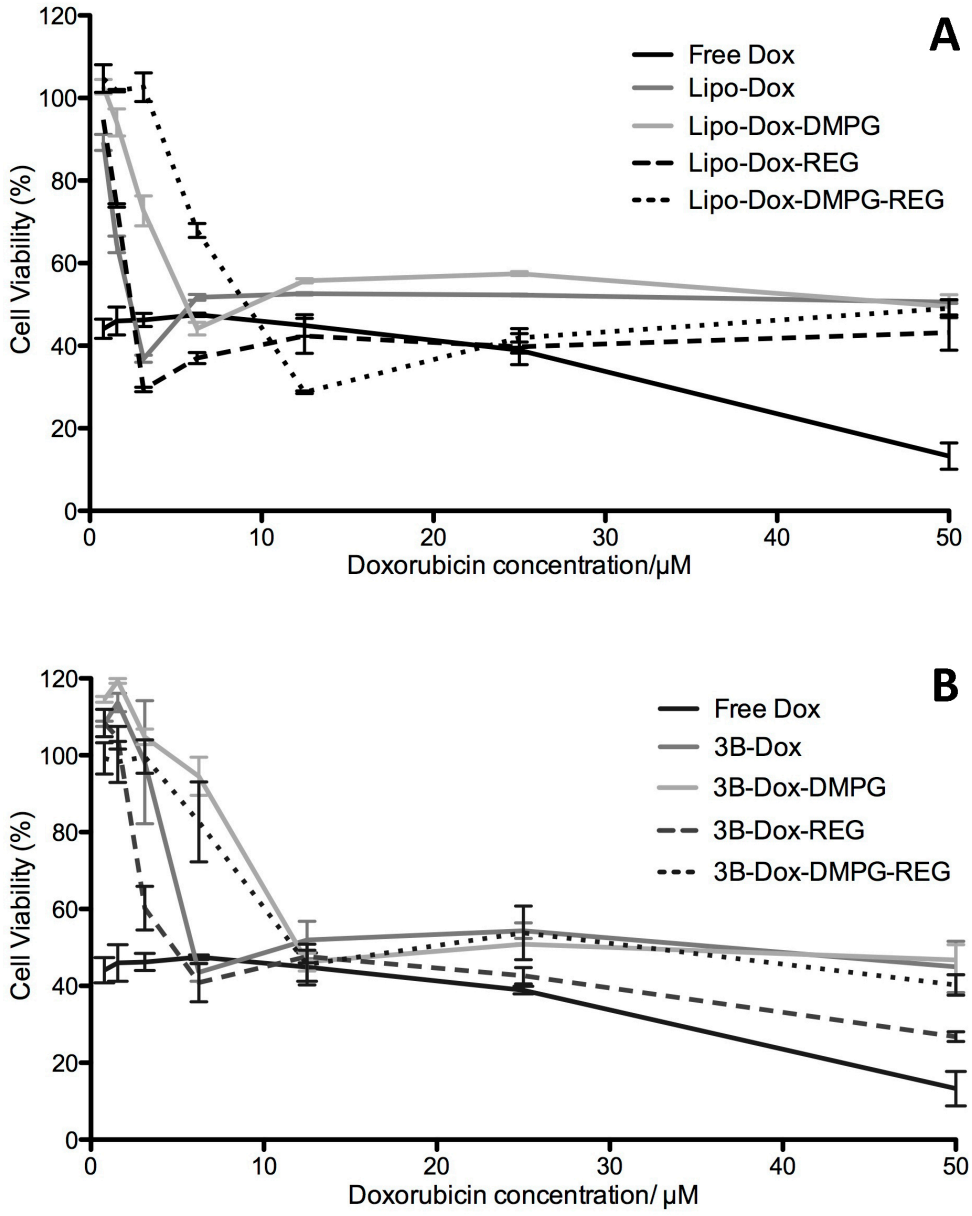

Figure 4.11: Cell viability (%) of MCF-7 after 48 h of treatment with free dox and doxorubicin-loaded MCF-7-targeted and non-targeted liposomes (A) and polymersomes (B) Data were presented as mean ± SD (n=3).

Generally, liposomal formulations (Figure 4.11A) showed slightly higher cytotoxicity than polymersomes in MCF-7 cells (Figure 4.11B), which is in good agreement with the faster release (Figure 4.8) and the higher uptake shown by liposomal formulations in MCF-7 cells (Figure 4.9). Comparing non-targeted formulations, fluorescence microscopy images already revealed that Lipo-Dox was focused in the nucleus while 3B-Dox was mainly distributed along the cytoplasm

(Figure 4.10), suggesting that doxorubicin found in the cytoplasm may exist as its encapsulated form and may therefore require a longer period to be released to become therapeutically active and show cytotoxicity.

Regarding targeted formulations, it was observed that MCF-7-targeted samples were slightly less cytotoxic than non-targeted ones, oppositely to what was expected, as uptake was higher in the presence of phage protein (DMPG). Taking into account the localization of DMPG-bearing formulations over the cytoplasm as shown by fluorescence microscopy, it is believed that escape from the endosomes would take longer so that free doxorubicin would not be released till longer periods, showing less cytotoxicity at shorter times although the uptake is higher.

BBB-targeted formulations bearing Regulon peptide showed similar levels of cytotoxicity compared to non-targeted liposomes (Lipo-Dox). This fact may indicate that regulon peptide did not have a negative effect in Lipo-Dox-REG uptake and contributed positively to the uptake of 3B-Dox-REG in MCF-7 cells. An explanation for this behaviour might be the low levels of LRP-1 found in MCF-7[39,88,89]. However, when DMPG and regulon peptide were combined in dual-targeted formulations, toxicity was much lower, indicating a possible negative cooperativity phenomenon between DMPG and Regulon pepide.

Figure 4.12 shows U87MG cell killing of doxorubicin-loaded formulations and free doxorubicin. Cell killing ability of polymersomes was higher than liposomes at all concentrations tested, as IC_{50} of 3B-Dox was approximately 2.24 µM, which is lower than Lipo-Dox IC_{50} that was around 7.86 µM.

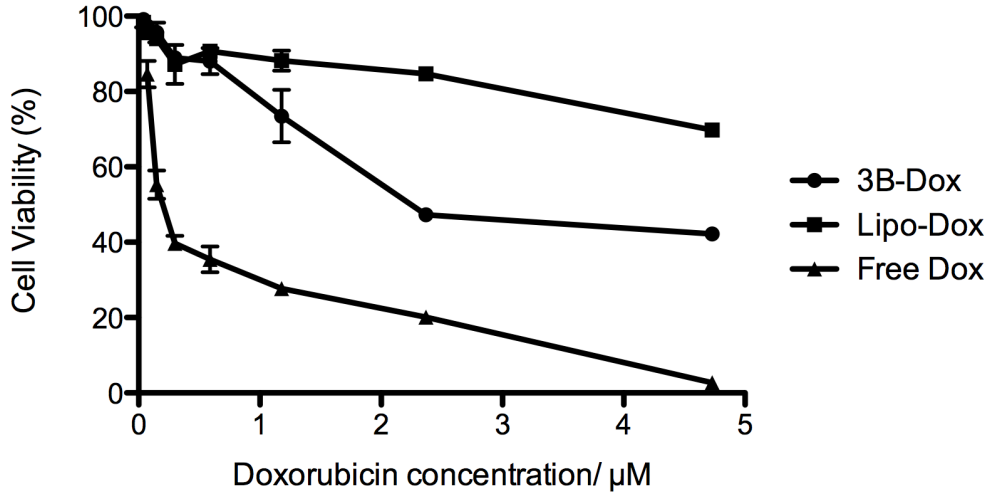

Figure 4.12: Cell viability (%) of U87MG after 48h of treatment with free dox and doxorubicin-loaded liposomes and polymersomes Data were presented as mean ± SD (n=3).

Cell viability (%) of U87MG cells decreased up to 80% and 45% for Lipo-Dox and 3B-Dox respectively, while in MCF-7 cells, these formulations were nearly non-cytotoxic (Figure 4.11).

Tumor cell killing results obtained for MCF-7 and U87MG cells suggest that U87MG cells are much more sensitive to doxorubicin than MCF-7 after 48 hours of treatment[38,90], as the uptake was higher in MCF-7 than in U87MG cells (Figure 4.9).

4.3.12 Evaluation of endosomal escape ability of MCF-7-targteted Polymersomes

As the presence of phage protein (DMPG) did not involve a clear increase of doxorubicin-loaded polymersomes cytotoxicity in MCF-7 (Figure 4.11B), their endosomal escape ability was tested. As mentioned before, it has been previously shown that phage protein (DMPG) possesses endosome-escaping ability due to the protonation in acidic conditions of their aspartic and glutamic residues causing a change in its conformation and a subsequent destabilization of the endosomal membrane. Therefore, in order to examine the possible involvement of the endocytic pathway in 3B-Dox-DMPG-induced cell death, targeted and non-targeted polymersomes were incubated with bafilomycin A1 (BFA), an endosomal acification inhibitor, and chloroquine, an endosome disrupting agent, in MCF-7 (Figure 4.13).

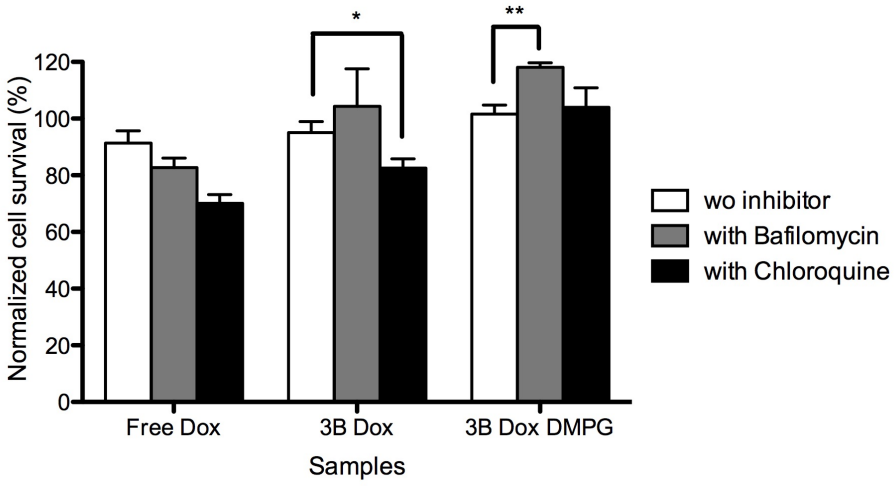

Figure 4.13: Effect of endosome acidification on DMPG-bearing Polymersomes after 24h of treatment. Data were presented as mean ± SD (n=3). Statistical analysis was determined using t test compared to "wo inhibitor" (*p < 0.05, **p<0.001)

The presence of BFA significantly reduced MCF-7 cell killing by 3B-Dox-DMPG, suggesting that endosomal acidification is required for 3B-DMPG-mediated cell death and that endocytosis is a pathway for 3B-Dox-DMPG internalization (Figure 4.13). In contrast, BFA co-incubation with non-targeted polymersomes (3B-Dox) did not cause a significant reduction in cytotoxicity, indicating that disruption of the endosome does not influence its killing efficiency, which is in good agreement with confocal microscopy results that show the retention of 3B-Dox inside endosomes (Figure 4.10).

Chloroquine is known to disrupt the endosome integrity by swelling and bursting the endosome[91], and to inhibit endosome delivery to lysosomes[92]. As expected, chloroquine treatment significantly enhanced 3B-Dox tumour cell death, but had a negligible effect on the 3B-Dox-DMPG cell death, suggesting that endosome disruption by chloroquine facilitates the escape of the endosome-entrapped 3B-Dox into the cytosol thus increasing its cytotoxicity, whereas 3B-Dox-DMPG escapes from endosomes without the help of chloroquine. This, along with results of bafilomycin A1

inhibition, suggests that phage protein, like chloroquine, stimulates the endosomal release of 3B-Dox-DMPG and promotes drug access to the cytosol.

In the light of the results, it can be concluded that the presence of phage protein into 3B-Dox-DMPG provides the system with the endosomal-escape ability, but at longer times than expected, thus not showing an evident increase in cytotoxicity compared to non-targeted polymersomes (3B-Dox) (Figure 4.11).

4.3.13 Transport across the BBMVECs monolayer and dual-targeting effects in vitro

4.3.13.1 Cytotoxicity in BBMVECs

Before evaluating the capability of a drug delivery vehicle to cross a BBB model, it must be ensured that the formulation to be tested does not compromise the barrier integrity. For this reason, cytotoxicity of MCF-7-targeted and non-targeted doxorubicin-loaded liposomes and polymersomes in Bovine Brain Microvascular Endothelial cells (BBMVECs) was assessed.

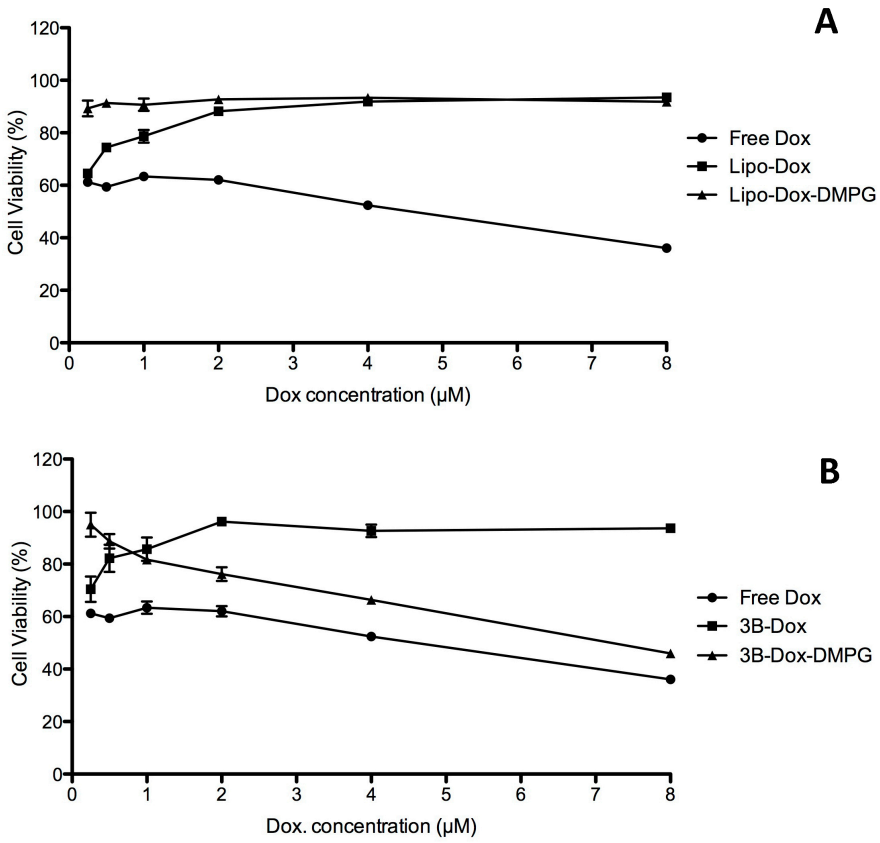

Figure 4.14: Cytotoxicity of doxorubicin-loaded liposomes (A) and polymersomes (B) in BBMVECs, after 18 hours of treatment at 37°C

Regarding liposomal formulations (Figure 4.14A), no cytotoxicity was observed in BBMVECs after 18 hours of incubation with doxorubicin-loaded MCF-7-targeted and non-targeted liposomes at an equivalent concentration of doxorubicin of 10 μM. In the case of polymersomes, doxorubicin-loaded non-targeted samples did not show any

cytotoxic effect in BBMVECs. However, MCF-7-targeted polymersomes showed increasing cytotoxicity as doxorubicin concentration increased. Generally, chemotherapeutic agents cause minor cytotoxic effects to the BBB as endothelial cells express a quiescent phenotype[93], thus drugs, such as paclitaxel or doxorubicin do not affect them as their mechanism of toxicity are based on blocking cell replication[94,95]. It must be said that in this experiment BBMVECs did not reach the optimum confluence, typical of BBB-like monolayers, thus cells were able to keep replicating, and therefore samples, such as free doxorubicin, showed cytotoxic effects. Nevertheless, transport experiments across the BBMVECs monolayer were performed at shorter times, in order to avoid cytotoxic effects.

4.3.13.2 Establishment of BBB model

Once all formulations demonstrated that they did not represent a threat for BBMVEC cell viability, their suitability as drug delivery vehicles able to cross a blood-brain barrier model and kill tumour cells in the brain was assessed. To do so, a preliminary study was performed using an *in vitro* co-culture model. Blood-brain barrier was represented by a Bovine brain microvascular endothelial cells monolayer (BBMVECs) cultured on the upper side of cell culture inserts, while tumor cells were placed at the bottom of a six-well plate[96], U87MG cells as primary glioblastoma brain tumour and MCF-7 cells as metastatic breast cancer (Figure 4.15).

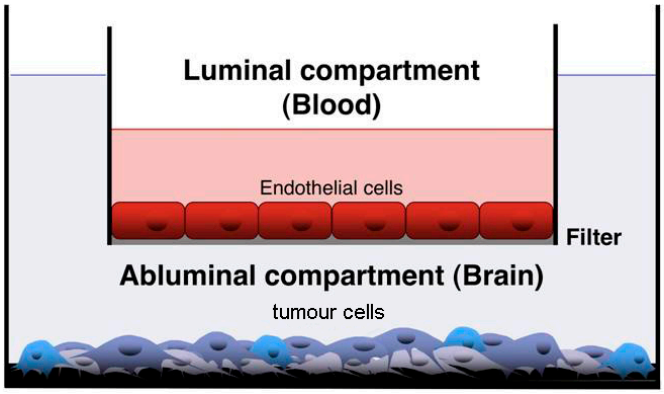

Figure 4.15: In vitro co-culture model of the blood-brain barrier and tumour cells in the brain.

The establishment of the BBMVECs monolayer was achieved by culturing cells for three days in Bovine brain endothelial growth media, which was substituted by supplemented DMEM, and further incubated for 3 days. It has been demonstrated that supplemented media with cAMP[61,97,98] and corticosteroids, such as hydrocortisone[99,100], improved barrier function in vascular endothelial cells, allowing the establishment of valid BBB models for the evaluation of the permeability of different compounds[96,101,102] and nanoparticulate systems[103,104]. In these BBB *in vitro* models, BBMVECs monolayer integrity is generally characterized measuring Transendothelial Electrical Resistance (TEER) and Permeability coefficient (P_e) of Lucifer yellow. In the experiments performed in this work, monolayers showing TEER values above 230 $\Omega.cm^2$ and P_e below 0.8 $x10^{-3}$cm/min were considered feasible for transport experiments, as this is the limit value usually accepted[41,105]. Once the

BBMVECs monolayer was achieved, the insert was placed over the well with tumour cells and were cultured for 24 hours.

4.3.13.3 Transport experiment across BBMVECs monolayer

At this point, BBB model crossing potential of targeted and non-targeted doxorubicin-loaded liposomes, bearing MCF-7 phage protein and BBB-specific peptide (REG), was assessed. The co-culture was assembled by placing BBMVECs monolayer inserts over U87MG wells. Samples with an equivalent doxorubicin's concentration of 10 µM were added to the upper compartment of the co-culture and incubated for 5 hours at 37°C without shaking. Afterwards, inserts were removed and tumour cells were further incubated with the abluminal media containing the transported liposomes for 48 hours. Then, fractions were collected from upper and lower compartments to measure transport ratio (penetration) referring to doxorubicin's concentration. U87MG were further incubated for 24 hours, then media was changed for fresh MEM and their cell viability was evaluated 24 hours later with CellTiter Blue assay. As the aim of this approach was that the dual-targeted system crosses the BBMVECs monolayer without being internalized by the barrier itself, uptake of formulations by BBMVECs was measured by flow cytometry. This experiment was performed at low doxorubicin's concentration (10 µM) in order no to compromise BBB model integrity.

Figure 4.16 shows transport across the BBMVECs monolayer, BBMVECs uptake and U87MG cell viability of non-targeted (Lipo-Dox), MCF-7-targeted (Lipo-Dox-DMPG), BBB-targeted (Lipo-Dox-REG) and dual-tageted (Lipo-Dox-DMPG-REG) doxorubicin-loaded liposomes after 5 hours of co-culture incubation at 37°C.

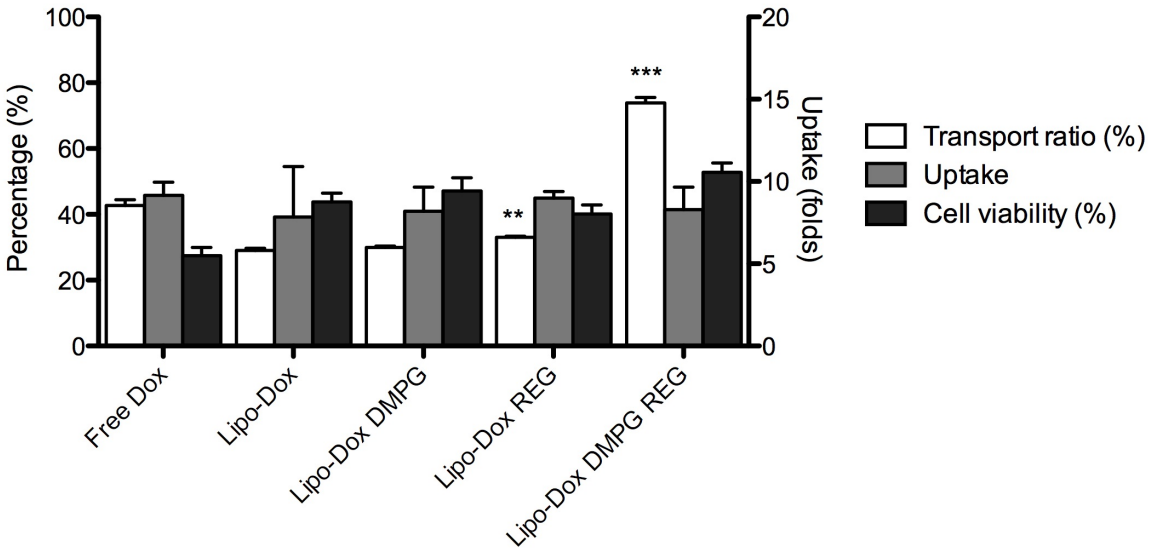

Figure 4.16: Co-culture model of BBB (BBMVECs) and glioblastoma (U87MG) Transport ratio (%) of doxorubicin across BBMVECs monolayer (white) and doxorubicin uptake by BBMVECs in folds respect to non-treated BBMVECs (control) after 5 hours of incubation (grey). Cell viability of U87MG after 72 h of incubation. Uptake is represented as folds increase respect to non-treated cells. Data were presented as mean ± SD (n=3). Statistical analysis was determined using t test compared to Lipo-Dox (**p<0.001, ***p<0.0001)

Transport experiment (Figure 4.16) showed that doxorubicin itself was able to cross the BBMVECs monolayer, as other authors have already demonstrated[106].

However, dual-targeted liposomes (Lipo Dox DMPG REG) were able to enhance free doxorubicin's crossing ability by a factor of 1.74, suggesting a synergetic effect of Regulon peptide with DMPG protein, as no other targeted formulation was able to improve free doxorubicin's permeability. On the other hand, Regulon peptide demonstrated his efficacy as its presence lead to an increase in non-targeted liposomes' transport ratio (Lipo Dox) by a factor of 1.14, in the case of Lipo Dox REG, and 2.52, for Lipo Dox DMPG REG. It seemed that DMPG alone did not contribute to the penetration of liposomal doxorubicin. After transport experiment, BBMVECs monolayer's integrity was again evaluated in terms of marker's permeability. The permeation coaefficient (P_e) of Lucifer yellow was below 0.8 $x10^{-3}$cm/min, indicating that after 5 hours of incubation with the samples tested monolayer's integrity was not compromised.

In terms of uptake, no significant difference was observed between samples. These uptake values were much lower in BBMVECs than in the tumor cells tested, MCF-7 and U87MG cells (Figure 4.9), suggesting transcytosis of liposomal formulations as they do not accumulate in BBMVECs.

After 72h of incubation, U87MG cells showed cell viabilities below 50% with no significant differences between targeted samples. These results are in good agreement with liposomes' cytotoxicity data after 48 h of incubation (Figure 4.12) as doxorubicin's concentration in the abluminal compartment is between 3 and 4 µM.

Surprisingly, dual-targeted liposomes showed an equal cytotoxicity, while it achieved the higher transport ratio. This could be explained by the large shell this formulation has, as both DMPG and Regulon peptide are very large targeting moieties, with molecular weights of 46 KDa and 7295 g/mol, respectively, which might interfere in doxorubicin's diffusion and release.

Once having evaluated the permeability of liposomal formulations, transport of targeted and non-targeted polymersomes across the BBMVECs monolayer was assessed. In order to mimic a breast cancer metastasis scenario in the brain *in vitro*, the previous co-culture model was established culturing MCF-7 cells at the abluminal compartment instead of U87MG.

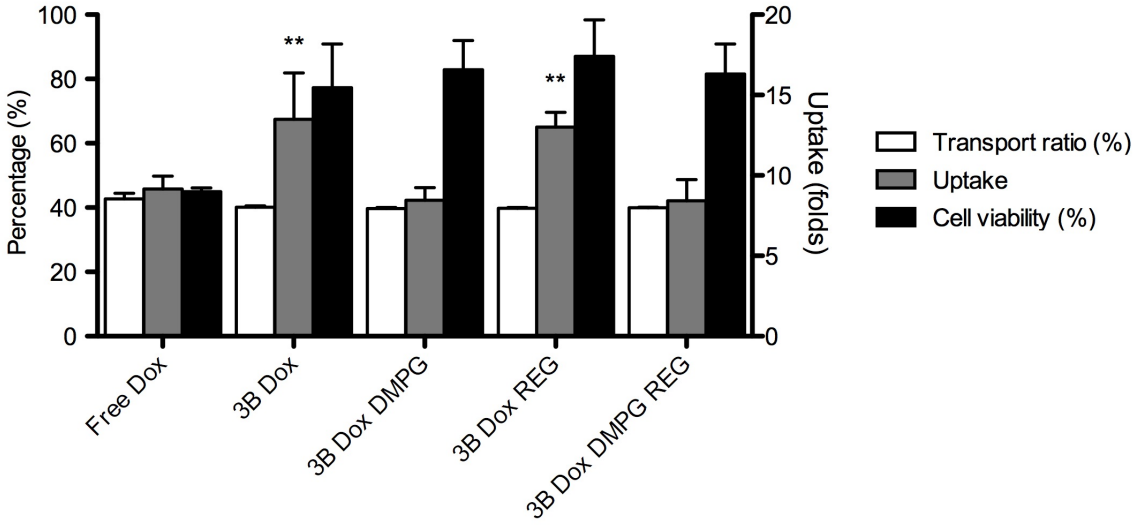

Figure 4.17: Co-culture model of BBB (BBMVECs) and breast adenocarcinoma (MCF-7) Transport ratio (%) of doxorubicin across BBMVECs monolayer (white) and doxorubicin uptake by BBMVECs in folds respect to non-treated BBMVECs (control) after 5 hours of incubation (grey). Cell viability of MCF-7 after 72 h of incubation. Data were presented as mean ± SD (n=3). Statistical analysis was determined using t test compared to Free Dox (**p<0.001)

As Figure 4.17 shows, transport ratio (%) across the BBBMVECs monolayer reached 40% for targeted and non-targeted polymersomes with no significant difference among them, being higher compared to liposomal's formulations, except from dual-targeted ones (Figure 4.16). These transport ratio values for both liposomes and polymersomes represent an improvement compared to what has been published before about drug delivery of chemotherapeutic agents to the brain, which achieved transport ratios across BCECs between 2 and 5% of paclitaxel-loaded angiopep-conjugated PEG-PCL[105] and PEG-PLA[41] nanoparticles after 5 hours of treatment in vitro.

Regarding the uptake, no improvement in polymersomes' crossing ability was observed when using a BBB-targeting moiety (REG), as there was not a significant difference between non-targeted (3B Dox) and BBB-targeted (3B Dox REG) polymersomes. What was surprising of this fact was the high transport ratio achieved by 3B Dox, as normally non-targeted nanoparticulate systems do not even reach a 3% of penetration through the monolayer after 5 hours of incubation[41,105].

We hypothesized that this high transport ratio of non-targeted formulations could be related to the cholesterol content of polymersomes' structure, although it was thought that the hydrophobic block containing cholesterol was not exposed to the surface. Several studies confirmed that the low density lipoprotein receptor-related LRP-1 is involved in LDL cholesterol metabolism[107-109] in the brain and contributes to its transcytosis across the BBMVECs monolayer towards the abluminal side[110]. Indeed, it has been shown that the increase of cholesterol content of cholesterol-based nanoparticulate systems can enhance permeability across a BBMVECs monolayer[111]. Therefore, polymersomes (3B Dox) themselves could be able to cross the BBB model through receptor-mediated transcytosis by the LRP1 and the effect of Regulon peptide on 3B Dox REG uptake might have been masked.

However, in the presence of DMPG, for both single and dual-targeted polymersomes, there's a significant reduction of uptake compared to non-targeted polymersomes. This decrease in uptake could be explained as a reduction of cholesterol exposure to the surface because of the presence of DMPG phage protein, that is a voluminous moiety with a molecular weight of 46 kDa. On the other hand, it was not expected that conjugation with DMPG would somehow contribute on polymersome's uptake as DMPG interacts with nucleolin, which is just expressed in activated and angiogenic endothelial cells[85].

Regarding cytotoxicity in MCF-7 cells, no significant difference was observed between polymersomes formulations. However, these results are in good agreement with polymersomes' cytotoxicity data after 48 hours of incubation (Figure 4.11), taking into account that doxorubicin's concentration in the abluminal compartment was approximately 4 μM. Again, U87MG cells showed higher sensitivity towards doxorubicin compared to MCF-7 as previously shown in cytotoxicity assays (Figure 4.11 and Figure 4.12).

4.4 Concluding Remarks

In this chapter, a comparative study between liposomes and polymersomes as potential drug delivery systems for breast cancer metastasis in the brain has been presented by doxorubicin delivery through a BBB model.

First of all, it has been demonstrated that both systems can be decorated with targeting moieties by two different approaches, such as covalent binding and insertion into their membranes. On one hand, a thiolated peptide was covalently bound to the thiolated-liposomes' surface by thiol coupling, as it had been already shown in previous chapters of this thesis. On the other hand, it was shown the feasibility to decorate polymersomes' surface thanks to the post modification of the triblock copolymer by transforming its CTA-end group through aminolysis and further thiol coupling, thus allowing the attachment of thiolated macromolecules. In addition, insertion of amphiphilic transmembrane, such as phage protein, into polymersomes' membrane was achieved as well as in liposomes but at lower percentage, probably due to the higher rigidity of cholesterol-bearing polymersomes.

As expected, size of targeted liposomes and polymersomes was higher than plain formulations, being larger the peptide-bearing ones as it is attached on the nanostructures' surface and not inserted into the membrane like phage protein. Comparing phage-bearing formulations, it has been observed that phage protein is better embedded in liposomes' membrane rather than in polymersomes probably due to differences in membranes fluidity and morphology, leading to smaller nanostructures in the case of liposomes. Similarly to liposomes, polymersomes were able to encapsulate doxorubicin by the pH remote loading method although loading efficiencies and capacities were lower than in lisposomes, again due to membrane's higher rigidity. Loading was influenced by the presence of targeting moieties as well, being lower for dual-targeted samples, as both moieties complicated drug diffusion.

It was demonstrated that doxorubicin's release from both liposomes and polymersomes was pH-dependent. Thus, when pH decreased up to 6.5 breaking the pH gradient required for doxorubicin's remote loading, both formulations released 80% of their payload. Oppositely to polymersomes, liposomes were able to release the total of entrapped drug at pH 5.5. Both systems showed slight leaking at physiological pH (7.4), being higher for liposomes, suggesting that they would be able to keep much of their content until they reach the target site, such as in the tumour environment, where the pH drops down causing the drug's release.

Regarding binding specificity of phage-bearing formulations, flow cytometry assay showed a dramatic increase in uptake of MCF-7-targeted polymersomes both in MCF-7 and U87MG. This significant increase is in good agreement with fluorescence microscopy, which revealed that phage protein presence not only increased polymersomes uptake but also escape from the endosome, as phage bearing-polymersomes were observed both in endosomes and cytoplasm compared to non-targeted polymersomes, only located in endosomes. Regarding liposomes, the presence of DMPG implied just a slight increase in uptake, as non-targeted liposomes showed a high uptake by themselves already. In addition, microscopy images showed that incorporation of phage protein into liposomes drove the uptake to the

endosomes, preventing liposomes to fuse with cell membrane and release their content. These differences in DMPG contribution to doxorubicin's release from the endosomes between Lipo-Dox-DMPG and 3B-Dox-DMPG may suggest that DMPG presented a synergetic effect with polymersomes but not with liposomes, causing the disruption of polymersomes with subsequent release of their payload at endosomal pH due to phage buffering capacity.

In terms of cytotoxicity, it was observed that liposomal formulations presented higher cytotoxicity in MCF-7 compared to polymersomes, which is in good agreement with their faster release at acidic pH and their higher uptake shown by flow cytometry. However, phage-bearing formulations did not caused an increase in cytotoxicity as expected, although their endosomal escape capacity was also proved. This fact may suggest that escape from the endosomes of these formulations take longer times than that here tested. At this point, it can be concluded that U87MG cells are more sensitive to doxorubicin than MCF-7 cells as cytotoxicity was higher in the first ones although the uptake was higher in MCF-7.

The transport experiment of non-targeted, single-targeted and dual-targeted liposomes across a BBB model showed that dual-targeting approach was especially beneficial, achieving almost an 80% of penetration through a BBMVECs monolayer, suggesting a synergistic effect between regulon peptide and phage protein (DMPG). The uptake of these formulations was lower than that observed in MCF-7 and U87MG, suggesting transcytosis of liposomal formulations across the BBMVECs monolayer. Cytotoxicity in U87MG caused by liposomes that had crossed the monolayer was around 50% for all formulations, including dual-targeted ones, probably because of a lower release due to their larger shell. In contrast, permeation of polymesomes' formulations through the BBMVECs monolayer did not show any difference depending on targeting, however, a 40% of crossing represent an improvement compared to what has been published about drug delivery to the brain. We hypothesized that this high uptake of polymersomes regardless of their targeting could be related to cholesterol content of these formulations that may interact with LRP-1 present in BBMVECs, involved in LDL cholesterol metabolism in the brain. As a result, an eventual regulon peptide enhancement of transport across the BBB model may have been masked by the high affinity that cholesterol has shown for the BBB model. In the case of polymersomes, the presence of phage protein as a ligand may have a negative effect on the affinity for the endothelial monolayer, probably because it prevents cholesterol and regulon peptide from interacting with LRP-1 receptor. Cytotoxicity in MCF-7 caused by the percentage of sample that crossed the monolayer was in good agreement with previous cytotoxicity results.

Summarizing, in this chapter it has been demonstrated that polymersomes obtained from the self-assembly of amphiphilic triblock copolymers are promising delivery systems as it is possible to decorate their surface with thiolated biomacromolecules through post-modification of their CTA-end group, insert transmembrane proteins into their membrane, load them with doxorubicin through pH remote loading and release their payload at acidic pH (tumour), while showing low leaking at physiological pH. In terms of targeting, the insertion of an MCF-7-specific phage fusion protein is especially remarkable in the case of polymersome as it has

shown a dramatic increase of their uptake in MCF-7 and U87MG cells, and the capability to escape from the endosome. However, polymersomes themselves demonstrated that conjugation with BBB-specific targeting moieties is not required to achieve a successful transport across BBMVECs monolayer.

Therefore, in the light of the results, it can be concluded that polymersomes obtained from the self-assembly of the amphiphilic triblock copolymer, pHEMA-*co*-pCHOL-*co*-pHEMA, arise as a promising drug delivery platform for the delivery of anticancer drugs to the brain.

4.5 References

1. Steichen, S. D., Caldorera-Moore, M. & Peppas, N. A. A review of current nanoparticle and targeting moieties for the delivery of cancer therapeutics. *European journal of pharmaceutical sciences : official journal of the European Federation for Pharmaceutical Sciences* **48**, 416–427 (2013).

2. Coghlin, C. & Murray, G. I. Current and emerging concepts in tumour metastasis. *J. Pathol.* **222**, 1–15 (2010).

3. Kenchappa, R. S. *et al.* Novel Treatments for Melanoma Brain Metastases. *Cancer Control* **20**, 298–306 (2013).

4. Nishida, N., Yano, H., Nishida, T., Kamura, T. & Kojiro, M. Angiogenesis in cancer. *Vascular Health and Risk Management* 213–219 (2006).

5. Caffo, M. *et al.* Innovative Therapeutic Strategies in the Treatment of Brain Metastases. *IJMS* **14**, 2135–2174 (2013).

6. Palmieri, D., Chambers, A. F., Felding-Habermann, B., Huang, S. & Steeg, P. S. The Biology of Metastasis to a Sanctuary Site. *Clinical Cancer Research* **13**, 1656–1662 (2007).

7. Klein, C. A. CANCER: The Metastasis Cascade. *Science* **321**, 1785–1787 (2008).

8. Greco, F. & Vicent, M. J. Combination therapy: Opportunities and challenges for polymer–drug conjugates as anticancer nanomedicines. *Advanced Drug Delivery Reviews* **61**, 1203–1213 (2009).

9. Sledge, G. W. Phase III Trial of Doxorubicin, Paclitaxel, and the Combination of Doxorubicin and Paclitaxel as Front-Line Chemotherapy for Metastatic Breast Cancer: An Intergroup Trial (E1193). *Journal of Clinical Oncology* **21**, 588–592 (2003).

10. Komarova, N. L. & Boland, C. R. Calculated treatment. *Nature* **499**, 291–292 (2013).

11. Bozic, I. *et al.* Evolutionary dynamics of cancer in response to targeted combination therapy. *eLife* **2**, (2013).

12. Bertrand, N., Wu, J., Xu, X., Kamaly, N. & Farokhzad, O. C. Cancer nanotechnology: The impact of passive and active targeting in the era of modern cancer biology. *Advanced Drug Delivery Reviews* 1–24 (2013).doi:10.1016/j.addr.2013.11.009

13. Greco, F. F. *et al.* Investigating the mechanism of enhanced cytotoxicity of HPMA copolymer-Dox-AGM in breast cancer cells. *Journal of controlled release : official journal of the Controlled Release Society* **117**, 12–12 (2007).

14. Zucker, D., Andriyanov, A. V., Steiner, A., Raviv, U. & Barenholz, Y. Characterization of PEGylated nanoliposomes co-remotely loaded with topotecan and vincristine: relating structure and pharmacokinetics to therapeutic efficacy. *Journal of controlled release : official journal of the Controlled Release Society* **160**, 281–289 (2012).

15. Valencia, P. M. *et al.* Synergistic cytotoxicity of irinotecan and cisplatin in dual-drug targeted polymeric nanoparticles. *Nanomedicine* **8**, 687–698 (2013).
16. Chandrawati, R. & Caruso, F. Biomimetic Liposome- and Polymersome-Based Multicompartmentalized Assemblies. *Langmuir : the ACS journal of surfaces and colloids* **28**, 13798–13807 (2012).
17. Torchilin, V. P. Recent advances with liposomes as pharmaceutical carriers. *Nature reviews. Drug discovery* **4**, 145–160 (2005).
18. Le Meins, J. F., Sandre, O. & Lecommandoux, S. Recent trends in the tuning of polymersomes' membrane properties. *Eur. Phys. J. E* **34**, 14 (2011).
19. Allen, T. M. & Cullis, P. R. Liposomal drug delivery systems: From concept to clinical applications. *Advanced Drug Delivery Reviews* 1–13 (2012).doi:10.1016/j.addr.2012.09.037
20. Zhang, M., Garbuzenco, O. B., Reuhl, K. R., Rodríguez-Rodríguez, L. & Minko, T. Two-in-one: combined targeted chemo and gene therapy for tumor suppression and prevention of metastases. *Nanomedicine* **7**, 185–197
21. Meng, F., Zhong, Z. & Feijen, J. Stimuli-Responsive Polymersomes for Programmed Drug Delivery. *Biomacromolecules* **10**, 197–209 (2009).
22. Onaca, O., Enea, R., Hughes, D. W. & Meier, W. Stimuli-Responsive Polymersomes as Nanocarriers for Drug and Gene Delivery. *Macromolecular bioscience* **9**, 129–139 (2009).
23. Howse, J. R. *et al.* Templated formation of giant polymer vesicles with controlled size distributions. *Nature materials* **8**, 507–511 (2009).
24. Lorenceau, E. *et al.* Generation of Polymerosomes from Double-Emulsions. *Langmuir : the ACS journal of surfaces and colloids* **21**, 9183–9186 (2005).
25. Pang, Z., Feng, L., Hua, R., Chen, J. & Gao, H. Lactoferrin-conjugated bodegradable polymersome Holding Doxorubicin and Tetrandrine for Chemotherapy. *Molecular pharmaceutics* **7**, 1995–2005 (1995).
26. Hammady, T., Rabanel, J.-M., Dhanikula, R. S., Leclair, G. & Hildgen, P. Functionalized nanospheres loaded with anti-angiogenic drugs: Cellular uptake and angiosuppressive efficacy. *European Journal of Pharmaceutics and Biopharmaceutics* **72**, 418–427 (2009).
27. Brannon-peppas, L. & Blanchette, J. O. Nanoparticle and targeted systems for cancer therapy. *Advanced Drug Delivery Reviews* **64**, 206–212 (2012).
28. Perche, F. & Torchilin, V. P. Recent Trends in Multifunctional Liposomal Nanocarriers for Enhanced Tumor Targeting. *Journal of Drug Delivery* **2013**, 1–32 (2013).
29. Torchilin, V. P. Multifunctional, stimuli-sensitive nanoparticulate systems for drug delivery. *Nature Publishing Group* 1–15 (2014).doi:10.1038/nrd4333
30. Debbage, P. Targeted drugs and nanomedicine: present and future. *Current pharmaceutical design* **15**, 153–172 (2009).

31. Silva, G. A. Nanotechnology approaches to crossing the blood-brain barrier and drug delivery to the CNS. *BMC neuroscience* **9 Suppl 3**, S4 (2008).

32. Pestalozzi, B. C. Brain metastases and subtypes of breast cancer. *Annals of Oncology* **20**, 803–805 (2009).

33. Thomas, F. C. *et al.* Uptake of ANG1005, A Novel Paclitaxel Derivative, Through the Blood-Brain Barrier into Brain and Experimental Brain Metastases of Breast Cancer. *Pharmaceutical research* **26**, 2486–2494 (2009).

34. Rahmathulla, G., Toms, S. A. & Weil, R. J. The Molecular Biology of Brain Metastasis. *Journal of Oncology* **2012**, 1–16 (2012).

35. Jain, R. K. *et al.* Angiogenesis in brain tumours. *Nat Rev Neurosci* **8**, 610–622 (2007).

36. Goldfarb, S. B., Hudis, C. & Dickler, M. N. Bevacizumab in metastatic breast cancer: when may it be used? *Therapeutic Advances in Medical Oncology* 85–93 (2011).

37. Kodack, D. P. *et al.* Combined targeting of HER2 and VEGFR2 for effective treatment of HER2-amplified breast cancer brain metastases. *Proceedings of the National Academy of Sciences of the United States of America* **45**, 3119–3127 (2012).

38. Gabathuler, R. Approaches to transport therapeutic drugs across the blood–brain barrier to treat brain diseases. *Neurobiology of Disease* **37**, 48–57 (2010).

39. Lillis, A. P., Van Duyn, L. B., Murphy-Ullrich, J. E. & Strickland, D. K. LDL Receptor-Related Protein 1: Unique Tissue-Specific Functions Revealed by Selective Gene Knockout Studies. *Physiological Reviews* **88**, 887–918 (2008).

40. Fillebeen, C., Descamps, L., Dehouck, M.-P. & Fenart, L. Receptor-mediated Transcytosis of Lactoferrin through the Blood. *Journal of biological chemistry* **274**, 7011–7017 (1999).

41. Zhang, B. *et al.* LDLR-mediated peptide-22-conjugated nanoparticles for dual-targeting therapy of brain glioma. *Biomaterials* **34**, 9171–9182 (2013).

42. Xin, H. *et al.* Anti-glioblastoma efficacy and safety of paclitaxel-loading Angiopep-conjugated dual targeting PEG-PCL nanoparticles. *Biomaterials* **33**, 8167–8176 (2012).

43. Hu, K. *et al.* Lactoferrin-conjugated PEG–PLA nanoparticles with improved brain delivery: In vitro and in vivo evaluations. *Journal of controlled release : official journal of the Controlled Release Society* **134**, 55–61 (2009).

44. Demeule, M. *et al.* Identification and Design of Peptides as a New Drug Delivery System for the Brain. *Journal of Pharmacology and experimental therapeutics* **324**, 1064–1072 (2008).

45. Regulon Inc. Novel peptide for crossing the blood-brain barrier (BBB) discovered at regulon. *www.regulon.org* (2009).at <http://www.regulon.org/prs/pdf/5.pdf>

46. Du, J. *et al.* Dual-targeting topotecan liposomes modified with tamoxifen and wheat germ agglutinin significantly improve drug transport across the blood-brain

barrier and survival of brain tumor-bearing animals. *Molecular pharmaceutics* **6**, 905–917 (2009).

47. Ying, X. *et al.* Dual-targeting daunorubicin liposomes improve the therapeutic efficacy of brain glioma in animals. *Journal of controlled release : official journal of the Controlled Release Society* **141**, 183–192 (2010).

48. Kuhn, A. Major coat proteins of bacteriophage Pf3 and M13 as model systems for Sec-independent protein transport. *FEMS Microbiology Reviews* **17**, 185–190 (1995).

49. Wang, T. *et al.* Enhanced binding and killing of target tumor cells by drug-loaded liposomes modified with tumor-specific phage fusion coat protein. *Nanomedicine* **5**, 563–574 (2010).

50. Wang, T., Petrenko, V. A. & Torchilin, V. P. Paclitaxel-Loaded Polymeric Micelles Modified with MCF-7 Cell-Specific Phage Protein: Enhanced Binding to Target Cancer Cells and Increased Cytotoxicity. *Molecular pharmaceutics* **7**, 1007–1014 (2010).

51. Fagbohun, O. A. *et al.* Landscape phages and their fusion proteins targeted to breast cancer cells. *Protein Engineering Design and Selection* **25**, 271–283 (2012).

52. Wang, T., Yang, S., Petrenko, V. A. & Torchilin, V. P. Cytoplasmic Delivery of Liposomes into MCF-7 Breast Cancer Cells Mediated by Cell-Specific Phage Fusion Coat Protein. *Molecular pharmaceutics* **7**, 1149–1158 (2010).

53. Boyer, C. *et al.* Bioapplications of RAFT polymerization. *Chemical reviews* **109**, 5402–5436 (2009).

54. Boyer, C., Bulmus, V. & Davis, T. P. Efficient Usage of Thiocarbonates for Both the Production and the Biofunctionalization of Polymers. *Macromolecular Rapid Communications* **30**, 493–497 (2009).

55. Bulmus, V. RAFT polymerization mediated bioconjugation strategies. *Polymer Chemistry* **2**, 1463 (2011).

56. Mortisen, D., Peroglio, M., Alini, M. & Eglin, D. Tailoring thermoreversible hyaluronan hydrogels by 'click' chemistry and RAFT polymerization for cell and drug therapy. *Biomacromolecules* **11**, 1261–1272 (2010).

57. Nardin, C., Thoeni, S., Widmer, J., Winterhalter, M. & Meier, W. Nanoreactors based on (polymerized) ABA-triblock copolymer vesicles. *Chem. Commun.* 1433–1434 (2000).doi:10.1039/b004280n

58. Setijadi, E. *et al.* Biodegradable Star Polymers Functionalized With β-Cyclodextrin Inclusion Complexes. *Biomacromolecules* **10**, 2699–2707 (2009).

59. Petrenko, V. A., Smith, G. P., Gong, X. & Quinn, T. A library of organic landscapes on filamentous phage. *Protein Engineering Design and Selection* **9**, 797–801 (1996).

60. Brigati, J. R., Samoylova, T. I., Jayanna, P. K. & Petrenko, V. A. *Phage Display for Generating Peptide Reagents*. (John Wiley & Sons, Inc., 2001).doi:10.1002/0471140864.ps1809s51

61. Deli, M. A., Dehouck, M.-P., Abraham, C. S., Cecchelli, R. & Joó, F. Penetration of small molecular weight substances through cultured bovine brain capillary endothelial cell monolayers: the early effects of cyclic adenosine 3‘,5’-monophosphate. *Experimental Physiology* **80**, 675–678 (2005).

62. Siflinger-Birnboim, A. *et al.* Molecular sieving characteristics of the cultured endothelial monolayer. *Journal of cellular physiology* **132**, 111–117 (2004).

63. Barner-Kowollik, C. *Handbook ofRAFT Polymerization*. 1–558 (Wiley-VCH, 2014).

64. Boyes, S. G. *et al.*in *Multifunctional Nanoparticles for Drug Delivery* (Svenson, S. & Prud'homme, R. K.) 1–371 (Springer, 2012).

65. Skrabania, K., Miasnikova, A., Bivigou-Koumba, A. M., Zehm, D. & Laschewsky, A. Examining the UV-vis absorption of RAFT chain transfer agents and their use for polymer analysis. *Polymer Chemistry* **2**, 2074 (2011).

66. Vázquez-Dorbatt, V., Tolstyka, Z. P. & Maynard, H. D. Synthesis of Aminooxy End-Functionalized pNIPAAm by RAFT Polymerization for Protein and Polysaccharide Conjugation. *Macromolecules* **42**, 7650–7656 (2009).

67. Hu, Y., Sun, W. & Vang, D. *Electrochemistry of flotation of sulphide minerals*. (Springer).

68. Na, D. H., Woo, B. H. & Lee, K. C. Quantitative Analysis of Derivatized Proteins Prepared with Pyridyl Disulfide-Containing Cross-Linkers by High-Performance Liquid Chromatography. *Bioconjugate chemistry* **10**, 306–310 (1999).

69. Hermanson, G. T. *Bioconjugate Tecniques*. (Academic Press, 2013).

70. Pretsch, E. & Bühlmann, P. *Determinación estructural de compuestos orgànicos*. (Elsevier masson, 2002).

71. Biswas, S., Dodwadkar, N. S., Sawant, R. R. & Torchilin, V. P. Development of the Novel PEG-PE-Based Polymer for the Reversible Attachment of Specific Ligands to Liposomes: Synthesis and in Vitro Characterization. *Bioconjugate chemistry* **22**, 2005–2013 (2011).

72. Chaw, C.-S. *et al.* Thermally responsive core-shell nanoparticles self-assembled from cholesteryl end-capped and grafted polyacrylamides:; drug incorporation and in vitro release. *Biomaterials* **25**, 4297–4308 (2004).

73. Li, L. *et al.* Self-assembled nanoparticles of cholesterol-conjugated carboxymethyl curdlan as a novel carrier of epirubicin. *Nanotechnology* **21**, 265601 (2010).

74. Sevimli, S., Inci, F., Zareie, H. M. & Bulmus, V. Well-Defined Cholesterol Polymers with pH-Controlled Membrane Switching Activity. *Biomacromolecules* **13**, 3064–3075 (2012).

75. Li, X., Hirsh, D. J., Cabral-Lilly, D. & Perkins, W. R. Doxorubicin physical state in solution and inside liposomes loaded via pH gradient. *Biochimica et biophysica acta* 23–40 (1998).

76. Gillies, E. R. & Fréchet, J. M. J. pH-Responsive Copolymer Assemblies for Controlled Release of Doxorubicin. *Bioconjugate chemistry* **16**, 361–368 (2005).

77. Fritze, A., Hens, F., Kimpfler, A., Schubert, R. & Peschkasuss, R. Remote loading of doxorubicin into liposomes driven by a transmembrane phosphate gradient. *Biochimica et Biophysica Acta (BBA) - Biomembranes* **1758**, 1633–1640 (2006).

78. Lee, R. J., Wang, S., Turk, M. J. & Low, P. S. The Effects of pH and Intraliposomal Buffer Strength on the Rate of Liposome Content Release andIntracellular Drug Delivery. *Bioscience Reports* **18**, 1–10 (1998).

79. Barenholz, Y. & Haran, G. Method of amphipatic drug loading in liposomes by pH gradient. 1–16 (1993).

80. Sanson, C. *et al.* A simple method to achieve high doxorubicin loading in biodegradable polymersomes. *Journal of controlled release : official journal of the Controlled Release Society* 1–8 (2010).doi:10.1016/j.jconrel.2010.07.123

81. Discher, B. M., Hammer, D. A., Bates, F. S. & Discher, D. E. Polymer vesicles in various media. *Current opinion in Colloid \& Interface Science* **5**, 125–131 (2000).

82. Gabizon, A. A., Catane, R. & Uziely, B. Prolonged circulation time and enhanced accumulation in malignant exudates of doxorubicin encapsulated in polyethylene-glycol coated liposomes. *Cancer Research* **54**, 987–992

83. Upadhyay, K. K. K. *et al.* The intracellular drug delivery and anti tumor activity of doxorubicin loaded poly(γ-benzyl l-glutamate)-b-hyaluronan polymersomes. *Biomaterials* **31**, 2882–2892 (2010).

84. Soundararajan, S., Chen, W., Spicer, E. K., Courtenay-Luck, N. & Fernandes, D. J. The Nucleolin Targeting Aptamer AS1411 Destabilizes Bcl-2 Messenger RNA in Human Breast Cancer Cells. *Cancer Research* **68**, 2358–2365 (2008).

85. Koutsioumpa, M. *et al.* Interplay between v 3 Integrin and Nucleolin Regulates Human Endothelial and Glioma Cell Migration. *Journal of biological chemistry* **288**, 343–354 (2013).

86. Xu, Z. *et al.* Knocking down nucleolin expression in gliomas inhibits tumor growth and induces cell cycle arrest. *J Neurooncol* **108**, 59–67 (2012).

87. Sahay, G., Alakhova, D. Y. & Kabanov, A. V. Endocytosis of nanomedicines. *Journal of controlled release : official journal of the Controlled Release Society* **145**, 182–195 (2010).

88. Beaujouin, M. *et al.* Pro-cathepsin D interacts with the extracellular domain of the {beta} chain of LRP1 and promotes LRP1-dependent fibroblast outgrowth. 1–17 (2010).

89. Rozanov, D. V. The Low Density Lipoprotein Receptor-related Protein LRP Is Regulated by Membrane Type-1 Matrix Metalloproteinase (MT1-MMP) Proteolysis in Malignant Cells. *Journal of biological chemistry* **279**, 4260–4268 (2003).

90. K, L. N., Jagadeeshan, S., Nair, S. A. & Kumar, G. S. V. Evaluation of triblock copolymeric micelles of δ- valerolactone and poly (ethylene glycol) as a competent vector for doxorubicin delivery against cancer. *Journal of nanobiotechnology* **9**, 42 (2011).

91. Erbacher, P., Roche, A. C., Monsigny, M. & Midoux, P. Putative Role of Chloroquine in Gene Transfer into a Human Hepatoma Cell Line by DNA/Lactosylated Polylysine Complexes. *Experimental Cell Research* **225**, 186–194 (1996).

92. Mellman, I., Fuchs, R. & Helenius, A. Acidification of the Endocytic and Exocytic Pathways. *Annual Review of Biochemistry* **55**, 663–700 (1986).

93. Herbert, S. P. & Stainier, D. Y. R. Molecular control of endothelial cell behaviour during blood vessel morphogenesis. *Nature Publishing Group* **12**, 551–564 (2011).

94. Rowinsky, E. K. The development and clinical utility of the taxane class of antimicrotubule chemotherapy agents. *Annual Review of Medicine* **48**, 353–374 (1997).

95. Hurley, L. H. DNA and its associated processes as targets for cancer therapy. *Nature Reviews Cancer* **2**, 188–200 (2002).

96. Cecchelli, R. *et al.* In vitro model for evaluating drug transport across the blood-brain barrier. *Advanced Drug Delivery Reviews* **36**, 165–178 (1999).

97. Fukuhara, S. *et al.* Cyclic AMP potentiates vascular endothelial cadherin-mediated cell-cell contact to enhance endothelial barrier function through an Epac-Rap1 signaling pathway. *Molecular and cellular biology* **25**, 136–146 (2004).

98. Price, G. M., Chrobak, K. M. & Tien, J. Effect of cyclic AMP on barrier function of human lymphatic microvascular tubes. *Microvascular Research* **76**, 46–51 (2008).

99. Forster, C. *et al.* Differential effects of hydrocortisone and TNF on tight junction proteins in an in vitro model of the human blood-brain barrier. *The Journal of Physiology* **586**, 1937–1949 (2008).

100. Glaser, A. W., Buxton, N. & Walker, D. Corticosteroids in the management of central nervous system tumours. *Archives of disease in childhood* **76**, 76–78 (1998).

101. Franke, H., Galla, H. J. & Beuckmann, C. T. An improved low-permeability in vitro-model of the blood-brain barrier: transport studies on retinoids, sucrose, haloperidol, caffeine and mannitol. *Brain Research* **818**, 65–71 (1999).

102. Culot, M. *et al.* An in vitro blood-brain barrier model for high throughput (HTS) toxicological screening. *Toxicology in Vitro* **22**, 799–811 (2008).

103. Lockman, P. R. *et al.* In Vivo and in Vitro Assessment of Baseline Blood-Brain Barrier Parameters in the Presence of Novel Nanoparticles. *Pharmaceutical research* **20**, 705–713 (2003).

104. Ragnaill, M. N. *et al.* Internal benchmarking of a human blood-brain barrier cell model for screening of nanoparticle uptake and transcytosis. *European journal of pharmaceutics and biopharmaceutics : official journal of Arbeitsgemeinschaft f\"ur Pharmazeutische Verfahrenstechnik e.V* **77**, 360–367 (2011).

105. Xin, H. *et al.* Angiopep-conjugated poly(ethylene glycol)-co-poly(ε-caprolactone) nanoparticles as dual-targeting drug delivery system for brain glioma. *Biomaterials* **32**, 4293–4305 (2011).

106. Gil, E. S., Li, J., Xiao, H. & Lowe, T. L. Quaternary Ammonium β-Cyclodextrin Nanoparticles for Enhancing Doxorubicin Permeability across the In Vitro Blood−Brain Barrier. *Biomacromolecules* **10**, 505–516 (2009).
107. Liu, Q. *et al.* Amyloid Precursor Protein Regulates Brain Apolipoprotein E and Cholesterol Metabolism through Lipoprotein Receptor LRP1. *Neuron.* **56**, 66–78 (2007).
108. Orth, M. & Bellosta, S. Cholesterol: Its Regulation and Role in Central Nervous System Disorders. *Cholesterol* **2012**, 1–19 (2012).
109. Segatto, M., Di Giovanni, A., Marino, M. & Pallottini, V. Analysis of the protein network of cholesterol homeostasis in different brain regions: An age and sex dependent perspective. *Journal of cellular physiology* **228**, 1561–1567 (2013).
110. Gosselet, F. *et al.* Transcriptional profiles of receptors and transporters involved in brain cholesterol homeostasis at the blood–brain barrier: Use of an in vitro model. *Brain Research* **1249**, 34–42 (2009).
111. Kuo, Y.-C. & Wang, C.-C. Cationic solid lipid nanoparticles with cholesterol-mediated surface layer for transporting saquinavir to the brain. *Biotechnology Progress* **30**, 198–206 (2013).

Chapter 5

Impact and future trends

In this thesis, different drug delivery systems have been explored to provide know-how on their fabrication in order to fulfil the requirements of size, charge, targeting, loading, release and biocompatibility that make them suitable as drug delivery systems.

The development of a core-shell approach for obtaining ready-to-use targeted micellar and vesicular systems in water by means of classic chemistry with controlled size and LCST, arises as a promising method to prepare thermosensitive targeted systems through a simple and fast method. The simplicity and versatility of this targeting approach contributes to the broadening of the applicability of these systems, which have not reached clinical trials yet despite the attractiveness of thermo-responsive polymeric systems.

Free radical polymerization is of enormous industrial importance due to its speed and easiness. However, this leads to the synthesis of polymers with wide molecular weight distributions, due to the high reactivity of the propagating radicals. To overcome these limitations, a controlled/living radical polymerization, such as RAFT polymerization, was explored as well, showing that the presence of a proper chain transfer agent (CTA) provided higher control over polymerization rate allowing the synthesis of a polymer of predetermined molecular weight with narrow molecular weight distributions. RAFT polymerization has shown the ability to achieve a fine-tuning control of the synthesized polymer thanks to the selection of a proper CTA, while keeping the versatility of radical polymerizations, allowing the utilisation of a wide range of monomers. Concretely, DSPA has demonstrated the ability to control polymerization of both monomers used, with PDI below 1.3, which is typical from trithiocarbonates[1]. In addition, block copolymers can be synthesized through subsequent reactions with the same CTA and with much lower polydispersities, PDI<2, than those from free radical polymerization for these kinds of polymer.

As pointed out, the possibility to target these systems to a specific target contributes to design much efficient therapies. Therefore, the ability to modify these systems to decorate their surfaces with specific targeting moieties in a simple and fast way is crucial. In the first chapter, the core-shell strategy employed has been found to be a simple, fast and versatile method to decorate nanoparticles' surface with any desired targeting moiety, fluorophore or biomacromolecule using an acrylic linker. Regarding RAFT polymerization, the presence of functional groups on both sides of the polymeric chain, provides end groups amenable to a wide range of simple transformation procedures to achieve conjugation to peptides and proteins, allowing the easy attachment of targeting moieties, such as biomacromolecules, as well. In addition, vesicular systems, such as liposomes and polymersomes, showed the ability to incorporate amphiphilic proteins in their structure thanks to their bilayer-like membrane. This additional method of targeting provides specificity for certain targets, while it can enhance the release of the entrapped payload to the cell cytoplasm thanks to their endosomal escape capacity, which may be an advantageous strategy to improve DDS efficacy. Generally, the importance of targeted systems was reflected in the attachment of a BBB-specific peptide on several drug delivery systems, such as thermoresponsive acrylamide-based nanoparticles and liposomes, which showed an enhanced uptake in brain endothelial cells or the increased uptake of phage protein-

bearing formulations in breast cancer cells. Dual-targeting approach is a promising strategy, which is nowadays being exploited by targeted drug delivery, in order to overcome multiple biological barriers. In this work, it has been demonstrated the permeation enhancement achieved by dual-targeted strategy in liposomes through a BBB model, by a factor of 1.74 folds compared to free doxorubicin's permeation, which is comparable to the increase in permeation achieved by quaternary ammonium ß-cyclodexrtin nanoaprticles[2]. Although, this improvement was not as clear for polymersomes, their transport ratio represented an improvement compared to literature regarding drug delivery of chemotherapeutic agents to the brain, which have shown transport ratios across BCECs monolayer between 2 and 5% of paclitaxel-loaded angiopep-conjugated PEG-PCL[3] and PEG-PLA[4] nanoparticles.

In terms of loading, all the systems tested showed high loading efficiency and capacity through a relatively simple procedure, such as thermal cycles in the case of thermoresponsive systems, showing an encapsulation efficiency of insulin similar to bibliographic values[5], or pH induced doxorubicin's loading into liposomes and polymersomes, whereas paclitaxel could be loaded directly during the self-assembling procedure. Vesicular systems, such as polymersomes, have shown a clear advantage over acrylamide-based nanoparticles as polymersomes have demonstrate their ability to entrap both hydrophilic and hydrophobic substances at high loading capacity for both systems, as it has been reported for liposomes too, thanks to their compartmentalized structure. In addition, the variation of copolymers composition allows the modulation of the loading capacity of the entrapped substances, reaching 7.2% for tetra- and pentablock, which is between the 3% of loading capacity showed by PEG-Polycarbonate polymersomes[6] and the 11% reached by Polybutadiene-PEO diblock copolymers[7]. Regarding doxorubicins' loading, the 4.8% of loading capacity shown by the system here developed represents a slight increase over MPEG-Polycaprolactone polymersomes loaded through the pH gradient technique, which achieved a 4.4% of loading capacity[8]. In this sense, nanocarriers obtained from the self-assembly of amphiphilic block copolymers provide higher versatility to the drug delivery system, allowing their application in combination therapy to address several molecular targets, a strategy often used in cancer therapy.

Similarly, to the modulation of the loading capacity in polymersomes by varying their composition, thermoresponsive systems also allowed the modification of their thermoresponsive behaviour, and thus their release profile, through the tuning of their monomers' ratio as well. Therefore, depending on the concrete application, the release temperature (LCST) of the system can be adjusted. Contrary to thermoresponsive nanoparticles, polymersomes' release system is modulated by pH, due to the pH gradient method used to encapsulate doxorubicin, showing release profiles comparable to other vesicular multiblock copolymers[9]. Consequently, this system is useful when addressing tissues where pH is typically lower, such as in tumours (pH 6.5) or in the endosomal compartment (pH 4) after endocytic uptake. Thereby, both systems permit the release of their payload easily in response to external stimuli, being useful for diverse applications. Hence, their selection must be done on the basis of the final application.

Regarding vesicular delivery systems, the polymersomes tested in this work have shown higher rigidity compared to liposomes, leading to lower loading capacities and lower release rate, due to the differences in membrane fluidity of both systems. However, polymersomes provide high versatility to this kind of delivery systems as their properties can be varied by modifying their structures at a molecular level. Thus, the fine adjust of monomer nature and ratio or copolymers' molecular weight can have a significant influence on the membrane permeability, the size of the resulting nanostructure or loading capacity.

Last but not least, both systems have shown satisfactory results in terms of cytotoxicity and hemocompatibility, allowing them to be used as drug delivery systems. In the light of the results obtained in this thesis, it can be concluded that both systems provide high versatility to the design of drug delivery systems thanks to the possibility to tune their structure and composition, which have a strong influence in nanocarriers' properties and behaviour. The final application is what generally influences the selection of one system delivery system or another. Therefore, thermoresponsive systems may be more appropriated for the treatment of inflammations, cancer or oral delivery applications, whereas the polymersomes platform can be used in the treatment of cancer as well, or to enhance intracellular release. However, between the two polymerization systems that have been explored, it can be concluded that RAFT polymerization provides higher control over polymer's structure and polydispersity, which will have a big impact on nanocarrier's behaviour. In addition, this method shows higher versatility regarding the polymerization conditions, the fine-tuning of polymer characteristics, loading of substances of diverse amphipathicity and different targeting approaches.

1. Boyer, C. *et al.* Bioapplications of RAFT polymerization. *Chemical reviews* **109**, 5402–5436 (2009).

2. Gil, E. S., Li, J., Xiao, H. & Lowe, T. L. Quaternary Ammonium β-Cyclodextrin Nanoparticles for Enhancing Doxorubicin Permeability across the In Vitro Blood−Brain Barrier. *Biomacromolecules* **10**, 505–516 (2009).

3. Xin, H. *et al.* Angiopep-conjugated poly(ethylene glycol)-co-poly(ε-caprolactone) nanoparticles as dual-targeting drug delivery system for brain glioma. *Biomaterials* **32**, 4293–4305 (2011).

4. Zhang, B. *et al.* LDLR-mediated peptide-22-conjugated nanoparticles for dual-targeting therapy of brain glioma. *Biomaterials* **34**, 9171–9182 (2013).

5. Leobandung, W., Ichikawa, H., Fukumori, Y. & Peppas, N. A. Preparation of stable insulin-loaded nanospheres of poly(ethylene glycol) macromers and N-isopropyl acrylamide. *Journal of controlled release : official journal of the Controlled Release Society* **80**, 357–363 (2002).

6. Chen, W., Meng, F., Cheng, R. & Zhong, Z. pH-Sensitive degradable polymersomes for triggered release of anticancer drugs: A comparative study with micelles. *Journal of controlled release : official journal of the Controlled Release Society* **142**, 40–46 (2010).

7. Li, S., Welsh, J., Byrne, B. & Palmer, A. F. Self-assembled poly(butadiene)-b-poly(ethylene oxide) polymersomes as Paclitxael carriers. *Biotechnology Progress* **23**, 278–285 (2008).

8. Pang, Z., Feng, L., Hua, R., Chen, J. & Gao, H. Lactoferrin-conjugated bodegradable polymersome Holding Doxorubicin and Tetrandrine for Chemotherapy. *Molecular pharmaceutics* **7**, 1995–2005 (1995).

9. Sanson, C. *et al.* A simple method to achieve high doxorubicin loading in biodegradable polymersomes. *Journal of controlled release : official journal of the Controlled Release Society* 1–8 (2010).doi:10.1016/j.jconrel.2010.07.123

Chapter 6

Conclusions

As the aim of this thesis stated, the exploration of diverse drug delivery systems' fabrication has provided know-how regarding the modification of polymer's structure to obtain systems with the desired size, surface charge, targeting, loading capacity, drug release and biocompatibility. The conclusions obtained are as follows.

The obtaining of a versatile smart delivery system trough a core-shell approach has been achieved.

- Free-radical polymerization in microemulsion has been a simple and fast method to synthesize acrylamide-based nanoparticles, allowing the tailoring of their size and LCST. Core-shell approach using poly(pentafluorophenyl methacrylate) (pPFM) as a linker has been found to be a simple and fast method to coat nanoparticles with a large variety of molecules containing amino groups with different molecular weights and structures. The final size of the nanoparticles depends on the size of the coating moieties added to the shell, hence the larger the coating moieties are, the larger the nanoparticle will be. Therefore, nanoparticles size can be tuned by regulating the amount of PFM added to the core, and thus controlling the amount of coating moieties.

- It has been demonstrated that the thermo-responsive behaviour of nanoparticles is a reversible process as they increase in size above LCST and decrease to their initial size below LCST, shown by DLS and AFM. LCST can be tuned by varying nanoparticles' core composition and is also influenced by coating moieties. It has been suggested that this increase in size, in contrast to the characteristic shrinkage of thermosensitive polymers, is caused by a change in nanoparticles conformation from micelle to vesicle due to a change in hydrophobic/hydrophilic interactions that lead to the formation of a bilayer structure above LCST. Nanoparticle's thermosensitivity allowed the loading of insulin and ECM collagen booster at a loading efficiency of 41 and 53%, respectively.

- The importance of targeting has been demonstrated through the selective uptake of targeted nanoparticles with BBB-specific peptides, RP3 and AGBBB015I, in HCMEC, suggesting the specificity of both peptides tested. On the other hand, other endothelial cell lines, such as HUVEC and HDMEC, showed non-specific endocytosis of coated and non-coated nanoparticles, as they are less restrictive than HCMEC.

A versatile vesicle-like delivery system has been synthesized by RAFT polymerization.

- Multiblock copolymers of HEMA and Ma-acap-CHOL, ranging from diblock to pentablock, have been synthesized through RAFT polymerization with DSPA, as chain transfer agent (CTA), in a controlled manner, obtaining predetermined molecular weight polymers with narrow molecular weight distributions.

- Amphiphilic multiblock copolymers, ranging from diblock to pentablock copoymers, self-assembled into round-shape nanostructures with low polydispersity in water as shown by DLS, NTA and TEM. Increasing number of blocks rendered smaller nanostructures but with higher tendency to aggregate, as

indicated by zeta potential. This trend was kept through all techniques employed, nanoprecipitation and film hydration. For lower copolymers, the self-assembled nanostructures showed the same size with all the techniques tested, whereas for higher copolymers, nanostructures obtained by film hydration technique were larger than those obtained by nanoprecipitation, indicating that is more difficult for the rehydrating solution to penetrate through the polymeric film's pores in the case of larger copolymers, thus larger vesicles are formed.

- The obtained nanostructures showed the ability to encapsulate a hydrophobic drug, such as paclitaxel, at high loading efficiency and capacity. Higher loading of paclitaxel can be achieved by raising the number of hydrophobic blocks, from triblock to pentablock copolymers. In addition, nanostructures from triblock copolymers showed the ability to encapsulate both hydrophilic and hydrophobic substances with high loading efficiencies and drug content of paclitaxel and doxorubicin.

Liposomes and polymersomes have been compared as potential drug delivery systems to breast cancer metastasis in the brain through a dual-targeting approach.

- The polymersomes developed in this thesis can be easily decorated with biomolecules through covalent binding by post-modification of their CTA-end group or by insertion of an amphiphilic protein into their membranes, without loosing its function. It has been demonstrated that the obtained polymersomes show also membrane permeability, although the resulting loading capacity was slightly lower compared to liposomes. The higher mechanical stability of polymersomes is translated into a lower drug leaking.

- The incorporation of phage protein into both systems, led to an increase in uptake in MCF-7 and U87MG, which was especially remarkable for polymersomes. In addition, phage presence determined the uptake pathway of the formulations, contributing to the endosomal escape of polymersomes and preventing membrane fusion in the case of liposomes. Cytotoxicity of liposomes is higher than polymersomes, due to their higher uptake and faster release.

- Dual-targeting approach has been found to be a good strategy to increase liposomes permeability through a BBB model, suggesting a synergistic effect between both ligands, whereas in the case of polymersomes, no differences in permeability were observed depending on the targeting. This fact indicates that cholesterol present in polymersomes' structure contributes to the permeation across the BBB model, thanks to its high affinity for LRP-1, masking an eventual enhancement of transport through the BBB monolayer of Regulon peptide.

List of publications

M. Sanchez-Purrà, B. Oller, B. Albaiges, K. Pickl, E. Fröhlich, C. Grandfils and S. Borrós (2013) **New method to decorate thermosensitive nanoparticles for biomedical appplications.** *Journal of Nanopharmaceutics and Drug Delivery (Accepted)*

M. Sánchez-Purrà, V. Ramos, V.A. Petrenko, V. P. Torchilin and S. Borrós (2013) **Polymersomes and Liposomes as potential Drug Delivery Systems to Breast Cancer Metastasis in the Brain: Comparative Study of Doxorubicin Delivery through a BBB Model.** *Nanomedicine (Submitted)*

G. H. Bode, K. E. Pickl, M. Sanchez-Purrà, B. Albaiges, S. Borrós, A. J.G. Pötgens, C. Schmitz, F. M. Sinner, M. Losen, H. W.M. Steinbusch, HG. Frank, P. Martinez-Martinez (2013) **Detection of peptide-based nanoparticles in biological fluids by ELISA.** *APLOS ONE (Accepted)*

Presentations and Courses

05/2012	**9th international Symposium on Polymer Therapeutics**, València, Spain Poster presentation: Amphiphilic multiblock copolymers as self-assembly drug carriers
09/2010	**2nd Summer School on Medicines**, Institut Claudius Regaud, Toulouse, France *The entire process of a drug: From the idea to the market*
05/2010	**8th international Symposium on Polymer Therapeutics**, València, Spain Poster presentation: A new method to decorate acrylamide-based nanoparticles
02/2010	**Particle Size Analysis Training**, CEIB, University of Liège, Belgium *General overview of the main techniques suitable to characterize nanodispersions*
09/2009	**22nd European Congress on Biomaterials**, Lausanne, Switzerland Poster presentation: Tailoring the thermosensitivity of acrylamide-based nanoparticles through particle size control
09/2009	**Euronanomedicine**, Bled, Slovenia Oral presentation: A new method to decorate thermosensitive acrylamide-based nanoparticles ***Member and chair of the organizing committee of the Young researchers' technical workshop in the frame of Euronanomedicine***
02/2009	**Citotoxicity and immunological tests of nanoparticles**, Medizinische Universität, Graz, Austria